The Numerical Prediction of the Dent Resistance of Medium Scale Aluminum Structural Panel Assemblies

by

Blake Hodgins

A thesis
presented to the University of Waterloo
in fulfillment of the
thesis requirement for the degree of
Master of Applied Science
in
Mechanical Engineering

Waterloo, Ontario, Canada, 2001

I hereby declare that I am the sole author of this thesis. This is a true copy of the thesis, including any required final revisions, as accepted by my examiners.

I understand that my thesis may be made electronically available to the public.

Abstract

An examination of static and dynamic dent resistance of structural panel assemblies representing automotive hoods is described in this thesis. Fabricated panel assemblies incorporating typical components of real automotive parts were tested. The panel assemblies included an AA5754 inner panel using an array of teacup supports and an AA6111 closure panel joined with automotive mastic. The assemblies allowed for parametric assessment of numerous factors affecting dent resistance including: panel thickness, panel curvature, panel support configuration and dent site location.

An extensive experimental program evaluated various panel combinations under both static and dynamic denting conditions. The measured results illustrate various trends of the different factors affecting dent resistance. The experimental database allows a qualitative assessment of dent resistance for full-scale automotive parts. The importance of support conditions is highlighted. The influence of mastic thickness is found to be a critical consideration.

Numerical simulations of the dent test were undertaken using finite element techniques. The numerical predictions offer varying degrees of accuracy. The quantitative results are limited, due to numerical concerns, but the qualitative trends are generally well captured. As well, the relative importance of the various parametric factors is well represented in the numerical results. The interaction of the components at the teacup supports proved to critical to the predictive ability of the models. The method developed to model the interaction was somewhat limited by the available material models within the numerical code used, but offers promise for improved results in future simulations. The modelling method is readily transferred to full-scale automotive panels for assessment of dent resistance early in the design cycle.

Acknowledgements

To my family,

To my parents for pushing me without pushing me,

To my sister for her friendship,

And to my grandparents for their support and inspiration,

Thank you.

Contents

List of Tables

List of Figures

x

xiii

xv

xvi

xvii

1 Introduction

1.1 *Motivation*

The current research is concerned with the prediction of aluminum alloy, automotive panel dent resistance. In order to understand the impetus for this research and the introduction of aluminum into automotive design it is essential to understand the historical context and factors which led to the drive for vehicle weight reduction. Once the motivation for the introduction of aluminum into an increasing range of automotive applications is clear, the specific importance of dent resistance can be examined. The automotive industry operates within a highly competitive global market in which the need for constant innovation is essential. The market is driven by numerous critical factors, which directly influence a company's ability to compete. In the case of the automotive market the varying needs of the public, government and profitability all must be accommodated in the design of vehicles.

One key factor in the development of automotive design over the last 25 years has been the supply and cost of oil and the implications of vehicle fuel efficiency that arise in this regard. Historically, the North American marketplace had some of the lowest global fuel costs, and the effect of gasoline prices and vehicle fuel efficiency on automobile purchases has been limited. In the current marketplace it is debatable that increasing fuel costs will have any noticeable effect on automotive purchasing, as the reliance on the car, particularly in North America, is so pervasive. This has not always been the case, as was apparent in the mid to late 1970's when the Middle East oil embargoes saw dramatic rises in fuel costs and fuel shortages. This fuel shortage translated somewhat into public demand for more fuel-efficient vehicles, but the greater effect was political. As a result of mounting public pressure for government relief from the crisis, political action was undertaken to address the situation.

The U.S. government reacted to the heavy reliance of America on foreign oil in the Energy Policy and Conservation Act of 1975 [1]. The key element of this legislation, with respect to the automotive industry, was the corporate average fuel economy (CAFE) standards. In an attempt to lower consumer use of oil, the CAFE standards introduced minimum fuel efficiency requirements, effectively an average fleet efficiency that each automotive manufacturer had to meet. These standards outlined increasingly stringent minimum fuel efficiencies for successive model years. Initial efficiency levels of 18.0 miles per U.S. gallon were introduced for 1978, and this minimum increased to 27.5mpg by 1985. It is important to realize that these standards applied to passenger cars, while a less stringent standard was applied to light trucks. The CAFE standards remain in effect to this day, with the current level for passenger cars being 27.5mpg and the light truck standard being 20.7mpg. These standards have effectively remained at these levels since 1990, with only slight increases in the light truck standards over the past ten years.

The impact of the CAFE standards on the automotive industry was dramatic as fuel efficiency levels as late as 1974 were only 12.9mpg [1]. In order to meet these new requirements the need for new design approaches was apparent. Numerous improvements in a range of areas were introduced, with weight reduction being prominent. Weight reduction can be achieved in two main ways in the design of the automotive structures and body panels:

1- Down gauging, the reduction of panel thickness
2- Material Substitution

One of the most likely candidates as a material substitute for steel body panels was aluminum alloy sheet, which potentially offers a three times weight reduction at a constant thickness. Thus the oil crisis of the 1970's and the resulting CAFE standards served as a driver for the introduction of aluminum in a wider range of automotive applications.

However, the political climate changed dramatically in the 1980's as the oil crisis ended and the economic impact of further increases of the CAFE standards began to be questioned. Up to the mid 80's, when oil prices began to drop and consumer demand for smaller cars receded, meeting increasing CAFE standards was a relatively minor concern. When the marketplace changed in the mid 80's and demand for larger cars, which tended to be less efficient, escalated, automotive manufacturers began to view the CAFE standards as a

2

growing concern [1]. With increasingly less efficient vehicles making up the core of vehicle sales, fleet efficiency averages began to climb and meeting CAFÉ standards became more difficult. When this was coupled with increasing competition from foreign manufacturers, political pressure began to mount against the CAFE standards. The importance, both financially and politically, of the automotive sector had to be balanced against standards whose importance was less quantifiable. This led to slight decreases in the standards starting in 1986 before they stabilized at the current levels in 1990. This change in standards saw the focus on weight reduction, and hence aluminum substitution in the automotive industry, curtailed, as the 1990's were entered.

The next shift in automotive design philosophy with regards to weight reduction occurred in the early 90's with a new administration in the United States. While increases in the CAFE standards proved politically impractical or impossible, the introduction of the Partnership for a New Generation of Vehicles (PNGV) provided a stimulus for further research into material substitution with aluminum. The PNGV initiative was a cooperative research alliance between government labs and domestic automotive manufacturers, which had as one of its main objectives, a threefold increase in fuel efficiency [1]. One of the main areas of research of the PNGV program was lightweight materials, chiefly aluminum. Another emerging factor in the 90's was increasing environmental awareness that led to both domestic and global influences on fuel emissions. Global treaties such as the 1997 Kyoto accord on global emissions provided further impetus for improved vehicle fuel efficiencies. A final factor that emerged in the late 90's was the rise in sport utility vehicle (SUV) sales. While SUVs and mini-vans are currently classified as light trucks for CAFE purposes, and hence must meet lower standards, these vehicles tend to be some of the heaviest in the fleets. With this trend towards increasingly large and expensive vehicles, the push for lighter materials increased. Aluminum offers significant weight savings but at a cost penalty. While smaller cars cannot absorb the cost increase and remain financially viable, more expensive, large vehicles offer the perfect opportunity for aluminum substitution where a reasonable cost increase can be absorbed.

Currently, a new U.S. administration is in power and its political philosophy with regards to oil costs, fuel efficiency and emission standards is only beginning to take shape. The Kyoto accord has recently been officially rejected, and a renewed push for domestic oil

exploration appears imminent, yet the need for improved fuel efficiency remains strong. Current gasoline prices are reaching all time highs in North America, the impact of which is sure to be felt by the automotive industry. Regardless of what the political outcome will be with regard to changes in the CAFE standards, the need for improved fuel efficiency should remain.

With the spread of aluminum into a broader range of automotive applications the need for a better understanding of its behaviour has emerged over the past 25 years, with dramatic increases in the past 10 years. As the push for fuel efficiency has driven the need for weight reduction, the competition between steel and aluminum has intensified. At the same time that aluminum began to make serious inroads in the automotive industry, steel manufacturers countered with down gauging options using high strength steels. The Ultra Light Steel Auto Body (ULSAB) project was introduced in 1994 as a cooperative venture between steel and parts manufacturers to better exploit the potential of these new high strength steels. The ULSAB has demonstrated significant structural performance improvements, along with a 25% weight reduction while maintaining cost levels [2]. In 1998 a similar program for outer panels, the Ultra Light Steel Auto Closure (ULSAC) program, focused on further possible weight savings with new steels [3]. With increasing improvements in steel properties, coupled with a well established manufacturing infrastructure for steels, widespread introduction of aluminum remains difficult.

To achieve a broader use of aluminum alloys requires a complete design approach that considers all performance parameters of potential aluminum parts. The need for this detailed examination of new parts has led the aluminum suppliers to offer comprehensive evaluation of aluminum in all aspects of its automotive implementation. This includes careful design of material properties to meet part requirements with respect to formability, manufacturability and in-service performance.

One potential area for widespread introduction of aluminum sheet in automotive applications is in body panels, such as hoods and doors. Among the key factors that must be assessed in the design of body panels are formability, stiffness, torsional rigidity and dent resistance. At first glance, dent resistance appears to be an insignificant, cosmetic concern, however, that is far from the case. The ability of a panel to resist denting deformation or damage may be an aesthetic concern, but it can become very expensive in terms of both

4

warranty claims and public perception. In fact, with the need for lower sheet thickness, the susceptibility of body panels to denting increases, to the point where dent resistance may become the limiting design factor. In the end, a seemingly minor cosmetic concern may control the final sheet thickness, and corresponding panel weight.

The research to be described was part of a larger program with ALCAN International that looked to evaluate the dent resistance and stiffness response of aluminum sheet in automotive applications. Previously completed work examined the denting behaviour of two different alloys in a medium scale formed panel that approximated actual panel curvatures and levels of pre-strain [4]. The current work is focused on the evaluation of the interaction between outer panels and supporting inner panels during denting. A key component of this research has been the use of finite element modeling as a tool for the assessment of dent resistance.

The use of numerical simulation continues to grow in the automotive industry, as the potential to improve and optimize designs early in the design cycle is highly desirable. The number of commercially available numerical modeling packages has grown dramatically over the past decade and numerical simulation has become a key component of automotive part design. It is particularly important for new materials, such as aluminum, that feasibility be demonstrated before material substitution will be considered. Thus it is imperative that successful numerical approaches are available to help assess all design concerns, including dent resistance. As a result, a key focus of this work is the development of effective numerical modeling methods for complex multi-part body panels.

In order to gain insight into what areas need to be examined a survey of existing research identified the areas of most importance. A range of previous dent resistance studies for steel and aluminum, both numerical and experimental, offer a wide assessment of different factors that may be critical to denting behaviour. Papers as early as 1960 [5], offer insight into denting behaviour. Historically, research on denting has been associated with periods during which there was a requirement for vehicle weight reduction. Thus, the two largest concentrations of denting papers occurred in the mid 70's and the early 90's, corresponding to the initial CAFE standards and the PNGV program respectively.

1.2 Static vs. Dynamic Dent Resistance

The study of dent resistance can be divided into two main areas, corresponding to two distinct phenomena: static and dynamic denting. In general, denting of a panel refers to a secondary loading, that is a load not related to the vehicle's operation, which results in a permanent deformation of the panel. Depending on the nature of this load the denting process can be classified as either static or dynamic, in either case the end result being some form of permanent surface deformation on the panel.

Static denting is defined by a gradual loading of the panel, that can be approximated as quasi-static. Static denting is typified by someone leaning on a hood or door with their hand or elbow. The loading will tend to be relatively gradual, and the response will be governed by the global stiffness of the panel. As a result, evaluation of static dent response is often combined with stiffness analysis of panels. The effective performance criteria will be the "feel" of the panel, its stiffness, and the residual displacement or deformation, the static dent depth. A critical factor in static dent resistance and stiffness analysis is the so-called "oil canning load", the load at which localized panel curvature reverses. Oil canning or snap-through appears as a transition from an initial stiffness to a secondary stiffness in the load-displacement curve in static loading.

Dynamic denting refers to a process at a higher velocity involving the impact of an object with the panel surface. Dynamic denting is typified by a hailstone or small stone impact. In the case of dynamic denting the phenomena is more localized, with the deformation more focused in the impact region. The dynamic dent depth is the resulting permanent deformation in the panel. As noted by DiCello and George [6], the main difference between the two types of denting is explained by examining how the applied loads are supported. The static denting load is dispersed continuously, and is supported globally by the panel with both bending and membrane stresses. Dynamic denting response will be highly localized and will depend primarily on the radial-in-plane membrane yield stress.

In surveying the research related to denting it is important to distinguish which denting behaviour is being studied. Many studies will focus on one form of denting, often ignoring the other, which can lead to confusion when comparing results. It is thus important to understand the loading case being studied at all times, as the results are greatly affected by the type of denting process. Static denting studies usually refer to a load/unload cycle that

was used to generate both a stiffness response, from the load vs. displacement data, and a dent resistance profile, from the unloaded displacement or dent depth vs. load. Dynamic denting analyses will reference dent depths to either indentor velocity, applied through various mechanisms, or indentor drop height. Both types of denting are also function of the indentor used in testing. Unfortunately, common denting standards, load levels, velocities and indentor geometry, have not always been in place and thus variation in test procedures further confound comparisons of different studies.

1.3 Dent Testing Procedures

Some of the earliest documented dent testing occurred to 1960 in research done by Dow metals [5] that investigated dynamic denting of aluminum and steel using relatively small panels, 37mm by 37mm, and a 5kg [11lb], 50.4mm diameter, hemispherical tipped indentor. A range of drop heights was used to produce data over a spectrum of impact energies. While this work represents a common approach to dynamic dent testing, the high mass of the indentor is not typical of current testing methods. Other early work reported data for both static and dynamic denting of steels [7]. Interestingly, the motivation for weight reduction in this case was the lower shipping costs of thinner steel. An Olsen test was used for the static testing procedure. A clamped test sheet with a 25.4mm diameter exposed area was gradually loaded using a 22.2mm diameter spherical indentor, to thousands of pounds. The load levels, and subsequent dent depths, greatly exceeded the levels seen in current test procedures. The dynamic testing procedure used was similar to current testing methods, as a 25.4mm diameter, 599g, indentor was dropped from a height of 736.6mm. Two sets of boundary conditions were used in the tests, locally and globally restrained samples, which led to dramatic differences in the results. Other early testing related to dent resistance of automotive panels includes studies of hailstone impacts of roofing panels. This research considered a range of hailstone sizes from 38-70mm, and used ice as a hailstone simulant [8]. These early studies highlight the varied nature of early dent testing standards that persisted as more automotive denting studies began to appear.

As more focused automotive denting research began to emerge in the 1970's, a variety of testing procedures persisted. Early dynamic testing of steel sheet used a 12.5mm indentor, weighing between 0.227kg to 2.27kg, that was dropped from between 19mm and

477mm [9]. This range of drop heights is relatively low as the impact velocity reaches only 3.05m/s at the highest height. DiCello and George [6] at Chrysler also presented preliminary dynamic denting results based on tests using a 25.4mm diameter sphere with velocities up to 30m/s. Other early dent testing performed by Reynolds Metals Co. used an air gun to fire projectiles at both steel and aluminum panels [10,11,12]. These studies used a 25.4mm diameter, spherical indentor with velocities ranging from 4.5m/s to 26.8m/s. These velocities would correspond to drop heights of 1.0m to 36.7m, with the high velocity tests falling well outside today's test standards. Other studies [12] considered the effect of larger diameter indentors (31.75mm and 38.1mm), finding that for equivalent amounts of impact energy the denting response was similar. The indentor size chosen was based partially on hailstone samples in an attempt to better mimic actual, in service, denting conditions. Other early work on dynamic denting included use of a 38.1mm diameter indentor with a velocity of 7.72m/s [13] and further air gun based testing using relatively high impact velocities from 12.5m/s to 27.8m/s with a 22.2mm diameter indentor [14]. A set of dynamic dent tests was reported by Kobe Steel [15], covered indentor sizes from 20mm to 30mm in diameter, and drop heights from 300mm to 2200mm (2.45m/s to 6.56m/s). This range of test cases brackets the range of most current tests. For the most part, early dynamic dent tests used indentors with diameters of 25.4mm but the range of velocities tested was large.

Static dent testing in this period was more limited and the test procedures varied to a large extent. The landmark paper in denting, particularly with respect to static denting, of DiCello and George [6] used a 25.4mm diameter spherical indentor and loads up to 100N. Other early studies saw the use of 25.4mm square indentors [16], 12.5mm diameter spherical indentors [17] and 50mm diameter indentors [18]. The other common variable in these tests was the range of applied loads. Depending on the nature of the testing, a range of loads could be specified or a maximum desired deflection could determine the peak loading.

In the 1990's, when the next grouping of dent studies appeared, a more standardized denting procedure emerged. The 1996 Auto Steel Partnerships denting guidelines [19] provided a standardized experimental procedure for both static and dynamic dent testing procedures. The majority of testing from this period used these standards which suggested a 25.4mm diameter indentor for both static and dynamic testing. The guidelines also categorized a dent as static for loading speeds of less than 127mm/min (0.002m/s) and

dynamic for indentor speeds greater than 894mm/s (0.89m/s). The guidelines were sensitive to the varying nature of different test setups and offered recommendations for these different cases, while leaving room for the tailoring of specific tests to meet particular needs. The suggested static load method involved a 50.8mm/min loading speed and a successive load/unload cycle such as, 67N (15lbf), 133N (30lbf), 200N (45lbf) and then 267N (60lbf). A common alternative would see smaller load steps, using every 22.2N (5lbf), with 178N (40lbf) as a denting assessment load. With respect to dynamic denting, a procedure for high-speed actuator loading was outlined, as well as a range of impact energies for drop height or projectile based test systems. The suggested range of impact energies was 0.2J (2.45m/s) to 0.5J (3.87m/s) in 0.1J increments, with 0.2J as a low-end threshold for the achievement of visible dents.

The 25.4mm diameter indentor is largely the standard geometry used in dent testing today. There are some static dent studies that use larger indentors, often for stiffness assessment, but for the most part the 25.4mm sphere is the indentor of choice. Some studies have examined the influence of indentor geometry on both stiffness and dent resistance. Comparison of a 25.4mm and 102mm indentor with respect to stiffness showed little difference in the mean values measured [20]. Similarly, a lack of indentor geometry effect on stiffness measurements was noted in testing using 25.4mm and 100mm spherical indentors [21]. A more detailed analysis by Vreede *et al.* [22] of indentor geometry in dynamic denting used 4 different indentor diameters, ranging from 6.25mm to 50mm, with a range of masses between, 33g and 100g. They reported no significant effect of indentor geometry. An alternative study of dynamic denting indentors, with a more pronounced geometric variation comparing a 37mm spherical indentor to a 1.59mm tipped cone, showed an indentor effect of 20%-80% on dent resistance [13]. Despite the difference in dent resistance values, the general trends remained consistent for both indentors.

The 178N peak load for static dent assessment is quite common [23,24,25,26,27,28,29,30]. Other static peak loads, using 25.4mm diameter indentors, include, 267N [20], 300N [31], 350N [32], 400N [33] and 578N [34]. This variety of load levels is predicated on the individual test setups and panel configurations, along with the resulting level of denting deformation observed. Other studies using different load and indentor combinations are also available [17,35].

9

Fewer dynamic dent studies are available from the 1990's. Two studies by M. Shi of US Steel used quite different test procedures. His earlier study [36], used a drop tower procedure with a 12.7mm indentor and a 1.75m/s impact velocity, while his later work [37] used a high-speed actuator driven, 25.4mm indentor at 0.5m/s. The later study used a relatively slow speed for a dynamic dent test as it represents only a 12.5mm drop height. A comprehensive study assessing both the static and dynamic denting of aluminum sheet performed by Thorburn [30] used a 25.4mm indentor and 3 different drop heights that imparted velocities of 3.46m/s, 4.24m/s and 4.89m/s respectively. Finally, the work of Vreede *et al.* [22] used a similar test setup, measuring dynamic denting with a 25.4mm indentor dropped from heights between 0.3m to 1.2m (2.45m/s to 4.89m/s). Thus, the range of adopted velocities in dynamic testing is quite broad, but the 25.4mm indentor is a well agreed upon standard.

A final source of variation in test standards remains the automotive companies. Each major manufacturer tends to have different thresholds, in terms of both velocity and static load level, at which minimum dent requirements must be met. This leads to varying test methods by the material and parts suppliers between parts depending on who the end customer will be. As such, when developing any test procedure it is important to consider what the study's goal remains and to tailor the testing procedure to meet those needs while attempting to remain within the range of commonly used load levels.

1.4 Assessment of Dent Resistance

Another common area of variation in denting studies centers on the assessment of dent resistance. This problem was alluded to in the overview of the various test procedures, as different studies will adopt static load levels and dynamic impact velocities depending upon how they wish to assess dent resistance. Firstly, what constitutes a dent must be determined, whether it is a qualitative assessment of damage, a "visible dent" or a quantitative depth of deformation, a critical dent depth. This is reflected in the existing studies that define a dent in numerous different ways. Some studies use criteria where dents are ranked subjectively, using an alphabetic grading system [38]. Testing that quantifies dents with an actual measured value often sets an arbitrary dent depth at which a panel is deemed to have dented, referred to as a visible dent. In some cases, a maximum allowable depth of dent is specified,

termed a failure depth, or often no visible dent is allowed. Determining the magnitude of a visible dent is subjective, dependent on numerous secondary factors such as paint color, lighting and panel shape. Still, some arbitrary depth is useful in comparing results between studies. The most common dent depths that are classified as visible are 0.1mm [9,15,17,18, 26,32,37] 0.06mm [24,34] and 0.02mm [6,38,39,40]. The most comprehensive examination of what constitutes a visible dent correlated qualitative alphabetic grades of the degree of denting with measured dent depths [38]. Based on the reported results the mean value of a visible dent was 0.08mm with a standard deviation of 0.06mm. While the array of dents considered in that study was limited, the results suggest 0.02mm as a minimum depth for dent visibility. Studies often refer to the formation of a visible dent as the onset of plastic yielding, and attempt to associate a very small level of deformation with this yield point. This was the approach used by DiCello and George [6], when they selected 0.025mm as their approximation of minimal deformation at yielding. Ekstrand and Asnafi [21], suggest 0.01mm as a dent depth reflective of initial yielding but suggest using 0.1mm for assessment of dent resistance. This reflects that accurately capturing the depth at dent initiation can be very difficult and subjective, while a more relaxed standard such as 0.1mm is more reasonable for comparisons.

Another consideration is the dent load that the panel must withstand in service. This leads to tests where the applied load is governed by various performance requirements. This is reflected in the numerous studies cited that evaluated static denting at 178N, an arbitrary critical load or a specified drop height or impact velocity. These two requirements can lead to studies that will dent panels until they reach some critical level of denting deformation, while others will simply test dent response up to a threshold load or velocity [10-13,30,35,37,41,42]. This can lead to difficulties in comparison between studies, as the data sets will lack a basis for comparison.

In order to quantify the static dent resistance of a given panel, a value of load to cause a critical dent is often reported. This form of assessment often leads to confusion in comparisons between studies due to the differing nature of the dent resistance quantifiers. Some studies will report the critical value to cause the onset of denting, while others will report the critical value to cause a specific dent depth, often 0.1mm. Furthermore, how the load state is quantified also varies. A force based approach will use the applied load to cause

a 0.1mm dent, $P_{0.1}$, as a quantifier [17,18,21, 28,35,42]. Alternatively, an energy based approach will use the dent energy applied [6,13,39,43,44,45] or absorbed [41] to quantify dent resistance. Static dent energy is calculated after testing as the area under the force-displacement curve and is a function of the panel stiffness. These different means of quantifying dent resistance can lead to contradictory findings with respect to the effect of various parameters on dent resistance, as illustrated in Figure 1. Quantifying dynamic dent resistance does not cause the same degree of confusion as the applied energy and velocity are directly related.

The confusion with regard to the static dent resistance assessment is highlighted by the contradictory findings of two early papers. DiCello and George [6] used the concept of applied work or energy, while Yutori *et al.* [18] used a critical applied load. The applied energy approach for the assessment of static dent resistance used two non-dimensional terms to plot denting results and then used a regression analysis to relate the two terms. The resulting equation relates applied denting energy, a measure of dent resistance, as a function of panel yield strength (σ_y), thickness (t), and stiffness (S) such that:

$$W = K \frac{\sigma_y^2 \cdot t^4}{S} \tag{1}$$

where K is constant. The paper outlines methods for relative comparisons of panels using the above equation by holding a given parameter constant. This relation, and the resulting comparison equations, have been cited and used by numerous subsequent studies. Ford [16] used equation (1) in a material substitution analysis of load floors of various station wagons, comparing the relative dent performance of steel and aluminum panels of the same stiffness. This equation also became the foundation of various different panel assessment tool sets that combined different theoretical panel stiffness formulas with the denting energy relation. Through the use of theoretical equations for stiffness of circular shells and discretized regions of unsupported areas, a set of design equations can be developed for general assessment of panel performance [39,43]. The equations and methodology of these studies were subsequently used to produce dent resistance assessments, over a range of parameters in other studies [27,44].

The alternative method of dent resistance assessment presented by Yutori *et al.* [18], based on a critical load to cause a dent, yielded the following relationship:

$$P_d = K \cdot \sigma_y \cdot t^n \qquad\qquad\qquad (2)$$

where P_d is the load to cause a permanent dent, K and n are constants, t is the panel thickness and σ_y is the yield strength. The suggested value for n, based on curve fitting of experimental data, is 2.3-2.4. This equation does not explicitly include the effect of stiffness but based on the results presented, increased stiffness results in increased P_d. This stiffness effect contradicts the findings of DiCello and George, who observed an inverse relationship between dent resistance and stiffness. Numerous studies [17,21,24,28,35,46] have since pointed out this discrepancy before choosing one method for dent resistance assessment. Depending on the nature of the study the impact of this stiffness difference will vary. For cases that assume a constant stiffness when making comparisons between panels, the two approaches provide the following relations:

$$DiCello \ \& \ George: \sigma_{y2} = \sigma_{y1} \cdot \left(\frac{t_1}{t_2}\right)^2 \qquad\qquad Yutori \ et \ al.: \sigma_{y2} = \sigma_{y1} \cdot \left(\frac{t_1}{t_2}\right)^{2.3}$$

The above equations are quite similar with the load based equation being slightly more conservative as noted by Shi in a material substitution study [28]. The greater concern in choosing which assessment method to use arises when the stiffness is not assumed to remain constant. For down-gauging analyses, where the Young's modulus remains constant and only small changes in panel stiffness occur, either approach can be effective. However, if the panel geometry is used as a design variable in an attempt to control dent resistance the choice of assessment method will clearly be a key factor.

As outlined previously, many dent test studies use a load based approach. As a result, most studies that attempt to correlate their results with these dent resistance assessment methods tend to find that Yutori *et al.*'s [18] observations with regard to stiffness are correct [24,35,37,47]. While theoretically DiCello and George's findings [6] can be valid, for the majority of applications that use load based testing, their findings cause erroneous conclusions with respect to the role of stiffness. In cases where a given load is applied and an assessment of resistance to dent initiation is desired, Yutori *et al.*'s [18] load based equation is more appropriate as it better reflects the testing approach.

Considering typical dent testing, where a peak load is used and a residual dent depth is recorded, the more appropriate method for dent resistance assessment appears to be the load based approach, using a $P_{0.1}$ type quantity. As illustrated in Figure 1, by Thomas [4],

both methods can produce a force-displacement profile, for a common dent depth, which support their contradictory conclusions with respect to stiffness. It then becomes a matter of determining which is the more appropriate measure of dent resistance, an applied load, which is effectively independent of the panel, or an energy, which will be a function of the panel stiffness.

Load Versus Displacement
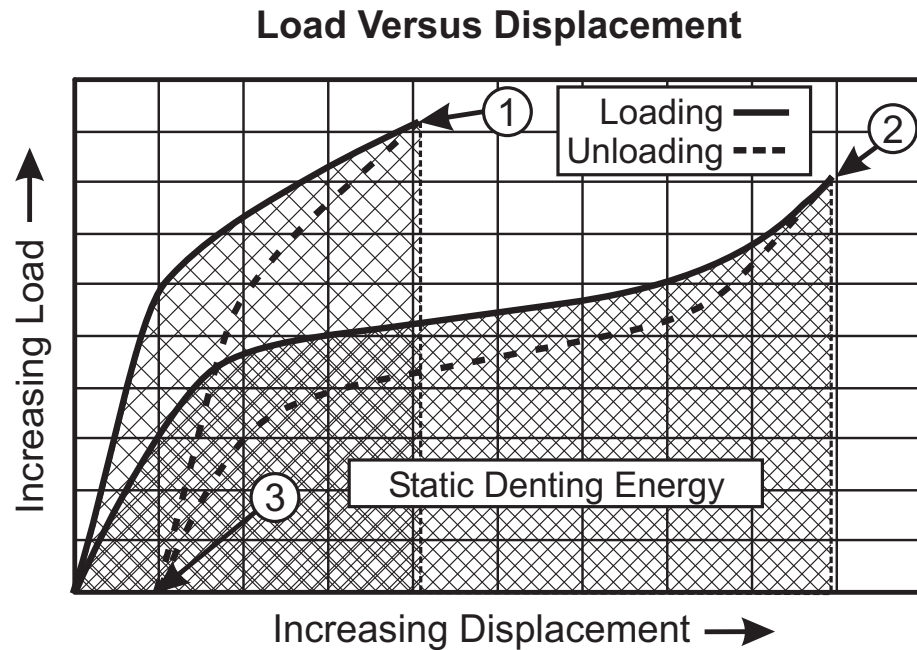
Figure 1: Hypothetical comparison of stiffness response for two curved panels. The panels are assumed to unload to identical dent depths at (3), but suggest alternative conclusions with regard to dent resistance. A higher load, (1), is reached for the stiffer panel but at lower level of denting energy than the low load, (2), soft panel case.

The energy based approach will tend to suggest that more compliant panels are superior with respect to dent resistance since they allow a larger elastic deformation, leading to a large area under the force-displacement curve and a higher subsequent measure of applied energy. This energy approach is highly dependent on the panel geometry, which controls the force-displacement response. This limits applied energy as a design criteria. The load based approach allows for a specified load to be applied independent of panel geometry. Essentially the load method allows a design load to be applied and the residual dent measured and an assessment of the panel can be made relative to an allowable dent depth.

14

1.5 Factors Affecting Dent Resistance

As was highlighted in the previous section, various factors affect dent resistance and their relative importance is a continuing area of study. While there is confusion in quantifying the effect of stiffness, most factors are clearly understood.   Various material properties affect dent resistance, such as yield strength, Young's Modulus, strain hardening and strain rate sensitivity. Geometric factors such as thickness, curvature, panel size and support conditions also play a critical role in denting response. Finally, the level of applied load or velocity will have an obvious effect on dent resistance.   The effect of different parameters is often dependent on the nature of the dent test, with opposite trends emerging for static and dynamic testing.

1.5.1 Yield Strength

One of the principle factors that affect both static and dynamic dent resistance is the yield strength of the material. A dent is a plastic deformation of the surface of a panel is directly related to the onset of yielding in the material. Associated with the yield strength is the general stress strain response of the material reflected in the strain hardening and strain rate hardening behaviours. Another factor that will affect panel strength is its age hardening characteristics, particularly as they pertain to paint bake heat treatments common in automotive applications. Numerous studies have addressed the effect of yield strength on dent resistance, suggesting various methods for the optimization of the yield strength and stress-strain response of the material.

Dent resistance is directly related to yield strength in that an increase in yield strength will lower dent depths [6,9,13,15,18,21,22,26-38,42,44-46,48,49,50,51,52,53]. Regardless of the material, panel geometry, thickness or any other factors, the benefit of high yield strength remains. The relationship of dent resistance resulting to yield strength will vary depending on the quantities used to describe denting. In cases where dent resistance is quantified as the load to cause a specific dent depth, dent resistance is linearly related to yield strength [18,21,22,34,42]. A typical linear relationship between denting load and yield strength is presented in Figure 2 for a set of different panel curvatures (300R corresponds to a radius of curvature of 300mm).
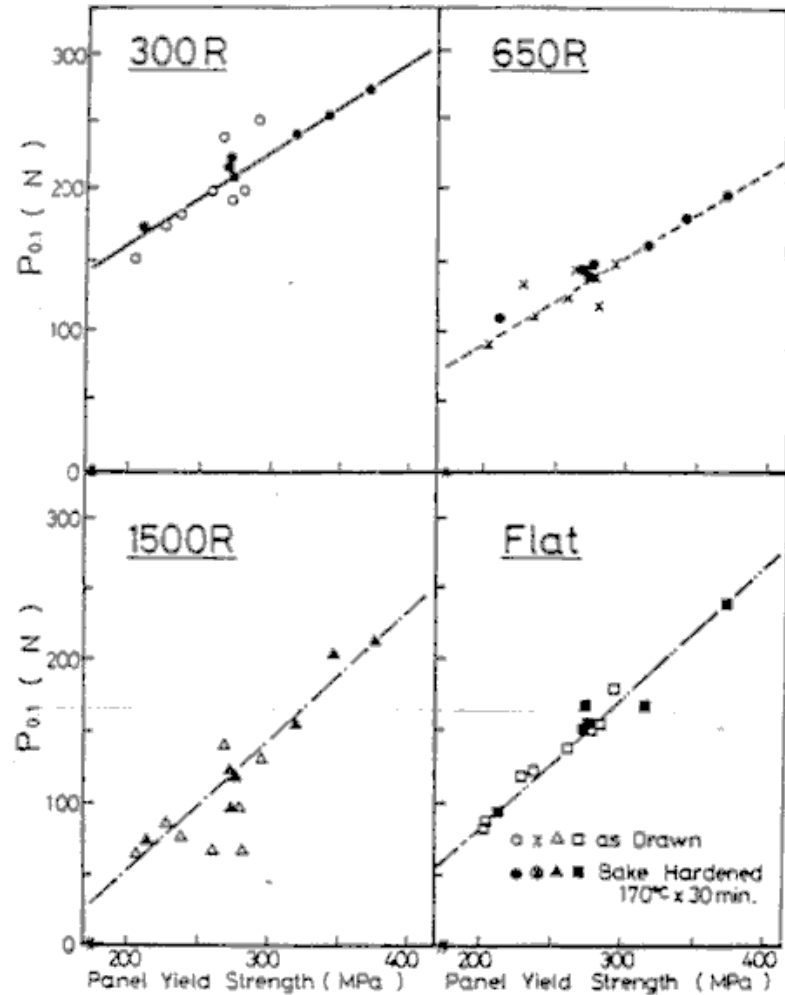
Figure 2: Linear relationship between load to cause a 0.1mm dent, $P_{0.1}$, and panel yield strength for a variety of panel curvautres, as observed by Yutori *et al.* [18].

The linear nature of this relationship seems reasonable since the load to cause a visible dent, or a very small measurable dent, is slightly above the onset of yielding. Therefore, as the yield strength is increased the load needed to reach yielding will increase linearly as long as the force displacement response remains linear. Using the same analogy with respect to energy, the reason for the yield strength being squared in equation (1) is apparent. If the loading is linear up to yield the area under this curve, the denting energy, will be increasing quadratically.

Van Veldhuizen *et al.* [35] attempted to quantify the relationship between yield strength and critical denting load for different panel curvatures using an equation similar to (2) but saw the exponent for the σ_y term range from 1.1-1.6. The highest exponent applies to

16

the lowest curvature panel, the most likely panel to exhibit snap through and a non-linear loading response. This may explain the varying exponent. Observations of dent depth, for a given load over a range of yield strengths, show diminishing benefits as yield strength increases. Generally dent depth is observed to decrease exponentially as yield strength is increased [9,18,37]. Figure 3 illustrates this yield strength effect from the work of Yutori *et al.* [18].
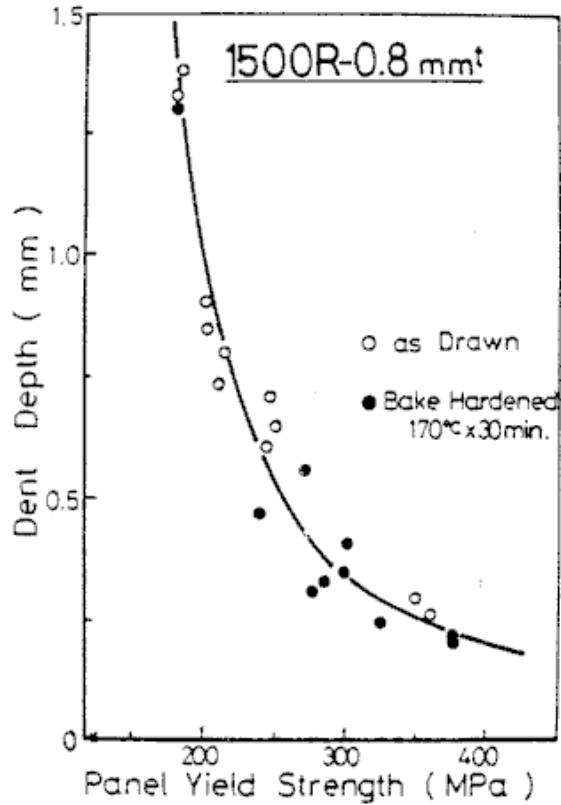
Figure 3: Decaying effect of panel yield strength on static dent depth as observed by Yutori *et al.* [18].

Based on the influence of yield strength on dent resistance, it becomes a matter of determining how best to exploit its benefits. Material substitution of higher strength alloys becomes a desirable goal. Numerous studies have examined the benefits of the introduction of high strength steels in autobody panel applications [6,9,17,18,22,26-29,32,34,37,38] and high strength aluminum alloys [6,11,13,45,49,51,53]. The studies reflect the benefits of improved yield strength for a variety of material grades and alloys. A concern with the use of high strength materials is the potential loss of formability. Lower strength materials tend to be ductile and more easily formed into complex automotive panels and part formability

17

must be taken into account when considering high strength alloys. A common method to improve strength, while retaining formability, is through the introduction of bake hardenable alloys. These alloys take advantage of the elevated temperature cycle used to cure panel paint. The age hardening process is accelerated at the high temperature and the material is strengthened after it has been formed but prior to being put into service. This effectively allows for complex autobody parts to be formed while still exploiting the benefits of higher strength. The use of bake hardenable steels is examined in several studies [26,28,30,34,36-38] outlining the potential weight reduction benefits associated with the strength gains. An interesting effect possibly related to the paint bake cycle arose in studies that attempted to quantify the effect of yield strength on dent resistance. McCormick *et al.* [26] studied a range of different steels and saw some outlying points when attempting to use equation (2) to model their results. The main outlying point was for a grade of bake hardenable steel, and the authors suggest that perhaps the baking kinetics have added benefits for dent resistance beyond simply increased yield strength. This observation is also noted by Shi *et al.* [37] in another study where the expected linear relationship also failed to appear. Both studies allude to yield point elongation as a possible reason for the extra dent resistance encountered in some bake hardenable steels.

Similar work with aluminum [31,49,51,53], specifically with 6000 series alloys, illustrates how paint bake cycles can be exploited with that alloy. In an optimization exercise of an aluminum hood by Saab [31], specific reference is made to the relative merit of bake hardening as a method of strength increase. The optimization of paint bake cycles and kinetics is beyond the scope of this research, but potential means of maximizing the benefits are possible through careful modification of the alloy's metallurgy [51].

An alternative method of exploiting strength benefits in automotive applications is through the use of the strain hardening and strain rate hardening responses of the material. Strain hardening, often quantified with a strain hardening exponent, n, refers to the increase in yield strength experienced by a material as it undergoes plastic deformation. Material used in automotive applications will exhibit varying degrees of strain hardening over a range of strain levels. Furthermore, materials will exhibit a rate dependent response to strain hardening. Strain rate hardening or strain rate sensitivity, often measured as a strain rate hardening exponent, m, will tend to be more of a concern in dynamic denting. However,

compared to aluminum only steels exhibit positive strain rate hardening effects in the range of strain rates experienced in typical denting analysis.

Consideration of strain hardening in denting analysis can take two forms. Firstly, it is essential to account for yield strength increases due to strain hardening when attempting to predict dent depths or dent resistance. This is particularly important when attempting to numerically model the denting process, as will be explored later. In terms of design and panel optimization, the more important impact of strain hardening is tied to the actual level of strain in a panel prior to denting. Through the pre-straining of panels in the forming process the yield strength of a sheet can be increased without having to switch materials. As such, it becomes imperative that the level of a strain in a panel prior to denting be taken into account when assessing dent resistance and comparing applications. A range of work has addressed the various issues associated with pre-strain levels and strain hardening behaviour [9,17,26-28,32,33, 36,37,42,44,46,48,52].

The need to quantify the level of strain and corresponding yield strength in a formed panel has been highlighted by Shi *et al.* [48]. This work developed a method for extracting this information for a range of applications, only one of which was denting analysis. Several studies have examined the effect of pre-strain level in formed parts, suggesting varying degrees of pre-straining as optimum. No consensus has been reached regarding an ideal level of strain but all studies point to a level of pre-strain which after there are only limited gains in dent resistance. This will correspond to leveling off of the stress strain curve for the given material; a point beyond which the increases in yield strength for a given strain increment becomes negligible. The level of beneficial pre-strain cited ranges from 5% [46] to 20%[32]. The 20% level was cited for a highly anisotropic, rephosphorized IF steel with greater strain hardening potential to exploit before thinning offsets further gains. This particularly study attempted to illustrate that lower strength steel actually offers the same potential dent resistance as bake hardenable steels since it exhibits greater hardening response. The effect of anisotropy is considered in some theoretical dent resistance work that attempts to account for pre-strain levels in dent resistance assessments. Shi *et al.* [28] incorporated Hill's [54] anisotropic yield function in Yutori *et al.*'s [18] denting load relationship in work with steel. Asnafi [42], using current strain, initial yield strength and a material's anisotropy, measured as its r-value has developed a more generic equation. A set of design curves [44], based on

the denting energy assessment method, attempts to quantify strain effects by presenting design criteria for a range of strain states $(\varepsilon_1, \varepsilon_2)$.

In many cases even a small level of pre-strain and the corresponding increase in yield strength, offers substantial benefits. This suggests that the introduction of even minimal levels of strain throughout a formed panel is desirable. This small level of pre-strain can be achieved by optimizing the forming process to promote stretch forming. The ULSAC program [3] highlighted this approach by recommending a hydro-forming process for its closure panels that would introduce a small, 2%, level of pre-strain in the parts. Consideration of strain hardening, through stretch forming, was also highlighted as an effective means of exploiting yield strength benefits in down gauging work with steel sheet by Shi *et al.* [46]. Similar examination of the benefits of promoting stretch forming has been undertaken by Dauby *et al.* [27] to promote high formability steels as alternatives to bake hardening steels. This study explored the effect of strain path on dent resistance by comparing samples formed in a biaxial state $(\varepsilon_1 = \varepsilon_2)$ to samples formed in a plane strain state $(\varepsilon_2 = 0)$. Both cases illustrated the benefits of promoting pre-strain, as shown in Figure 4.
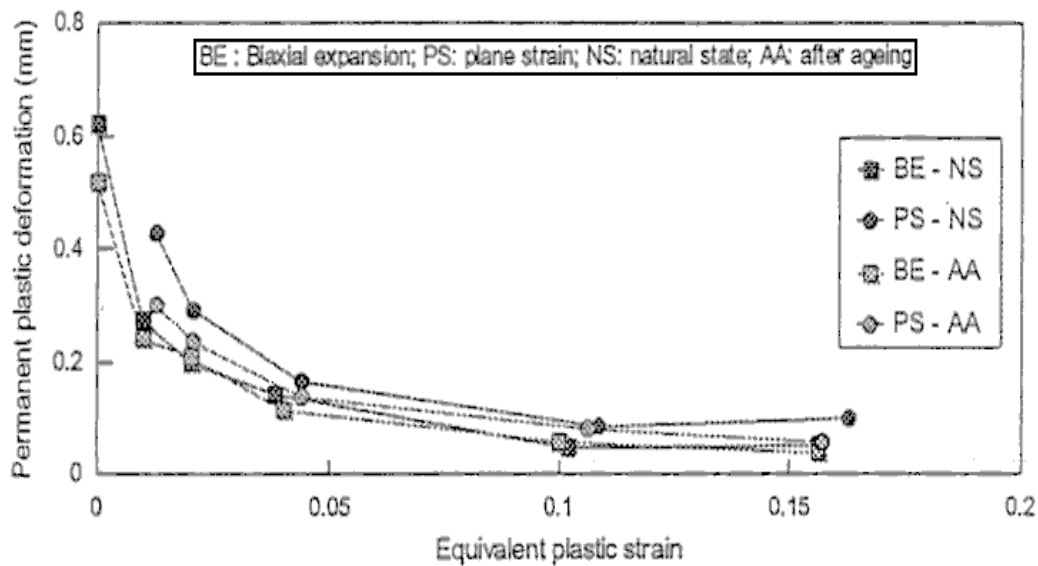
Figure 4: Effect of pre-strain and strain path on static dent resistance of steel for a load of 50kg, observed by Dauby *et al.* [27].

Dauby *et al.* [27] found that the parts formed by biaxial expansion showed improved dent resistance for an equivalent level of effective plastic strain. The role of strain path in pre-straining on dent resistance result is left unexplained. The study does suggest that the

20

benefits of paint bake response can be matched with small levels of pre-straining. It is clearly advisable to promote straining in the more dent susceptible regions of formed parts to take advantage of the associated strength increases.

The influence of strain rate hardening is also important when assessing dent resistance, as strain rate sensitivity will affect the deformation response during denting. The influence of strain rate hardening has been examined in various studies, particularly those involving the dynamic denting of steels [6,9,22,36,37,52]. Adjustment of yield strength, due to steel strain rate sensitivity, was cited as a key element in early denting work [9], even at low speeds, in achieving experimental agreement with a theoretical relationship between denting energy and yield strength. Preliminary work by DiCello and George [6] comparing the dynamic dent resistance of aluminum and steel suggested that steel's positive strain rate hardening would allow it to outperform aluminum. The work stipulated that as velocities increased the rate hardening of steel would make it superior. This analysis only examined the denting process from a strength perspective and thus its findings are limited. The effect of strain rate hardening between different steel grades was examined and found to be a key factor in dynamic dent performance by Shi *et al.* [36]. The study noted that low strength steels tended to have higher m values than high strength steels. As such, as strain rates increase in dynamic testing the lower strength steels eventually match the high strength steels' performance. Finally, work that compared dynamic and static denting of steels [37], using an actuator driven indentor at various speeds, reported superior dent resistance at higher speed. This improvement was attributed to the strain rate hardening of the material. Thus, consideration of the m value of steels should be made when selecting a material. As noted, aluminum alloys exhibit little strain rate hardening in the typical range of dent testing and thus no research in that area was found.

1.5.2 Thickness

The importance of thickness with respect to dent resistance is also relatively well understood. As thickness is reduced a panel will lose its load carrying capacity and become more susceptible to plastic deformation. In most cases, a decrease in thickness will increase denting susceptibility. Thus, weight reduction through down gauging requires careful consideration with respect to dent resistance.

Attempts to quantify the effect of thickness are limited, as changes in thickness lead to changes in overall stiffness. The early work of DiCello and George presented in equation (1) suggested a fourth order relationship between thickness and static denting energy. Their work further explored thickness effects when considering panel stiffness as they cited different stiffness-thickness relationships for curved and flat panels. The higher order relationship between critical denting force and thickness presented by Yutori *et al.* in equation (2) has been used to assess the thickness effect in other studies. Van Veldhuizen *et al.* [35] related their denting force data to sheet thickness, for a range of panel curvatures, using similar values for the thickness exponent. This work, shown in Figure 5, found values for the thickness exponent of 2.1-2.3, slightly lower than the range predicted by Yuotri *et al.* [18] of 2.3-2.5, as. Asnafi [42] related denting force to thickness through a complicated second order relationship.
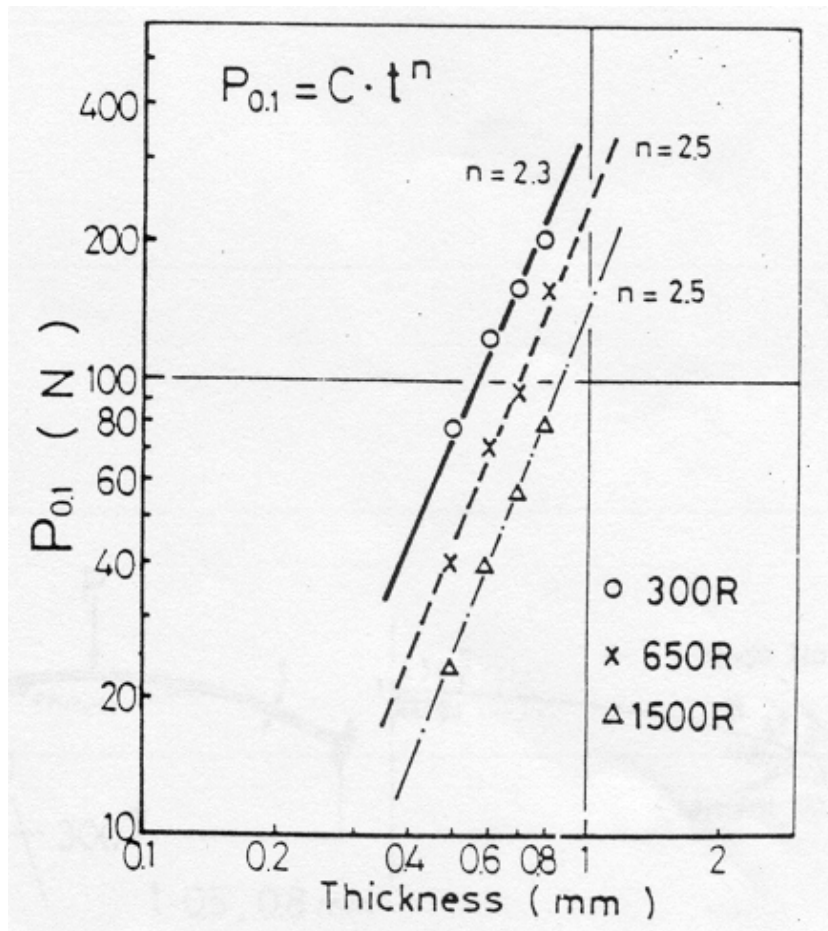
Figure 5: Correlation of denting load to cause a 0.1mm dent, $P_{0.1}$, and thickness by Yutori *et al.* [18] for panels of different curvature.

The effect of thickness on dynamic denting has generally been treated as similar to the static case. The accepted view is that a decrease in thickness will produce greater dynamic dent depths. Studies [7,36] have noted that the thickness effect is less pronounced in dynamic denting, suggesting that down gauging will be of greater concern in static denting. However, Nomura *et al.* [15] examined dynamic denting over a wide range of applied energy, produced using 2 different indentors and a range of drop heights, and reported the complex thickness effect shown in Figure 6.
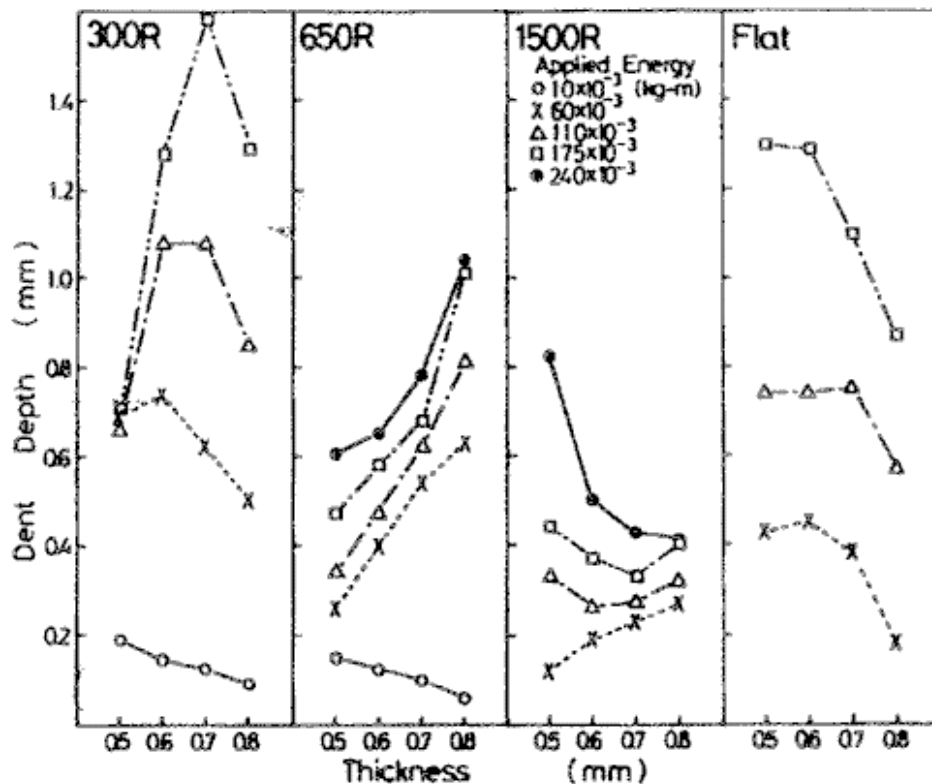
Figure 6: The effect of thickness on dynamic dent depth for a range of panel curvautres and applied energies as observed by Nomura *et al.* [15].

Depending on the panel curvature and the level of applied energy the role of thickness could be reversed from the expected trend. All flat panels exhibited an increase in dent depth with decreasing thickness. The relationship was much more varied for curved panels. At energy levels greater than that corresponding to denting with a 25.4mm and a velocity of 4.24m/s, increasing thickness shows a reducing dent resistance. At even higher energy levels, not typical of current dynamic denting standards, the behaviour becomes more clouded as the thickness effect becomes non-linear and highly curvature dependent. The

paper suggests an elaborate system of classifying the dynamic denting process in an attempt to explain the varied nature of the dent response. The explanation offered is closely tied to both thickness and curvature and will be addressed in the stiffness section. This study highlights that assuming increasing thickness will retard dynamic denting can be dangerous. However, the majority of the cases where lower thickness is beneficial are for non-typical test conditions, so the general trend of thickness should prevail in most cases.

1.5.3 Stiffness and Panel Curvature

As mentioned, panel curvature plays a major role in dent resistance. A panel's curvature can be approximated as a circular radius for a given span, with the resulting geometric stiffness being inversely proportional to this measure. The combined effect of material stiffness and geometric stiffness contributes to the complex nature of dent resistance that often leads to contradictory findings. Attempts to quantify stiffness effects are very difficult, as isolating the geometric stiffness contribution is nearly impossible. For example, geometric stiffness cannot be held constant in a down gauging analysis, as any change in thickness will cause slight changes in curvature and stiffness. Asnafi [42] pointed out this difficulty in attempting to develop a complex relationship for denting force. The numerous possible panel configurations, and thus stiffness, leads to a range of observations of curvature effects.

To better understand the role of stiffness, an analysis of the deformation mechanisms during the denting process is necessary. Static denting is controlled by membrane and bending straining that vary during the denting process depending on the panel curvature. The static dent response of a curved panel can be divided into three segments, the initial, secondary and final stiffness, as shown in Figure 7.
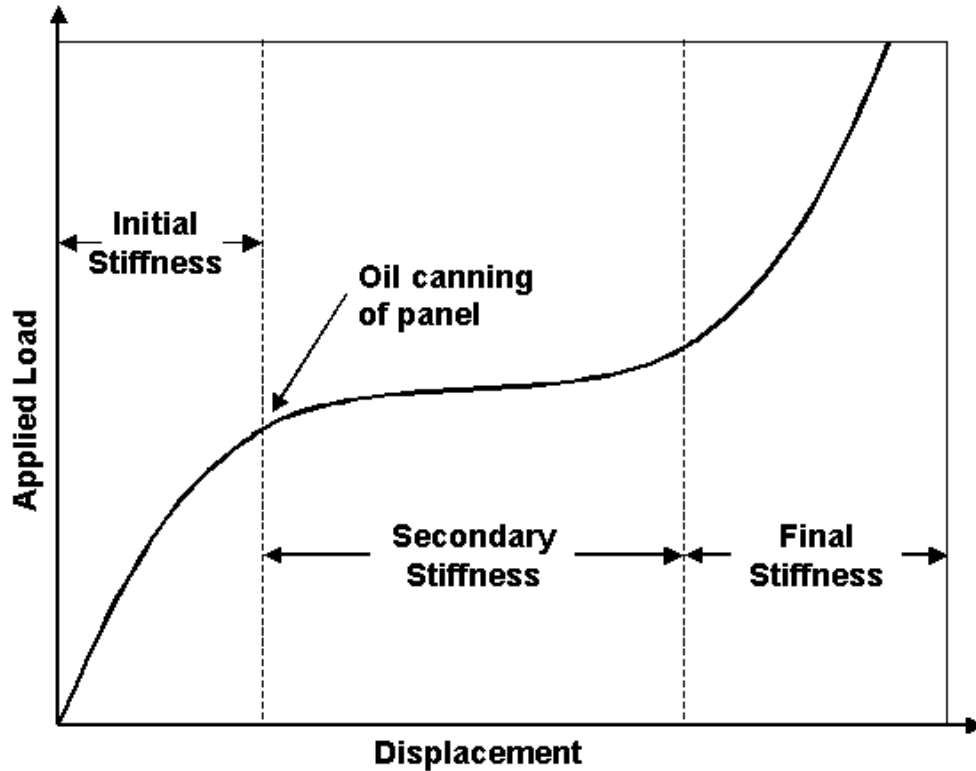
Figure 7: Multi-stage stiffness response of typical panels under static loading. The stiffness response is divided into three distinct stiffness regions.

In the initial stiffness stage local bending and compressive membrane stresses control the panel deformation. A load level is eventually reached at which the local panel curvature is reversed. This is called the oil canning or snap-through load, after which the panel carries the load predominantly in membrane tension. This snap-through state is observed as a circular ring in the panel, inside which the panel curvature is locally reversed. This region will grow radially from the dent site as the load level increases. Yutori *et al.* [18] refer to this transition point of panel curvature as the nodal point of deflection. The movement of the nodal point of the deflection, illustrated in Figure 8, is controlled by the secondary stiffness, until the surrounding edges or support conditions prevent further movement of the nodal point. At this point, the panel stiffness begins to increase as shown by the final stiffness region. Each stiffness region, along with the transition between regions, introduces complicated non-linear stiffness effects with respect to dent resistance. For example the role of initial stiffness on dent resistance may be opposite that of secondary stiffness.
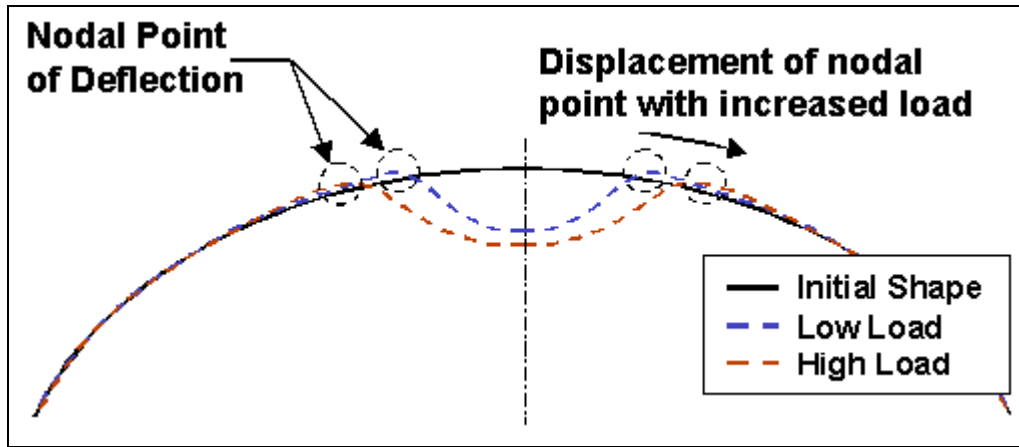
Figure 8: Illustration of the movement of the nodal point of deflection as the pane loading is increased. The displacement will be resitricted as it approaches the panel periphery leading to a corresponding increase in stiffness.

As mentioned earlier, the two prominently cited papers in dent resistance offer opposing views on the role of stiffness on dent resistance. This difference is further highlighted in examination of the literature, with respect to stiffness, where a wide variety of stiffness effects are presented. Numerous studies [10,13-15,18,20,22,24,26,28,30,35,38,46,55] have found that the effect of curvature will be complex, often varying with the load level, support conditions and dent type. The conclusion of Yutori *et al.* [18] that high stiffness will improve dent resistance was not found universally, as shown in Figure 9.
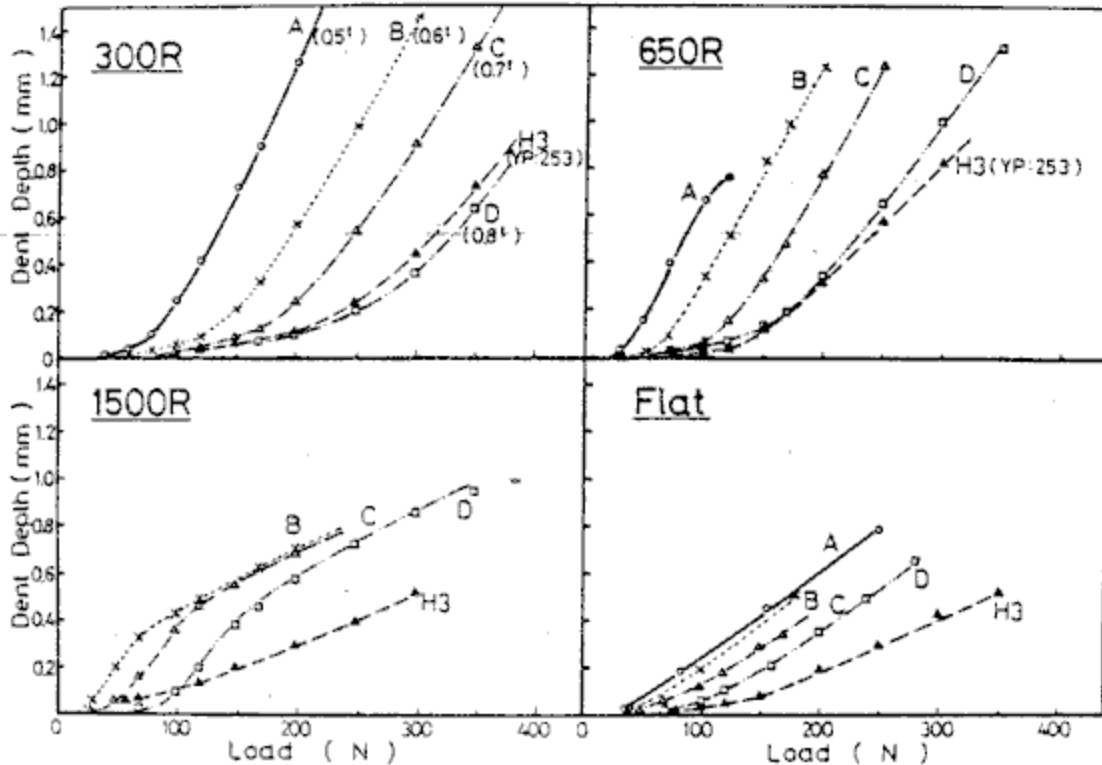
Figure 9: Effect of curvature on static dent depth as observed by Yutori *et al.* [18]. The various letters correspond to increasing thickness values (A=0.5mm to D=0.8mm).

Yutori *et al.* [18] noted that the flat panel, with lower stiffness, outperformed the largest curvature panel, 1500R (R=1500mm),in static denting. The two stiffest panels, R300 and R650, showed the best static dent resistance for low levels of dent depth (dent depth < 0.2mm). It is noted that the 1500mm panel exhibits denting behaviour similar to the highly curved panels initially, before behaving as a flat panel after oil canning. The testing used strain gauges located on the underside of the panel to record the strain history of the dent in order to study the nature of the deformation mechanisms. The nodal point of deflection was defined as the location at which the measured strains reach a maximum in compression. The authors postulated that as the large curvature panel was loaded the nodal point of deflection's movement away from the dent site was restricted by the panel's edges and introduced the complex stiffness effect. The importance of edge or support conditions on stiffness was also highlighted in other parametric studies of dent resistance [20,21]. One study [21] used four separate boundary conditions and then selected the least stiff case as the worst case for static denting. At the same time, this study mentioned that while reducing stiffness will generally reduce dent resistance, attempting to quantify the effect would be very difficult.

27

When the multi-staged nature of static denting deformation is considered, the role of dent resistance assessment method may be explained. Th force-governed method indicated superior dent resistance in panels with high initial stiffness, while the energy based method favoured panels with low secondary stiffness and high elastic deflections. Studies have presented findings that support both conclusions [24,55] depending on the load level. For low load levels, highly curved panels, with high initial stiffness offer the best dent resistance. At higher load levels, less curved panels, with low secondary stiffness, demonstrate superior dent resistance. Montgomery & Brooks [24] observed that the transition in stiffness effect was directly tied to the transition from initial to secondary stiffness at the oil-canning load. The results for a range of panel curvatures between R=350mm and R=2000mm, at low, 89N, and high, 178N, loads suggested that the stiffness effect was strongly load dependent. The belief was that once the panel passes through the transition to a secondary stiffness, the less stiff panels delay denting by allowing greater elastic deformation. Similar findings, with respect to load level were reported in testing of 500mm square panels [55]. This paper also noted the differing effect of initial and secondary stiffness. For denting predominantly in the initial stiffness stage, the resistance to local bending or deformation, is the controlling factor. For cases in the secondary stiffness region, the nodal point of deflection is referenced as a controlling factor. Again, the panel with low secondary stiffness promotes nodal point movement, which in turns lessens the permanent deformation and dent depth. Seel [38] argued that visible dents only occurred after the knee in the force displacement curve. This conclusion is debatable, though the magnitude of dent depths does tend to increase dramatically after the onset of oil canning. Still, the importance of the transition in stiffness regions is further reinforced. Thorburn [30] compared aluminum and steel under static denting loads and alluded to the load carrying mechanisms in order to explain results. While both steel and aluminum panels with high stiffness exhibited similar denting behaviour, a noticeable difference at flatter locations was observed. In the lower stiffness regions the aluminum panels outperformed the steel panels. This difference was attributed to the higher deflection of the aluminum panel, which represents higher membrane loading thus lessening bending that would cause local yielding. This reflects a benefit of lower material stiffness for aluminum, which translates into lower secondary stiffness and improved dent resistance.

Veldhuizen *et al.* [35] evaluated static dent resistance of 4 different curvature panels, 1m, 2m, 4m and flat, and found results in good agreement with Yutori *et al.*'s work [18]. Plotting of both data sets showed similar, non-linear trends in dent resistance with curvature as presented in Figure 10.
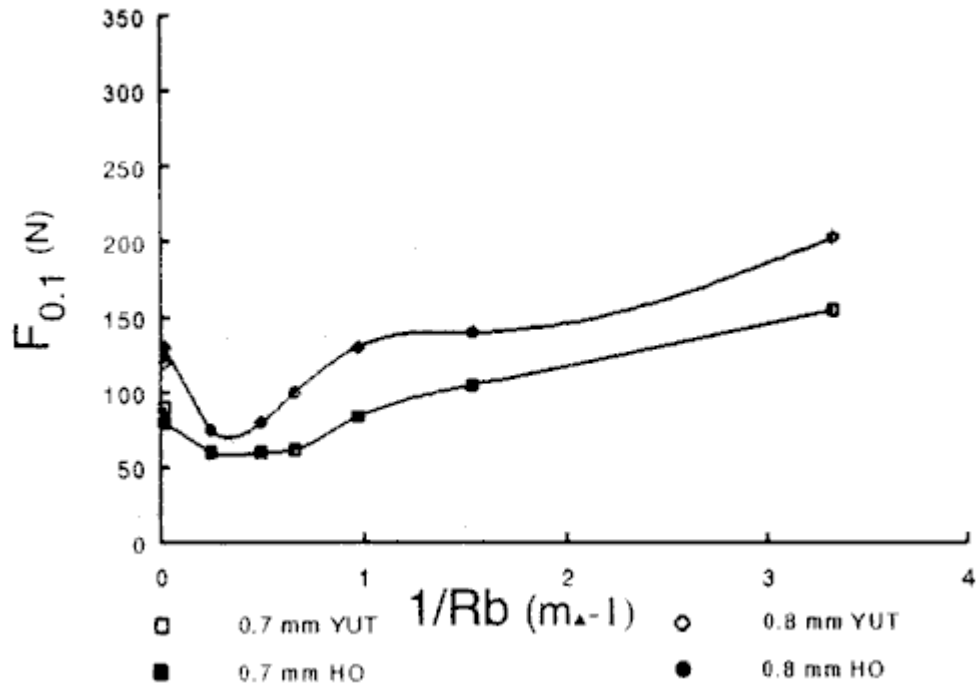
Figure 10: Curvature effect on the load to cause a 0.1mm static dent, $F_{0.1}$, for steels of two different thickness. Veldhuizen *et al.* [35] combined their test data with the results of Yutori *et al.* [18].

Studies with a wide range of panels have shown that high initial stiffness is beneficial for dent resistance. For example, static testing of automotive doors with low curvature and highly curved fenders showed superior dent resistance for the stiffer fenders [28]. The benefit of high stiffness was reinforced in another study of a door under static dent loads that examined the benefits of local reinforcements [29].

The effect of stiffness on dynamic denting shows more consistent findings, with the general trend showing increased stiffness as detrimental to dynamic dent resistance [13-15,22,30]. Nomura *et al.* [15], with the same co-authors as Yutori *et al.* [18], detailed dynamic dent resistance of various curved panels finding non-linear stiffness effects on dynamic dent resistance, as shown in Figure 11. The panel thickness is indicated on each figure with the superscript "t".

29
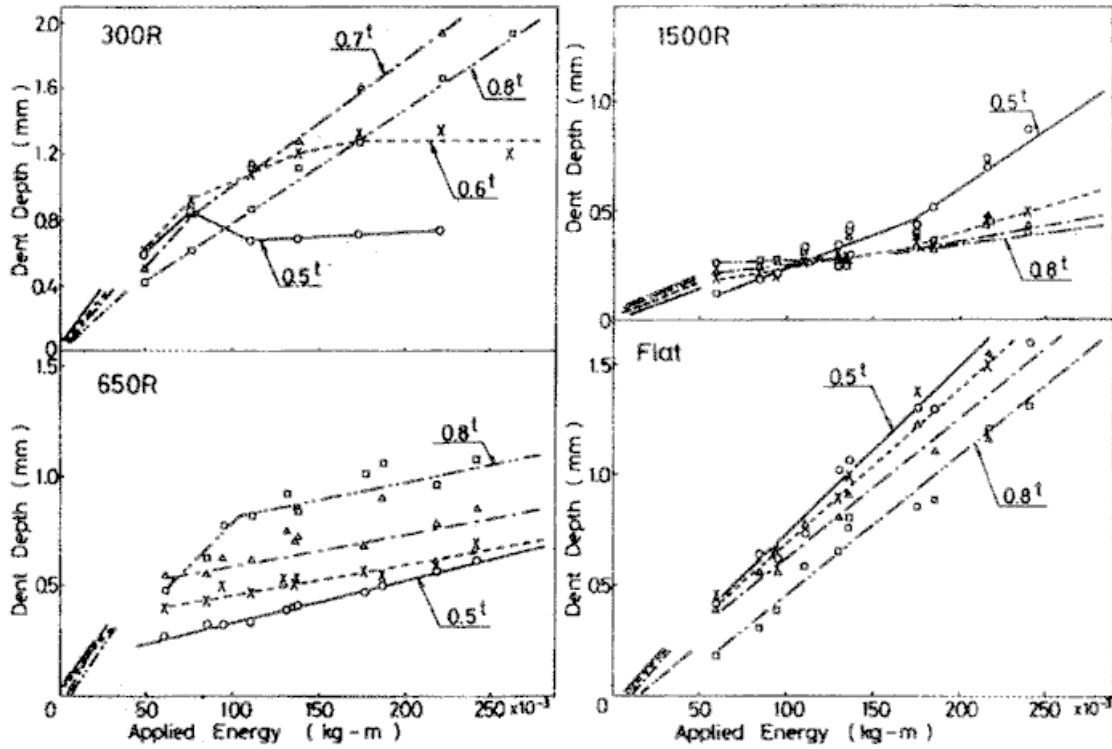
Figure 11: Dynamic denting results of Nomura *et al.* [15] for a range of applied energies, panel curvatures and thicknesses.

The work presented the difference in complexity between flat and curved panels. While flat panels presented more linear denting response with various parameters, the curved panels exhibited complex, non-linear behaviour. The panel response is again related to the three stiffness regions. The benefits of low secondary stiffness are highlighted as a means of promoting the panel elastically catching the indentor and limiting permanent deformations. This concept of catching the indentor is explained as effective momentum transfer in a study of impacting on steel, aluminum and composite sheets [14]. Similarly, work comparing aluminum and steel sheets by Thorburn [30] alluded to the ability of the lower stiffness aluminum panels to more readily deflect and hence avoid permanent local deformations. Also poorer overall dent performance was observed for both materials at the stiffest locations.

Two studies have suggested that the overall influence of curvature on dynamic dent resistance is not large. Vreede *et al.* [22] suggested that while larger panels, with greater unsupported regions, were beneficial, the effect of curvature was less significant. The concept of the panel catching the indentor was used, but it was argued that panel size, or lack

30

of boundary restraints, was more critical in limiting panel deflection. The study did suggest that as panels became thinner that the role of curvature would be more pronounced. The stiffness regions encountered in dynamic denting explain these findings. Two studies [36,38] have suggested that due to the high speed of the dynamic denting process that the initial stiffness stage is rapidly overcome and that secondary and final stiffness effects will control the majority of the deformation. Initial bending resistance is quickly overcome and the panel deformation is controlled by membrane straining in the secondary stiffness region. Panels free to deflect in the secondary stiffness region will reduce dynamic dent depths. However, panels with high levels of restraint will experience localized bending and high dent depths. Localization of bending may be caused by edge effects that cause the transition into stiffer final stiffness regions, however, the dangers of very high initial stiffness should not be overlooked. Depending on the level of applied energy, the denting process may never induce global deflections and only a highly localized deflection, governed by initial stiffness, will occur. Thus, panels with high initial stiffness may never experience the secondary deflection stage and this will promote deep dents. In cases where the panel's deflection is restricted by inner supports one could argue that the initial and final stiffness are the same as the panel is never allowed to deflect globally, in the secondary stiffness regime.

Panel curvature also has some secondary benefits for dent resistance. Higher curvature panels will experience increased pre-strain, which leads to increased yield strength [13]. Shi *et al.* [46] suggested that the relative benefit of pre-strain was greater in flatter panels than curved panels. These findings are questionable as the study was based on the energy based dent resistance equation, which had distinct differences in its stiffness term depending on the panel curvature. The change in the thickness effect, due to the stiffness term, between a flat and curved panel was quite pronounced.

1.5.4 Support Conditions

As was seen in examining the role of stiffness on dent resistance, panel support conditions often play a crucial role. The support conditions are normally defined at the panel perimeter, where the constraining actions of the edges restrict panel deflection. The other major consideration regarding support conditions is the influence of internal panel supports. Most automotive applications will involve assemblies of two or more parts that form the body

panel. For example, a hood will usually consist of an inner support panel, which serves as a stiffening device, covered by an outer panel that will experience the denting loads. The interaction of these panels can be critical in assessing dent resistance of in-service parts.

Many studies stress the importance of support conditions and the significant impact they will have on denting performance [9,12,13,15,18,20-22,29-31,34,37,45,55,56,57]. However, few studies actually attempt any type of comprehensive parametric evaluation of support conditions. Rather, studies will tend to mention the role of support conditions or assess a very limited set of conditions, specific to a given application. Studies by Yutori [18] and Nomura [15], outlined in the examination of stiffness effects, referred to the onset of final stiffness when panel deflection becomes restricted by the panel edges. This effect is a concern, particularly for smaller panels when global deflection will more rapidly be influenced by edge effects. However, the onset of final stiffness usually only controls the denting response in cases where relatively high load levels are reached. As such, this boundary condition effect will usually not be critical in the initiation of visible dents or small dents.

The accurate capture of in-service boundary conditions for global panel support, such as attachment points to the main car body, can be crucial in dent resistance assessment. Several studies have stressed the importance of global panel supports in their respective testing. Alaniz and Borchelt [20] tested doors under static loading using three different global support methods stressed the importance of the support setup used. The doors were supported in three ways: (i) the complete assembly mounted on the actual body in white (BIW), (ii) the assembly rigidly mounted to a test rig and (iii) the outer panel only rigidly mounted to a test rig. As expected, the test results showed high levels of variation between test setups, though the general trends observed were comparable. One interesting result of the study was the comparison of the stiffness in regions where the inner panel and outer panel were joined with an adhesive or mastic. For tests using the entire assembly, the stiffness over a mastic region was 46.8N/mm, while the stiffness in that region without the inner support was only 29.8N/mm, a loss of over 35% in stiffness. While the difference is to be expected, the importance of the inner panel is highlighted. It is noted that for dent tests in regions away from the edges and global support points, the rigid and BIW mounted assemblies perform similarly, but differences in tests near the perimeter are observed. Similar considerations of

edge effects were noted in other studies [37,57] that specifically avoided testing near the supports and panel edges. The need to capture global support conditions is highlighted, if accurate assessment of dent resistance around the edges is desired. Ekstrand and Asnafi [21], attempting to achieve the worst case scenario for dent testing of panels, evaluated four different boundary conditions. This testing used increasingly constraining edge supports and then selected the least restrictive boundary condition as a worst case for static dent resistance. Other studies [9,29,30] have also stressed the importance of global support conditions in achieving accurate and applicable results. Thorburn [30] observed that the need to accurately mimic real boundary conditions was particularly important in static dent testing. This is a result of the more predominant role of stiffness in static dent response.

Another area of study focuses on the design of inner supports to optimize denting response. By considering the inner spacing of supports, the deflection response and resulting denting performance may be controlled. Chen *et al.* [34] found that inner support spacing was a more important factor than yield strength in overall performance while examining the effect of steel properties on a variety of performance criteria, including static dent resistance. Swenson and Traficante [45] examined the spacing of inner supports for hoods, in an optimization analysis that considered dent resistance, stiffness and oil canning limits, finding that only cases of small inner spacing were critical. The results of this study are questionable as the dent resistance criterion used was based on the energy assessment method, which recommends low stiffness for superior dent resistance. In effect the study will only find static dent resistance to be a concern in highly stiff, low stiffener spacing, regions which would likely be the opposite finding if a force based assessment criteria was used. Regardless of the findings, the role of stiffener spacing remains a key concern. Sakai *et al.* [55] suggested that careful spacing design could enable control of panel deflection and thereby optimize stiffness and dent response. This approach to optimize the hood stiffness was used in a down-gauging exercise of a Saab hood that successfully replaced 1.4mm aluminum sheet with 1.0mm sheet [31]. A study that examined hail stone response [12] of outer panels noted the difference in dynamic denting behaviour at various locations. Differences between flat unsupported regions and regions supported by inner stiffeners were noted, as well as the impact of featurelines. Featurelines are an area of particular concern as they are highly stiff regions that will be extremely resistance to panel deflection are expected

33

to dynamically dent to large depths. The effect of highly localized reinforcement was also examined in a study that used small fiberglass patches to locally stiffen steel body panels [29]. Local dent resistance was found to improve twofold due to the increase in stiffness associated with the reinforcing patches.

A final area where accurate support conditions are crucial is numerical modelling. To accurately capture tested behaviour, careful consideration of boundary conditions and modelling simplifications is necessary. A common concern is the level of restraint used around a panel edge. The difference between a clamped sample, which can potentially move, and a fully restrained model is a concern [22]. Oda *et al.*[56] attempted to assess the effects of inner spacing and mastic presence on dent resistance in another numerical study. Sabbagh *et al.* [23] varied their modelling approach depending on the test location. At a test site relatively removed from inner supports, only the outer panel was modelled. However, for a test site that was close to inner supports, a complete assembly was modeled. These works highlighted the importance of understanding the interaction between inner and outer panels, as well as, the adhesive joining them.

1.5.5 Impact Velocity

The effect of impact velocity directly influences the dynamic dent depth as explored in [13-15,22,32,36,37]. Depending on the study, the effect of velocity is either explicitly examined, or a combined factor of impact energy is assessed. Studies using energy attempt to combine the indentor mass and velocity into a single quantifying term. As was discussed in the review of the various dent testing procedures, the effect of indentor geometry can play a role in dynamic dent depth therefore the combining of indentor mass and velocity attempts to remove this factor. Generally, the use of energy instead of velocity seems reasonable for indentors of similar geometry, such as spheres of similar diameter, but for cases with larger discrepancies issues may arise. For example, indentor geometry may alter the deformation response observed during the load transfer from the indentor to the sheet. Such changes could lead to confusion in the reported trends.

Most studies that report velocity versus dynamic dent depth show linear relationships, with increasing velocity yielding large dent depths [11,14,22]. Burley and Niemeier [11]

examined the effect of curvature on the velocity response and found a stronger velocity effect for panels with higher curvature, as shown in Figure 12.
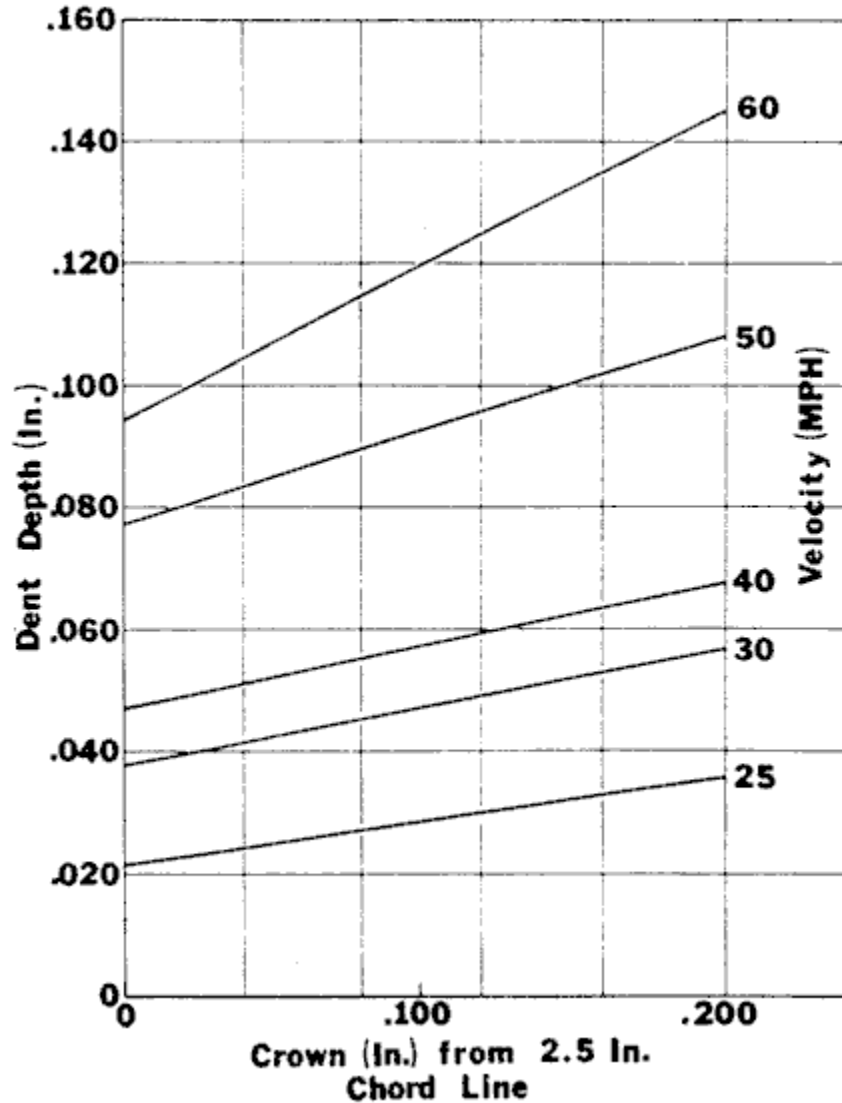
Figure 12: The increased effect of indentor velocity on dynamic dent depth as curvature is increased, as observed by Burley & Niemeier [11].

This relates to the role of stiffness in allowing panel deflection to absorb indentor energy elastically and avoid permanent dents. The stiffer panels will be unable to deflect and avoid denting, and as such will be more sensitive to increases in velocity. Panels with large deflections will conversely be less sensitive to increases in velocities as the change in deflection is small relative to the overall large panel motion. The other key element affecting the velocity relationship is the strain rate hardening behaviour of the material alluded to in the discussion of yield strength effects. Shi *et al.* [37] compared static and dynamic denting

using a test procedure with the ability to track the load level to cause a given dent depth, finding that as the indentor velocity increased higher loads were needed to produce the same dent depths. This increase in load for higher velocity was attributed to strain rate hardening. Zijp and Roelofsen [32] essentially argued that the benefit of increased material yield strength, prior to denting, was lessened as velocity increased. Again, the strain rate hardening allowed panels with lower yield strength to match stronger material as velocity increased and the contribution of strain rate hardening increased.

Nomura *et al.* [15] used an energy based approach to assess dynamic denting effects. This study used two different spherical indentors, 20mm and 30mm respectively, and a range of drop heights that led to impact energies from 0.1J to 2.4J, as presented previously in Figure 11. This range of energies is quite high; for example a 25mm indentor dropped from 1220mm will have a velocity of 4.89m/s and a corresponding energy of 0.8J. Therefore, some of the trends observed do not apply for current, typical dynamic dent tests. This paper outlined three energy ranges that lead to the three deflection regions tied to stiffness. Depending on the energy level and corresponding deflection region, the role of thickness is stipulated to vary. In the low energy region, where initial stiffness is controlling the deflection, higher thickness is beneficial in reducing dent depths. As the energy level increases, the secondary stiffness region is reached and large panel deflections are seen. In this region, lower thickness is beneficial as the panel will deflect more readily and thus better absorb the applied energy. At very high energy levels, the panel deflection is restricted by the outer edges and increased thickness is desirable. The dent depth versus energy relationships is mostly linear, with various transitions in slope as different regions are reached. Only the thinnest sheets, with thickness of 0.5mm, show a mostly non-linear response. For the flat panel, a fully linear response, with lower dents at all energy levels for thicker sheets, is observed as no transition from initial to secondary stiffness exists. The impact of the different indentors on dent response does not appear to be a concern as the variation of diameter was only 10mm and as such similar displacement responses would be expected. This study reinforces that as velocity increases to higher levels, more complicated effects may result.

1.6 Dent Resistance of Aluminum

Consideration of the dent resistance of aluminum has been mentioned in various assessments of the different factors that affect denting. Examination of existing studies presents various works that focus solely on aluminum, comparing the denting behaviour of different alloys. Also, various studies focus on aluminum introduction for automotive applications from a broader perspective. Numerous comparative studies evaluate dent resistance of steel and aluminum. In analyzing these comparative studies, the source of the work is often an important consideration, as there is often a vested interest in finding a particular material to be superior. This bias does not present itself as any overt manipulation of test data, rather, the choice of alloys often favours one particular material.

Numerous studies have compared various different aluminum alloys, ranging from 2000, 3000, 5000 and 6000 series alloys [5,6,10,12,13,21,22,45,53]. The specific alloys varied depending on the time and the corresponding alloying additions within a given series. Thus, detailing the exact alloys offers little with regard to today's alloy choices. Studies that report relative performance of the different alloys usually recommend 6000 series alloys for static and dynamic dent resistance considerations [12,13, 22,45,53]. Various other studies [21,30,31,35,49] only test 6000 series alloys when they considered aluminum denting. In all these studies, the principal reason for the superior denting performance of the 6000 series alloys is their paint bake response. As discussed in the examination of yield strength effects, the potential gains in strength through heat treatment of age hardening alloys offers an ideal means of improving dent resistance. Detailed studies [49,51] of the hardening kinetics of 6000 series offer various alloying and heat treatments designed to optimize the strengthening response. Bryant [51] outlined a pre-aging treatment that enhances precipitation kinetics during the paint bake cycle to better exploit strength gains. The same study noted that the paint bake response will be a function of pre-strain, a factor that should be taken into account in future work. On a related note, extreme bake hardening treatments can effectively reduce strain-hardening response, but the increased strength will offset any strain-hardening loss [31]. Another benefit of using a bake-hardening alloy is that formability at the lower pre-treatment strength is acceptable, while the increase in strength will help the in-service denting response. Also, a lower strength after forming, but prior to painting, is desirable for the reduction of part springback [49,51]. This allows for the replacement of the more

formable 5000 series alloys in outer panels. Gatto and Morri [53] examined the static dent resistance of 5000 and 6000 series alloys. They noted that at higher strain levels that the 5000 series alloys performed much worse than the 6000 series alloys. This is attributed to the higher strain hardening and increased strength of the 6000 alloy. Rolf *et al.* [13] assessed the relative increase in thickness needed in various aluminum alloys to meet steel's dynamic denting performance in flat panels, and found that while 2000 and 6000 series only needed 10-15% increases in thickness the 5000 series required a 50% increase in thickness. The same study also evaluated "mini-hoods" which had some curvature and found that the 6000 series alloy actually allowed for significantly thinner sheet than both the 2000 and 500 series. Swenson and Traficante [45], tested a range of alloys from the 1000-6000 series, in the early 1980's, for static dent resistance, springback, stiffness and oil canning load, and found that the 6000 series offered the superior performance in terms of cost to weight.

The last study was one of many that also included steel in their evaluations. These studies [6,7,11-14,16,30,31,35,53] usually compared aluminum performance relative to steels already in use for the given applications. The study of Rolf *et al.* [13] examining the "mini hoods" actually found that the 6000 series alloy could be thinner than steel for dynamic denting. Other studies [11,12,30] have found similar results, suggesting that in dynamic denting aluminum is equivalent or superior to steel. This response is attributed to the greater elastic deflection of the panel, promoted by the less stiff aluminum. The most detailed of these studies, that of Thorburn [30], found that as the stiffness of the dent locations decreased, the aluminum alloy increasingly outperformed the steel. This relates to the deflection occurring during the secondary stiffness region of the panel response discussed previously. DiCello and George [6] argued that the superior strain rate hardening of steels would actually make them superior in dynamic denting but no actual testing was performed to validate this theory.

Comparisons of static denting performance have also found acceptable dent resistance of aluminum relative to steel. These studies [16,30,31,35,53] usually require an increase in aluminum thickness to meet steel's performance, but still represent substantial weight savings. Thorburn [30] achieved equivalent static dent performance of 0.9mm thick aluminum and 0.7mm thick steel, as shown in Figure 13, and superior dynamic denting performance for the aluminum panels, as shown in Figure 14.
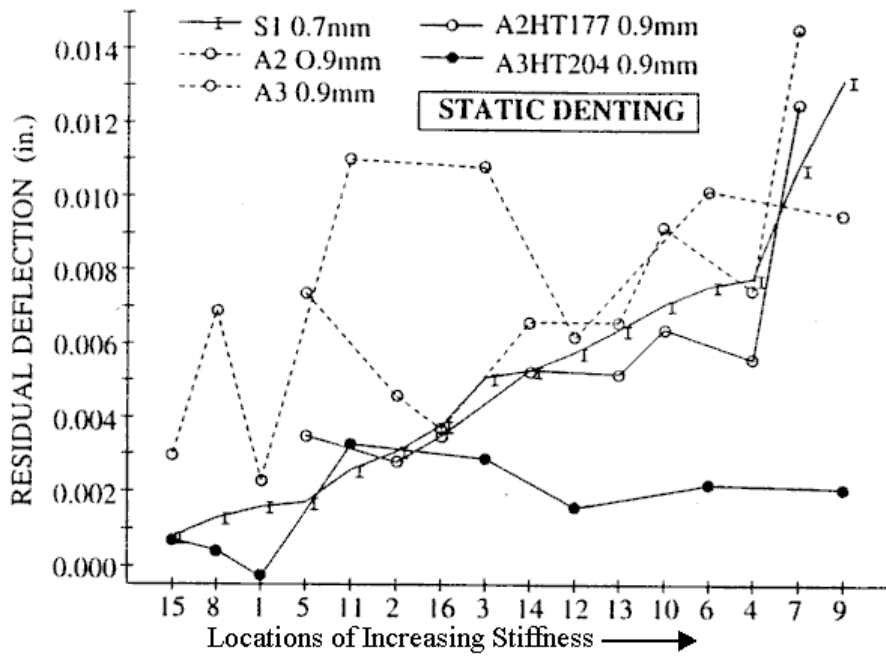
Figure 13: Comparison of static denting between 0.7mm steel and 0.9mm aluminum panels by Thorburn [30]. Heat treatment is designated using HT, followed by the temperature 177ºC or 204ºC.
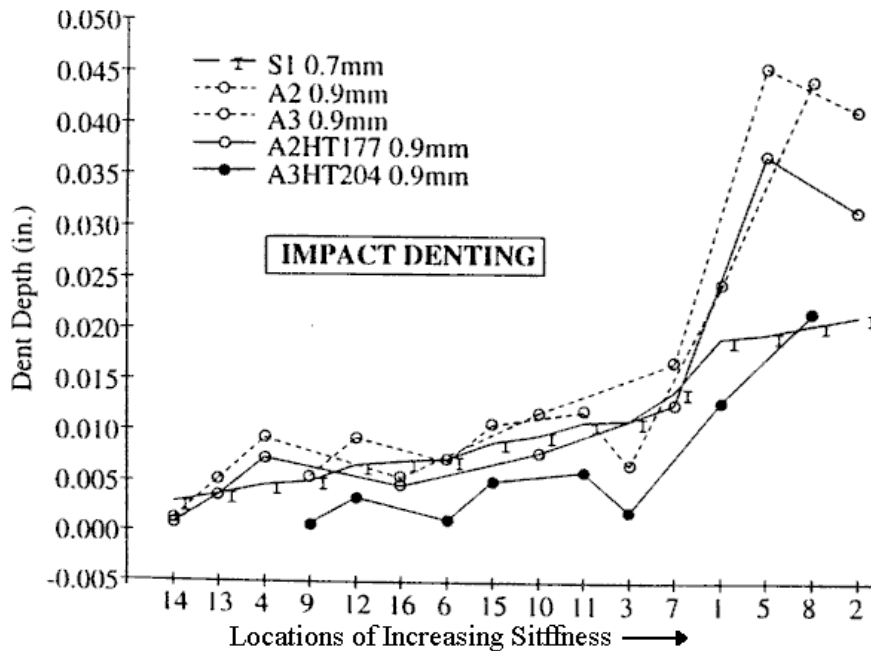
Figure 14: Comparison of dynamic denting between 0.7mm steel and 0.9mm aluminum panels by Thorburn [30]. Heat treatment is designated using HT, followed by the temperature 177ºC or 204ºC.

For this thickness difference, the static dent resistance variation was small, with the aluminum usually outperforming steel, with a small loss of stiffness. At this thickness ratio, the aluminum offers a 53% weight reduction. Other weight savings reported when considering only static dent resistance were 60-70% for a range of curved panels [35], 46-55% for a trunk floor [16] and 50% for a Saab hood [31]. Clearly, the potential for weight savings through aluminum substitution has been demonstrated in a range of applications.

1.7   Numerical Modelling

1.7.1   Explicit and Implicit Solution Methods

Numerical modelling of sheet metal forming has become increasingly common over the past decade. The benefits of detailed knowledge of part formability early in the design cycle are substantial. As computing power continues to increase so does the complexity of simulations. Multi-stage forming processes are now modelled with regularity, successfully capturing complete part histories. Various detailed studies [58,59,60,61] have examined the ability of numerical simulations to accurately capture sheet metal, specifically aluminum, forming processes. The use of numerical simulations is particularly helpful for aluminum applications, as there is a more limited practical knowledge base than for steel. The modelling of denting is very similar to forming simulations, and thus approaches and methods are readily transferred to denting applications.

Sheet metal forming simulations normally involve non-linear geometric and material responses, which necessitate a non-linear solution method. There are two main finite element methods commonly used in sheet metal forming simulations. Depending on the nature of the problem one solution method is often more suitable than the other. A simulation may be classified as either quasi-static or dynamic depending on the level of dynamic excitation involved in the process. For dynamic problems the fundamental differential equation that must be solved is:

$$\{r^{ext}\} = \{r^{int}\} + [M]\ddot{d} + [C]\dot{d} \tag{3}$$

where

$$\{r^{int}\} = \int_{V^e} [B]\{\sigma\} dV^e \tag{4}$$

40

{r^{ext}} is the vector of external forces, {r^{int}} is the vector of internal forces, [M] is the mass matrix, [C] is a damping matrix, [B] is the strain-displacement matrix, {σ} is the internal stress matrix and d is the nodal displacement vector, and it's associated derivatives for velocity and acceleration. The internal force vector incorporates material non-linearity and stiffness response. The damping term in the equation is often not included, as quantifying damping is difficult. When this term is included an arbitrary value is often selected.

Two different time integration algorithms are available for solving this differential equation. The explicit solution method is conditionally stable and allows for relatively inexpensive numerical iterations. The explicit solution is limited by its stability, with a limiting numerical time step, governed by the Courant condition:

$$\Delta t_{max} = \frac{L_{min}}{\sqrt{E/\rho}} \qquad (5)$$

The maximum time step, Δt_{max}, is controlled by the smallest element size, L_{min}, and the speed of sound of the material, which is a function of the Young's Modulus, E, and density, ρ. For most metals used in sheet forming this implies time steps on the order of 10ns-2μs. This extremely small time step limits the length of simulations to small intervals, which often necessitates artificial increases in tooling velocities in typical forming processes. The effect of increased velocity must be monitored as it may introduce artificial dynamic effects. Fortunately, the time steps are numerically inexpensive as a forward integration scheme is used that only requires the inversion of the lumped mass matrix. The explicit solution will solve for acceleration for the current time step by inverting the mass matrix and multiplying it by the difference in internal and external forces.

$$\{\ddot{d}\}_{n+1} = [M]^{-1}\left(\{r^{ext}\} - \{r^{int}\}\right) \qquad (6)$$

The mass matrix is a diagonal matrix, which makes the inversion of the matrix trivial and a numerically inexpensive operation. Thus while the number of time steps, or iterations, will be large, the numerical cost is relatively low.

The implicit solution method is the alternative numerical option. This method is unconditionally stable and thus time step size is not a function of the problem's material properties or mesh. However, this method is numerically very expensive as the solution method solves for the displacement at the end of a time step, {d$_{n+1}$}, finding equilibrium

between the out-of-balance forces and the displacement increment. The stiffness matrix, $[K]$, is inverted and multiplied by the effective force vector, R^{eff}, (Equation 7), which is a function of the external force and dynamic terms at the current time step.

$$\{d_{n=1}\} = [K]^{-1}\{R^{eff}\}_{n+1} \tag{7}$$

The formation, storage and inversion of the stiffness matrix are numerically expensive. Also, the size of the time step must be chosen with care for highly non-linear problems, where large steps may achieve equilibrium while missing details of the non-linear deformation. Non-linear numerical methods which iterate over a given time step to better capture non-linear deformation can be effective but add increased numerical costs as repeated formation and inversion of the stiffness matrix becomes necessary. This iterative stiffness updating when searching for equilibrium can lead to difficulties in achieving numerical convergence. The implicit solution is often well suited to quasi-static problems where the acceleration and velocity terms are both dropped from the governing equation. For these problems a simpler equation results but the expensive stiffness matrix inversion remains. In this type of solution the time step size is only a measure of discretization, and has no true meaning as an actual measure of time. The time interval is simply dividing the solution into manageable steps to find equilibrium. The static implicit solution method must solve:

$$\{r^{ext}\} = [K]d \tag{8}$$

For many problems that are not truly dynamic, it may still be advisable to use an explicit dynamic solution. The inherent non-linearity of many forming problems, coupled with the convergence issues that can arise with implicit solutions, often dictate that an explicit solver be used. The decision to use an explicit dynamic formulation for a quasi-static process again raises issues with the introduction of artificial dynamic effects, particularly when velocity scaling is required. Still, the faster solution times of the explicit formulations are often a predominate factor. One principle drawback of explicit solutions is the stage of the simulation after the forming process is complete. In an implicit solution the final step will represent an equilibrium state, but in an explicit solution the part will be oscillating. This vibration after forming will not affect the part's plastic strains, so the successful forming of the part can be assessed from a strain perspective, but the final shape of the part when the tooling is removed is not accurately known. In order to solve for the springback after the tooling is removed an explicit solution would require a large time period for the oscillation to

42

damp out. An implicit solution is more suited for this type of problem, as only a few implicit steps will find final equilibrium. Thus, the preferred numerical approach is often an explicit forming solution coupled with an implicit springback analysis. Naturally, the transition from the forming simulation to the springback simulation requires accurate transfer of the forming strains, stresses and thicknesses between solvers.

Another important consideration in numerical modelling is the representation of the material properties. The need to capture the strain hardening behaviour was highlighted in the discussion of yield strength effects. Most finite element codes will allow for the input of actual stress-strain data to capture the material hardening. This behaviour will be coupled with the yield criterion selected. Various yield criteria exist, but not all are available in all numerical codes. A detailed examination of suitable yield criteria for numerical modeling of sheet metal forming found that the Barlat anisotropic model was best suited for aluminum [60]. For denting simulations the level of plastic deformation is very localized and quite small so an isotropic material model such as Von Mises is acceptable.

The transfer of numerical methods for forming processes to denting simulations is relatively straightforward. Depending on the type of denting being modeled an appropriate finite element method is selected. Dynamic denting is ideally suited for explicit dynamic solutions as the indentor velocities allow for real time solutions. For efficient modeling of dynamic denting, a coupled explicit-implicit solver is needed to capture the post denting springback. Static denting simulations are well suited for static, implicit solutions. An implicit solution using a frequent stiffness matrix reformation algorithm is necessary in order to capture the non-linear deformation response.

1.7.2 Numerical Modelling of Dent Resistance

Numerical studies of denting have been concentrated in the past decade. Prior to that, only limited numerical simulations had been attempted. An examination of the history of numerical modeling of denting illustrates both the development of dent modelling and the improvements in the available software. There has been a larger focus on static denting and stiffness prediction than on dynamic dent modeling.

Rolf [13] published the earliest numerical work associated with denting studies in 1974. However, this work comparing aluminum and steel dynamic dent performance only

used numerical modelling for analysis of structural flutter. The analyses were performed using ANSYS, and no mention of attempting to model denting was made. Ni [52] introduced limited numerical methods for dynamic denting analysis in 1976. This work used a finite difference numerical solution to iteratively solve for the dynamic denting response of aluminum panels. An interesting source of error that caused over prediction of dent depths and deflection was the use of a point load in the analytical equation developed. The author postulated that a more dispersed contact area is necessary to accurately capture the testing procedure. In 1980 Yutori *et al.* used MARC, an implicit FEM package, for the study of the strain development of various curved panels under static loading. The model used 30 axi-symmetric elements and a point load. An elastic plastic material model was implemented that approximated the plastic response with two linear regions. The agreement of the predicted strain data and test data was good, but no attempt to capture dent depths was made. Sakai *et al.* [55] used MARC to assess static dent resistance and stiffness, but found difficulties in achieving convergence in the unloading of panels. As a result, the study did not model the unloading steps typical of static dent testing. Problems with the stiffness results arose after the onset of buckling. Prior to buckling, good agreement with the first stiffness response was found.

Chen and Salamie, in work for GM in 1984, detailed static dent modeling using an in-house implicit solver. A half-symmetry triangular mesh of a door outer panel was point loaded at various dent sites. The geometry used was simplified, such that sharp changes in geometry, such as feature lines, were not captured and denting in these regions was avoided. The model was used to measure plastic work done by the denting load as a means of quantifying the onset of visible dents. Validation of the force-displacement responses for the various sites was acceptable. The accurate capture of oil canning was noted as being particularly difficult. The stiffer locations showed better agreement, while regions that oil canned and demonstrated higher non-linear response proved more difficult to model. On average the oil canning load predicted was off by 10%. The study noted that the modeling method was limited, as it could not model full assemblies with inner panels.

Alaniz *et al.* [62] modeled static denting, in the early 1990's, using ABAQUS, with an implicit solver that used a modified Riks method for equilibrium searching along the force displacement curve. The formulation used automatically adjusted the step sizes in its

solution depending on the ease of convergence. This reduced step sizes in attempting to find equilibrium in regions of high non-linearity. The results again showed difficulties in capturing the non-linear stiffness response. The same authors also presented non-numerical work [20] that compared static testing of panels mounted rigidly and mounted to the BIW. The study highlighted that modeling of the joints and connections of panels in their in-service condition, mounted on the BIW, were difficult with the current software packages. This concern persists to this day.

In 1993 Werner [25] compared three software packages for static denting. Initially, two implicit codes were tested, ABAQUS and MARC. The principal difference between the two codes involved their stiffness matrix reformation strategy. The ABAQUS solution used the modified Riks method alluded to previously, while the MARC solution used a full Newton stiffness matrix update approach. The MARC solution reformed the stiffness matrix after every equilibrium iteration during a given time step. This approach is numerically more expensive but may better capture the non-linear deformation. Both simulations used the same mesh, with element size of 10-15mm, and a meshed, rigid indentor. The use of meshed indentor avoids the issues previously seen associated with the use of point load approximations. The contact of the indentor and panel was modeled differently in the two codes. MARC used an automatic contact method, while ABAQUS used "interface elements" that required a 1.0mm initial penetration. Both models used a material model that incorporated actual stress-strain data, but the specific yield criterion was not mentioned. Also, in later attempts to improve results a strain rate hardening material model was used but no significant changes in results were observed. Both codes under predicted secondary stiffness, again due to difficulties in the capture of the oil canning load. This study also was the first to report dent depths from their numerical results. Both codes under predicted dent depth by roughly 50%, with MARC slightly outperforming ABAQUS. In an attempt to improve the results, LS-DYNA, an explicit dynamic code, was used. In order to overcome the small step size inherent with the explicit solution, the indentor speed was increased by a factor of ten. The buckling response observed with the DYNA simulation was not in agreement with the test results. The increased speed and part geometry were blamed for the poor results. These results highlight that an explicit dynamic solver is poorly suited for modeling of quasi-static denting. The mesh size used in these models seems quite large

when the size of dent depth is considered. For dent depths on the order of 0.5mm, elements of near 10mm will not be able to capture the local deflection. Also, the buckling response will be sensitive to the mesh size.

The need for mesh refinement in the region of denting is noted in various subsequent studies. Montgomery and Brooks [24] illustrated the benefit of numerical solutions for parametric evaluation of panel properties and curvature using ABAQUS. This study also modeled static denting of door panels and included local mesh refinement in the denting region. Van Veldhuizen *et al.* used ANSYS [35] with a relatively fine shell mesh for a variety of curved panels and found little change in results for a mesh of twice the number of elements. The model used an isotropic, elastic-plastic material model based on actual stress-strain data. The size of the panels was 490x490mm and the initial meshes used 1500 elements. Assuming a uniform mesh this translates to only 12.5mm element edge lengths, which seem too high for accurate results. The refinement used yielded only a 1% change in the stiffness results which suggests that there was little mesh sensitivity for elements of those sizes, for these panels. Still, a higher level of refinement, particularly if dent depth is being studied, should be used. The stiffness results reported were found to be sensitive to panel curvature.

The role of inner and outer panel interactions has been examined in two studies. Sabbagh *et al.* [23] examined the static denting of door panels, at two different locations, using ABAQUS. This study used a different model for each test site. One location was in a relatively unsupported region and the model used only included the outer panel. A second model simulated a site close to a support point of the inner panel. This site was modeled with a linear spring, with stiffness based on actual compression test data, to represent the adhesive joining the inner and outer panels. The results again showed good correlation with initial stiffness, but were overly stiff in the secondary stiffness region. Oda *et al.* [56] performed a more detailed examination of inner and outer panel interaction and the role of mastic using MARC. This study modeled a 0.8mm steel outer panel supported by a 0.7mm inner panel. The inner and outer panels were joined with a non-linear adhesive mastic material. The mastic was modeled with gap elements with a linear stiffness that was deemed appropriate for the expected loading levels. The stiffness was approximated as follows:

46

$$K_s = \frac{E \cdot A}{h} \tag{9}$$

where K_s is the spring stiffness, E is Young's modulus, A is the mastic area and h is the mastic thickness. A cluster of 5 springs was used for the mastic directly under the impact site, while single springs were used at other locations. A quarter symmetry model of 800 shell elements, with nine evenly spaced through thickness integration points, with local refinement of the mesh to 1mm x 1mm sized elements in the denting region. The hardening behaviour of the sheet metal was modeled with a piecewise linear representation of actual stress-strain data. A distributed load was applied, but no indentor was meshed. The predicted stiffness responses were good for regions with and without reinforcement but dent depths were under predicted, as shown in Figure 15.
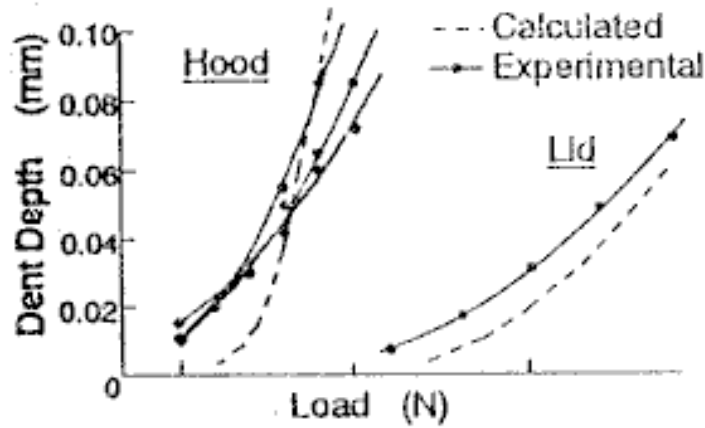
Fig. 13 Application to Actual Parts

Figure 15: Comparison of calculated and experimental static dent depth for a hood and trunk lid by Oda *et al.* [56].

The increase in stiffness when the outer panel contacts the inner was noted to reduce dent depths as expected. The modeling methods were applied to a hood and trunk with good results, that again under predicted dent depth. This study also examined the role of residual stresses, from the forming process, on subsequent denting performance. Depending on the nature of the residual stress profile, dent depths will be increased or decreased. This highlights the need to accurately capture the forming history of parts prior to denting in numerical modeling.

Studies that have attempted to model both the forming and denting processes have stressed the importance of accurately capturing the forming data in subsequent denting models. Chavali and Song [50] developed a program for transferring forming strains and thickness changes from an ABAQUS door forming model to a LSNIKE (LSDYNA's implicit solver) denting simulation. The program projected both meshes on a flat surface and then transferred data to the corresponding nodes and elements. The denting model also accounted for the paint bake response of steel by adjusting the stress-strain curve accordingly. A rigid indentor with a full contact surface and a highly refined dent site were used. The results showed good agreement for both stiffness and dent depth, but it should be noted that no panel buckling (oil canning) occurred. Raghavan and Arwashan [33] coupled a LSDYNA explicit forming simulation and an LSNIKE implicit static denting simulation. The effect of paint bake was again added by adjusting the stress-strain curve between simulations. The forming simulation was critical in accurately capturing the strain states prior to denting. At the time of this study, only limited forming data could be transferred between the two solvers. While element thickness data was transferred, forming strains and stresses were lost. The study designated five regions in the blank and manually assigned representative strain data. The results were limited for both dent depth and stiffness response and the need for an improved interface between the solvers was highlighted. Attempts to model the static dent with the implicit solver presented problems with panel vibrations that prohibited obtaining meaningful results. Another study [44] that ignored forming strains in formed doors, reported a 15% error in stiffness results using LS-NIKE.

Limited numerical modeling of dynamic denting has been published in the past decade. Vreede *et al.* [22] used ANSYS to examine the dynamic denting of various curved steel and aluminum panels. It appears that an implicit dynamic solution with Rayleigh damping was used. An axi-symmetric, 240 iso-parametric 4 node element mesh was impacted by a meshed, rigid indentor. A strain rate hardening material model was developed and implemented in ANSYS to improve the results. Concern regarding the boundary conditions was noted, as the model fully constrained the outer edge of the blank at a radius of 25mm, rather than attempting to model the actual clamps. This clamping is of concern when the size of the indentor is considered. Several indentor tip radii were tested, ranging from 3mm to 25mm, but the paper is unclear as to which test condition was modeled. Based on

the mesh illustrated in the paper, it appears that 12.5mm radius indentor was used, which represents a highly constrained condition. The results reported under-prediction of actual dent depths from 10% to 20%. The higher the initial velocity, the larger the error reported. It seems plausible that as the impact energy increased the tight, over constrained condition would increase the observed error. The need for accurate boundary conditions is reinforced, particularly when denting in close proximity to the constraints.

2 Waterloo-Alcan Automotive Dent Resistance Research Program

The work being reported is part of a large dent resistance program undertaken with ALCAN International Limited. Improved understanding of the dent resistance of aluminum is critical to increased use of aluminum sheet in automotive body panels. The overall program encompasses a range of increasingly more involved studies culminating in dent resistance assessments of complete automotive hood assemblies. A key component in the project's evolution has been the use and development of finite element techniques for the prediction of denting behaviour.

The full program was subdivided into five sub-projects:

(i) An initial numerical parametric study by Worswick *et al.* [63] to assess the static and dynamic dent resistance of small-scale panels.

(ii) A small scale modelling validation study using experimental dent testing of 152.4mm diameter hydraulically bulged specimens, was completed by the author [64].

(iii) A parametric study, by Thomas [4], examining various factors affecting dent resistance of medium-scale panels, using a multi-stage modelling approach. Local re-meshing was performed using D-Mesh, a software tool developed as part of the work.

(iv) A parallel study, by the author, of medium-scale structural assemblies, focusing on the interaction between the outer closure panel and the inner support panel.

(v) A numerical down-gauging study of various full-scale aluminum hoods, by Viertel *et al.* [65], using the techniques developed in the two medium-scale studies (iii) and (iv).

As indicated, the present research is the fourth sub-project, the numerical simulation of the dent resistance of medium-scale panel assemblies. Prior to introducing this topic, a brief overview of the first three sub-projects is given. Discussion of the full-scale hood models studied by Viertel *et al.* [65] will be included in the discussion chapter, Section 7.3, of this thesis.

2.1 Numerical Study of Small Scale Panels

The work, by Worswick *et al.* [63], served as the foundation of the current research initiative. It represents the initial attempts to assess the various geometric and material parameters that affect dent resistance using numerical simulations. Two panel sizes, 200x200mm and 600x600mm, of thicknesses, 0.8mm, 0.9mm and 1.0mm, were used for single and doubly curved panels. The range of radii of curvatures, 100mm to 4000mm, attempted to capture typical autobody curvatures. All panels were modelled as AA6111 with various heat treatments and levels of pre-strain. Both static and dynamic dent resistance were studied by modelling the test procedures used at ALCAN. Dynamic denting was assessed for three drop heights (610, 914 and 1219mm), using a 25.4mm diameter indentor. Static denting was assessed as the residual deflection after loading to 155N.

The numerical modelling was performed using LS-DYNA (explicit) and LS-NIKE (implicit) for the dynamic and static denting, respectively. A quarter-symmetry model with a fully restrained panel perimeter was used. A meshed indentor was used for the dynamic models, but a point load was used in the static models. A Mises yield criteria, with a piecewise hardening curve was used in both models, though limitations in the static implicit code allowed only eight points to represent the curve. The effect of paint bake and pre-strain was incorporated in the hardening curves employed. A coupled springback simulation was run after dynamic denting to find the final deformation.

The result of the study illustrate the role of the various parameters on dent resistance. A loss in dent resistance is observed for both types of denting as thickness is reduced. Also, the benefit of increased yield strength due to strain hardening and paint bake hardening is demonstrated. The effect of stiffness, as introduced by panel curvature, is presented in Figure 16. The stiffness effect is highly non-linear for both forms of denting, and the effect appears to be reversed for the static and dynamic cases.
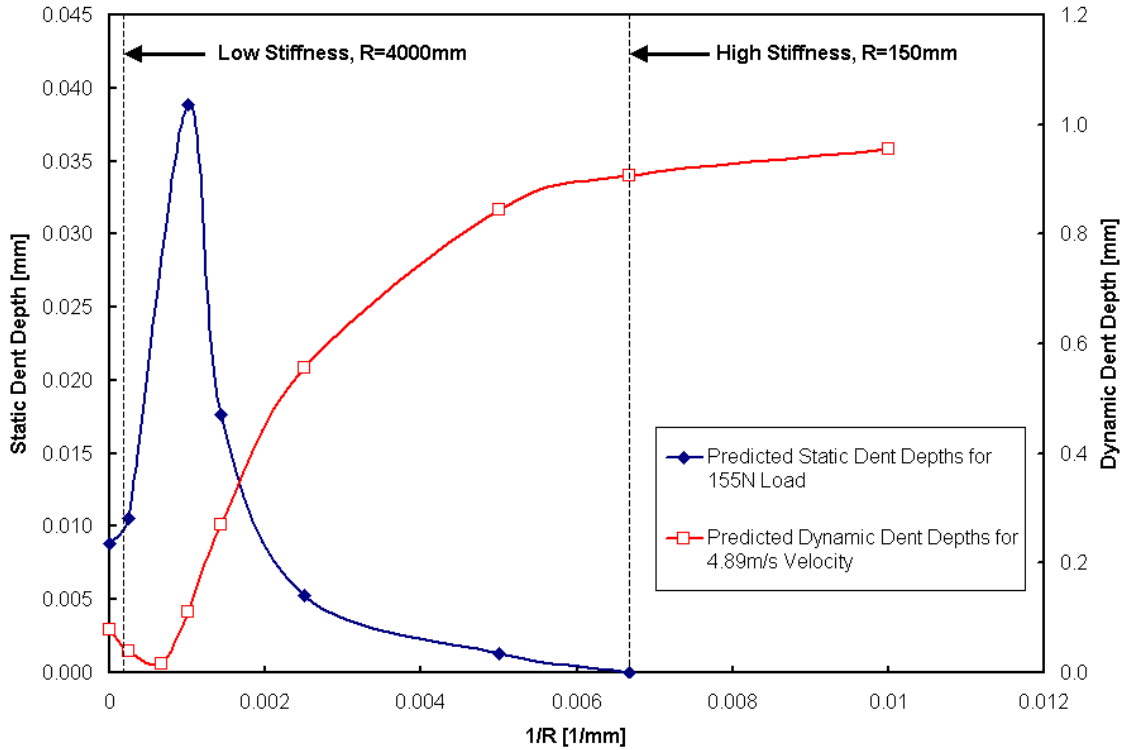
Figure 16: Comparison of predicted static and dynamic dents of 600x600mm panels vs. the inverse of the radius of curvature (Stiffness increases as the plot moves to the right). Static dents (left ordinate axis) are based on 155N applied point loads. Dynamic dents (right ordinate axis) are based on 4.89m/s impact of an elastic indentor.

The worst static dents occur in relatively shallow curvature panels, while under dynamic denting loads these panels show the best dent resistance. If the flat and nearly flat models are ignored, increasing curvature and stiffness appears to improve static dent resistance while lowering dynamic dent resistance. The contradictory stiffness effect is tied to the deformation mechanisms at work in the two cases.

The effect of panel size was shown to be minimal on static denting, while larger panels exhibit superior dynamic dent resistance, as shown in Figure 17. Local panel bending controls the static dent depth, which is a function of thickness and curvature, not panel size. For the dynamic case the reduced panel size increases the stiffness and leads to higher contact forces at impact.
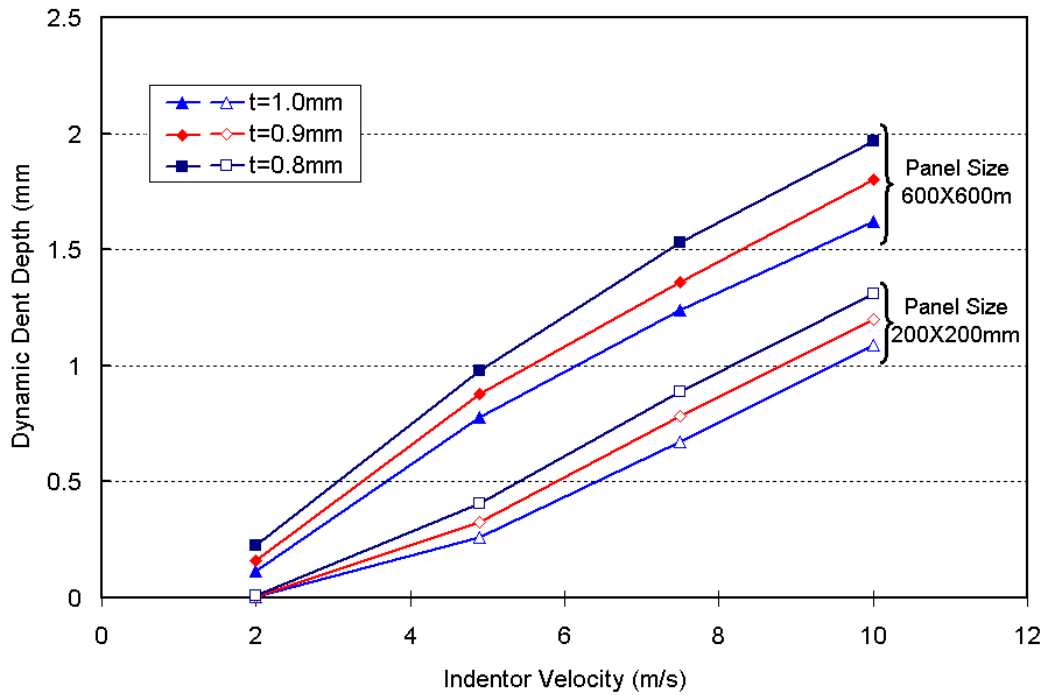
Figure 17: Effect of panel size on dynamic dent depth for a range of indentor velocities.

The simulations allow the plotting of force vs. time histories for the dynamic dent process, as shown in Figure 18, which help illustrate the role of panel geometry on dent depth. The stiffer panels exhibit higher contact forces, over shorter time intervals. Conversely, the low stiffness panels see a lower, longer force profile, as the indentor's energy is gradually transferred to the sheet as the panel deflects.
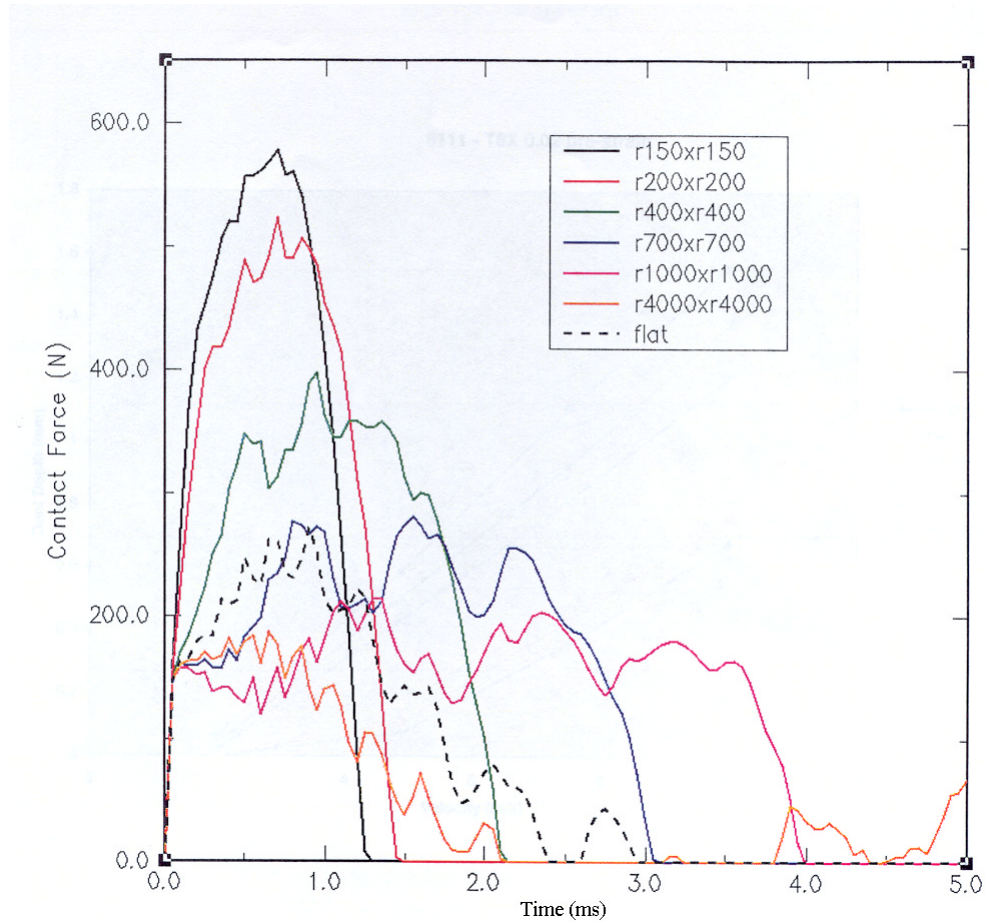
Figure 18: Contact force time histories for a range of panel curvatures.

The study served as a strong foundation for future work that expanded on these initial findings. The contradictory nature of static and dynamic denting with panel curvature was viewed as an area requiring further examination.

2.2 Small Scale Validation of Hydraulic Bulges

Prior to undertaking the current work, an initial small-scale validation exercise was undertaken by the author. This work was included as part of a paper presented at Numisheet 1999 [64]. The work served as a means of assessing various parameters affecting dent resistance, while developing a numerical foundation for future work. The validation was based on several dynamic and static dent tests performed on a range of 152.4mm diameter, circular blanks hydraulically stretched to various heights. The blanks were clamped around the periphery and then pressurized to form a dome. The use of hydraulic bulges provided biaxially stretched panels, with known levels of strain in the dome heights. Unfortunately,

the strain level, final thickness and curvature were coupled, but a range of test conditions was provided for numerical simulations. The modelling of these bulges required accurate capture of the forming conditions to ensure accurate dent predictions.

The forming of the bulges was modeled using LS-DYNA, with an explicit approach using a quarter symmetry model. Figure 19 shows the results of a forming simulation for an 8% strain hydraulic bulge. Both simplified and detailed forming models of the bulges were created. The initial simplified models only restrained the outer edge of the blank in forming, whereas the edges were clamped in the detailed model. The initial model was proven inaccurate, as only two of the three forming results (strain, height and thickness) could be captured. The addition of a clamp tooling model introduced clamping force as a variable, thereby allowing more accurate forming results. After forming, an LS-NIKE springback simulation was run prior to denting. Dynamic denting was modelled in LS-DYNA, while static denting was modelled in LS-NIKE. A rigid indentor, with full contact interfaces, was used for both types of denting. Similar material modelling techniques, as used by Worswick *et al.* [63], were employed, with the same eight stress-strain data point limitations in the LS-NIKE runs.
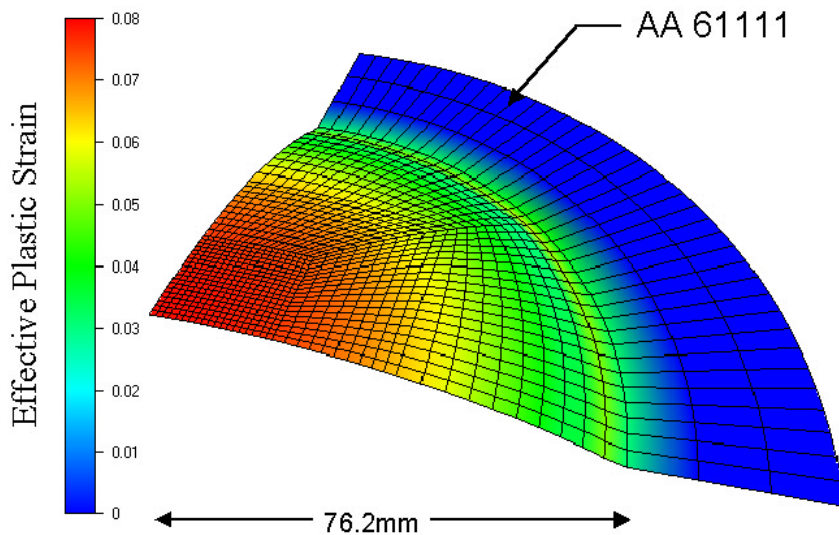
Figure 19: Forming model of 152.4mm hydraulic bulge for 8% pre-strain.

Results of this work demonstrated the potential of the numerical modelling approaches while highlighting several areas of concern. The dynamic simulations proved to be quite accurate as shown in Figure 20.
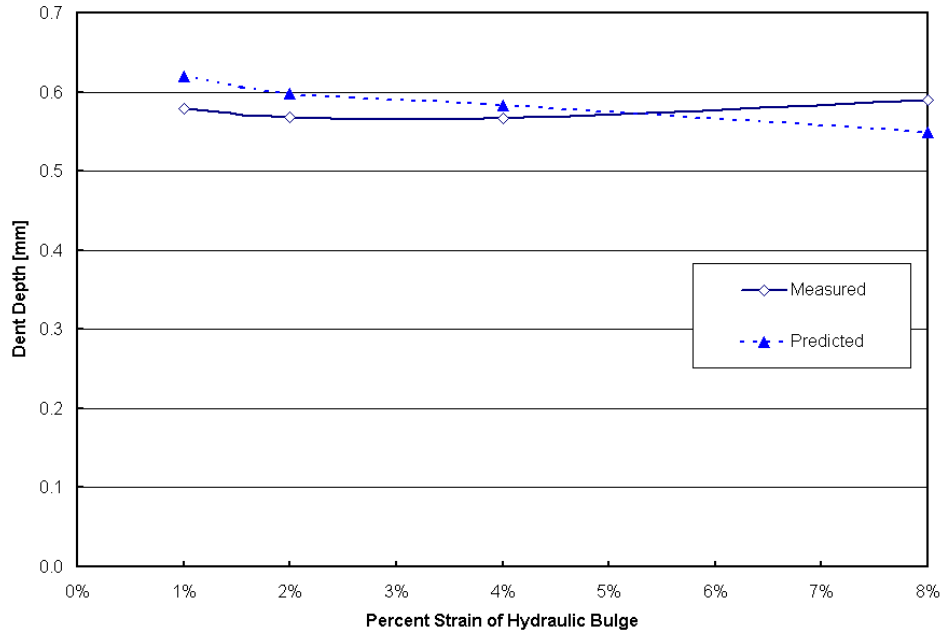
Figure 20: Comparison of measured and predicted dynamic denting results of 152.4mm hydraulic bulges for a range of pre-strains and corresponding dome heights.

The static simulations proved to be more limited in their success. The capture of oil canning was quite difficult and this translated into inaccuracies in dent predictions. The transition in the actual dent depth vs. load curves was poorly captured by LS-NIKE, shown in Figure 21, as the oil canning behaviour controls this transition region.
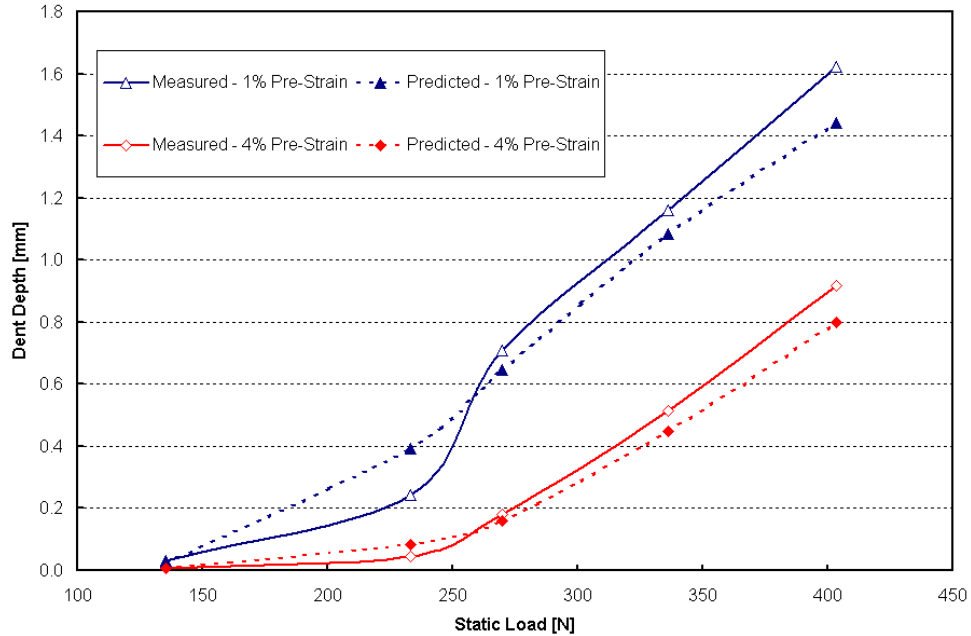
Figure 21: Comparison of measured and predicted static dent depths vs. load for two levels of pre-strain in 152.4mm hydraulic bulges.

In addition, excessive adjustment of the number of time steps and non-linear solver settings proved to be necessary in order to achieve convergence in many cases. These difficulties proved to an area of concern in the current work, and will be addressed in more detail in this thesis. Despite the numerical issues, the results of this preliminary study were promising and provided a foundation for the more detailed models that followed. The study also demonstrated that multi-stage numerical modelling of the entire forming and denting process was possible, but highlighted the need for improved interfaces and tools in order to optimize the process.

2.3 Medium Scale Panel Dent Prediction Incorporating Forming Strains

Thomas [4] reports a major study incorporating forming strains in panel dent predictions in his MASc thesis at the University of Waterloo. This study included a detailed forming simulation and subsequent static and dynamic denting simulations of a deep drawn part. The work also included the development of a software tool, D-Mesh, to ease the transition between forming and denting models. An important consideration in dent modelling is the level of local refinement needed at the dent site in order to achieve accurate results. For accuracy, forming models have high levels of mesh refinement in regions of high forming

strains. Unfortunately, these high strain regions are rarely in proximity to critical dent sites, which leads to a need for local mesh refinement prior to denting simulations. The software tool, developed by Thomas, allows for local mesh refinement, indentor insertion and translation between various input formats. Numerical models, at both the forming and denting stages, were presented and shown to have a high level of agreement with experimental results. Two alloys were tested and modeled, AA5754 and AA6111.

The modelling techniques developed are similar to those presented in this study, with special consideration for accurate models of forming. The forming process was modelled using LS-DYNA explicit and LS-DYNA implicit for the panel springback. Dynamic dent simulations were performed in LS-DYNA after local mesh refinement with D-Mesh. Static denting was modeled in ABAQUS implicit, after convergence in LS-DYNA implicit proved to be difficult. The study examined numerous numerical options that influenced all stages of the modelling process. Among these factors was the choice of yield criterion. As discussed previously, the use of an anisotropic material model is essential for accuracy in forming models and was used by Thomas. Unfortunately, the static dent simulations couldn't use this material model due to the limitations of ABAQUS. The effect of the anisotropic model on dynamic dent depth was examined and no significant trend was observed.

The results of the dent resistance analysis showed very good agreement, as illustrated in Figure 22, which compares the load-displacement curves and Figure 23, which compares the predicted and measured dent depths.
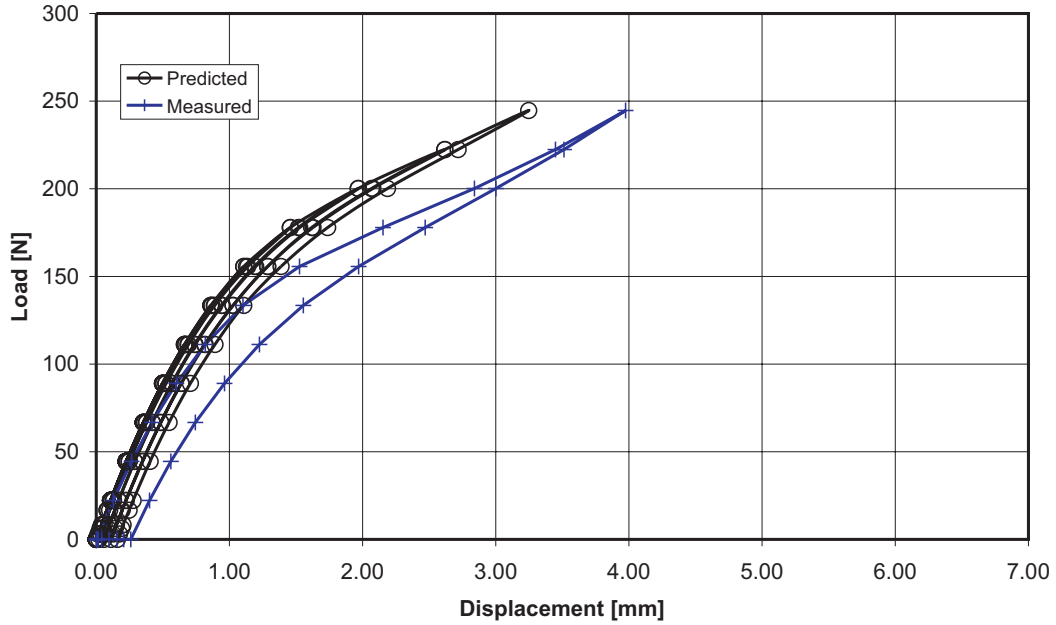
Figure 22: Predicted and measured load displacement curves for the 1.00mm AA6111 panel
at location B by Thomas [4].
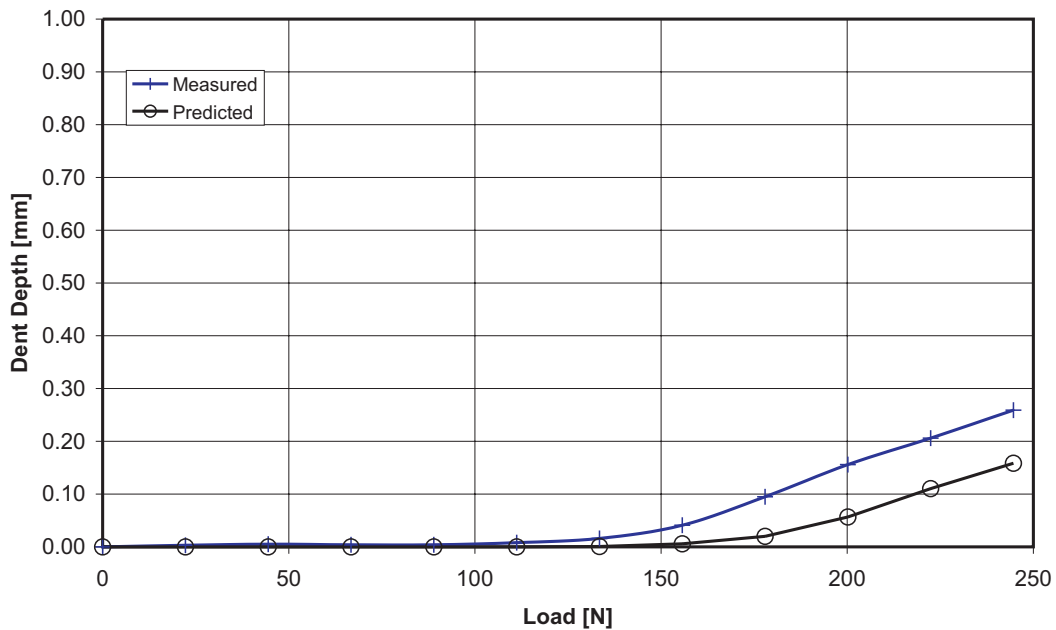
Figure 23: Predicted and measured residual static dent depths for the 1.00mm AA6111 panel
at location B by Thomas [4].

The relatively small scale of the dent depths predicted introduced some limitation in
the numerical accuracy. Thomas [4] suggests that numerical simulation of dent depth using
the current methods may be best suited for relative comparisons rather than absolute
measures. The results demonstrated sensitivity to the material used. The dynamic denting

59

results were superior for the AA6111 while the predicted static results were superior for the AA5754. The sensitivity of the static results to the prediction of oil canning load was stressed. The need for accurate material properties and sufficiently refined meshes was emphasized. The opposing effect of stiffness on static and dynamic dent resistance is again observed, as the stiffer locations perform poorly dynamically but well statically. Considering the complexity of the multi-stage process modelled and the small level of dent deformation to be predicted, the level of accuracy is very promising. The numerical approach used offers an effective method for dent resistance assessment that can be transferred to larger scale applications. The results and methods developed by Thomas [4] proved invaluable in the work presented in this thesis.

2.4 Current Work – Medium Scale Structural Assemblies

The focus of this thesis is the numerical modelling of medium-scale, structural panel assemblies. There is limited work in the literature that attempts to address the role of panel interaction in dent resistance performance. Most studies that have addressed such issues have only done so tangentially, with limited experimental testing or numerical simulation. The need for a more comprehensive examination of the role of the inner support panel and the panel support conditions on dent resistance is addressed in this thesis. This study served as a developmental tool for modelling techniques that could later be transferred to full-scale autobody panels. By focusing on medium-scale panels, the role of global support systems could be studied while maintaining manageable model sizes for parametric study. The medium scale panels measure 850mm by 550mm, roughly a quarter the size of full-scale automotive hoods. The medium-scale panels enabled the use of fabricated inners rather than expensive stampings with flexibility in support structure design. Also, experimental validation of the role of the mastic was possible with the panel assemblies.

Along with the development of modelling techniques for full-scale applications, this work also presents a comparison of static and dynamic denting for a range of parameters in representative panels. This knowledge base enables future design of full-scale panels to take dent resistance considerations into account on a qualitative level. Detailed numerical analysis can be pursued to address the relative impact of proposed modifications such as inner redesign or down-gauging using the numerical approaches outlined in this thesis.

The experimental procedure, panel configuration and fabrication are described in Chapter 3. These assemblies consist of an inner AA5754 panel, designed to mimic an existing commercial hood geometry, and an outer AA6111 panel joined together using automotive mastic. The assemblies allow a parametric study of inner support effects, assembly curvature and outer panel thickness. Both static and dynamic dent testing has been completed for a range of dent sites. The experimental results demonstrate the role of the various factors affecting dent resistance. Numerical simulations of the denting processes were performed, and the results were compared to the experimental findings. The details of the numerical approach are outlined in Chapter 4. The numerical modelling accounted for the inner and outer panel interaction using solid elements to model the mastic regions, as well as a contact surface between the two panels. The results of the numerical simulations illustrate various issues that arise in modelling of the panel interactions, with particular emphasis on the role of the mastic. Difficulties in modelling the mastic led to difficulties in achieving accurate results, but these issues are largely attributed to the overly thin mastic layer used. The experimental results are presented in Chapter 5, with accompanying examination of the observed denting performance trends. Discussion of the findings, subsequent transfer of the numerical methods to larger problems and outstanding experimental and numerical issues are presented in Chapter 7. General conclusions and recommendations for future work are included in Chapter 8.

3 Experimental Program

3.1 Medium Scale Panel Assemblies

The principal goal of the panel design, chosen for this work, was examination of the role of structural supports on denting behaviour. An assembly that incorporated both an inner support panel and outer closure panel was therefore needed. The assembly developed includes a teacup-based inner support panel joined to an outer closure panel with automotive mastic. The resulting assemblies are representative of large-scale hoods, and allow a parametric study of the factors affecting dent resistance. Various factors were examined using different inner and outer combinations, including panel curvature, closure thickness, support spacing, dent location relative to support points and dent type. The design of the assemblies incorporated various elements of actual hood design and manufacture in order to address issues, with the medium scale specimens, that would arise in future work with full-scale hoods. The interaction between the inner and outer panel through both the adhesive layer and other joints was of particular interest. In order to limit the number of assemblies constructed, reuse of the inner panels was a priority. Also, panel paint bake response was incorporated in the study in the materials selection.

3.1.1 Material Selection

Commercial hood designs and the current aluminum alloys used by ALCAN for these applications dictated the choice of materials. As outlined in the Chapter 1, 6000 series alloys are preferable for body panel design where dent resistance is concerned. The bake hardening of these alloys can be exploited during the paint curing stage of body panel manufacture making them ideally suited for outer panel applications. As a result, a developmental ALCAN 6111 alloy was selected for the outer panels. Three nominal thickness sheets, 1.0mm, 0.93mm and 0.8mm, were provided, a range that reflects typical

thickness values of actual hoods. It should be noted that the 0.93mm sheet was from a separate batch of material. The alloy provided was designated as AA6111 T4PD, in a proprietary unaged, pretreated condition. The pretreatment is designed to optimize the bake hardening response of the alloy for a typical automotive paint bake cycle while retaining relatively good initial formability.

Material selection for the inner panel design is less definitive. In the early stages of this project, the most common inner panel alloys in commercial panels were from the 5000 series, most likely due to the superior formability they offered. More recently, the recycling benefits of single alloy assemblies have become more prominent and 6000 series alloys have become the preferred alloys for commercial inners. However, for this project, the desire to reuse the inner panels for multiple closures dictated the use of a non-bakehardenable, 5000 series alloy. Furthermore, in this work, the complex inner panel geometries were fabricated through welding of the panel. 5000 series alloys are considerably more weldable than 6000 series aluminum, hence, 5754 was used to fabricate the inner panels in this research.

The material properties of the alloys selected were required for the numerical modelling. The inner panel undergoes little or no plastic deformation throughout the denting process and only the elastic modulus is necessary if the inner panel is treated as fully elastic material. The material behaviour of the outer panel alloy must capture both the paint bake and elastic-plastic behaviour. As a result, complete stress-strain histories for the various thickness and heat treatment conditions were compiled. Material anisotropy must be considered in numerical modelling.

The tensile tests were performed at ALCAN's Kingston Research and Development Centre (KRDC), using automated tensile testing. The tensile tester was an Instron 4200 Series IX, with a robotic specimen loader. Measurement of both axial and transverse deformation was recorded. A standard tensile specimen was used based on the ALCAN setup requirements. The Lankford coefficient or R-value was determined at 10% strain. The Lankford coefficient is a measure of sheet anisotropy that compares the degree of straining through the thickness, ε_t, to the transverse strain, ε_w across the width.

$$R = \frac{\varepsilon_w}{\varepsilon_t} \qquad\qquad (10)$$

The R-value is often measured for tensile specimens cut from various in-plane orientations to fully measure the anisotropy of a given sheet.

Tensile specimens were cut from the sheet at two orientations, 0º and 90º, to examine sheet anisotropy. In total 17 tensile specimens were tested, 6 for each thickness, except for 0.93mm. Two specimens were tested for both the 0º and 90º directions after paint baking, as well as single specimens in both directions in the as received condition for the 0.8 and 1.0mm sheet. Only one direction was examined for the 0.93mm sheet due to limited material availability. The averaged results, comparing the as-received and paint bake yield strengths, are presented in Table 1.

Nominal Thickness [mm]	Condition	Measured Thickness [mm]	Yield Strength [MPa]	Standard Deviation [MPa]
0.8	T4PD	0.805	139	3.21
0.8	T4PD PB	0.805	213	3.72
0.93	T4PD	0.927	154	n/a
0.93	T4PD PB	0.927	210	4.27
1.0	T4PD	0.998	142	0.02
1.0	T4PD PB	0.996	221	1.93

Table 1: Comparison of average yield strength in the as-received and paint baked conditions for AA6111 sheet.

The effect of the paint bake treatment is evident, as an increase of over 70MPa is observed in the 0.8mm and 1.0mm sheet. The 0.93mm sheet, from a different batch of sheet, exhibited a smaller strength increase of 56 MPa. The strength gain during paint bake offers substantial benefits for dent resistance. The 0.93mm sheet was older, and thus the higher initial yield strength, relative to the 1.0mm sheet, may be attributed to natural age hardening. A comparison of typical true stress-strain responses of the given sheets is presented in Figure 24. The true longitudinal strain (ε_l) was calculated from the axial extension data. The true stress was computed using the reduction in cross-sectional area based on the measured transverse strain (ε_w) and the calculated thickness strain (ε_t). The thickness strain was calculated using volume constancy during plastic deformation such that:

$$\varepsilon_t = -(\varepsilon_l + \varepsilon_w) \qquad\qquad (11)$$

The current thickness and width were then calculated from the strains, enabling the calculation of the current area and the corresponding true stress.
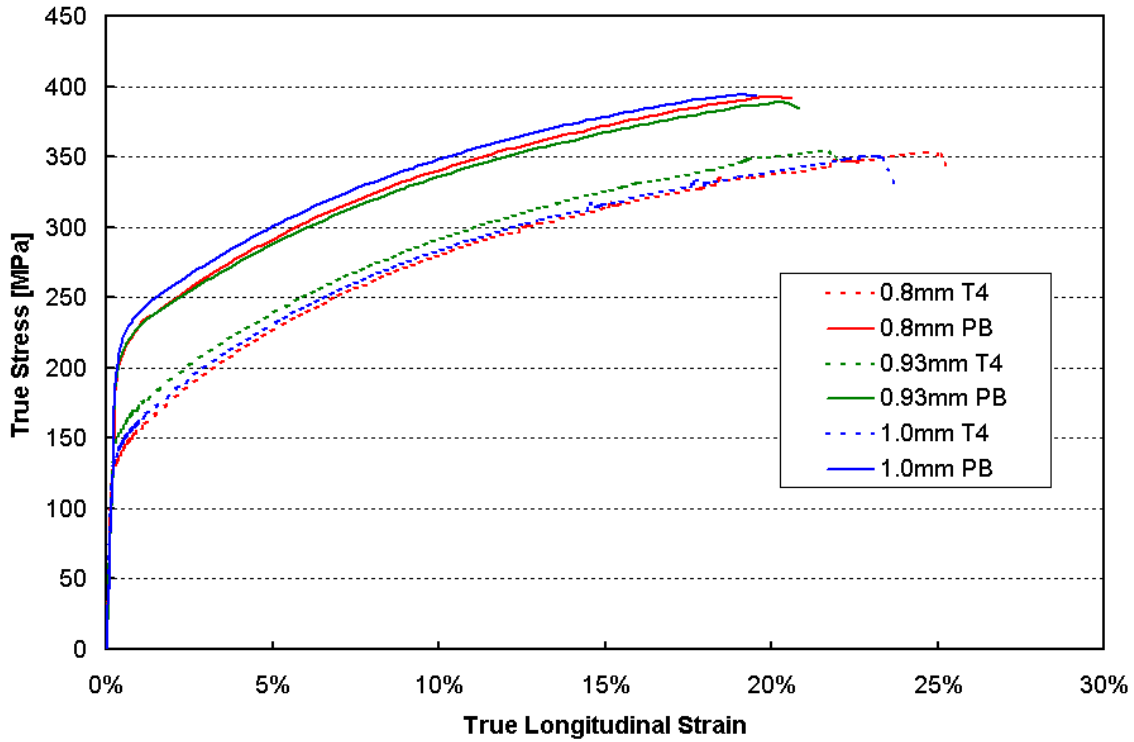
Figure 24: Typical Stress-Strain Response of AA6111 for 0.8mm, 0.93mm and 1.0mm thickness in the T4 and paint bake (PB) conditions.

The strain to failure for all specimens is greater than 20%. Similar hardening responses for the different thickness measures can be observed, along with the inferior bake hardening of the 0.93mm sheet. The loss of hardening of the 0.93mm sheet may be attributed to differences in the pre-treatments, but is more likely the result of natural age hardening reducing the bake hardening response.

The effect of anisotropy is presented in Table 2, which illustrates the change in yield strength depending on material orientation for both the as received and paint baked conditions. A small difference in yield strength with orientation is observed in the thinnest sheet, and no variation is evident at the highest thickness.

Nominal Thickness [mm]	Condition	Orientation	Yield Strength [MPa]	R Value
0.8	T4	0º	143	0.63
0.8	T4	90º	136	0.86
0.8	PB	0º	217	0.61
0.8	PB	90º	209	0.85
1.0	T4	0º	142	0.61
1.0	T4	90º	142	0.64
1.0	PB	0º	221	0.59
1.0	PB	90º	221	0.63
0.93	T4	90º	154	0.56
0.93	PB	90º	210	0.57

Table 2: Comparison of average yield strength for the two material orientations tested and the measured R values for the respective directions of AA6111 sheet

The R-values are also listed for all three thickness of sheet, at the given in plane orientation relative to the rolling direction. The thinner sheet exhibits a larger degree of anisotropy as the R-values change substantially between the 0º and 90º directions. Conversely, the 1.0mm sheet has similar R-values for both orientations measured.

3.1.2 Inner Panel Design

The inner panel was designed using an array of "teacup" supports, which provide local reinforcement of the outer panel at various points. The teacup concept was chosen as it is becoming increasingly common in automotive hoods as it allows for sharp transitions from supported to unsupported regions. The supports are referred to as teacups since they resemble inverted cup shapes, pressed into the inner panel. A model of a full hood inner is shown in Figure 25 to illustrate a typical teacup-based design. In fabrication of actual inner panels, the entire part would be formed into the final shape in a single process. For the simulated inners built for this study, it was impossible to form inners in a single process. The cost of developing tooling would be prohibitive and would require a detailed design study.

Instead, the inner panels were fabricated using individually formed teacups that were welded to a curved panel. All panels were constructed at the University of Waterloo machine shop.
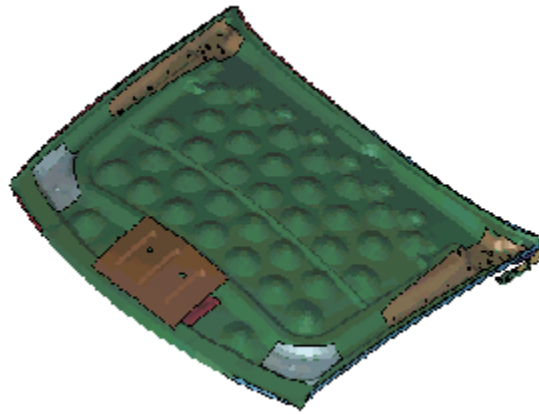
Figure 25: Teacup-based inner panel from an automotive hood

The shape chosen for the teacup was based on a teacup size from actual hoods. An approximate diameter and cup height was chosen and then adjusted based on the available manufacturing options. The cups were drawn from 171mm diameter circular blanks of 1.0mm AA5754. The blanks were formed using a custom punch built at the University of Waterloo from a 65,000lb hydraulic forming press shown in Figure 26.

Figure 26: Hydraulic press at the University of Waterloo used to form the inner panel teacup supports.

An existing 101.6mm circular die was used on the clamping perimeter. The teacup has a flat circular region at its top of approximately 25mm in diameter. The initial punch used to form the teacups consisted of a 25mm diameter cylindrical post attached to an existing 101.6mm diameter flat-bottomed punch extender. This initial post design proved incapable of successfully forming a 25mm high teacup as tearing at the post radius occurred for a range of lubrication and clamping loads. In order to avoid this localization at the post radius, a conic punch head was added to better support the sheet during cup forming. This modified punch is shown in Figure 27. The teacups were formed under displacement-based punch control and a clamping force of 250N was applied to the binder. Both sides of the blank were coated with an SAE 30 oil lubricant prior to forming.

Figure 27: Final modified 101.6mm diameter, conical flat-topped punch used to form the teacups.

A formed teacup is shown in Figure 28 and an outline of the profile is shown in Figure 29. The profile was measured using a milling machine to take touch measurements of height across a diameter. The profile is nearly symmetric with only small variations between sides. This profile was used as input into the subsequent numerical models. The profile of the teacup was not as critical as the cup height and top diameter. The profile of the formed teacup was sufficiently similar to that of an actual cup to be deemed acceptable. The teacup flange was subsequently trimmed to leave a 5mm outer rim for attachment to the inner panel. The approximate diameter of the trimmed teacups was 131mm.

Figure 28: Formed and trimmed AA5754 inner teacup support.
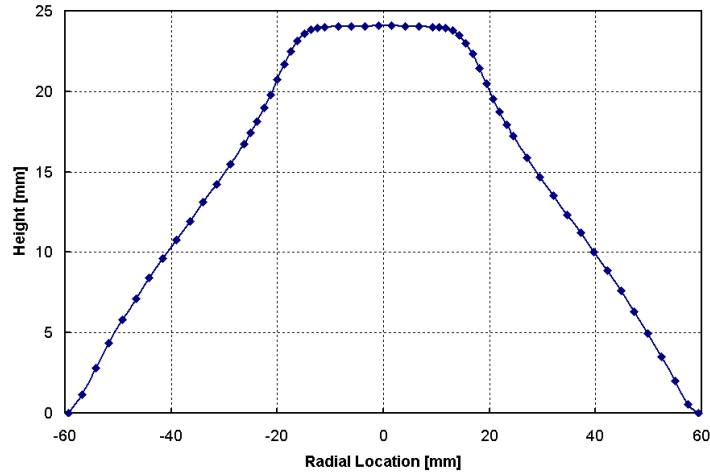
Figure 29: Measured cup profile showing cup height as a function of radial location for a typical formed teacup.

The base inner panels were sheared from 1.0mm AA5754 into 500mm by 900mm rectangular blanks. The long direction was then bent twice at each end to form a 25mm end wall and 25mm end flange. Additional 25mm wide strips were cut to form the enclosing sidewalls and flanges of the inner panel. Three panel curvatures were tested, a flat panel (FL) along with two curved panels. The curved panels are referenced as the medium curvature (MC) and high curvature (HC) cases with radii of curvature of 4580mm and 2370mm respectively. The actual radius of curvature in the finished assembly was a function of the panel construction. The sidewalls of the inner assembly were precut with nominal radii of 4010mm and 2020mm. The base panel was then TIG welded to sidewalls and a resulting curvature was reached after springback. The welding process led to some non-uniformity along the panel length as well as variation between separate inners due to distortions. After attachment of the sidewalls the inners were quite rigid. Various assembled inner panels, with attached teacups, are shown in Figure 30-Figure 33. The two teacup configurations used are shown, as well as both flat and curved inner panels. A side view of the medium curvature panel assembly is shown in Figure 33.

Figure 30: Assembled 1.0mm AA5754 inner panel with attached teacups and sidewalls with flanges. Teacup configuration #1 is shown.

Figure 31: Assembled 1.0mm AA5754 inner panel with attached teacups in configuration #2.

Figure 32: Assembled 1.0mm AA5754 medium curvature inner panel with attached teacups in configuration #2.

Figure 33: Side view of assembled 1.0mm AA5754 medium curvature inner panel.

The teacups were attached to the inner panel using a spot welder with roughly 10-12 spot welds per teacup. Some difficulty in achieving successful welds led to variation from cup to cup, but all teacups were successfully joined. Also, the welding process introduced some distortion in the panel that furthered the variations between teacup locations. Circular cutouts, with diameters of 108mm, were made in the base panel prior to attachment of the teacups. These cutouts reduced the panel stiffness and better reflected the geometry of a formed inner panel. The final dimensions of the inner panel with the flanges were 550mm by 850mm.

Two different teacup configurations were used to examine the effect of varied cup spacing. The primary configuration, as seen in Figure 30, configuration #1, was similar to those found in hoods and uses a staggered arrangement of teacups. A second teacup configuration, configuration #2, was also constructed as shown in Figure 31. This second configuration used a linear layout of the cups, with larger cup-to-cup spacing than configuration #1. As the study progressed the majority of testing was performed on the staggered configuration. Schematics of the two teacup configurations are shown in Figure 34. Due to the limitations of the cup layout, configuration #1 has two more teacups than configuration #2. Two inner panels of each configuration and curvature were built to lessen the required number of heat treatments.
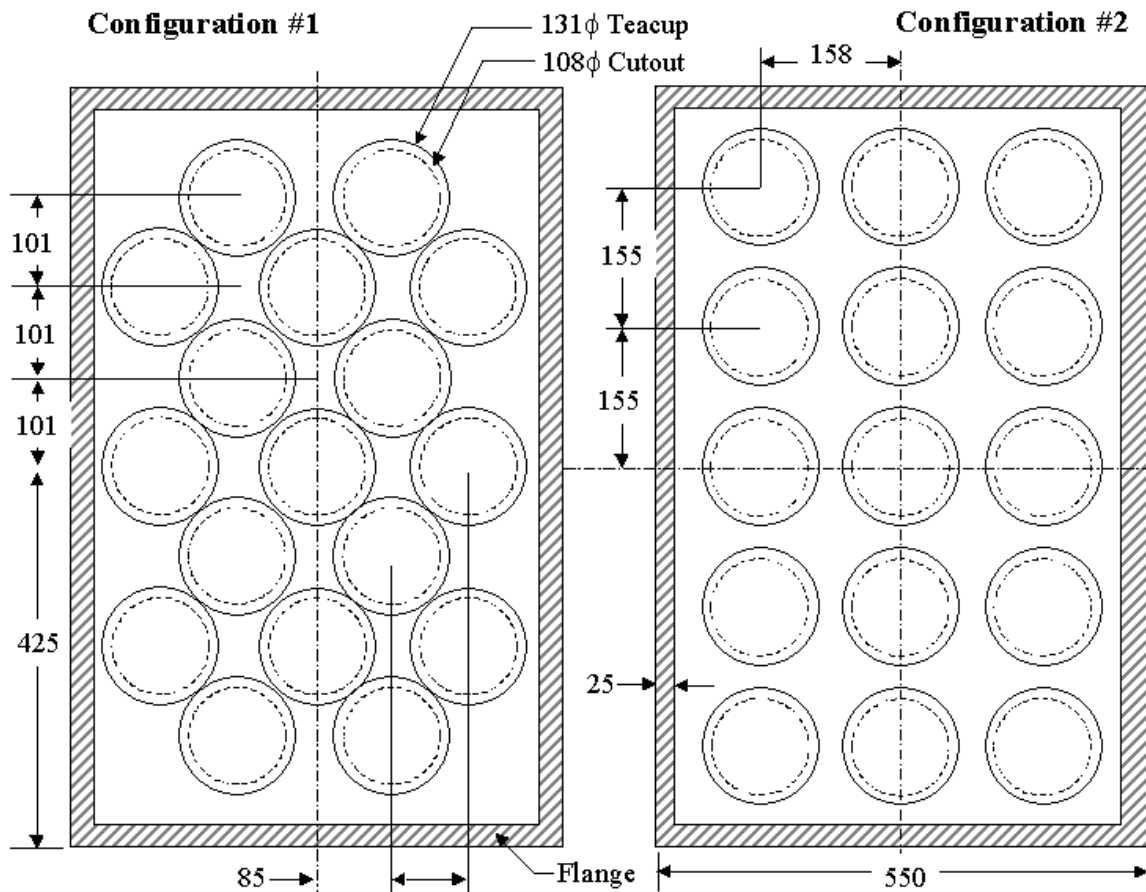
Figure 34: Teacup spacing configurations for inner panels. All dimensions are in mm.

In order to mount the panels on the test rig a set of four attachments brackets were added to the inner panel. These brackets were welded at corner of the panel and attached to four L-shaped mounting brackets. The welded attachments, shown in Figure 35, were

designed to rest against the sidewall and under the base panel with a ¼" threaded hole for bracket attachment. The L brackets had 25mm by 50mm footprints for ample clamping to the test rig. A ¼" threaded bolt was used to join each bracket to the inner panel. The fixtures allowed the panel to be rigidly mounted on the test rig in a manner that could later be modelled as four fixed points. A close-up of the mounting brackets attached to the test rig is shown in Figure 36.
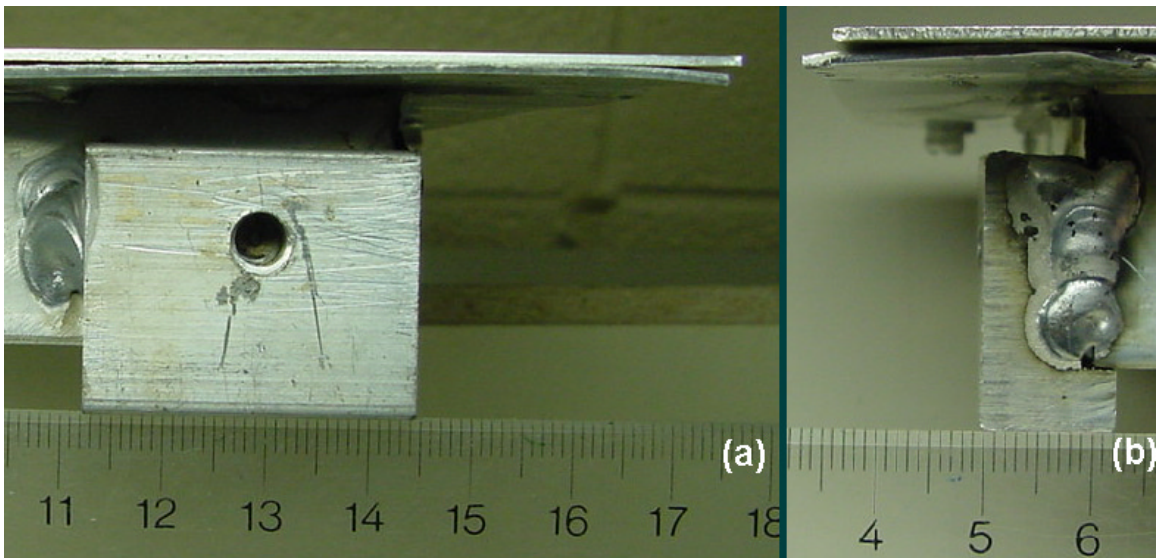
Figure 35: Attachment bracket welded to inner panel corners.

Figure 36: Close-up of inner panel mounting bracket for attachment to dent testing rig.

3.1.3 Outer Closure Panel Design

The closure panels were sheared from AA6111 sheet with three different thicknesses, 0.8mm, 0.93mm and 1.0mm. The closure panels were cut into 550mm by 860mm rectangles that were then attached to the inner panels. The outer panels were all initially flat, with the final curvature resulting from attachment to the inner panel. The outer panels were attached to the inner panel using automotive mastic at the top of each teacup and with 3/8" rivets around the flange perimeter. The rivet spacing was chosen to assure reasonable conformity of the inner and outer panels around the flange. Initial testing with fewer rivets saw large gaps between the flange and outer panel that were deemed unacceptable. The final rivet spacing is shown in Figure 37.
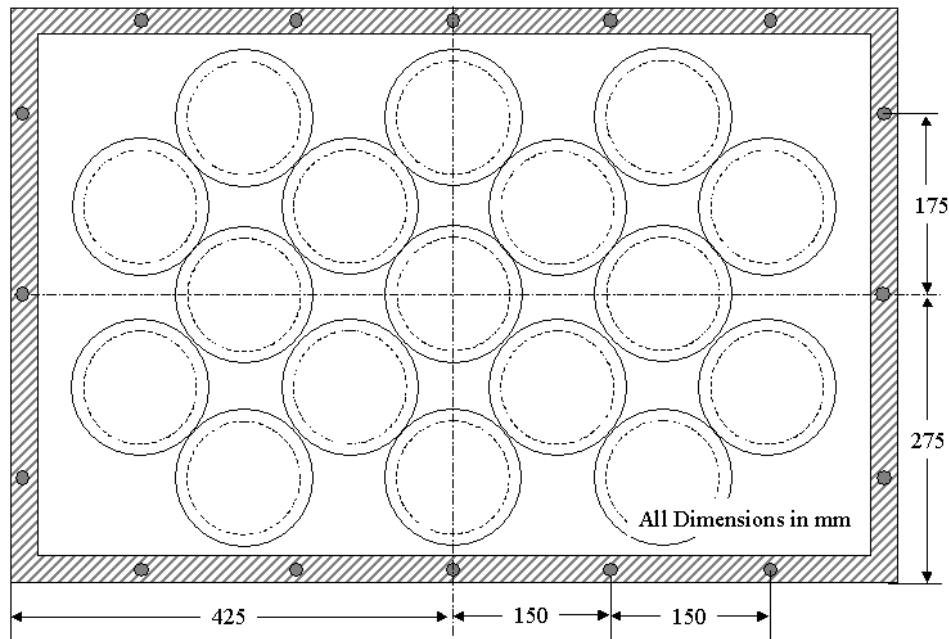
Figure 37: Rivet spacing for outer closure panel

After the closure panels were attached to the inner support panels, the entire assembly was baked in an oven at ALCAN. The cycle was designed to achieve the same degree of bake hardening in the closure panels that actual hoods would experience in multi-stage painting processes. The bake cycle used was 32 minutes at 177ºC. The initial ten minutes of the cycle is required for the sheet to reach the desired temperature and the sheet is then baked at the peak temperature for approximately 22 minutes. A typical temperature profile is

shown in Figure 38. The tensile specimens for the paint bake condition were included in the oven during the assembly's treatment to assure similar baking temperature-time histories.
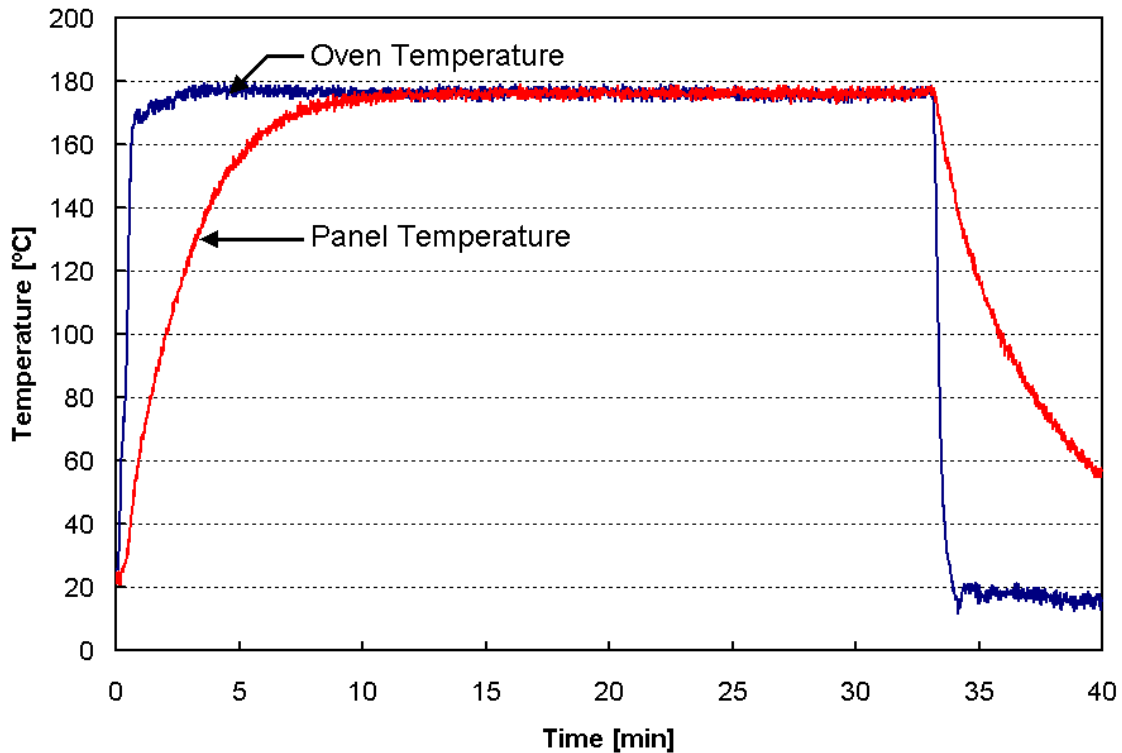
Figure 38: Paint bake temperature profile for panel assemblies.

The various permutations of outer panel thickness, inner panel curvature and teacup configuration, were too large for the testing time available. As a result, a limited combination of conditions was tested. A matrix of the selected test conditions is included in Table 3. The majority of testing was performed on panels with teacup configuration #1 as it best represented the commercial inner panels surveyed. Only a single test group for the high curvature panel was used as it was observed that this curvature may be overly stiff compared to actual hoods. Thus, the focus of the investigation was on the medium and flat curvature cases. The middle thickness, 0.93mm, was used as a baseline case for the high curvature and secondary teacup configuration.

Curvature	Teacup Configuration #1			Teacup Configuration #2		
	t=0.8	t=0.93	t=1.0	t=0.8	t=0.93	t=1.0
Flat	✓	✓	✓			
Medium	✓	✓	✓		✓	
High		✓				

Table 3 : Matrix of test conditions evalutated for static and dynamic dent testing of panel assemblies.

3.1.4 Automotive Mastic

The inner and outer panels are joined at the top of each teacup with mastic adhesive, commonly used in automotive applications. The mastic used in this testing was supplied to ALCAN by General Motors for use in actual hoods. The mastic in its uncured state has a consistency of thick peanut butter and is applied manually to the top of each teacup. The mastic was applied as uniformly as possible to each teacup top and then the outer panel was put in place and riveted to the inner. Any excess mastic would be pushed outwards from the teacup top, assuring full coverage over the entire region. Application of the uncured mastic is shown in Figure 39.
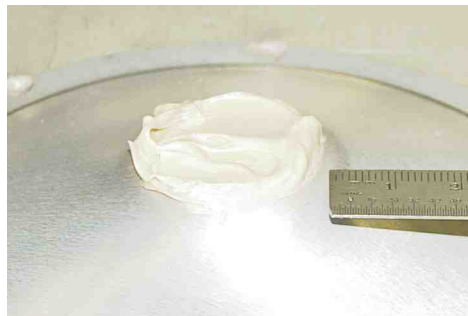
Figure 39: Application of uncured mastic to top of teacup.

The thickness of the mastic layer is controlled by the offset between the top of the teacup and the bottom of the closure panel resting on the outer flange. The thickness chosen for the testing was roughly 1mm, allowing for slight variations in teacup height. This thickness was based on discussions with people with experience in testing of full-scale hoods. It has been subsequently determined that a larger thickness would have better represented actual mastic thickness values. When cured, the mastic will tend to expand and this can lead to slight bulging of the outer panel if the constraints around the perimeter are

insufficient. A cross sectional view of an assembled panel is shown in Figure 40 to illustrate the variation in mastic thickness between sites. In some cases near metal to metal contact was observed which is a concern in future numerical analysis, as discussed below.
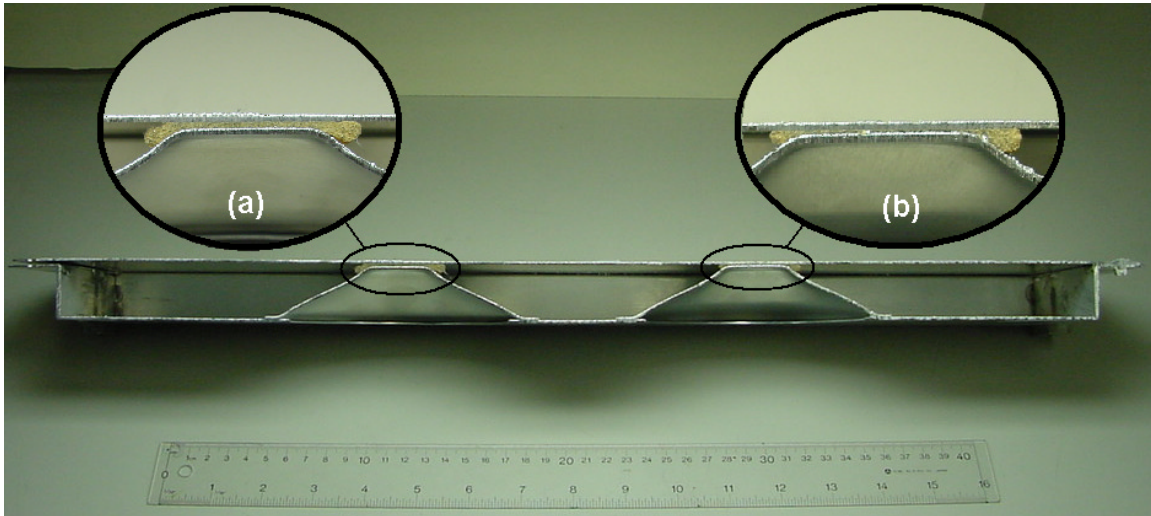
Figure 40: Cross-sectional view of assembled panel showing typical mastic thickness between inner and outer panels. Inset view (a) shows mastic thickness of roughly 1mm while inset view (b) shows a thinner mastic layer.

The mastic is cured during the paint bake cycle to a spongy foam state. Depending on the thickness of the mastic layer, the level of porosity observed in the foam will vary. The mastic will expand if unconstrained during curing. For the assemblies tested, the mastic is highly confined by the small gap between the top of the teacup and the outer panel. As the gap thickness is reduced, the foam will be increasingly compacted and the mastic stiffness will increase. A typical example of the cured mastic at the top of a teacup after removing the outer panel is shown in Figure 41. In actual hood applications, technicians [66] have noted that mastic adherence can be an issue, with teacups often being completely de-bonded from the outer panel. Examination of various teacup sites showed complete mastic coverage, indicative of excellent adherence as shown typically in Figure 41.

Figure 41: Cured automotive mastic on top of a teacup after removal of the outer panel exhibiting good mastic coverage and adherence.

It was essential to characterize the mastic for use in the numerical models. The sensitivity of the mastic's force displacement response to the mastic thickness was of particular interest. The mastic response in compression is of particular concern since a dramatic rise in stiffness is expected as the thickness is reduced. Accurate capture of this stiffness response became a key component of the numerical predictions. The mastic was initially tested in ALCAN's facilities at KRDC for fatigue purposes [67]. These tests entailed cyclic loading of the mastic from 100N in tension to 100N in compression. The testing was performed using 25.4mm cylindrical specimens. The specimens allowed the mastic to be squeezed outward in a radial direction as in the mastic's in-service conditions. These fatigue tests provided initial data for a range of mastic thicknesses. The tensile behaviour was similar for all thickness. Examination of the compressive response of mastic specimens of varying thickness showed substantial differences. Compressive force displacement data, for a range of thickness, is shown in Figure 42, along with the corresponding engineering stress-strain response in Figure 43. A dramatic increase in stiffness is observed as the thickness is reduced from 9.5mm to 1.3mm, which highlights the potential affects of an overly thin mastic layer. The increase in stiffness reflects a loss of the mastic's ability to absorb load that may translate into increased dent depths.
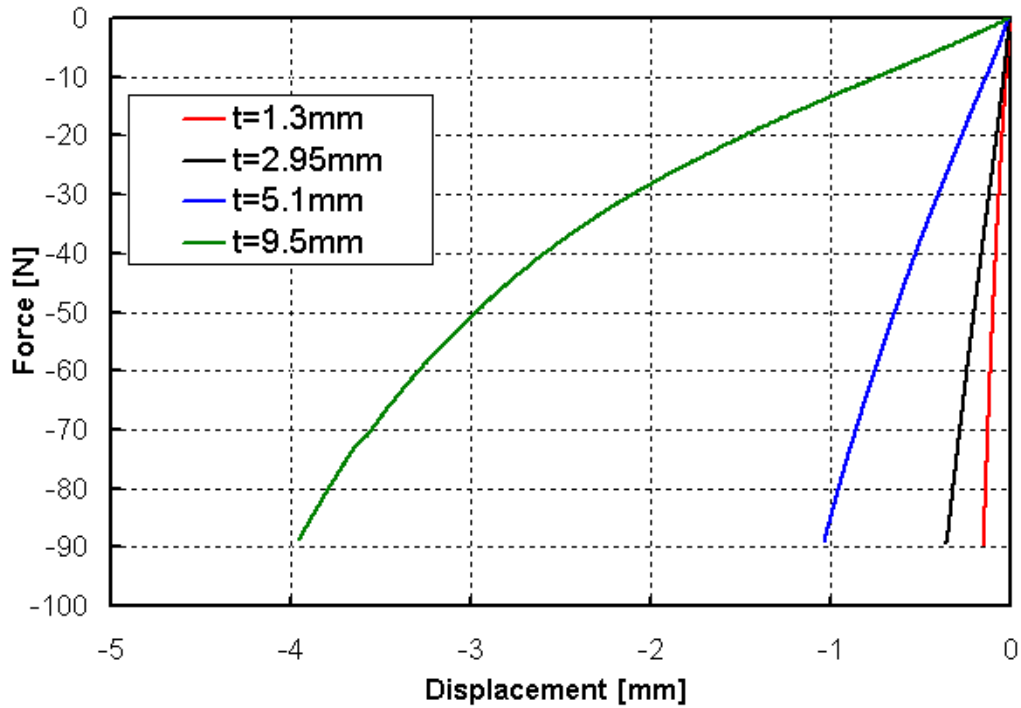
Figure 42: Compressive Force [N] vs. Displacement [mm] response of mastic of various thickness.
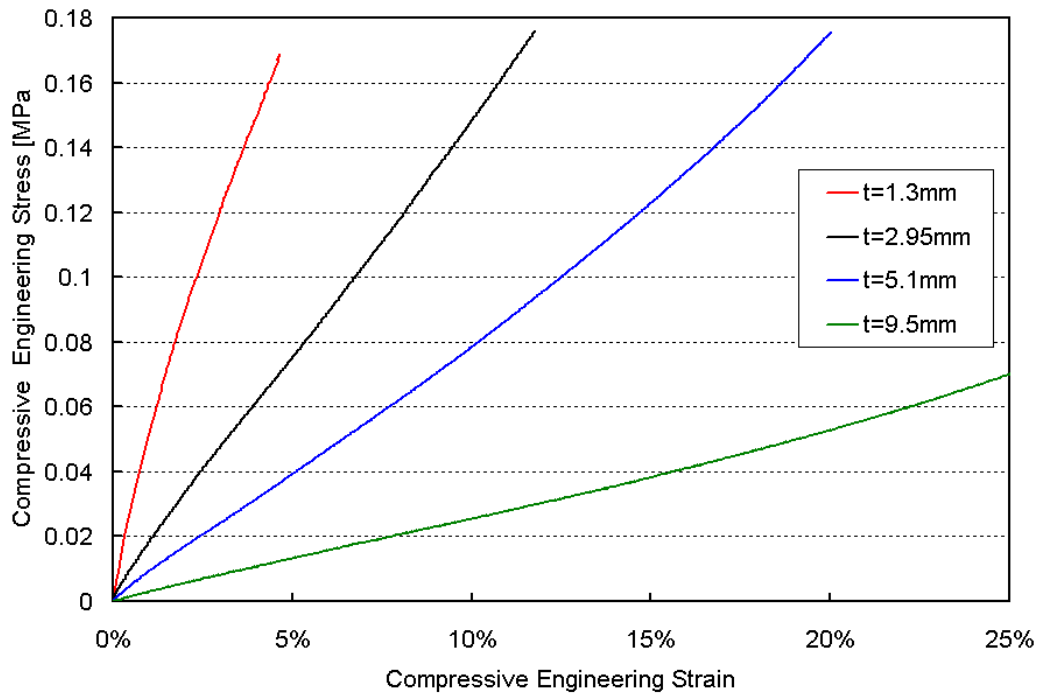
Figure 43: Compressive engineering stress [MPa] vs. compressive engineering strain for mastic of various thickness.

A concern with this initial testing was the low limit of the compressive loads. As the mastic thickness is reduced, the potential for increased reaction forces during denting necessitated the need for a larger compressive force range. The potential of high contact forces was of particular concern in dynamic denting of the medium-scale panel assemblies with a 1mm thick mastic layer. The original load range was based on load levels for thicker mastic layers found in typical hoods. Due to the overly thin layer used in this work, a larger load level was required to capture the different mastic response. Subsequent testing was performed on 1.0mm nominal thickness mastic specimens, using a peak load of 2000N. These tests provided a force-displacement history sufficient to cover the range of loads likely to be encountered in dent testing of the medium-scale panel assemblies. The results of the high-load compressive tests are presented in Figure 44 and Figure 45, for the force-displacement and stress-strain responses respectively.
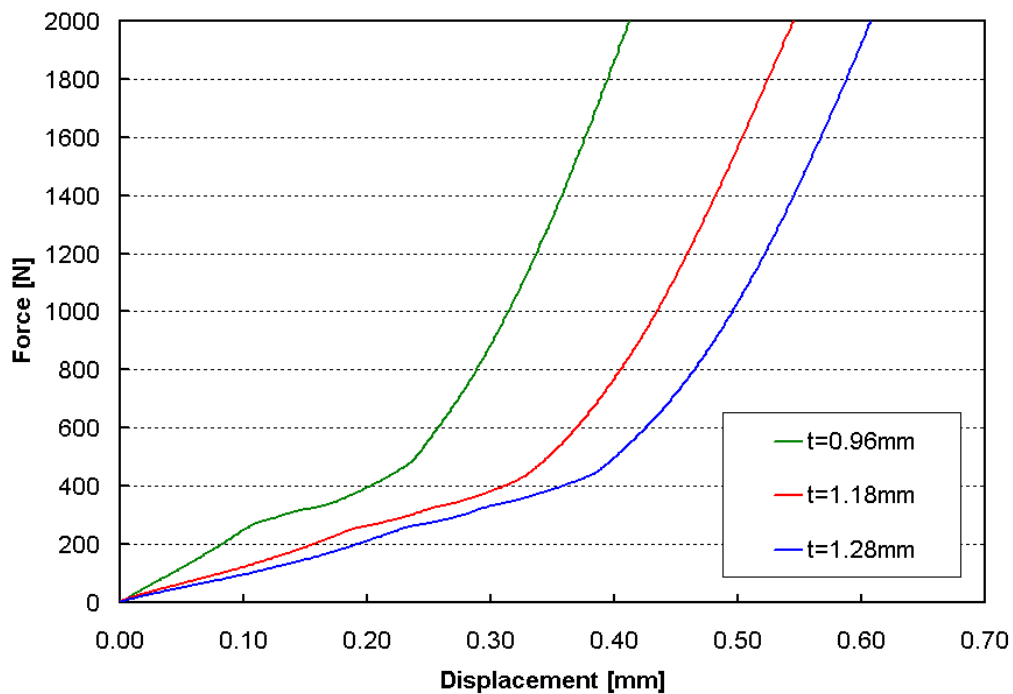
Figure 44: Compressive Force [N] vs. Displacement [mm] data for 1.0mm nominal thickness mastic specimens for loads up to 2000N.

81
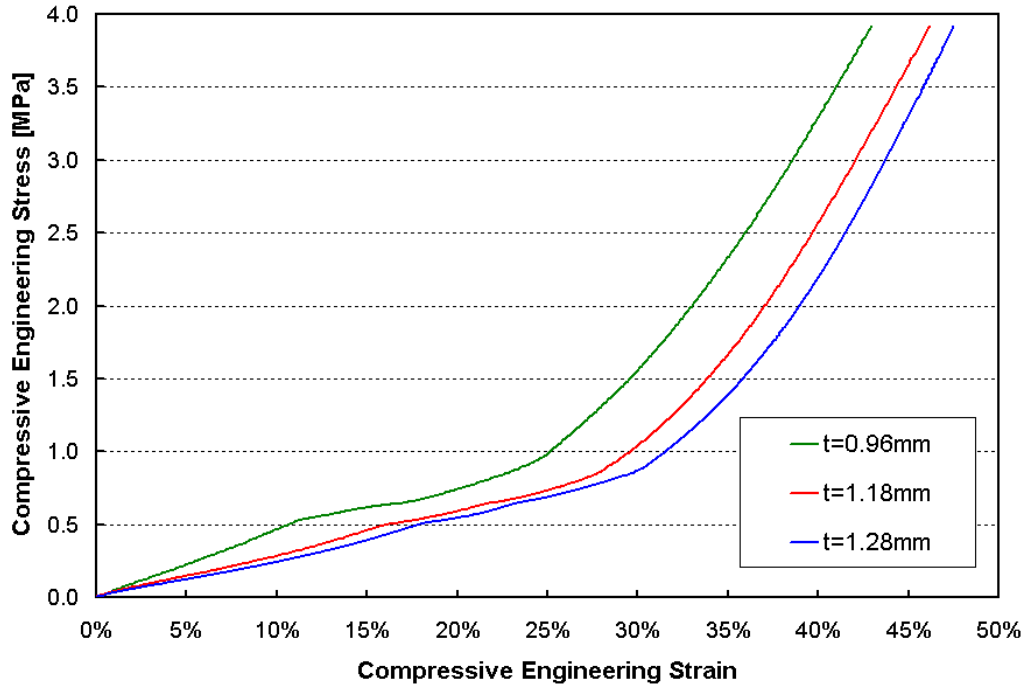
Figure 45: Compressive engineerin stress [MPa] vs. compressive engineering strain response for 1.0mm nominal thickness mastic specimens for loads up to 2000N.

A non-linear force displacement response is observed for all mastic thicknesses. For example, the 0.96mm thickness exhibits a transition around 300N that sees a marked softening of the response, similar to an oil canning response of a sheet. A transition to the final, highest, stiffness is then observed at 400N. This final stiffness is probably a result of the extreme compaction of the foam. As the foam is further compressed, any air pockets remaining are sealed and the mastic effectively behaves as a solid polymer layer. This multi-stage stiffness response becomes critical in numerical predictions. While the low load stiffness is roughly linear, this no longer remains true as the load level exceed 200N and should be accounted for in numerical models. As will be described later, limitations in the ability of the numerical simulations to capture this non-linear response became a limiting factor in the predictions.

3.2 Dynamic Dent Testing

3.2.1 Dynamic Dent Testing Setup

All dent testing was performed at ALCAN's KRDC facilities. A four-axis test bed was used for both the dynamic and static dent tests, with different loading apparatus for the each dent case. The dynamic test setup is shown in Figure 46, and schematically in Figure 47. The panel assemblies are clamped to the test bed with the four L-brackets shown in Figure 36.

Figure 46: Dynamic denting test setup.
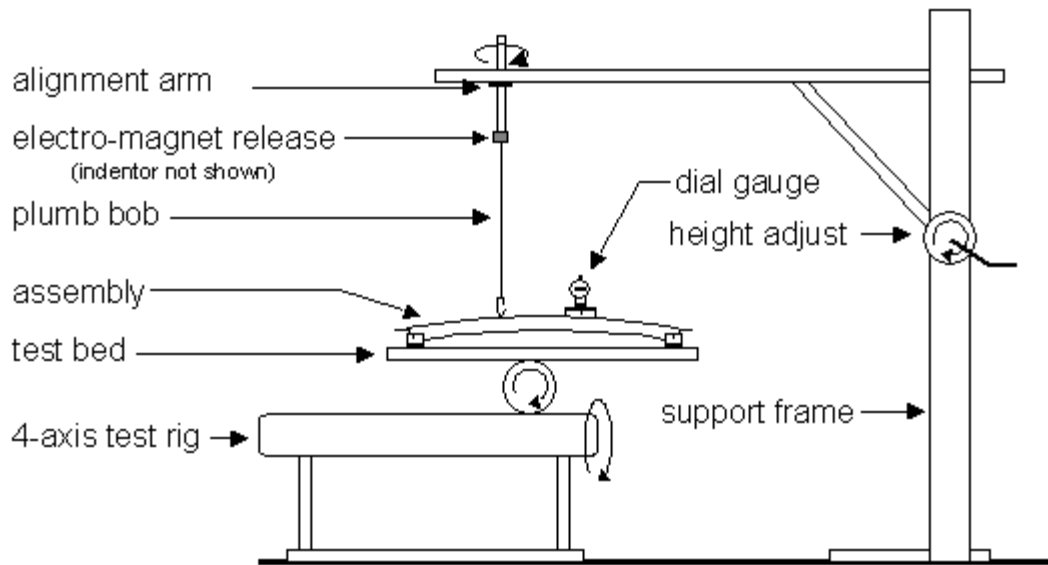
Figure 47: Schematic of dynamic denting test setup.

A normal impact is essential to ensure a maximum transfer of energy to the panel. The test bed can be rotated about two axes to level the assembly. A close-up of the rotational clamps is shown in Figure 48. The system allows for small adjustments in panel orientation to ensure a normal indentor impact. A small circular level, placed near the dent site, is used to verify the panel's orientation.

Figure 48: Close-up showing the rotational clamps on the denting test rig. The clamps can be unlocked allowing the cylinders to rotate freely in the supports.

The 25.4mm diameter spherical steel indentor is held above the dent site with an electromagnetic release mechanism as shown in Figure 49. The indentor is placed in a

magnetized nut, threaded to an adjustable alignment arm. The voltage to the magnet is adjusted as required to ensure the indentor is securely held in place. The alignment arm's height can be adjusted to achieve a desired drop height and its location can be maneuvered above the panel to a desired dent site. For large height adjustments a winch is used to raise and lower the main horizontal support bar. A plumb bob is attached to the release point and used to position the indentor over the desired dent site. Alignment of the release point using the plumb bob is shown in Figure 50. Once the release point is aligned, the indentor is put in place and then released via a remote switch. The indentor is caught after rebounding from the panel surface to prevent re-strikes of the dent sites. For the dynamic dent tests a drop height of 914mm, which translates to an impact velocity of 4.24m/s, was chosen. This height fell within typical drop height ranges, but most importantly it provided measurable dents for all the tests undertaken.

Figure 49: Close-up showing electromagnetic indentor release mechanism at end of the dynamic denting alignment arm. The 25.4mm spherical steel indentor is held by an alignment nut at the end of the threaded rod.
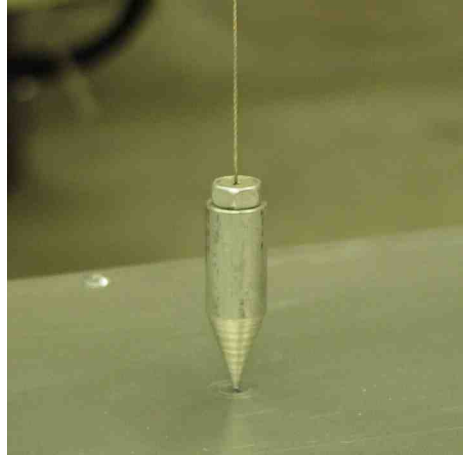
Figure 50: Close-up of plumb bob used to align the indentor release point above the dynamic dent site at the desired location and height.

3.2.2 Dynamic Dent Depth Measurements

The test appartus does not record the history of the displacement at the dent site during the denting process. As a result, a set of height readings is taken before and after the dent test to calculate the residual displacement at the test site. The height measurements were taken using a dial gauge mounted on an adjustable tripod platform, as shown in Figure 51. The tripod's feet, at a radial location of 38mm, are pointed and can be pressed into the outer panel leaving small permanent locating marks. These marks allow the tripod to be placed in the same position after the dent test. The tripod's feet can be adjusted to level the platform and ensure the height measurements are taken normal to the panel surface at the dent site. Three height measurements are taken and the difference between the averaged initial and final readings is recorded as the dent depth. The initial readings are taken at the centre of the dent site. After the test, the dial gauge is moved around the dent site, by sliding along the surface of the tripod, to locate the point of largest displacement, which is taken as the final reading. This manual location of the lowest point may introduce some error as the movement of the dial gauge tip can scratch the dent surface. Also, off-centre impacts will introduce small errors as the initial and final dent sites will not be identical. The dial gauge measures displacements to the nearest 0.001mm.

Figure 51: Close-up of dial gauge mounted on tripod platform. Three adjustable screws allow for leveling of the platform above the dent site to assure normal measurements. The screws are 38mm from the centre of tripod.

3.2.3 Dynamic Dent Test Sites

An array of dynamic dent tests was selected for both of the panel configurations. A schematic of the dent sites tested for configurations #1 and #2 are presented in Figure 52 and Figure 53 respectively. Material considerations limited the number of assemblies available for testing and so both static and dynamic tests were performed on the same assemblies by dividing the panel along the central axis. The array of dynamic test sites was chosen to examine the effect of the various support conditions on dent depth. Test sites directly above teacup locations were chosen to explore the role of the mastic, while locations centered between teacups examined the least supported sites. The effect of the panel edges, at both the wall and flange, were also considered. The difference in teacup spacing between the two configurations necessitated changes in the site array. Sufficient distance between dent sites ensured that the results of each test could be considered independent.
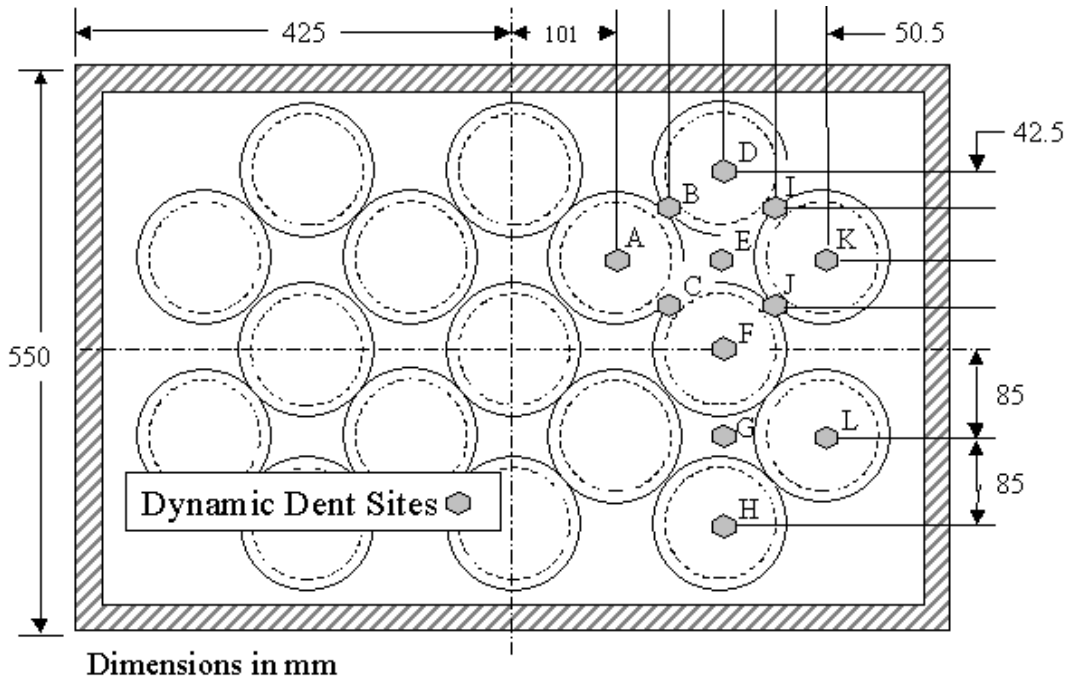
Figure 52: Dynamic dent sites for teacup configuration #1.
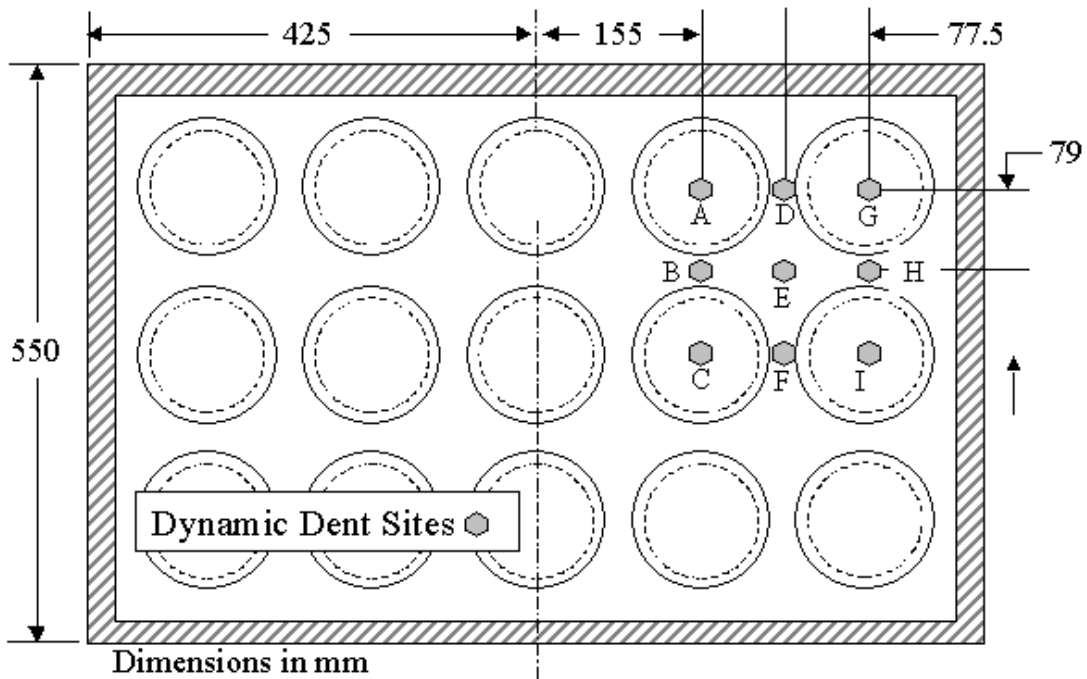
Figure 53: Dynamic dent sites for teacup configuration #2.

The assumption of symmetric panel conditions in the four quadrants of the assembly is limited by the variations in panel geometry due to welding distortion as well as the differences in mastic thickness, as discussed in Section 3.1.4. To examine the effect of

variations between quadrants, several symmetric dent sites were evaluated for some panel combinations. Sites D & H, E & G and K & L are symmetric for configuration #1 as shown in Figure 52.

The dent site arrays were laid out on the closure panels prior to testing. The locations were measured relative to the panel edges. The sites were marked with a circular sticker with an outer diameter of roughly 14mm and inner diameter of 7mm. The uncovered region was large enough to enclose the localized dynamic dents. A close-up of a typical dent is shown in Figure 54.
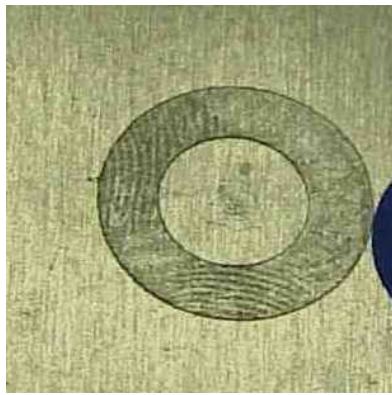
Figure 54: Close-up of a typical dynamic dent site showing the 14mm diameter sticker outlining the target site.

3.3   Static Dent Testing

3.3.1   Static Dent Testing Setup

The static dent tests were performed on the same basic test rig as used for the dynamic dent tests. The setup was altered for static testing by replacing the electromagnetic release mechanism with a cantilever loading arm. The static test used a set of loading weights, counterbalanced by another set of weights, to apply the desired static load. The static test setup is shown in Figure 55. A schematic of the setup showing the basic features is presented in Figure 56. The test bed is aligned as described in the dynamic test setup to assure loading normal to the dent site.

.

Figure 55: Test rig configured for static dent testing.
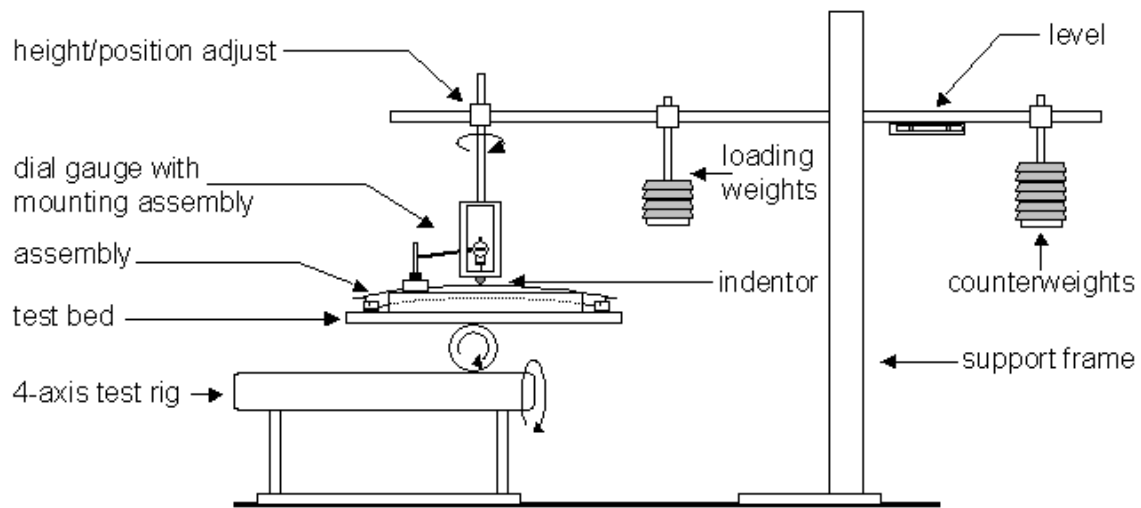
Figure 56: Schematic of static test setup.

Prior to application of the static load the horizontal arm of the setup must be leveled. The moment caused by the counterweights is balanced by the moments of the loading arm, located above the dent site, and the loading weight platform. The loading weight platform is located at the midpoint of the horizontal arm's pivot point and the indentor location. This establishes a 1:2 loading ratio such that the applied denting load is half the applied load weight.

The indentor is a 25.4mm diameter steel hemisphere mounted to the base of a rectangular section that acts as a loading arm as shown in Figure 57. This loading arm is located directly above the dent site, with a minimal initial contact at zero load. A dial gauge is mounted inside this section with its measurement tip normal to the dent site, above the indentor. The gauge itself is mounted with a magnetic clamp, supported on a moveable cross-member such that the gauge's weight is not applied to the panel. The dial gauge setup is also shown in Figure 57. The gauge measures the normal displacement of the indentor, which is equivalent to the deflection of the panel.
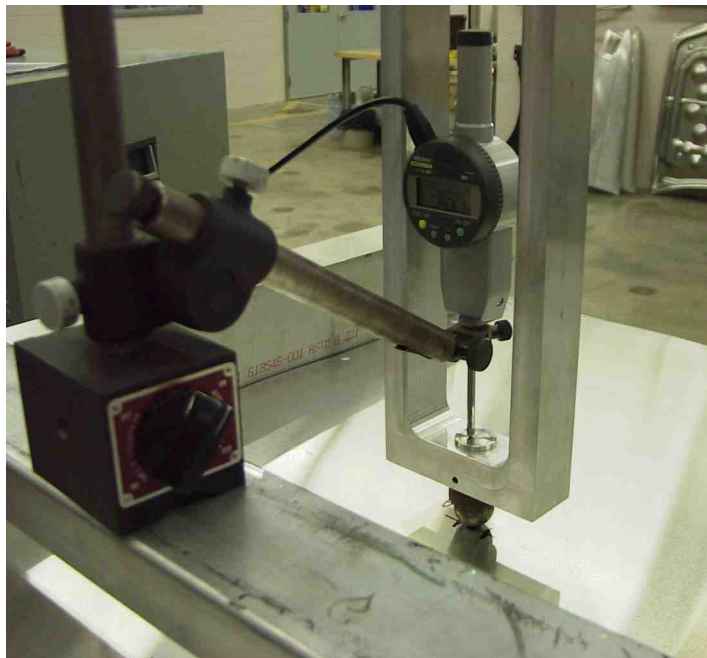
Figure 57: Close-up of dial gauge used in static dent testing. The gauge is suspended with a magnetic clamp mounted on a cross-member above the indentor. The dial gauge measures the normal displacement of the indentor.

3.3.2 Static Denting Procedure and Dent Measurement

The static tests consisted of several loading increments. An initial pre-load of 4.45N (1lbf) is applied to initiate contact between the indentor and panel prior to application of the loading weights. Static dent loading was performed in increments of 22.2N (5lbf) as listed:

1- the application of a 22.2N load increment
2- a one minute time delay to allow the panel to settle
3- recording of the panel displacement

4- steps 1 to 3 are repeated until the desired peak load is reached

5- unloading of the panel

6- a one minute time delay to allow the panel to settle

7- recording of the residual panel displacement

8- repeat steps 1 to 7 for the nest desired peak load

The peak loads were to progress from 22.2N to 244.7N in 22.2N increments. However, this was modified to reduce the testing period. The length of time the panel is allowed to settle is somewhat arbitrary as the degree of measurement drift varies for different tests. For the panel assemblies tested, the drift in the measurements was substantial, particularly after unloading. For the more compliant assemblies, recovery could cause the residual displacement to vary by over 0.05mm when a ten minute delay was used. For the stiffer panels the degree of recovery was lower. For consistency, a one minute delay between reaching the load state and recording of a measurement was used. The peak loads used in the loading sequence for the static tests were as follows: 22.2N, 44.5N, 66.7N, 111.2N, 155.7N, 200.2N and 244.7N. Each peak load was reached in 22.2N increments and a displacement was recorded for each interval. The loading profile is shown in Figure 58.

Each solid point represents a
1 minute dwell time
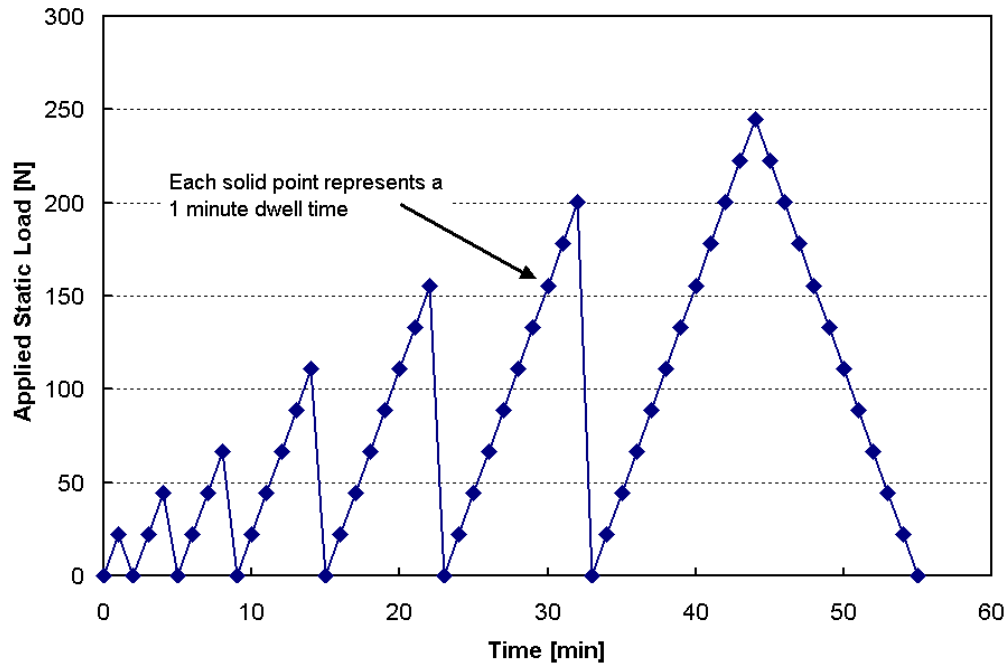
Figure 58: Loading profile used for static dent tests. The solid points on the graph represent loads at which a one minute dwell time was allowed prior to recording the displacement.

This process generated complete loading curves for all peak loads reached. Unloading was in a single step with no intermediate displacement measurements for all cases except the final 244.7N load. Panel stiffness can be examined by constructing a force-displacement curve using the displacements at each peak load. Between each peak load the panel was unloaded and a residual displacement was recorded. This residual displacement is treated as the static dent depth.

3.3.3 Static Dent Test Sites

The static dent sites were marked on the panel prior to testing. Due to the lengthy time requirements for static testing, only a smaller number of test sites were selected. Each panel was tested at three sites (A-C), with limited testing of symmetric dent locations (BB&CC). Again, a contrast between supported and unsupported regions was the key concern. The layout of the static dent sites for teacup configuration #1 and #2 are shown in Figure 59 and Figure 60, respectively. The effect of the sidewalls is examined through comparison of sites A and C. While both sites are directly above a teacup, they experience different interactions with the sidewalls and flanges. The static test sites are spaced at larger intervals, compared

to the dynamic sites, due to the larger area affected in static denting. As the load increases in static denting, a visible region of deflection moves outward from the dent site. Though the permanent deformation is localized, it is important to adequately space the static dent sites to prevent any site to site interaction and thereby maintain the independence of the individual dent tests.
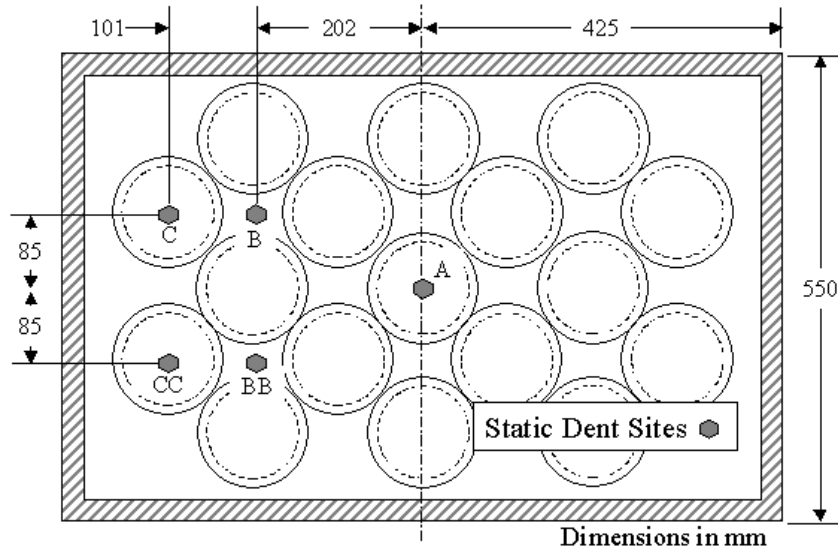
Figure 59: Static dent sites for panel assembly with teacup configuration #1.
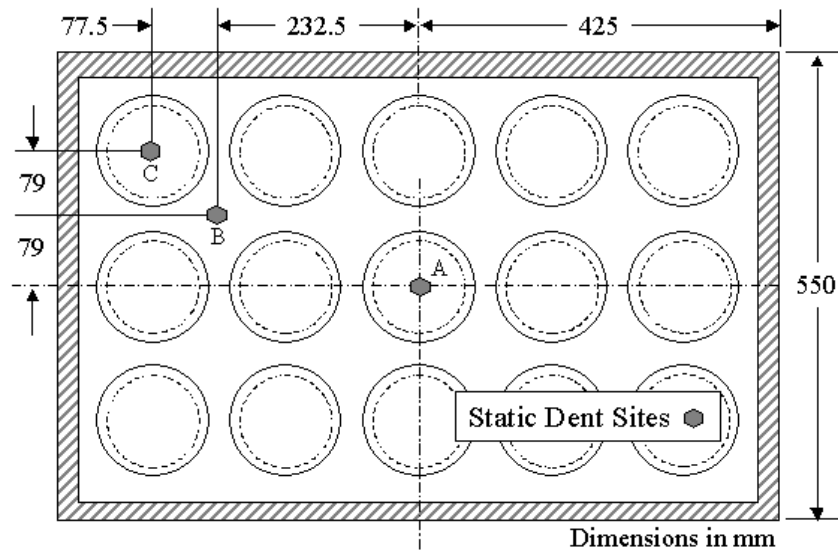
Figure 60: Static dent sites for panel assembly with teacup configuration #2.

4 Numerical Modelling

4.1 Numerical Modelling Overview

Numerical modelling of the denting of the panel assemblies involved several steps, with variations in the approach for the two different types of denting. The two denting processes are different physical problems that are best modelled with different numerical techniques. As outlined in Section 1.7.1, there are two time integration approaches available for the solution of the fundamental equation of motion, explicit and implicit time integration. As discussed, the explicit solution is well suited to dynamic problems where a reasonable velocity will allow for an efficient solution method. The dynamic denting process is ideally suited for explicit time integration methods as the indentor velocity leads to manageable simulation times. Conversely, the static denting process is best suited for implicit solvers, where quasi-static equilibrium states are found as the load is applied.

Regardless of the type of denting an initial mesh of the panel assemblies is required. These meshes were constructed using SDRC IDEAS [68], a solid modelling package with various finite element capabilities. While the IDEAS solvers are not well suited for the dent modelling, the package is an effective option for mesh generation. The development of the initial mesh must also incorporate the various boundary conditions, inherent in the experiments, in the numerical models. A key concern in the development of the finite element mesh is the degree of mesh refinement necessary for accurate results balanced with the computational costs. As several dent locations were modelled on each assembly, it was also desirable if one initial mesh could be re-used for various sites thereby limiting model development requirements. An ideal tool for the generation of various locally refined meshed assemblies, based on an initial general model, was the D-Mesh software developed by Thomas [4] as part of the overall dent resistance study at the University of Waterloo. This

software allowed for local mesh refinement of the base model at each of the dent sites. A typical refined mesh with a cutaway view of the assembly interior is shown in Figure 61.
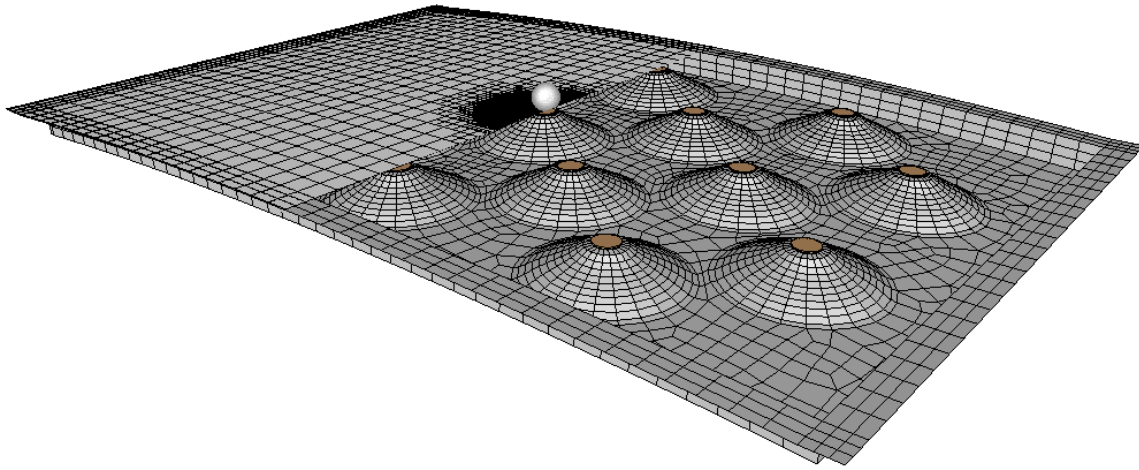
Figure 61: Cutaway view of a typical denting model with local mesh refinement at the dent site.

The numerical simulations were performed using LS-DYNA Version 960 [69], a non-linear finite element code with both explicit and implicit solvers. LS-DYNA was initially solely an explicit code, but has recently incorporated an implicit capability previously available in LS-NIKE. A main reason for the inclusion of the implicit capability was for springback modelling of sheet metal forming. After forming, it is often necessary to determine a part's final geometry after it is removed from the tooling. The need for springback solutions also arises in the case of dynamic denting. After the indentor impact, a springback analysis is necessary to determine the final deformed state of the panel, and thereby extract the dynamic dent depth. As a result, the dynamic denting process is modelled in two stages, first the dynamic dent is modelled using the explicit solver and then the springback solution is found using the implicit solver. For static dent analysis, the entire process is modelled using the implicit solver.

The simulations were performed at the University of Waterloo on a 4 processor Silicon Graphics Origin 200 with 2 gigabytes of memory, or later in the study, on a 16 node Linux PC cluster. The Linux cluster was configured with 256MB of memory on the majority of the nodes. Other the simulations were performed at ALCAN KRDC on an 18 processor Origin 2000 with 9 gigabytes of memory.

4.2 Numerical Models of the Panel assemblies

The numerical model was developed in two stages. The initial geometry and mesh were developed in the solid modelling package IDEAS and then translated into an LS-DYNA input format. This translation was performed using an in house software package [70] that transfers the node, element and boundary condition information. The second component of the model generation involved the implementation of the various model requirements in the LS-DYNA input deck. These requirements included the boundary condition necessary to capture the interaction between components of the panel assemblies, the appropriate constitutive models for the given materials and the element formulations used for the various meshed parts.

4.2.1 Finite Element Mesh of Inner and Outer Panels

The development of the base finite element mesh, prior to any local mesh refinement at a particular dent site, required consideration of the expected loading and deformation along with the interaction between the various parts. The shell element meshes, for the inner and outer panels, were constructed at the mid-plane of the particular part. This approach requires a half thickness offset above and below the mesh to account for the panel thickness as shown in Figure 62.
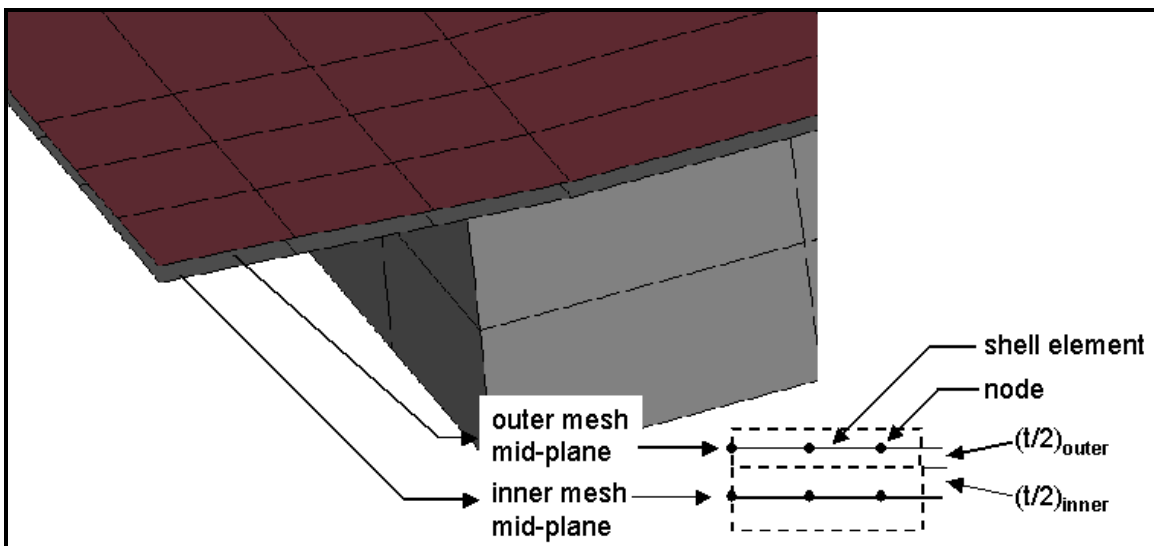
Figure 62: Shell element mesh at mid-plane of the inner and outer panels showing required half thickness offset.

The inner panel was the more challenging part to mesh, as developing a solid model that accurately captured the actual panel geometry was non-trivial. The inner panel was constructed by welding the teacups and sidewalls to the base panel as detailed in Section 3.1.2. Also, cutouts in the base panel were made below the teacups. Attempting to model the various welds and cutouts would add unnecessary complexity to the mesh development. Rather than model the teacups as separate parts, attached to the base plate through a numerical constraint simulating a weld, it was decided that a single, contiguous mesh was the optimal approach. The welded joints between the teacups and base panel are not a critical component of the simulation and thus can be excluded for simplicity. Similarly, the welds joining the sidewalls and flanges were ignored. The inner panel was thus modelled as a single part that could be meshed across these joints with a single mesh as shown in Figure 63.
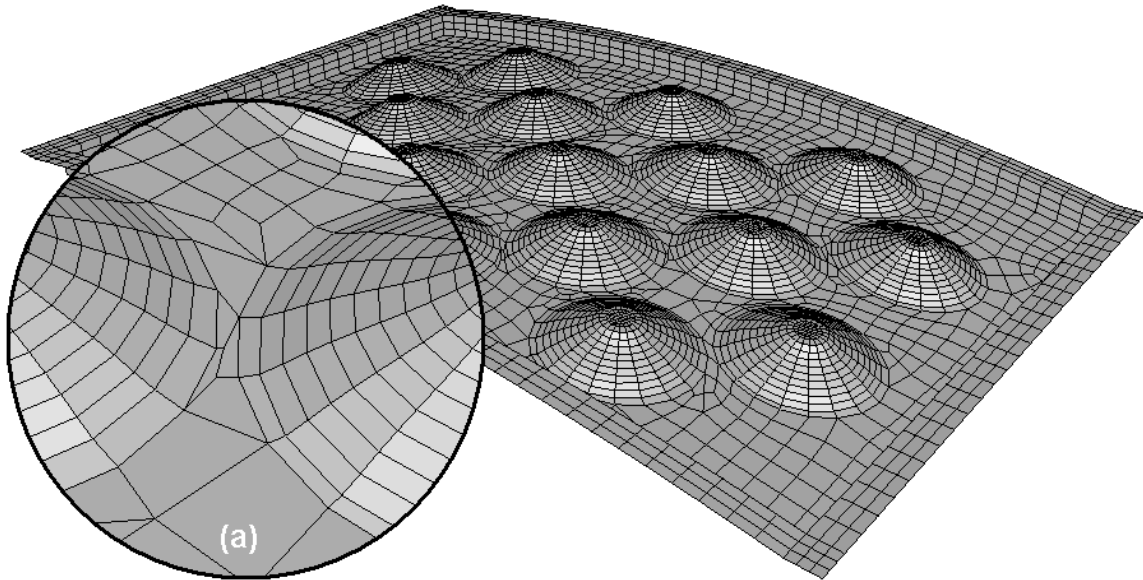
Figure 63: Typical mesh of inner panel generated in IDEAS. Inset (a) shows the region between teacups where the free meshed elements can become distorted.

The inner mesh was relatively coarse as the inner panel is expected to experience no permanent deformation. The panel geometry must be captured to accurately represent the inner stiffness and support of the outer panel, but this is accomplished without an overly refined mesh. The mesh is mapped on the teacups, to assure a reasonable representation of the teacup geometry, and around the edges and flanges. The base of the panel was meshed using the free meshing algorithm of IDEAS. Due to the relatively small spacing between the

98

teacups at their base, where they meet the inner panel, the free mesh elements are sometimes highly distorted which lead to longer simulation times. This mesh distortion is shown in the inset view of Figure 63.

The outer panel was partitioned into multiple regions corresponding to the outer flanges and the teacup locations. These partitions ensured that the mapped outer mesh would always have a node directly above the teacup. The presence of a node directly above the centre of each teacup simplified future mesh refinement. Also, the presence of a node on the outer panel directly above the centre of a teacup, combined with a node on the inner panel at the centre of a teacup would allow the implementation of a discrete spring element to simulate the mastic layer. The details of the mastic implementation will be described in a separate section. A typical, unrefined outer panel is shown in Figure 64, highlighting the correspondence between the inner and outer meshes. An element size of roughly 20mm by 20mm was specified. The initial meshes for the combined inner and outer panels consisted of 7500 to 9500 elements depending on the panel curvature.
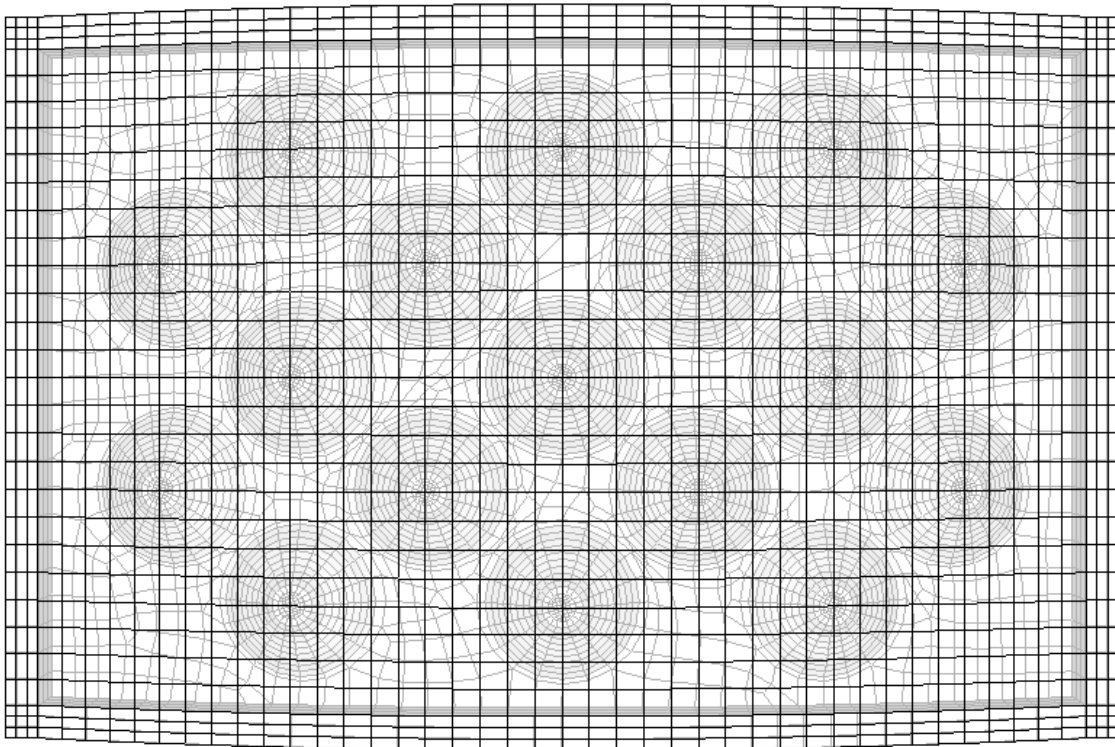
Figure 64: Unrefined mesh of the outer panel superimposed on the mesh of the inner panel. The meshes around the flanges and atop the teacups are aligned between the panels.

99

4.2.2 Simulation of the Mastic Layer

The mastic layer joining the inner and outer panels proved to be a critical aspect of the simulation. The mastic acts as a spring-damper between the inner and outer panel and its accurate representation is essential. The mastic undergoes a high degree of compression as the indentor loads the outer surface of the panel. The mastic controls the interaction between the inner and outer panels, particularly when denting directly above a teacup. Two options were explored for the numerical representation of the mastic.

Initial models were developed using discrete spring elements, defined in the input deck, which connected the inner and outer panel at the top of each teacup. These discrete elements could then be modelled using one of a variety of spring formulations available in LS-DYNA. For models using the discrete elements, the mastic would appear simply as a linear element joining the two nodes that defined the spring. The spring elements will only transfer loads in the direction of the spring. Another drawback with the use of spring elements is the concentration of the mastic reaction forces directly at the centre of the teacup, rather than over a distributed area.

The final models, used for the bulk of the numerical predictions, used solid elements to represent the mastic layer. The introduction of solid elements offers a more realistic representation of the mastic pads, as they are able to capture the crushing of the mastic layer. Also, the use of solid elements alleviated concerns with a discrete spring-based representation. The solid elements add numerical complexity and cost, as the mastic pads must be represented by small elements. The use of two solid element layers through the 1mm thickness of the mastic pad, coupled with mesh density to reasonably capture the circular shape of the pads, led to the small element size. A close-up of a meshed mastic pad on the top of a teacup is shown in Figure 65.
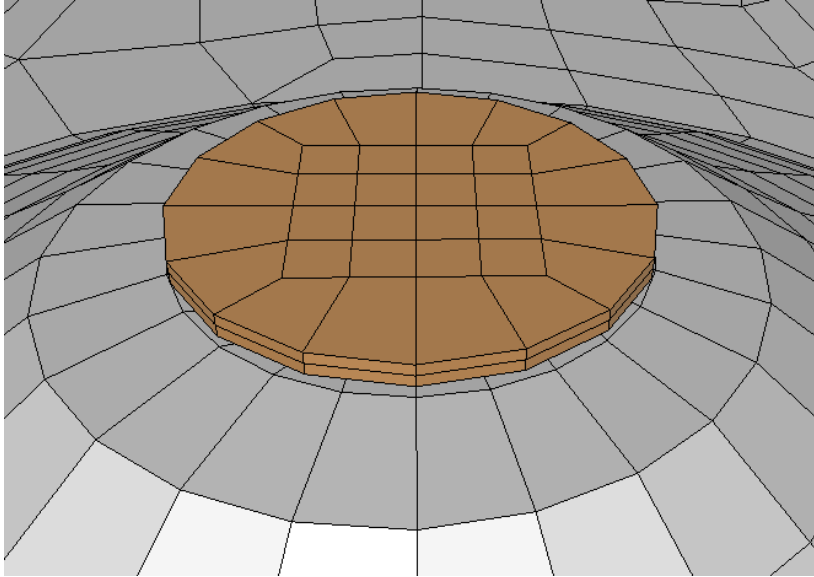
Figure 65: Close-up of a meshed mastic pad, with diameter of roughly 25.4mm, showing the two layers of solid elements through the 1mm thickness.

4.2.3 Element Formulations

In choosing an element formulation, a trade-off between accuracy and computational cost is often required. The degree of both in-plane and through-thickness discretization associated with the element formulation chosen will directly control the simulation time and will influence the accuracy of the results. The recommended element for springback analysis is shell element formulation #16 [71]. This formulation, based on the work of Simo & Armero [72], is fully integrated using a 2 by 2 array of in plane integration points. This element has replaced the reduced integration Belytschko-Tsay element formulation as the recommended element for forming simulations. Previous springback simulations had used the reduced integration element for the forming process and then switched to a fully integrated element for the implicit springback analysis. The limited in-plane stress data associated with the single integration point element caused convergence issues in the springback analysis. The new recommended formulation can be used throughout a simulation, with both the explicit and implicit solvers, and performs well in implicit solutions. The Simo & Armero element is substantially faster then the previously recommended fully integrated element, but does present a computational cost in comparison to the Belytschko-Tsay element formulation. The Simo & Armero element was used for both the explicit and implicit stages of all the

101

simulations performed. An added benefit of using a fully integrated element is the elimination of the need for hourglass control of the shell elements.

The second consideration with respect to shell element formulation is the type and degree of through-thickness integration chosen. The use of shell elements, as opposed to brick elements, is well suited for the inner and outer panels that undergo little through-thickness deformation. The shell elements use a through-thickness approximation to account for the bending effects experienced by the panels. The number and spacing of through thickness integration points is prescribed in the input decks for both the inner and outer panel meshes. A Gaussian distribution of five through-thickness integration points was assigned to the outer panel. The outer panel will undergo the majority of the deformation and, as such, a detailed through-thickness approximation is needed. Since the inner panel is assumed to see little deformation it was only assigned three through-thickness integration points.

The solid elements used to model the mastic can also use a reduced integration element if desired. However, the need for accurate stress data for springback again dictates the use of a fully integrated element. Also, for implicit solutions it is strongly recommended that a fully integrated element, solid element formulation #2 in LS-DYNA, be used [73]. The fully integrated element uses eight internal integration points arrayed in two layers of 2 by 2 points. Another benefit of the fully integrated element was that it helped prevent the mastic elements from crushing under high loads. The fully integrated element was better able to numerically support the load and helped prevent the elements from collapsing and reversing themselves.

4.2.4 Constitutive Models

For the panel assemblies the constitutive model chosen for each component of the model was based on the expected deformation of the part. In the case of the mastic, the material modelling options were limited by the choices available in LS-DYNA.

The AA6111 outer panel requires a detailed material model that incorporates the strain hardening behaviour of the material. Several material models in LS-DYNA allow the user to input a flow stress vs. effective plastic strain curve as part of a broader constitutive model. This option allows actual material test data, discussed in Section 3.1.1, to be used in the numerical simulations. In order to use the stress-strain data from the tensile tests, the data

must be changed into the necessary format. Using the true stress and true strain data (ε_{tot}), the effective plastic strain (ε_{pl}) for a given flow stress (σ) is found using the following equation:

$$\varepsilon_{pl} = \varepsilon_{tot} - \overline{\sigma}\big/E \qquad (12)$$

The resulting plastic strain vs. flow stress data is then entered in a piecewise linear curve along with the initial yield strength of the material and the elastic constants. The stress-strain curves used for the simulations are shown in Figure 66.
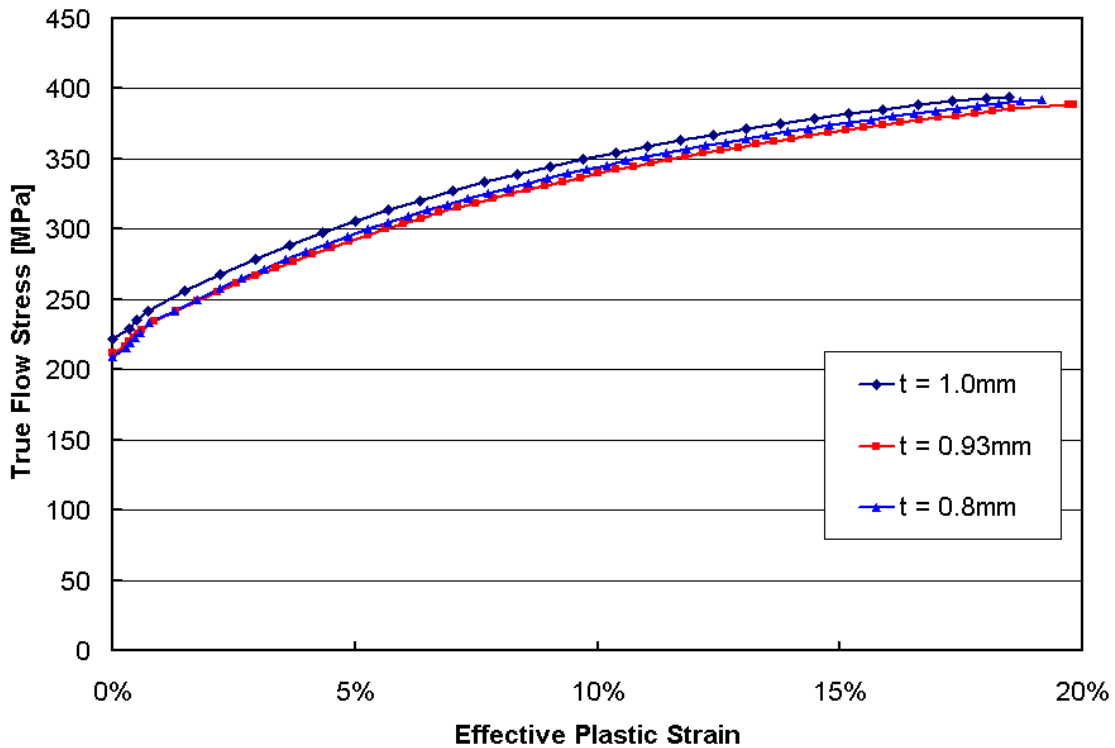
Figure 66: Effective plastic strain vs. true flow stress [MPa] used in numerical simulations for the three thickness AA6111 outer panels.

The second consideration of the material modelling is the constitutive model selected. As alluded to earlier, the use of an anisotropic material model is highly recommended for forming simulations. Lamontagne [60] examined the effect of various constitutive models in the forming of aluminum parts and recommended the anisotropic, Barlat material model [74]. However, for the small, localized deformations in denting analysis, the benefit of an anisotropic material model is questionable. A less expensive alternative from a numerical standpoint is the use of the isotropic Von Mises yield criterion. Thomas [4] examined the

difference in dent predictions, comparing the Barlat and Von Mises criterion, and found no notable improvement in accuracy in simulations with the anisotropic material model. For this study, the simpler Von Mises yield criterion was chosen for all the dent simulations.

The inner panel undergoes essentially an elastic deformation as the panel deflects and recovers with little or no permanent change in geometry. As a result an elastic material model was chosen for the inner panel and only the Young's modulus, 70,000 GPa, and Poisson's ratio, 0.3, were required for the material model. Simulations were performed using an elastic-plastic material model similar to that used for the outer panel and no notable difference in the dent depth predictions were observed. The use of the simplified elastic material model offers some computational savings.

The most challenging material to model has been the mastic. As outlined in the discussion of the meshing of the mastic, the material models available are tied to the representation chosen for the mastic. For the discrete spring elements, a variety of spring material models are available in LS-DYNA, while the number of alternatives for the solid element models are somewhat limited. The spring models allow for various levels of detail for the modeling the force-displacement response. The option chosen for the spring-based models was a non-linear elastic spring model. This non-linear elastic spring required a force displacement curve that covered the compressive and tensile regions of the spring behaviour. The material is modelled as fully elastic, using the same curve for loading and unloading. A more generalized non-linear spring allowed for the inclusion of unloading curves that impart some degree of permanent settling or residual deformation in the spring. These unloading curves are applied when the spring reaches a peak force in compression or tension. This option proved ineffective as the level of unloading confused the denting measures.

As will be discussed, the solid mastic elements were limited to a linear elastic material model. This approximation proved to be an area of great concern as the non-linear nature of the mastic material, seen in Figure 44, is poorly represented by a linear fit for many cases. In order to choose a value for the Young's Modulus of the mastic, initial models were run to examine the load levels experienced in the mastic layers. It would be impractical to attempt to determine an appropriate stiffness approximation for every individual simulation. As a result, a somewhat arbitrary load level of 500N was chosen as the upper limit for curve fitting. The resulting curve fits for the three thin mastic compression test are shown in Figure

67. The variation in stiffness approximations, the constant in the curve fitting equations, highlights the effect of even small changes in mastic thickness. The variation in the assembled panel mastic thickness layers, as presented in Figure 40, coupled with this variation in stiffness for this small range of thickness change, highlights the potential variation in dent depth predictions when assuming a constant mastic thickness.
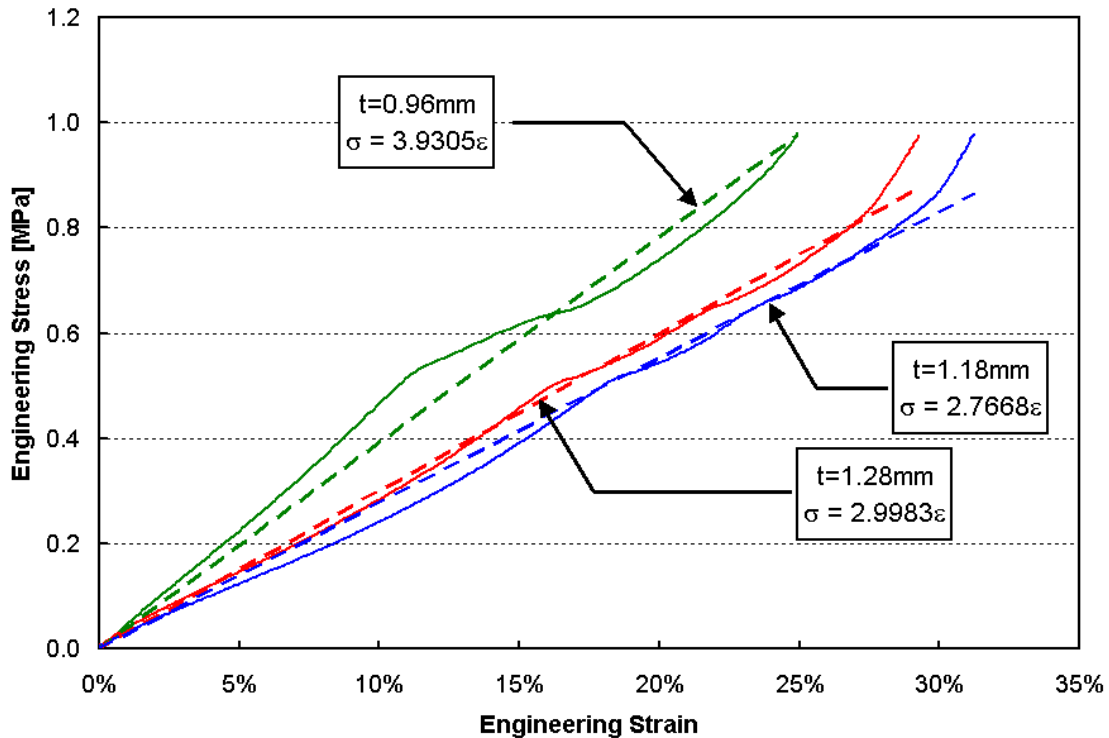
Figure 67: Linear approximations of mastic stiffness, based on force-displacement data up to 500N, for three test conditions. The load level is based on numerical contact forces observed in preliminary denting simulations at sites directly above teacups.

All simulations used a mastic stiffness approximation of 3.93 MPa, based on the 0.96mm mastic test. A single stiffness was used in both compression and tension. A consistent stiffness allowed the parametric evaluation of the other factors affecting the dent depths. However, this leads to errors in the dynamic predictions, particularly in regions away from the teacups and mastic pads. For dent sites away from the teacups, the magnitude of the contact forces experienced by the surrounding mastic pads will be significantly less than 500N and as such the linear approximations are often poorly suited for these cases. Further concerns with regard to the stiffness approximation are tied to the nature of the compressive tests themselves. The compression of the very thin mastic layer creates a highly constricted,

near plane strain condition, due to the lateral confinement of the material. As a result, the Young's Modulus approximation is no longer based on a standard uniaxial test, but rather on a stiffer test condition. This introduces further potential error in the mastic representation, in the form of an over prediction of stiffness. Alternative mastic stiffness values have been used for a limited number of dent predictions to examine the role of the mastic stiffness on the accuracy of results.

Attempts to model the mastic with non-linear elastic material models have been hampered by the lack of available material models of this type in LS-DYNA. Several material models designed to model foams and rubbers are available in LS-DYNA, some of which do include non-linear elastic stress-strain curves. However, the majority of these models are not available for implicit solutions. One material model, Material Type 57, that will function in the implicit stage of the simulation was designed to model low-density foams. This model allows for the input of a non-linear stress strain curve for the compressive response of material and a linear stiffness in tension. This material seemed promising for application with the panel assembly models. Unfortunately, the material model does not appear to be working correctly in the implicit stage of the solution. Failure to find convergence during implicit iterations or severe distortion of the solid elements occurred in all simulations using the low-density foam material model. As a result, the linear elastic material model is the only currently viable material modelling option for solid mastic elements.

4.2.5 Boundary Conditions

The modelling of the panel assembly boundary conditions includes both the attachment bracket support points and the rivets connecting the inner and outer panel flanges. The four nodes closest to the bracket locations were fully constrained, reflecting the test conditions at the supports. This approximation appropriately captures the physical behaviour of the panel assemblies with a simple and efficient approach.

The rivets were modelled using a simplified constraint-based boundary offered in LS-DYNA. A spot weld constraint, in this case the *constrained_generalized_weld_spot option, was used to model the rivets. This option was used primarily because it was supported by both the implicit and explicit solvers and could be used during both a dynamic dent and the

subsequent springback analysis. The rivets, or spot welds, are defined in nodal pairs, using one node from both the inner and outer panel flanges. The two nodes are tied such that their translational and rotational motions are identical creating a rigid beam between the corresponding nodes. The alignment of the inner and outer meshes highlighted in Figure 64 helps to assure the numerical constraints are aligned in a similar direction to the actual rivets.

4.2.6   Contact Surfaces

Several contact surfaces are defined for the panel assembly simulations. LS-DYNA offers three different contact methods. For the majority of numerical forming models the penalty method is the most appropriate choice. The penalty method places a normal interface spring between all penetrating nodes and the contact surface. This method is recommended in LS-DYNA as it conserves momentum at the contact interfaces and limits mesh distortion [75]. The interface stiffness values are of the same magnitude as that of the contacting elements and, as such, do not control the time step size. This method is well suited for cases where intermittent contact will occur, since it allows the contact surface to readily open and close.

Penalty based contacts were used for all the various interfaces in the assembly models. The contact between the indentor and outer panel was modeled using a simple surface to surface contact with a friction coefficient of 0.1. Frictional forces at the various contact surfaces are not critical in the panel assemblies and the 0.1 value was an arbitrary selection. Variation of the friction coefficient had a minimal impact on the results. The contact surface considers element thickness in the contact calculations.

The inner and outer panels are in contact around the surrounding flange and a contact surface was thus defined between the two parts. Models without this contact surface saw penetration of the two parts around the periphery in regions away from the rivet constraints. This penetration is unacceptable, particularly when the examination of support conditions is the principal goal of the work. A similar two-way contact surface as that used for the indentor to outer panel was defined for the inner to outer panel contact. However, a modification to the contact surface was required after difficulties in achieving implicit convergence were observed. Based on recommendations from LSTC [73] an optional control card was used for the inner to outer contact surface. LS-DYNA introduces "numerical sticking", between parts that attempt to separate, to improve implicit

convergence. This increased sticking is the default setting for implicit contact, but is not used in the explicit portions of simulations. This sticking option applies a gradually increasing contact stiffness prior to penetration of the contacting parts, which is designed to anticipate contact and thereby stabilize the solution. This sticking does not apply any contact force prior to actual penetration. The improved sticking option is illustrated in Figure 68.
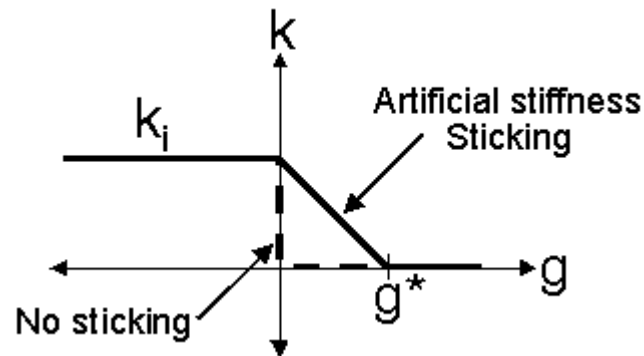
Figure 68: Artificial stiffness introduced in implicit contact to cause sticking between surfaces. Starting from a surface to surface gap (g) of g* a contact stiffness is prematurely introduced until contact is achieved (g=0) with the corresponding interface stiffness k_i.

In the case of the inner and outer flange contact, this sticking causes problems since the contact surface naturally wants to open and close intermittently. In essence the contact around the flange can be visualized as a wave like motion as the inner and outer panel contact opens and closes. The introduction of sticking attempts to hold the two panels in contact and introduces convergence difficulties due to this artificial numerical stiffness. In order to achieve implicit convergence, particularly during springback, it was necessary to deactivate the sticking option.

The final contact surfaces required in the models were between the mastic and the inner and outer panels. When modelling the mastic as solid elements it is necessary to define contact surfaces between the top of the teacups and the bottom of the mastic, as well as between the top of the mastic and the outer panel. These contact surfaces should reflect that the mastic layer is bonded to the panels and does not separate. A kinematic constraint based contact surface, used in initial models, which tied the nodes of the mastic to the appropriate panel surface, were not supported in the implicit solution phase when other penalty based contact surfaces were present. As a result, a modified tied interface that uses the penalty method was used to model the mastic contact surfaces. The penalty-based tied interface

requires an offset between the node and the surface that is maintained throughout the simulation. This offset distance must be within a minimum distance that is based on the size of the elements on the contacting surface. The offset method maintains the initial gap between the nodes and surface using a modified penalty method implementation. The modified penalty method enforces contact interface stiffness in both the opening and closing directions to maintain the position of the nodes relative to the panel surface, as shown in Figure 69. A tensile force is generated to maintain the initial gap in cases where the surface tries to open. This contact was defined by selecting all the nodes on a given mastic surface and tying them to corresponding panel elements.
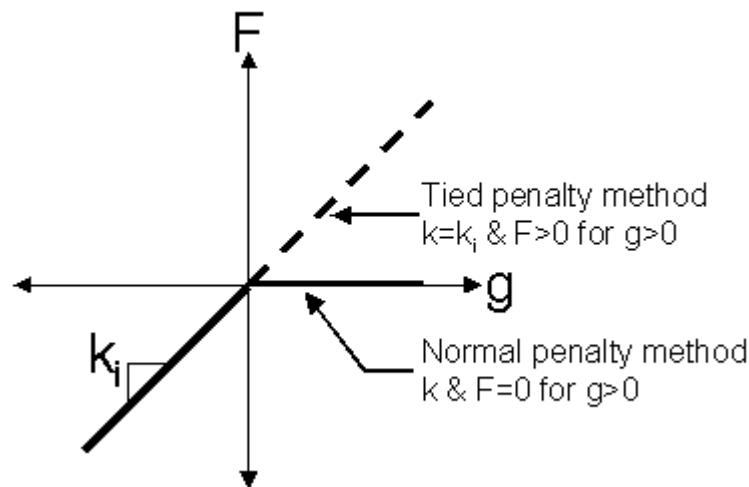
Figure 69: Tied contact penalty method implementation. An identical contact stiffness is applied for gap (g) opening and closing, where g=0 is the initial gap between the mastic and surrounding panel. A tensile force is generated to maintain the node position relative to the surface when the parts try to separate.

4.3 Local Re-Meshing

Prior to running the denting simulations, the initial base meshes were locally refined for each dent site. Generally, a model of a formed part will have insufficient mesh refinement in the flatter regions of low straining, which are of interest in subsequent dent resistance analysis. A formed part will require fine meshes, often using an adaptive mesh refinement algorithm, in areas of high strain such as corners and sharp bends. While the initial meshes for the panel assemblies were not defined by forming requirements, the use of a local re-meshing utility was still desirable. A base model was meshed with a coarse element distribution on the outer panel, as seen in Figure 64, that could later be refined at the node above each dent site. This

reduced the meshing time substantially and provided a consistent degree of mesh refinement for each dent site. The effect of mesh refinement, on the resulting dent depths, could also be easily explored.

The re-meshing was performed using a software tool, D-Mesh, developed by Thomas [4]. This tool allowed for local mesh refinement at specified nodal or Cartesian locations using one of two re-meshing algorithms. Both re-meshing algorithms require a radius of refinement, and retained all the original node positions. The first algorithm uses a specified number of refinements and then constructs increasingly refined, generally evenly spaced, refinement bands. The final element size is a result of the number of refinements and the refinement radius specified. The second, area-based, refinement algorithm uses a target element size and creates a large highly refined region, with small transitional refinement regions connecting to the base mesh. A comparison of meshes using the two algorithms, with a 100mm radius of refinement, is shown in Figure 70. The transition between different sized elements requires the introduction of mid-edge nodes at various locations. The mid-edge nodes may be replaced using triangular elements if desired.
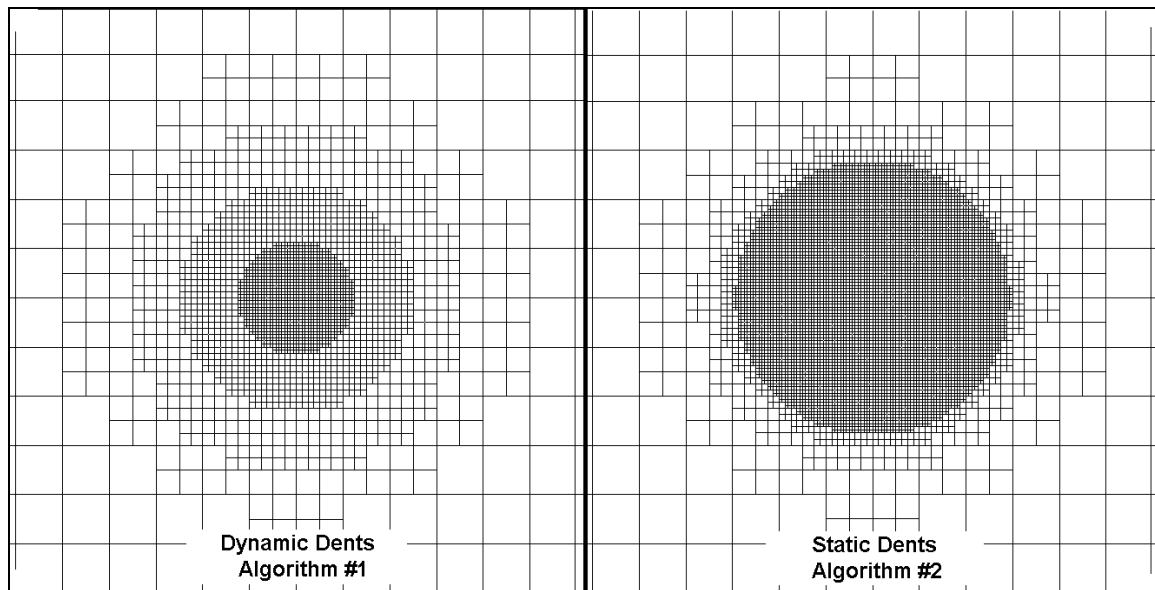
Figure 70: Comparison of D-Mesh refinement algorithms for a 100mm radius of refinement. Algorithm #1 used in dynamic dent simulations has a more gradual element refinement gradient. Algorithm #2 used in static dent simulations has a large region of high refinement.

110

Algorithm #1 was used in the dynamic dents as it provided sufficient local refinement directly at the impact region. The static dent sites were refined using algorithm #2 to provide a larger region of highly refined elements to better capture the larger, more global deformation. Both algorithms provided elements of roughly 1.3mm by 1.3mm in the most refined regions. D-Mesh also recaptures lost panel curvature resulting from insufficient mesh resolution. The software approximates the panel curvature, using the existing nodes, by fitting a series of bi-hermite patches to the base mesh surface. The additional nodes generated in mesh refinement are then projected on to these interpolated patches thereby recapturing lost panel curvature. This option improves the model accuracy and allows better representation of the panel geometry.

The re-meshing utility was also used to insert the indentor at the required location. The indentor is oriented along the normal direction at the dent location and a specified initial velocity is generated as three vector components. The magnitude of the velocity vector, 4.24mm/ms, corresponds to the experimental drop height. The indentor is treated as rigid in all dent simulations. The meshed indentor is shown in Figure 71, illustrating the refined solid element mesh at the base of the indentor in the contact region. The refinement in the contact region, using elements measuring 1mm by 1mm, captures the indentor geometry better.
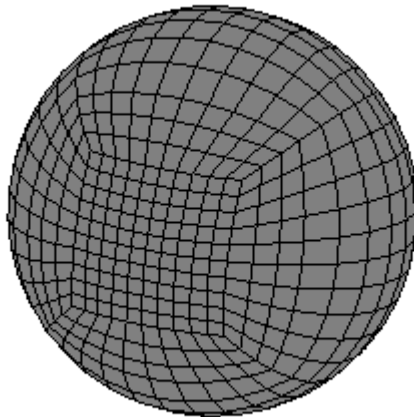
Figure 71: Meshed solid element indentor, with local mesh refinement at the contact area, inserted normal to the dent location using D-Mesh.

Earlier work comparing elastic and rigid indentors found no significant changes in results for different indentor properties. For the dynamic dents an offset of 0.5mm from the outer panel surface was used. For the static simulations the indentor was inserted to touch the panel with minimal initial penetration. This was achieved by inserting the indentor at one-half of the shell thickness from the mid-plane nodes of the outer panel. This initial contact was required for the implicit solver as discussed below. The re-meshing utility has several other options that were not required for these models, including the ability to map forming stresses and strains from the unrefined mesh to the refined mesh.

4.4 Dynamic Dent Simulations

Denting simulations require several considerations specific to the type of denting being modelled. For dynamic denting, the need for springback modelling after the indentor has rebounded from the panel surface has been noted. This two-stage process requires the use of both the explicit and implicit solvers in the same simulation, which was achieved using a new switching option available in the latest version of LS-DYNA. A final consideration for the dynamic dent simulations was the extraction of the dent depth.

4.4.1 Explicit-Implicit Switching

Earlier versions of LS-DYNA offered various options for coupled explicit forming and implicit springback simulations. After completion of the forming simulation, a restart file that includes the mesh of the formed part along with the residual stresses and forming strains was generated. This file was then used as an input condition for an implicit springback simulation. Unfortunately, this option could not be used for the modelling of the panel assemblies since the contact forces at the various interfaces are lost in the restart deck. An alternative method that was pursued involved the use of the so-called "seamless" springback option. This option transfers a list of specified parts from the explicit stage to the implicit analysis in a continuous simulation. These methods are both based on the assumption of a typical springback case, where the tooling is removed and a formed part is allowed to reach its final equilibrium position. This assumption leads to the elimination of contact forces and restraints in a model when the simulation changes from explicit to implicit. For the panel assembly models, this meant the loss of all the riveted joints along with the contact forces in the mastic and between the inner and outer panels.

The latest version of LS-DYNA includes an "explicit-implicit switching" option that avoids the above problems. The switching option allows the simulation to change between the implicit and explicit solvers repeatedly, at user specified times. All contact surfaces and restraints are maintained throughout these transitions. As a result, the switching option proved to be an important addition that enabled the dynamic denting simulations to be successfully completed. For each of the dent sites modelled, an explicit-implicit switching curve was specified, as shown in Figure 72. The curve was based on the contact period of the indentor with the outer panel, such that the implicit stage of the simulation was not begun until the indentor had been fully released from the closure sheet. In cases where the indentor was still in contact with the outer panel, when the switch to the implicit solution occurred, implicit convergence was often impossible to reach. Only when the implicit transition point was adjusted, by increasing the length of the explicit solution, could springback convergence be achieved.
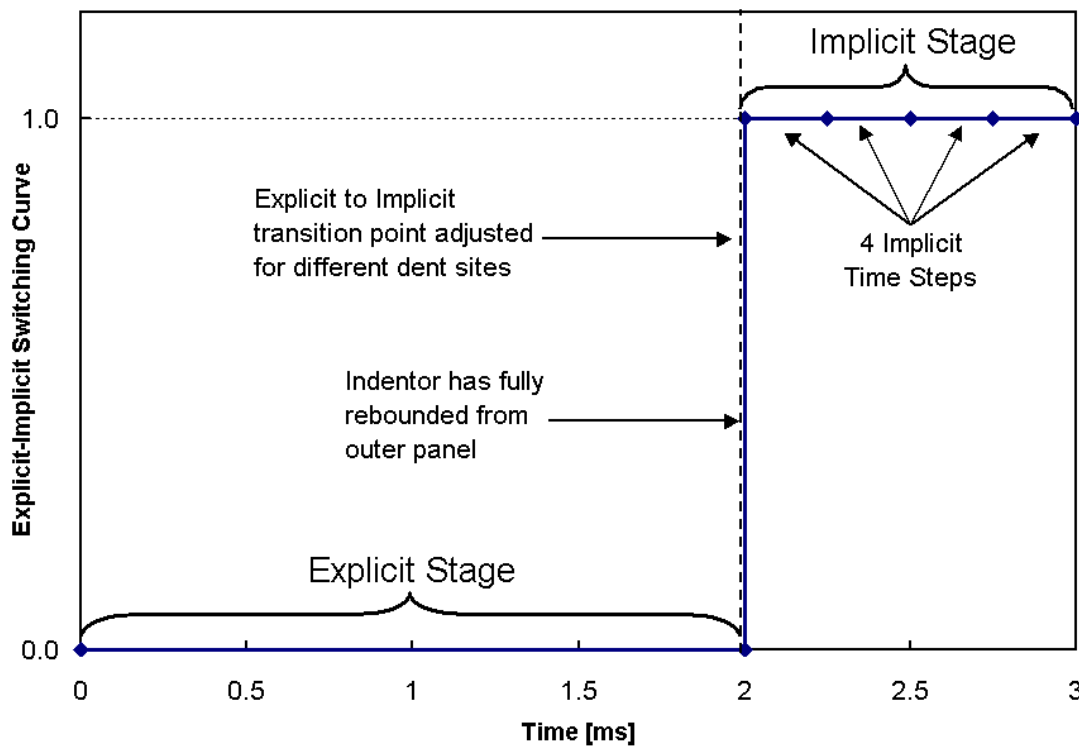
Figure 72: Typical explicit-implicit switching curve defined for dynamic dent simulations. The transition point is dependent on the dent site and is determined by the indentor contact period. Four implicit time steps are prescribed for the springback analysis.

113

4.4.2 Springback Modelling

The modelling of springback, after dynamic denting, requires several considerations involving the implicit solver. Achieving implicit convergence of springback analyses is often a challenging problem. It is particularly difficult in the case of denting simulations where a very small, localized deformation relative to the overall panel size, is involved. LS-DYNA offers various methods of improving springback convergence that are outlined in recent forming simulation guidelines [71]. These methods are specified using various implicit control cards. As noted previously, modelling of springback led to the adoption of fully integrated elements for improved convergence. Also, the contact surface definition between the inner and outer flange proved critical to the implicit convergence.

The implicit solution is divided in to artificial time intervals to improve convergence. The size of the time steps is physically meaningless, rather they serve as solution intervals that divide the analysis into smaller, more manageable, segments. The suggested number of time steps for springback analysis is four. In cases where convergence over a given step proves too difficult an automatic time step adjustment algorithm may be used. Automatic time step control will repeat a failed set of equilibrium iterations by subdividing the initial step into several smaller intervals. For the springback analysis of the panel assemblies, automatic time step control was enabled, but was only required in a few simulations.

The equilibrium iterations for a given time step can be performed using one of several implicit solvers available in LS-DYNA. The default solver is a quasi-Newton BFGS solver [75] that does a complete update of the stiffness matrix after 10 equilibrium iterations. A full-Newton solution, that updates the stiffness matrix after each iteration, is currently recommended for springback analysis and was used for all simulations. A maximum number of iterations within which equilibrium must be achieved, 150 for these simulations, is specified. The equilibrium convergence is based on a displacement and an energy criterion, equations (13) and (14) respectively.

$$\frac{|du|}{|u|} < 0.001 \quad Displacement\ Norm \qquad (13)$$

$$\frac{E_i}{E_0} < 0.01 \quad Energy\ Norm \qquad (14)$$

The displacement norm is the ratio of the total of the nodal displacements increments, du, to the maximum displacements, u. The energy norm is based on the initial and final nodal energies, E_i and E_0 respectively, which are based on the residual nodal forces at the beginning and end of the iteration. The convergence tolerances were the default LS-DYNA settings.

The linear solver that performs the expensive stiffness matrix inversions is coupled with the non-linear equilibrium solver. The default sparse matrix linear solver for stiffness matrix inversion was used. This solver is a new addition to the latest version of LS-DYNA and offers improved numerical results. Alternative solvers for the stiffness matrix inversion are available that offer increased numerical precision. In some cases the increased precision may improve convergence, or enable convergence that was previously unattainable. The double precision solver option only applies to the stiffness matrix inversion; for full double precision analysis, a separate version of the code is required. The use of double precision solver entails computational costs that increase run time significantly. While earlier springback simulations had required the double precision version of the code, the panel assemblies converged successfully with the new, single precision, solver.

A final aspect of the springback simulation was the inclusion of artificial stabilization. Artificial stabilization is a numerical device that introduces spring elements that attempt to spread the springback deformation evenly over the implicit time steps. The springs are applied with a default stiffness that can be adjusted to better partition the springback displacements. For the dynamic denting simulations, the default stiffness was scaled by a recommended 0.001 factor. It is important to note that intermediate time step solutions, prior to complete removal of the stabilization springs, have no physical meaning. The addition of stabilization greatly improves convergence of the springback analysis. In general the springback solutions converged in four time steps with roughly 10 equilibrium iterations per step.

4.4.3 Determination of Predicted Dynamic Dent Depth

The numerical predictions of dynamic dent depth required consideration of the experimental dent measurement method, outlined in Section 3.2.2. Initial dent depth predictions were extracted from the nodal displacement histories at the dent sites. Unfortunately the

displacement measurements did not agree as they failed to include the overall panel deflection. For comparison, a group of nodes surrounding the dent site at a radius equivalent to that of the dent-measuring tripod (Figure 51) was selected. A typical selection of surrounding nodes is shown in Figure 73. The average of the displacements of these nodes was used to assess panel deflection. The resulting dent depth prediction was calculated as the difference between the centre node displacement, δn_c, and the average of the surrounding node displacements, δn_r. The nodal displacements used were the normal displacements, which best reflect the normal loading conditions.

$$Dent\ Depth = \left| \delta n_c - \overline{\sum \delta n_r} \right| \tag{15}$$
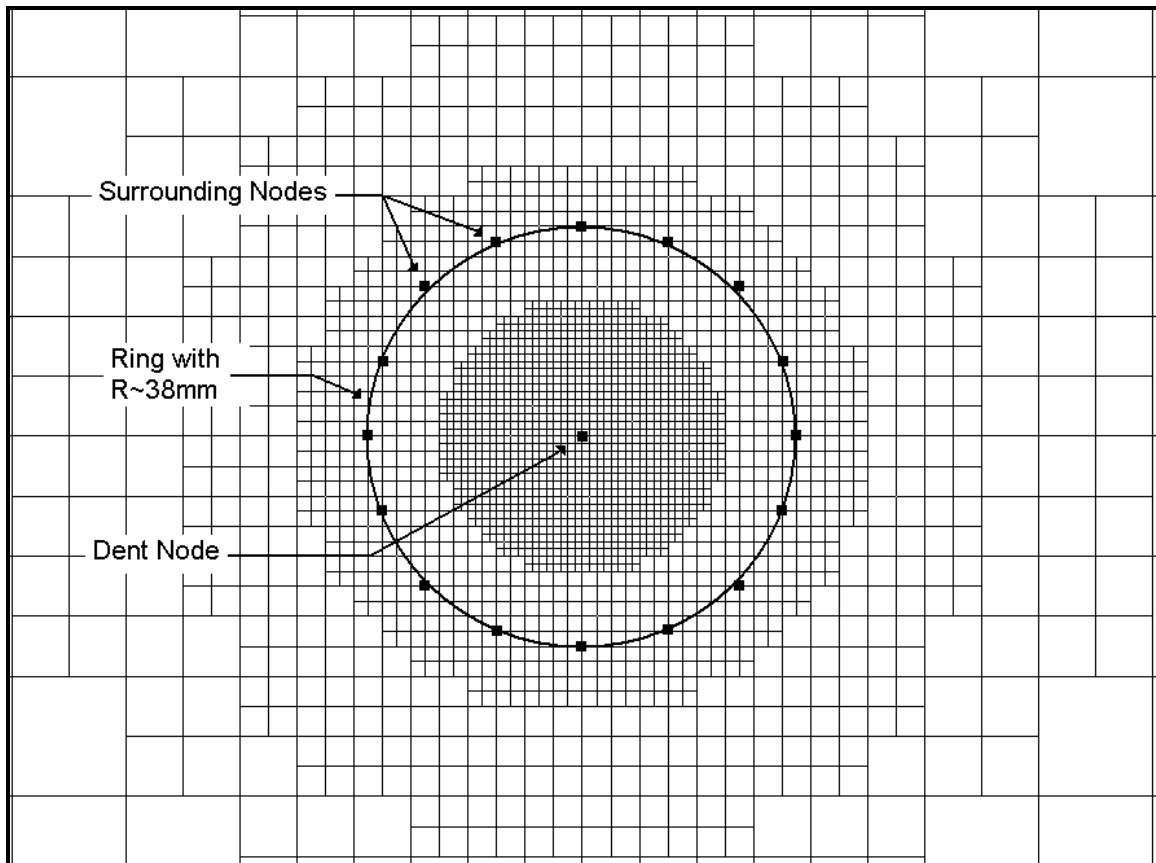
Figure 73: Measurement of numerical dynamic dent depths using the surrounding nodes at a radius of approximately 38mm.

An alternative dent measurement method was developed that used the deflections of the dent node and three nodes at positions matching the tripod support points. This method was used in subsequent modelling of full-scale hoods where more complex surface geometry

116

made previous method inaccurate. The tripod points were arbitrarily chosen, since the exact placement is a manual task in a real experiment. The initial and final coordinates of these four locations in the denting simulation were then used to approximate the experimental measurement. A schematic of the measurement method is shown in Figure 74.
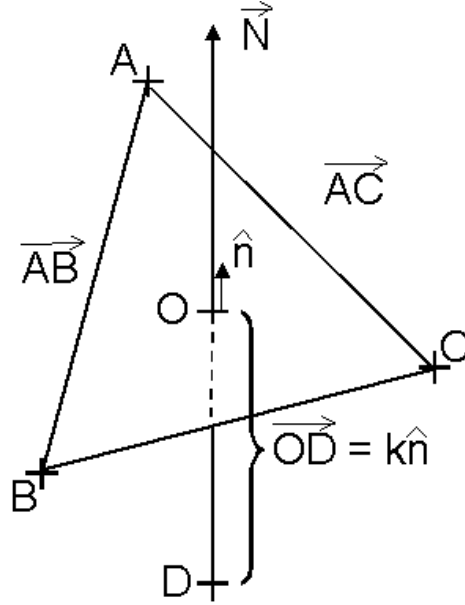
Figure 74: Schematic of measurement method of dynamic dent depths from numerical simulations.

A plane is defined using the three surrounding nodes, A, B and C. The unit normal vector, n, and a constant Q define the plane ABC as shown in equations 16-18.

$$\vec{N} = \overrightarrow{AB} \times \overrightarrow{AC} \tag{16}$$

$$\hat{n} = \frac{N_x + N_y + N_z}{\left| \vec{N} \right|} \tag{17}$$

$$n_x x + n_y y + n_z z + Q = 0 \tag{18}$$

A vector OD, parallel to the normal of the plane, is defined between the dent site D and a point on the plane O. This vector is also equivalent to a scaling of the unit normal by a factor k.

$$OD = (O - D) = k\hat{n} \tag{19}$$

$$O = \left(D_x + kn_x, D_y + kn_y, D_z + kn_z \right) \tag{20}$$

117

The value of k is found by substitution of point O, equation (20), into the equation of the plane, (18). The distance from the plane to the dent site, the magnitude of vector OD is equal to the factor k and is found using equation (22).

$$n_x(D_x + kn)_x + n_y(D_y + kn_y) + n_z(D_z + kn_z) + Q = 0 \qquad (21)$$

$$k = -(n_x D_x + n_y D_y + n_z D_z + Q) = \left| \overrightarrow{OD} \right| \qquad (22)$$

The values of k before and after denting are then used to determine the dent depth. This method could be repeated for several surrounding node groups to assess the variability due to peripheral node selection. For the panel assemblies, the uniform curvature and smooth deflections observed rendered the more detailed measurement method unnecessary. Predictions using the simplified averaging of surrounding nodal displacements proved nearly identical to those done using the detailed approach. All reported dynamic dent predictions used the simple averaging method.

4.5   Static Dent Simulations

The static dent simulations were run completely with the LS-DYNA implicit solver. The meshes were identical to those used in the dynamic analyses, except for the mesh refinement. A wider region of refinement, as shown in Figure 70, was chosen in an attempt to better capture the snap-through behaviour of the outer panel. Various issues associated with implicit convergence arose in the static simulations.

4.5.1   Implicit Solver Considerations

The implicit control parameters used for the static dent simulations were similar to those used in the springback analysis of the dynamic denting simulations. The number of time steps was governed by the prescribed load/unload cycle. The full-Newton non-linear solver was used for the implicit iterations, along with the default matrix inversion solver, as was detailed in Section 4.4.2. The same convergence criterion was also imposed. No artificial stabilization was used, as it would render any results meaningless.

The only significant change to the implicit control parameters involved the automatic time step algorithm. The base automatic time step control algorithm will allow the solver to automatically increase or decrease the step size depending on the ease of convergence over the last step. This can be quite useful in achieving convergence in a more optimal number of

iterations by automatically dividing the problem into appropriate segments. However, a problem may arise when the automated time steps cause a desired loading point to be missed. The loading curve specified for a simulation will specify a time at which a given load should be reached, for example each 22.2N increment should be reached at a specific time. If the exact time is missed due to changes in the time step, the displacement for a particular applied load is no longer readily known. Through the assignment of "keypoints" this problem is avoided. Lists of times at which iterations must be completed are specified assuring specific load levels are applied. For the panel assembly these keypoints were assigned for each 22.2N loading increment along the more coarsely defined load/unload curve as shown in Figure 75. Keypoints were only specified on the final unloading portion to mimic the test procedure used.
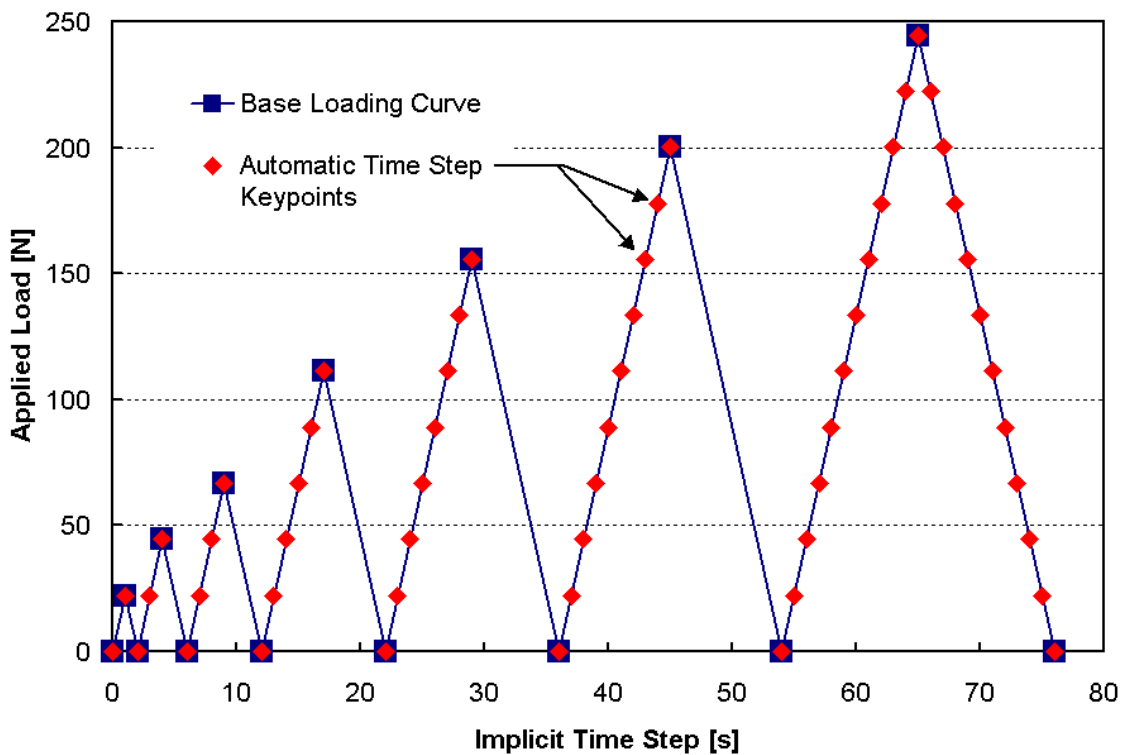
Figure 75: Static load/unload curve with automatic time step control keypoints defined to assure desired loading increments are reached.

4.5.2 Loading of the Assembly

The application of the static load is applied along the outward normal at the dent site, as calculated by D-Mesh. A common loading curve, scaled by the unit normals and applied in

the three Cartesian directions, is used. The basic loading curve could be specified using the desired loads in the normal directions making changes in the loading scheme easy to implement. A complete load/unload curve, shown in Figure 75, that mimicked the experimental loading curve (see Section 3.3.2) using 22.2N increments to reach 244.7N was prescribed. For some dent sites, difficulties in achieving convergence led to modification in the applied load curve.

The implicit solution is very sensitive to unconstrained parts and as such it is critical to assure that all parts in the simulation are restrained in some manner. For the inner panel this is achieved through the four constrained nodes at the support points. The outer panel and mastic are connected through their respective contact surfaces. Initial contact between the indentor and the outer panel is achieved through careful placement of the indentor. This contact does result in some minimal artificial initial contact force. In some cases, convergence was not achieved despite the initial indentor proximity. This required modification of the loading curve, such that the initial 22.2N increment is excluded and 44.5N is applied over the first time step. The use of the higher initial load causes contact and alleviates the unconstrained indentor from causing convergence problems. Also, the unloading period, from various peak loads, had to be adjusted in some cases to achieve convergence. This could introduce some numerical precision concerns.

4.5.3 Stiffness and Static Dent Measurement

Due to the experimental static dent measurement technique the extraction of the static dent predictions was straightforward. The normal displacement of the node at the dent site corresponds to the experimental static displacement readings. The normal displacement versus time is taken from the simulation and the corresponding applied load at the specified keypoint times is assigned. This generates a detailed loading history that represents the predicted stiffness response. The static dent depths are taken as the residual displacement after unloading from the various peak loads.

5 Experimental Results

5.1 *Dynamic Denting Results*

The experimental dynamic dent results are presented in a series of figures for the various test conditions. The effect of various parameters, thickness, curvature and test location, is examined. The assumption of panel symmetry is also explored through comparison of the mirrored dent sites tested for several panels. All results are presented using the dynamic dent site labels defined in Figure 52 and Figure 53 for teacup configurations #1 and #2, respectively. The notation used for the dynamic dent depth plots designates the curvature (FL-flat, MC-medium curvature, HC-high curvature) followed by the thickness (1.0mm, 0.93mm, 0.8mm).

5.1.1 Comparison of Mirrored Dynamic Dent Sites

The examination of the test results at the mirrored dent sites illustrates the validity of the symmetry assumption used. The variation in results, for nominally identical sites, demonstrates the impact of geometric differences and measurement repeatability. Sites D-H and K-L were mirrored dent sites directly over teacups, while sites E-G were located in the centre of four teacups. The results are presented in Table 4 and Figure 76.

Panel	Dent Site	Dent Depth [mm]	Mirrored Dent Site	Dent Depth [mm]	Difference [mm]
FL/0.93	D	0.340	H	0.361	-0.021
	E	0.053	G	0.033	0.020
	K	0.318	L	0.389	-0.071
FL/0.8	D	0.444	H	0.464	-0.020
	E	0.079	G	0.111	-0.032
	K	0.463	L	0.404	0.059
MC/0.93	D	0.299	H	0.305	-0.006
	E	0.029	G	0.040	-0.011
	K	0.305	L	0.349	-0.044
MC/0.8	D	0.419	H	0.471	-0.052
	E	0.076	G	0.071	0.005
	K	0.472	L	0.468	0.004

Table 4 : Comparison of measured dynamic dent depths of three mirrored dent sites for four panel combinations.
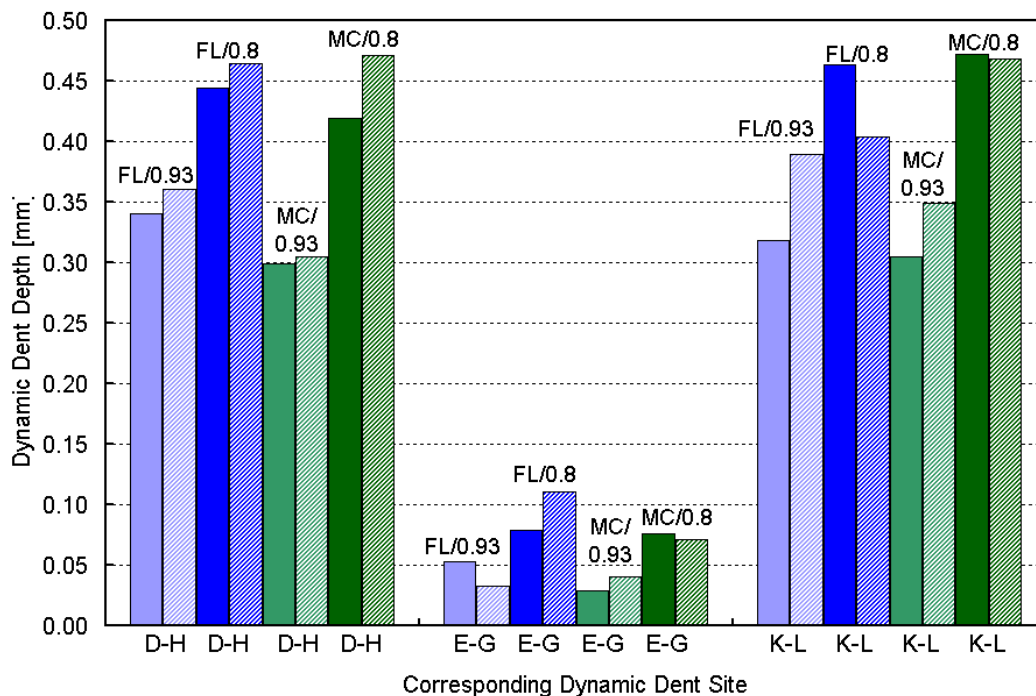
Figure 76: Comparison of dynamic dent depths at mirrored dent sites for various panel configurations. Sites D-H and K-L are above teacups. Sites E-G are between 4 teacups.

The largest variation in measured dent depth was 0.071mm, with the majority of differences less than 0.020mm. It should be noted that the average measurement error was roughly +/- 0.006mm. The highest variations were for test sites located directly above teacups, which can be attributed to the variations in both the teacup height and mastic

thickness, as shown previously in Figure 40. For the unsupported sites, E-G, the magnitude of the variations is smaller, with the largest difference being 0.032mm, however the percentage difference is larger due to the smaller dent depth. The differences between the unsupported locations are likely less influenced by the teacup-related variations. The accuracy of the initial and final readings, and their difference, will play a larger role in the case of small dent depths. It is important to recall the magnitude of the dent depths and realize that accurately capturing displacements of this magnitude using manual techniques is difficult. Generally, the agreement between sites is considered good, but in subsequent examination of dynamic denting results the potential for atypical results, for a particular site, should be recalled.

5.1.2 Effect of Dent Location of Dynamic Dent Depth

A comparison of the dynamic dent depths for the various test sites for teacup configuration #1 is presented in Figure 77. The results shown are the averaged dynamic dent depth for the seven different cases tested (see Table 3) for this teacup configuration. As a result the magnitude of the dent depth only offers a general idea of the expected dent depths at the various sites. The general trend between sites is well represented. It should be noted that sites A, D, F & K are located directly above a teacup support and experience high local support. Sites B, C, I & J are located on the diagonal between two teacups and thus experience some support from the teacups. Finally, site E is located in the centre of four teacups, and is the least supported of the test sites.
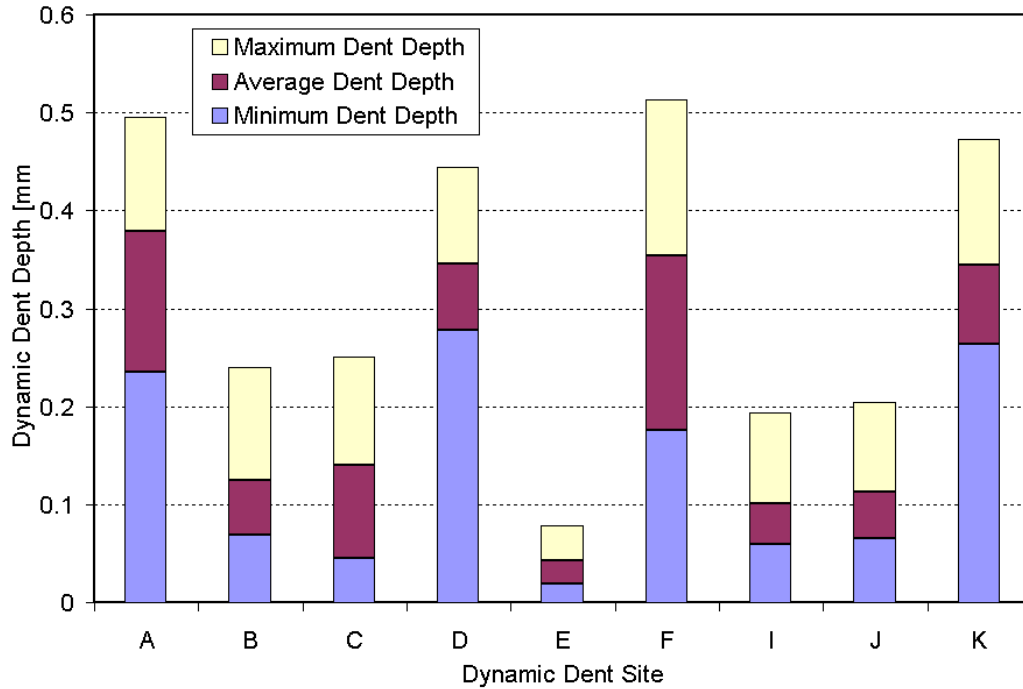
Figure 77: Comparison of measured average dynamic dent depth for various test locations of the panel assembly with teacup configuration #1.

The results illustrate the effect of the teacup supports quite clearly. The four test sites directly above teacups show significantly larger dent depths than the other test locations. The unsupported site, E, shows the smallest dynamic dent depth. The intermediate sites dent more substantially than the unsupported site, but still offer much better dent resistance than the teacup sites. The local support of the teacup locations appears to limit the assemblies' ability to elastically absorb the dynamic denting energy, leading to the large dents observed. This behaviour is contrasted by the unsupported location, which catches and releases the indentor, effectively transferring momentum and limiting residual dent depths. These trends are consistent with the observations of several of the studies outlined in the literature survey [13-15,22,30], which suggested that high local stiffness promoted large dent depths.

However, the dynamic dent testing of actual hood panels [65], at teacup locations, generally reveals superior dent resistance. This disagreement with the current results is attributed to the overly thin mastic layer used in the current panels. In actual hoods, with mastic layers of roughly 7mm, the mastic acts as a damper and cushions the indentor impact. The mastic thereby absorbs the majority of the impact energy and limits the permanent deformation. In the panel assemblies, the thin mastic layer is already highly compacted and

is no longer capable of absorbing the indentor energy. This stiff mastic interface leads to high local reinforcement and large dynamic dent depths.

The results for teacup configuration #2 are based on the sole set of tests performed on this configuration, the medium curvature, 0.93mm thick, outer panel case. The sites A, C, G and I are located above teacups, while site E is centred between four cups. The remaining sites, B, D, F and H, are in line between two teacups. The dynamic dent depths for teacup configuration #2 are shown in Figure 78.
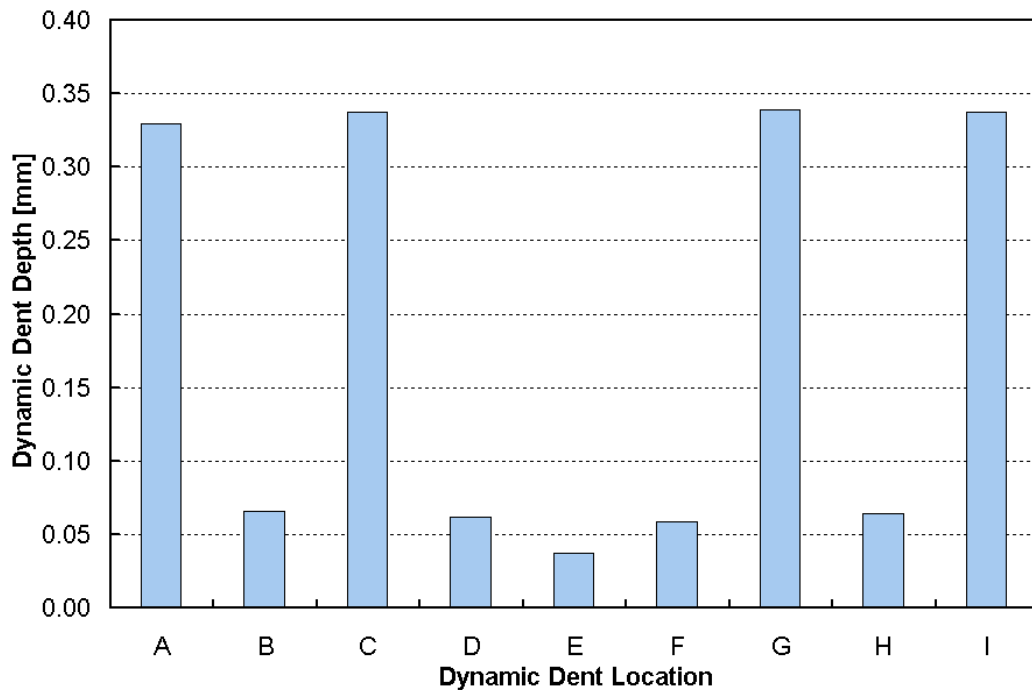
Figure 78: Comparison of measured dynamic dent depth for various test locations of the panel assembly with teacup configuration #2.

The results for the two teacup configurations are similar when comparing the supported and unsupported sites, as shown in Figure 79 for the medium curvature, 0.93mm panel assemblies. The results are nearly identical for the teacup sites, reflecting the highly local nature of the teacup support effect on dynamic dent depth. The results for the unsupported region, centred between four cups, are also very similar. The small difference in the results can be attributed to the differences in cup spacing and the total number of cups for the two configurations. The results for configuration #2, for the sites between 2 teacups, show smaller dents than the results for configuration #1. The linear cup spacing for

125

configuration #2 is greater than the tight diagonal spacing of configuration #1 thereby lessening the influence of the teacups. This suggests that the larger the teacup spacing, the lower the resulting stiffness and the smaller the dynamic dents.
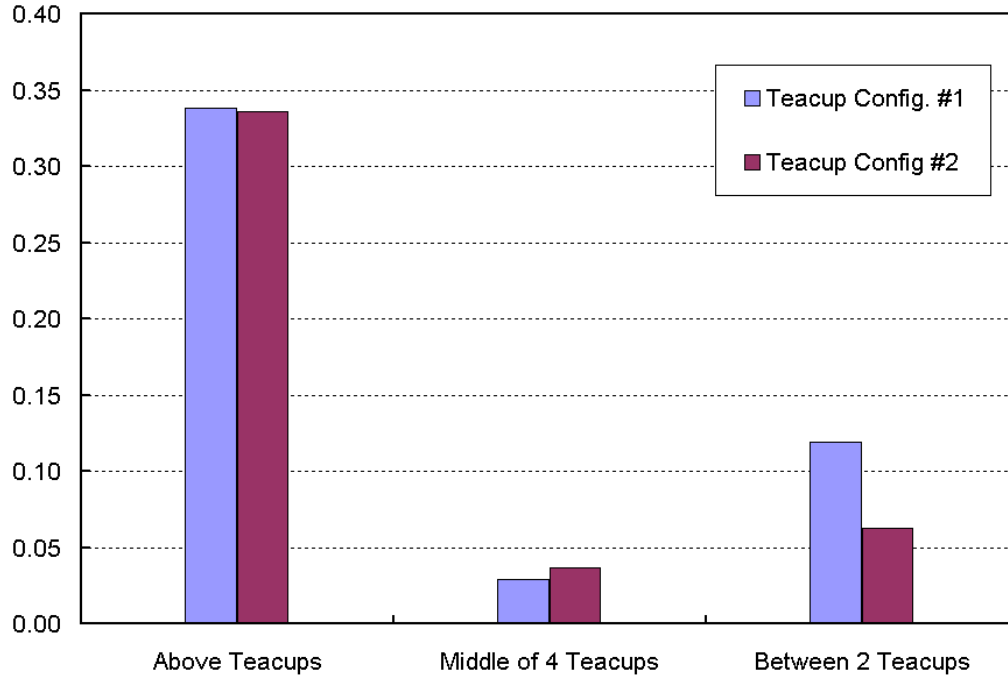
Figure 79: Comparison of dynamic dent depths for the two teacup configurations at the teacup sites and the least supported sites. The results are compared for the medium curvature, 0.93mm panel combination and the dent depth for the sites above and between teacups are averaged

For both teacup configurations, the surrounding flange and sidewalls appear to have minimal influence on dynamic dent depths for impact in proximity to the edge of the panel. No perceptible trend is found for either the unsupported or teacup locations as they approach the panel periphery. The localized nature of the dynamic dent tests limits the overall panel deflection and thus limits the role of the surrounding supports. Perhaps for higher indentor velocities a wider region of deformation might result, which would introduce an edge boundary condition effect in the unsupported dent tests. The teacup sites would remain highly localized and thus more independent of the other support conditions.

5.1.3 Effect of Thickness on Dynamic Dent Depth

The effect of thickness on dynamic dent depth for the panel assemblies with teacup configuration #1 is presented in Figure 80 for the medium panel curvature and in Figure 81

for the flat panel. The trends observed are similar for both the curved and flat panels, suggesting that the thickness effect is not significantly altered by changes in panel curvature.
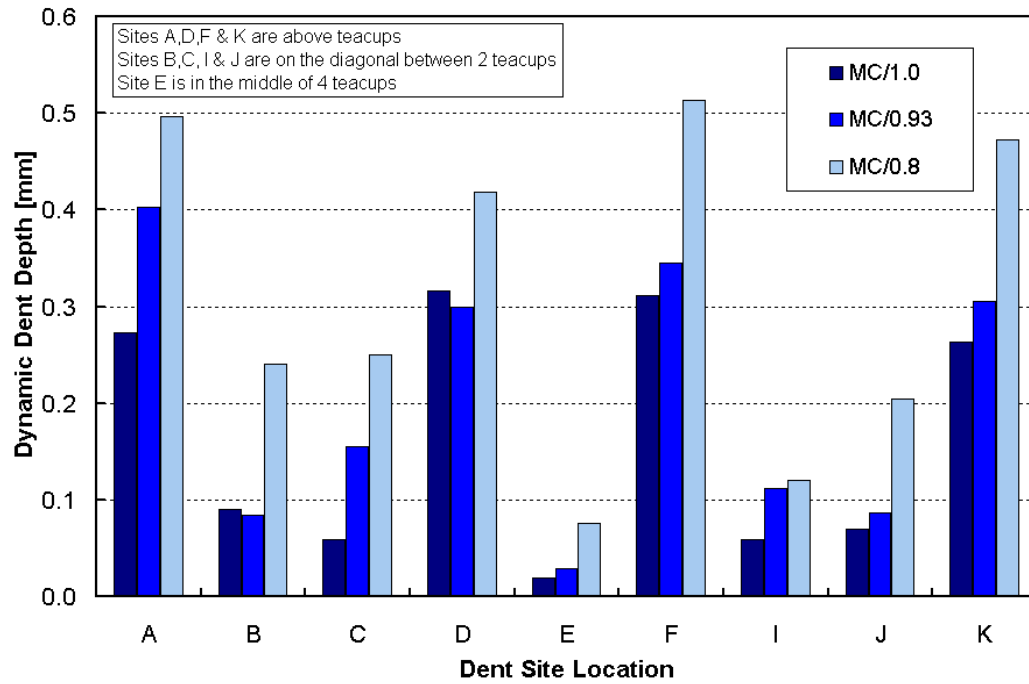
Figure 80: Measured dynamic dent depths for the medium curvature, teacup configuration #1, panel assembly for the three tested thickness values, 1.0mm, 0.93mm and 0.8mm.
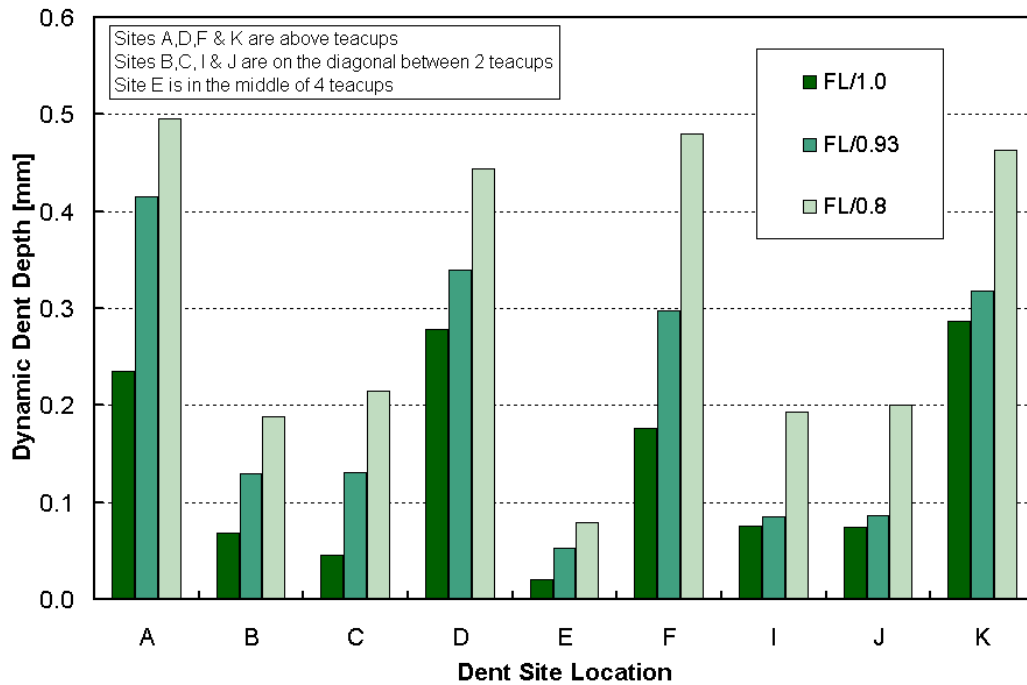
Figure 81: Measured dynamic dent depths for the flat, teacup configurations #1, panel assembly for the three tested thickness values, 1.0mm, 0.93mm and 0.8mm.

The effect of sheet thickness is consistent for nearly all test sites. The expected increase in dent depth, with reduced thickness, is observed at almost all test sites. Only sites B and D for the medium curvature assemblies saw the 0.93mm sheet outperform the thickest sheet. Generally, a dramatic increase in dent depth for the 0.8mm sheet is observed. It should be recalled that the 0.93mm sheet was from an earlier batch of AA6111. This may contribute to the small variation between the dent depths of the 1.0 and 0.93mm sheet for numerous sites. The expected, mainly linear, increase in dent depth, with increasing thickness, may be lost due the material property differences. The potential of geometric variations causing some of the unexpected test points should also be considered.

5.1.4 Effect of Panel Curvature on Dynamic Dent Depth

The effect of panel curvature on dynamic dent depth is compared for the 0.93mm thick, teacup configuration #1, panel assemblies in Figure 82. No consistent, discernible trend is observed with respect to the role of curvature on dynamic dent depth. For locations directly over teacups opposing curvature effects are seen, as in the comparison of sites A and F. The lack of a consistent curvature effect at teacup locations seems probable, as the highly

128

localized support at these sites would negate the influence of a global parameter. The panel above each teacup is more likely to take on the shape of the teacup, as the mastic holds the sheet in place, thereby altering the panel curvature. The variability in local mastic thickness and teacup geometry will be more significant than the nominal panel curvature. For the test sites away from the teacups an increase in panel curvature tends to reduce the observed dent depths. There are some cases where the flat panel outperforms the medium curvature panel, but the high curvature panel always provides the lowest dynamic dent depth.
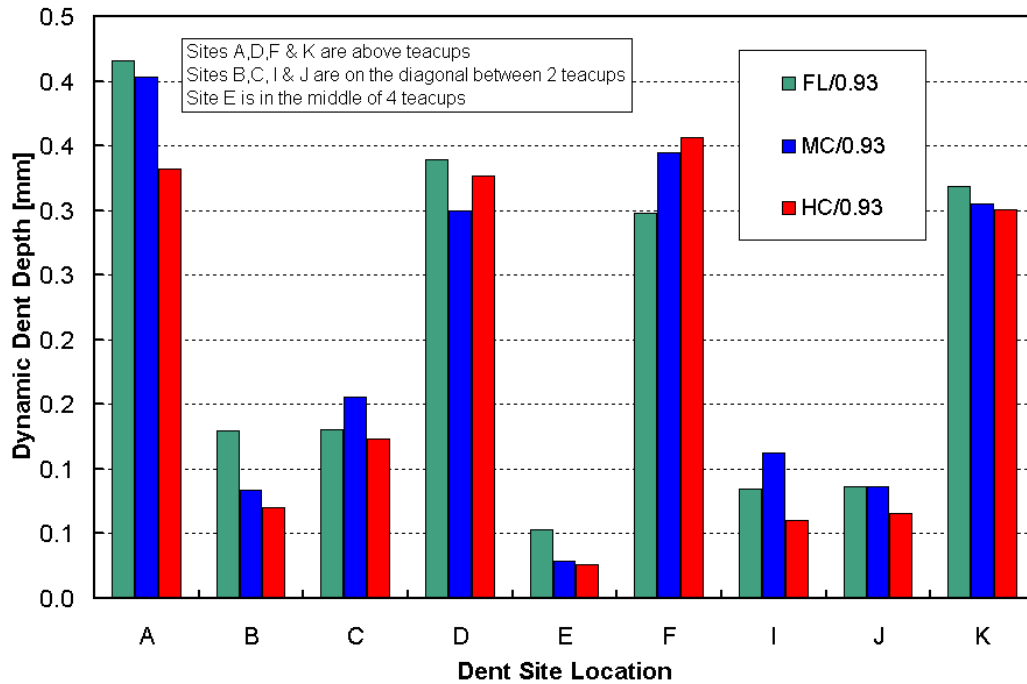
Figure 82: Measured dynamic dent depths for the 0.93mm, teacup configurations #1, panel assembly for the three tested panel curvatures, flat (FL), medium (MC) and high (HC).

Further examination of the unsupported site is presented in Figure 83. Upon first examination, the measured results appeared to contradict the expected trend of increased dynamic dent depth with increased panel curvature. However, in recalling the work of Worswick *et al.* [63], discussed in Section 2.1, the importance of the range of panel curvatures is illustrated. The panel assemblies the curvatures tested are large and fall within the range typical of automotive hoods. As a result, the region of pronounced increase in dent depth, with increasing curvature, as shown in Figure 16, is not encountered in the panel assembly tests. The comparison presented in Figure 83 is an enlarged view of Figure 16, and

includes two sets of data from the work of Worswick *et al.* [63], for different unsupported span lengths. The panel assembly data shown is for the unsupported site E, with teacup to teacup spacing of 170mm and 202mm. The magnitude of the dent depths can only be loosely compared as the material and test conditions are different. The current results follow similar trends as the predictions of Worswick *et al.* [63], as dynamic dent depth decreased with reduced radius of curvature for large radii. The relative importance of curvature in this region remains small when compared to the thickness effect.
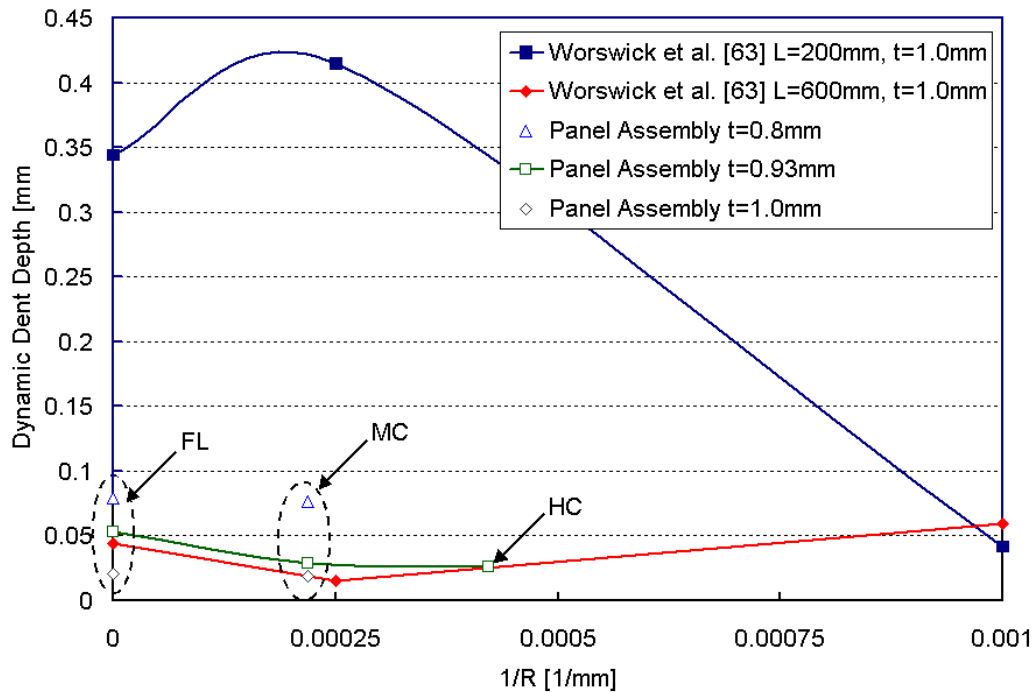
Figure 83: Comparison of measured dynamic dent depths of the panel assemblies and the predicted results of Worswick *et al.* [63]. The predicted results are shown for two different unsupported span lengths L. The measured results are for site E, which has an unsupported span lengths of 170mm or 202mm between teacup centres.

5.2 Static Denting Results

The experimental static dent results are presented in a series of figures for the various test conditions. Both the stiffness response (force vs. displacement) and the static dent depth (residual displacement vs. load) are examined for the various sites. The effect of various parameters including, thickness, curvature and test location, is examined. The assumption of panel symmetry is also explored through comparison of the mirrored dent sites tested for several panels. All results are presented using the static dent site labels defined in Figure 59

and Figure 60 for teacup configurations #1 and #2, respectively. The static stiffness curves will include the unloading profile for some cases, however unloading may be omitted for improved clarity in other instances. The dent depth curves are generated using the unloaded displacement, after each peak load, as the dent depth. A typical load/unload cycle is presented in Figure 84. The magnitude of displacement drift, highlighted in the inset view of Figure 84, during successive load-unload-reload to increasing load levels, was deemed acceptable.
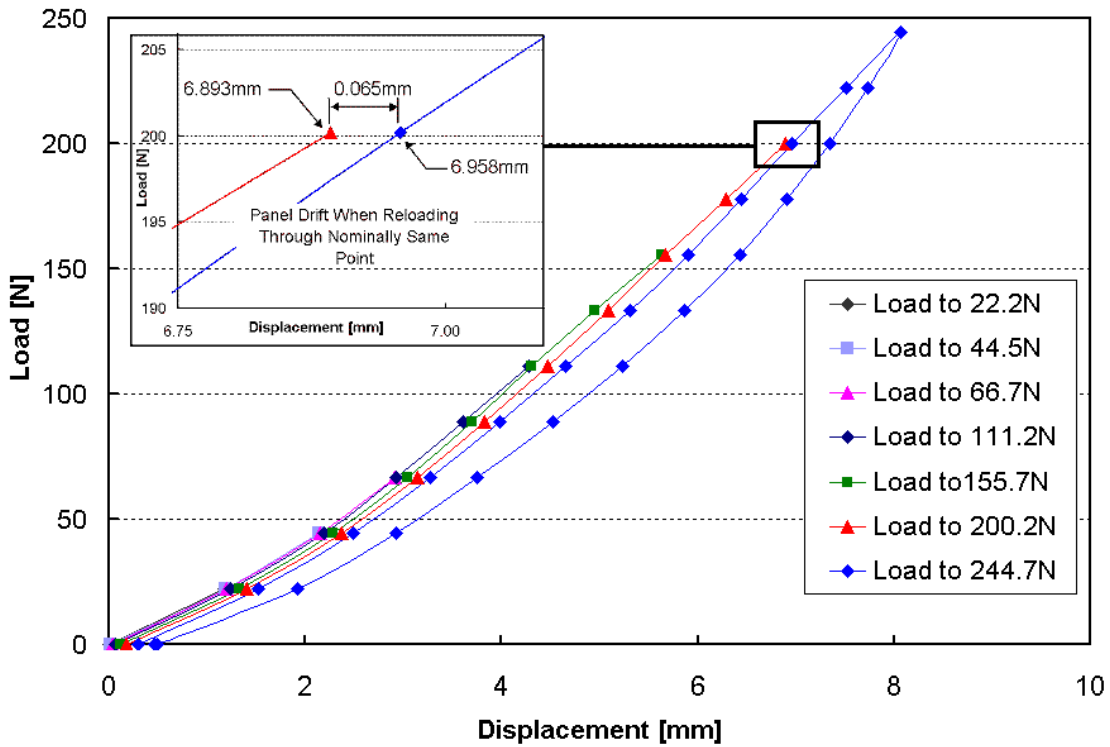
Figure 84: Typical load/unload data generated during a static test (MC/0.93/B configuration #1). The intermediate unloading steps are omitted for clarity. Panel drift upon reloading is highlighted in the inset view.

5.2.1 Comparison of Mirrored Static Dent Sites

A limited number of mirrored static dent sites were tested for assemblies with teacup configuration #1. Comparison of the resulting stiffness and dent depths are presented in Figure 85 and Figure 86, respectively. The sites B & BB are located between four teacups, while sites C & CC are located above a teacup near the outer edge of the assembly. The stiffness response for the unsupported sites, for two different thickness values, are well

matched. The peak displacements in both cases are nearly identical and the general shapes of the stiffness curves are similar. Considering that an arbitrary time was used for measurement intervals, good correspondence of the mirrored unsupported sites indicates satisfactory results.

The comparison of the stiffness response for the mirrored teacup locations is poorer than that of the unsupported regions. This is again attributed to the teacup geometry and mastic thickness variations discussed previously. The stiffness at the teacup site will affect the results, however the agreement between sites C & CC is still considered quite good.
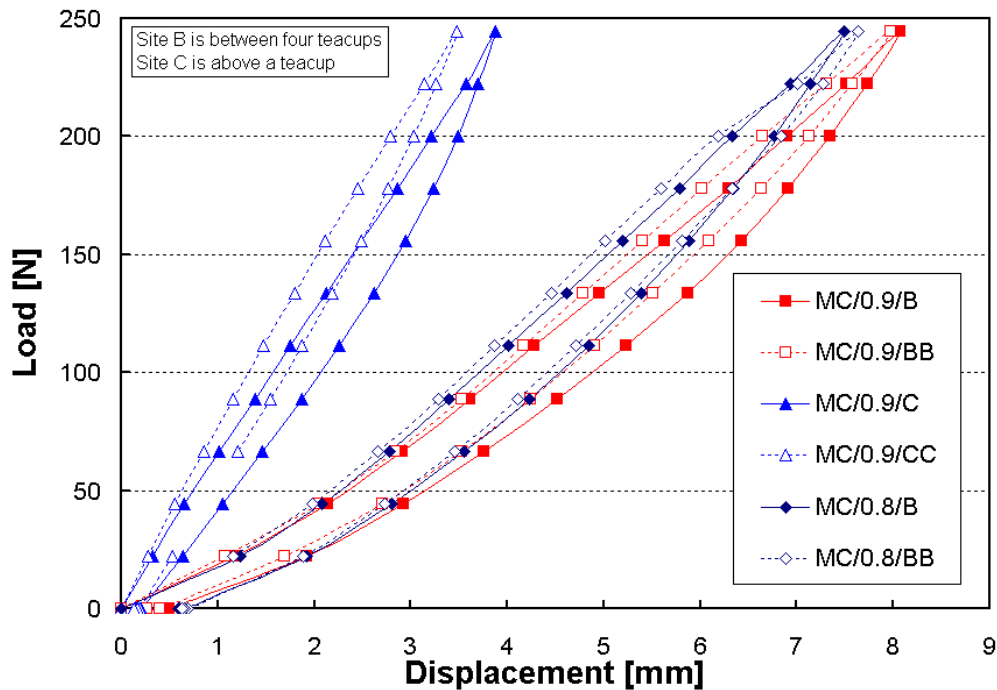
Figure 85: Comparison of static stiffness response of three mirrored dent sites for various panel combinations.

Comparisons of the static dent depths for a range of loads at the mirrored sites, Figure 86, again shows reasonable agreement. The level of agreement varies for the three different sites, with the worst case occurring for an unsupported location (MC/0.9/B&BB). This may be attributed to more dramatic nature of the panel recovery after removal of the loading weights. Panel settling is a concern in the stiffness response, but the observed settling when the panel is being loaded was less severe than when the panel was being unloaded. As a result, the residual displacements, recorded as static dent depths, will tend to be more sensitive to settling effects. The static dent depth trends are consistent for all the mirrored

sites. The good agreement of the static dent depth at teacup locations, C&CC, and poor agreement of stiffness (Figure 85), suggests that the stiffness and static dent depth measurements are somewhat independent. The static denting response is a function of panel yielding, which may occur at different points along the stiffness curve for nominally similar sites. Thus, while some sites could have similar stiffness responses, the onset of local yielding may vary which in turn leads to different dent depth results.
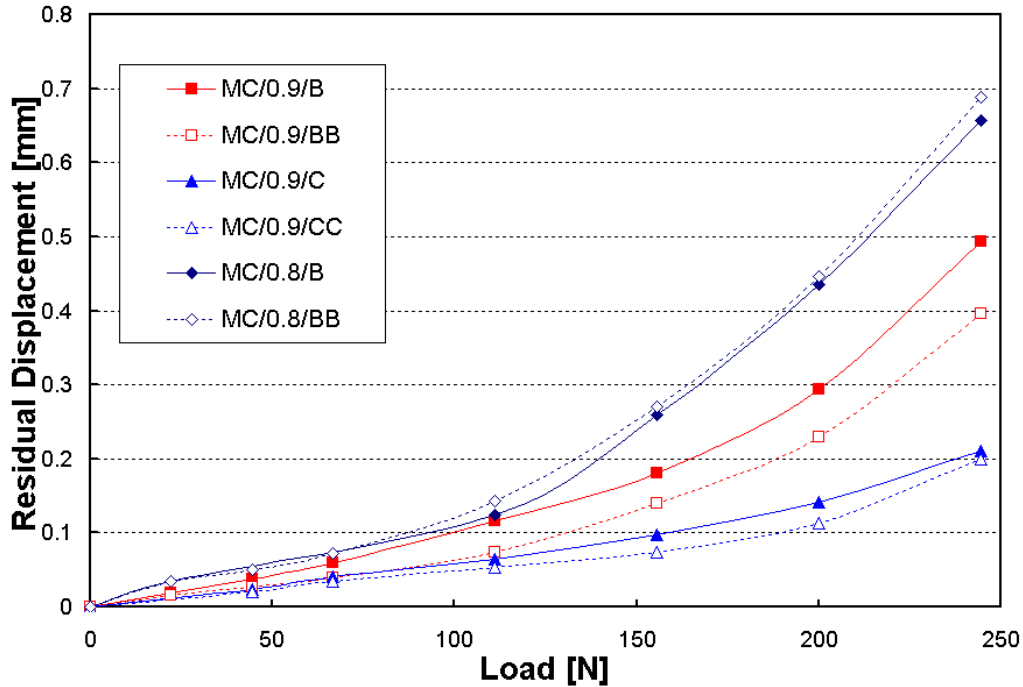
Figure 86: Comparison of static dent depth vs. load of three mirrored dent sites for various panel combinations.

5.2.2 Effect of Dent Site Location on Static Stiffness and Dent Depth

The effect of dent location on stiffness response, for teacup configuration #1, is examined in Figure 87. The curves presented are based on the averaged force-displacement results for the seven test conditions used, as outlined in Table 3. Comparison of the stiffness response at sites A & C shows dramatically different behaviour between two sites, both located directly at teacups. This suggests that the surrounding flange and sidewalls substantially influence the stiffness response of site C with the stiff edges of the assembly contributing significant stiffness to the assembly. The centrally located teacup, site A, is remote from these edge supports and deflects more freely. As a result, site A has a stiffness response similar to that

133

of site B, the unsupported test location. Initially, site A has a stiffer response than the unsupported region, but as the load increases the lack of panel edge support allows greater deflection. Conversely, the surrounding edge supports appear to restrict deflection at site C and prevent softening of the stiffness response. Thus, global support conditions have an important effect on static behaviour.
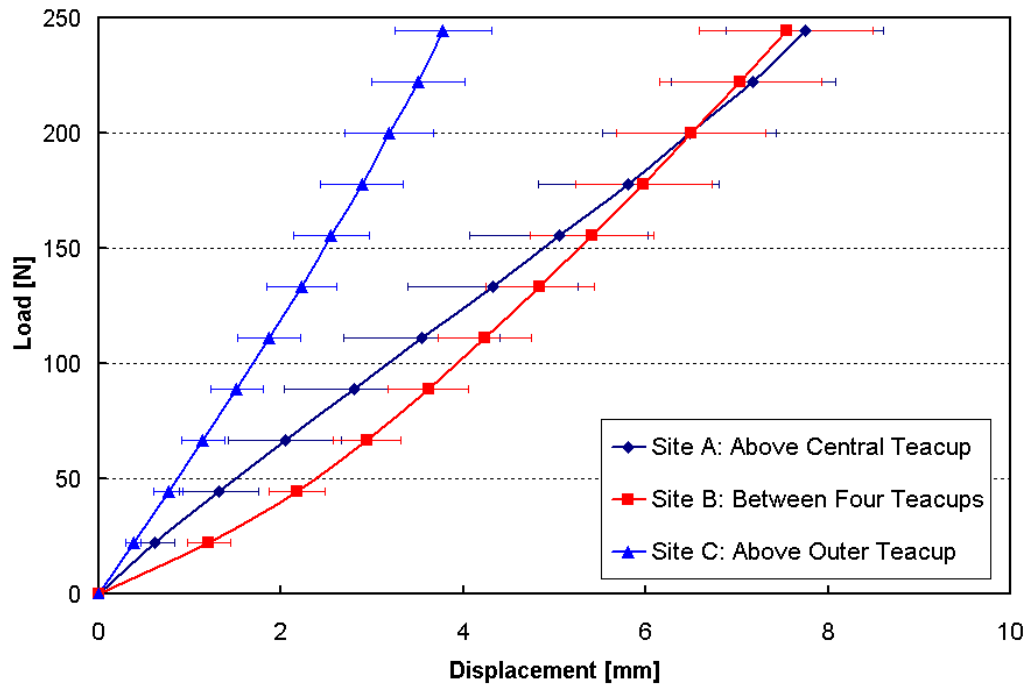
Figure 87: Stiffness response of the static dent sites for teacup configuration #1. The stiffness curves are based on the averaged results of the seven test conditions used.

The effect of dent location on static dent depth, for teacup configuration #1, is shown in Figure 88. The results are again based on the averaged data for all assembly combinations tested. All dent sites exhibit increasing static dent depth with increasing load level. The dent depth increases in a non-linear fashion, with larger increases corresponding to softening of the stiffness response. Site C, the stiffest site, offers the greatest dent resistance as predicted in the literature. The nearly linear stiffness at site C translates into a similarly linear denting profile. This result confirms that for panels undergoing relatively simple deflection response, the correlation between stiffness and dent depth is more evident

In contrast,the dent depth results for sites A and B are more difficult to explain. Site B is free to deflect and has the lowest initial stiffness. It appears that site B exhibits a secondary stiffness mode from the outset, such that initial buckling or oil-canning appears to

134

have occurred nearly immediately upon loading. A final stiffness appears to emerge as the load level exceeds 75N. Site A seems to exhibit a more discernible transition for initial stiffness to secondary stiffness, with buckling occurring around 50N. A final stiffness is also seen at site A in the latter stages of loading. This complicated stiffness variation may explain the dent depth behaviour observed. While site A begins with a stiffer response, it quickly softens at which point a corresponding increase in dent depth is observed. Site B is initially less stiff, but quickly transitions into a higher final stiffness which appears to reduce the static dent depth. The complicated relationship between the multi-stage stiffness response and the corresponding dent depth behaviour demonstrates that the stiffness effect on static dent resistance is complex.
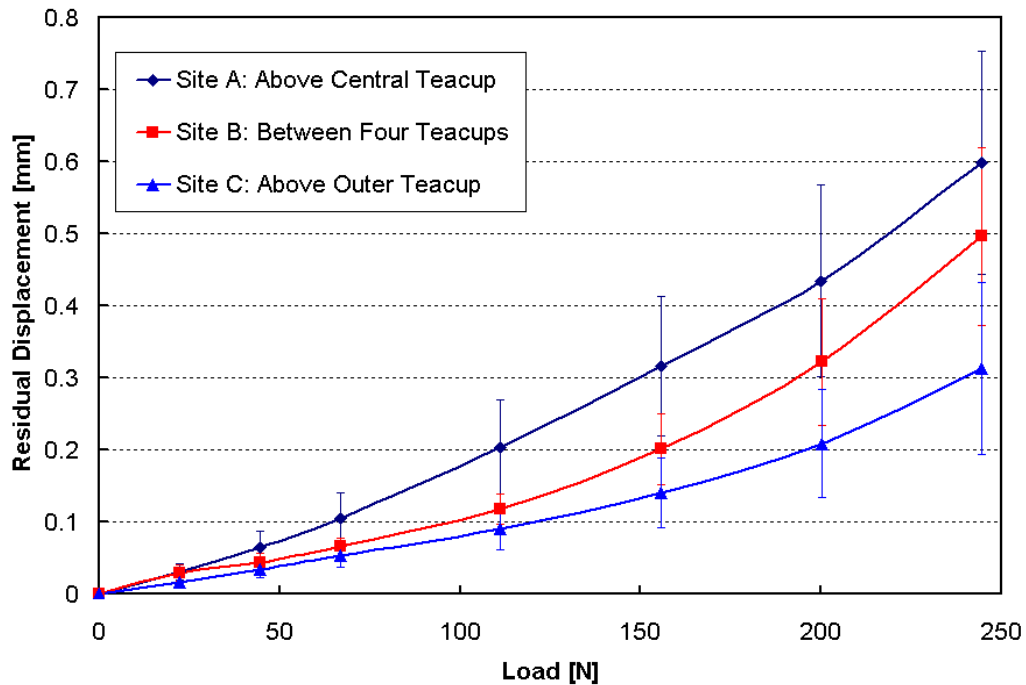
Figure 88: Static dent depth vs. load for teacup configuration #1. The stiffness curves are based on the averaged results of the seven test conditions used.

The stiffness and dent depth results for teacup configuration #2 are shown in Figure 89 and Figure 90 respectively. The results for the same panel combination, that is, medium curvature with 0.93mm outer panel, for teacup configuration #1 are also included for comparison. The sites are not identical for the two teacup configurations but they are similarly supported. Site A is located above the centre teacup and site C is located above an

outer teacup for both configurations. Site B is located between four teacups for both arrangements. As in the case of teacup configuration #1, site C is again the stiffest location for configuration #2. The unsupported site, site B is initially very soft, before dramatically stiffening as the loading increases. Site A exhibits a three stage stiffness response.
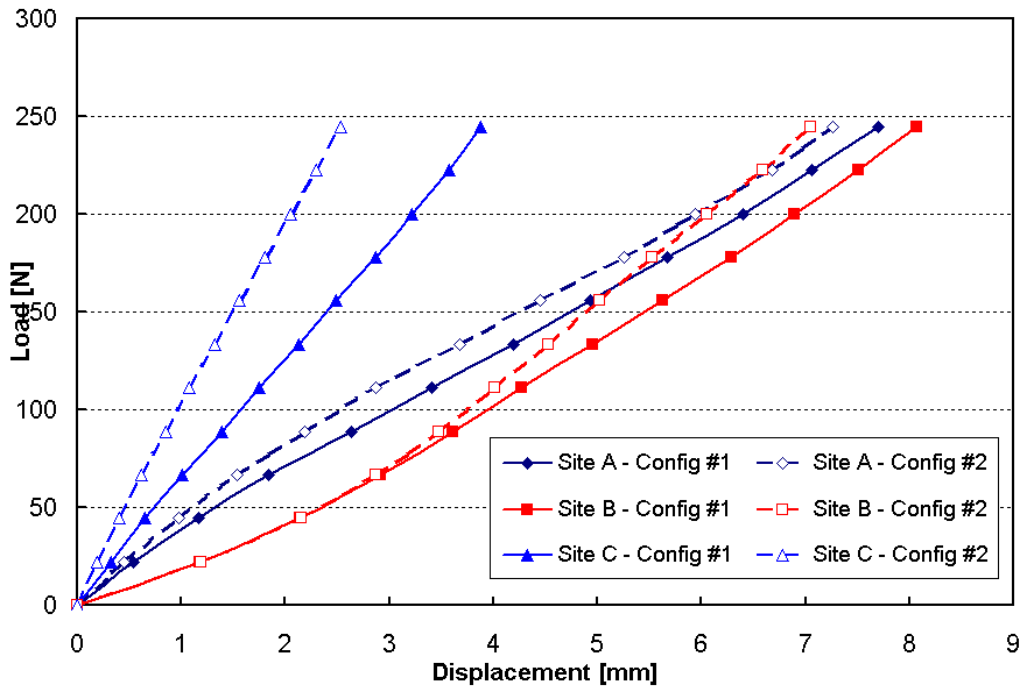
Figure 89: Comparison of stiffness response at three dent sites for the 0.93mm medium curvature assemblies of different teacup configurations. Sites do not correspond directly but are similarly supported.

Comparisons of similarly supported test sites show similar stiffness and dent depth behaviours. In comparing the results for site C, the effect of global supports is more pronounced for teacup configuration #2. Site C for configuration #2 is located closer to the periphery and this translates into the stiffer response observed. However, this increase in stiffness does not appear to translate into an increase in dent resistance, as both site C's dent similarly. Both the central dent site and the unsupported dent site perform better in the second teacup configuration. The unsupported site is closer to the outer supports in configuration #2, which may account for the increased stiffness and improved dent resistance relative to site B in configuration #1. The higher stiffness of site A for configuration #1 also explains the superior dent resistance it exhibits. However, explaining the improved stiffness is difficult. The increased number of teacups in the first configuration would presumably

have increased the overall stiffness of that assembly, yet the second configuration with wider cup spacing exhibited stiffer results at the central teacup. This discrepancy could be due to variation in teacup geometry that confounds the expected results. Due to the limited test data for the second configuration further examination of the observed behaviour is not possible.
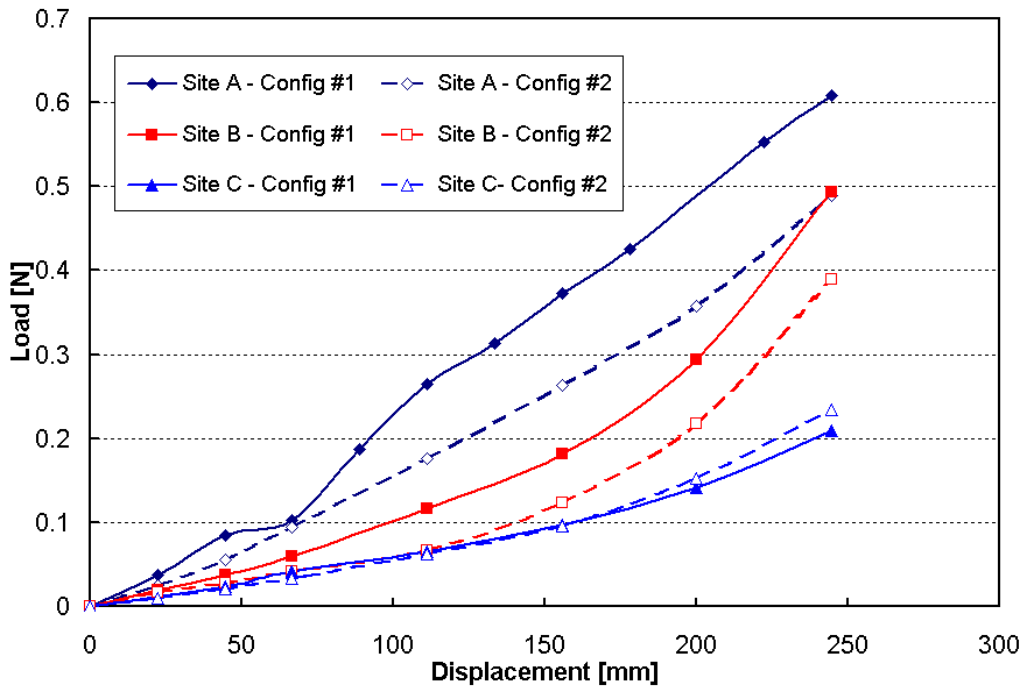
Figure 90 Comparison of static dent depths at three dent sites for the 0.93mm medium curvature assemblies of different teacup configurations. Sites do not correspond directly but are similarly supported.

5.2.3 Effect of Panel Thickness on Static Stiffness

The effect of panel thickness on stiffness is compared for both the flat and medium curvature assemblies. The medium curvature assemblies are compared in Figure 91, Figure 92 and Figure 93, for sites A, B and C respectively. The flat assemblies are compared in Figure 94, Figure 95 and Figure 96, for sites A, B and C respectively. All curves include only the loading portion of the response for improved clarity. A fixed load and displacement range is used to enable comparison of the figures.
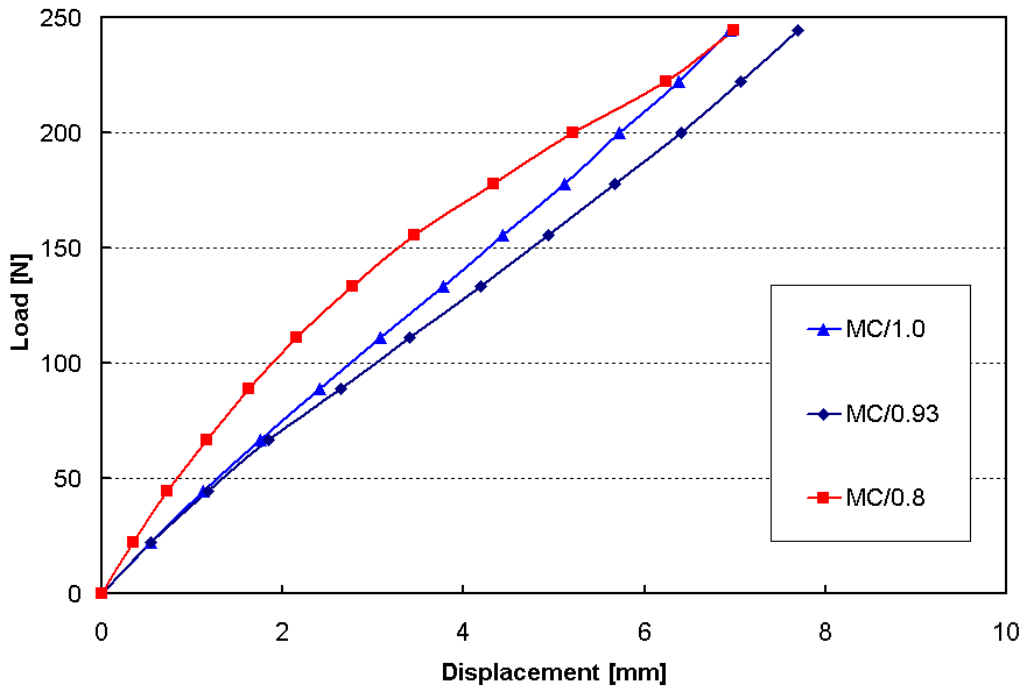
Figure 91: Static stiffness responses at site A for medium curvature assemblies of three outer panel thickness values.
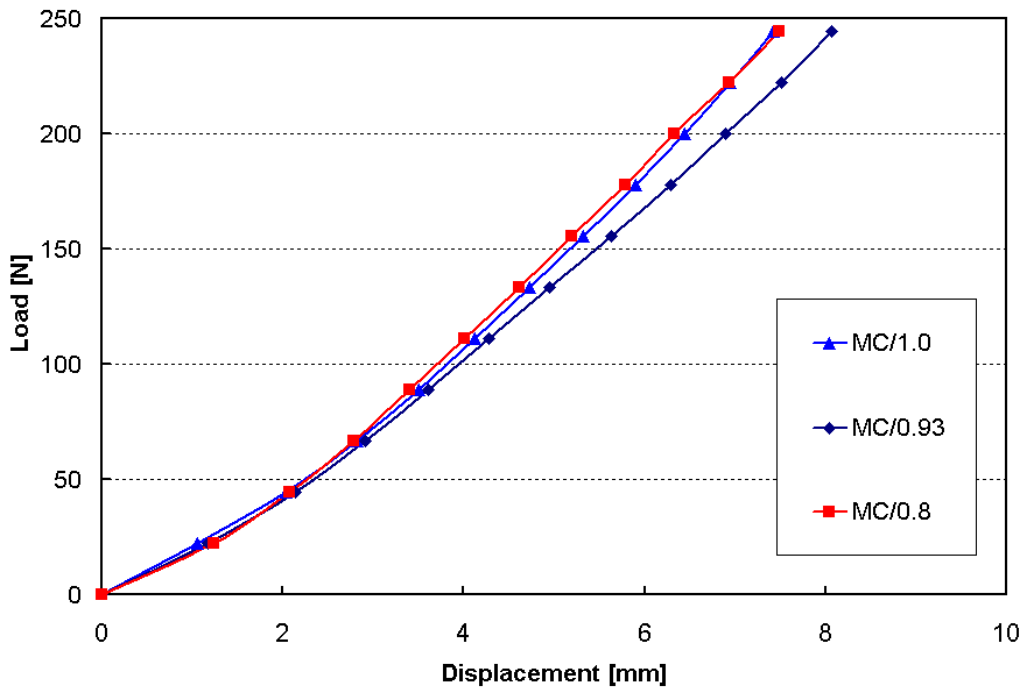
Figure 92: Static stiffness responses at site B for medium curvature assemblies of three outer panel thickness values.
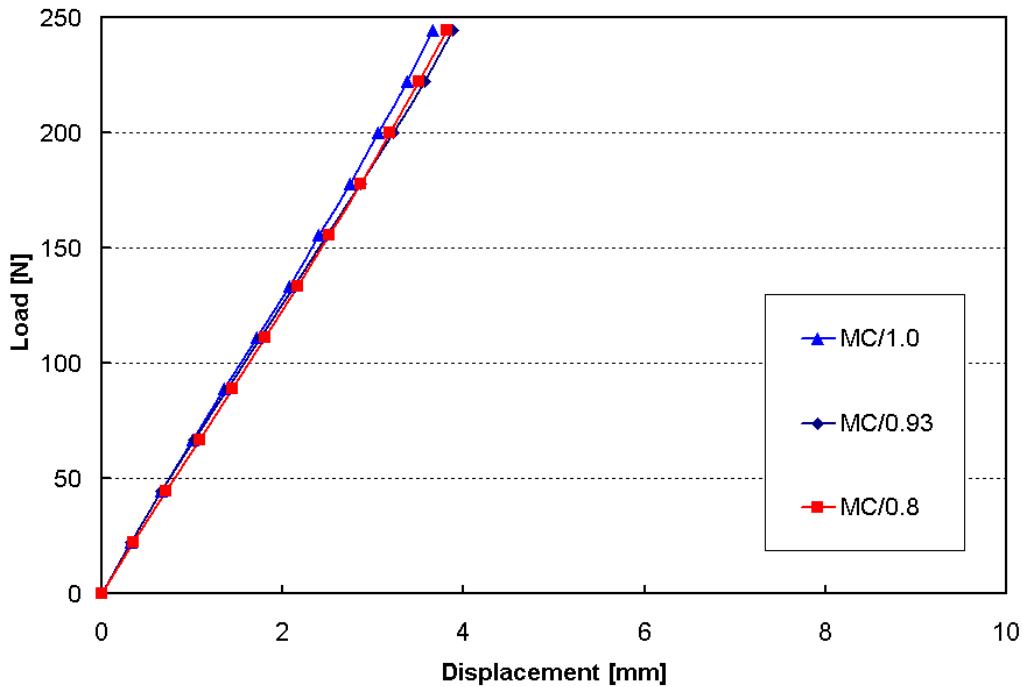
Figure 93: Static stiffness responses at site C for medium curvature assemblies of three outer panel thickness values.

Examination of the medium curvature assembly results reveals some unexpected results. The stiffness response should nominally decrease as thickness is reduced, but this is not always the case. For site A, Figure 91, the thinnest gauge displays a markedly different, and stiffer, response. This observed stiffness increase at site A may be explained due to teacup-related factors that saw this particular site supported differently than the other sites. Perhaps, the thinner sheet is more sensitive to an overly thin mastic layer, which could result in a more direct coupling of the outer panel with the teacup and a stiffer overall response. For sites B and C, there is a negligible difference in stiffness between the 1.0mm and 0.8mm assemblies. This suggests that the global supports have more of an influence on stiffness than panel thickness. This is particularly interesting at site B, Figure 92, that is not directly supported by a teacup, where presumably any thickness effect would be most likely to emerge.

The 0.93mm assemblies consistently offer the least stiff response, with larger differences observed at the lower stiffness sites A and B. This lower stiffness, particularly when compared to the 0.8mm assemblies, is counter-intuitive until the hardening response of the 0.93mm sheet is considered. The 0.93mm sheet displays lower work hardening (Figure

139

24), which may account for the relative loss of stiffness. This may help explain the results observed, but the increased strength of the 1.0mm sheet, compared to the 0.8mm sheet, does not appear to translate into a stiffness effect. Another possible explanation for the increased stiffness for the thinnest sheet is that the mastic may more readily push out the thinner sheet during curing.
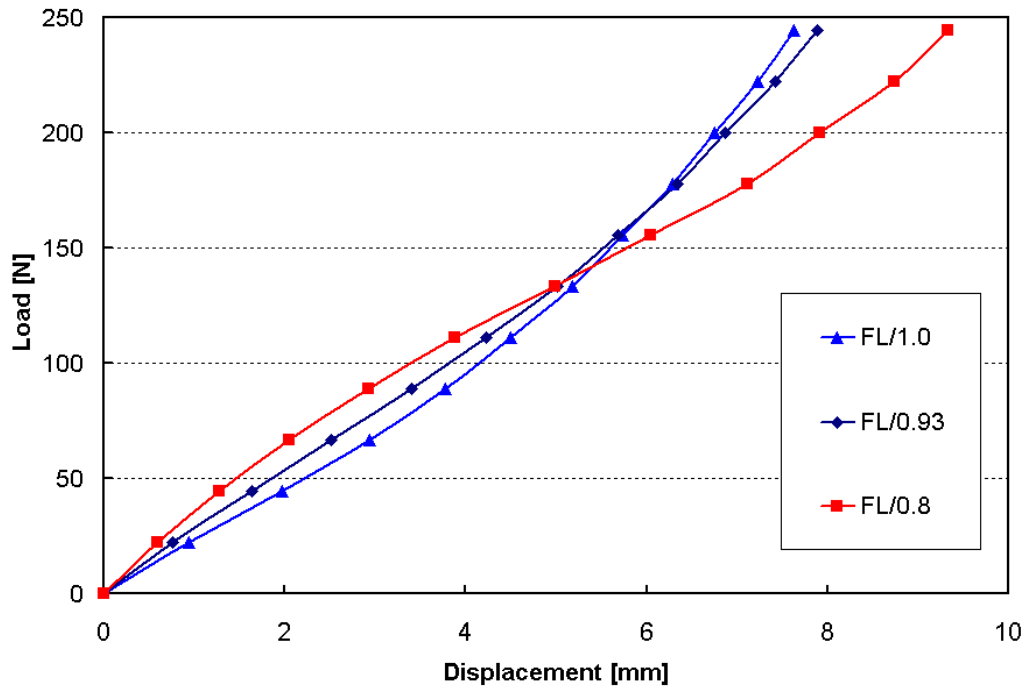
Figure 94: Static stiffness responses at site A for flat assemblies of three outer panel thickness values.
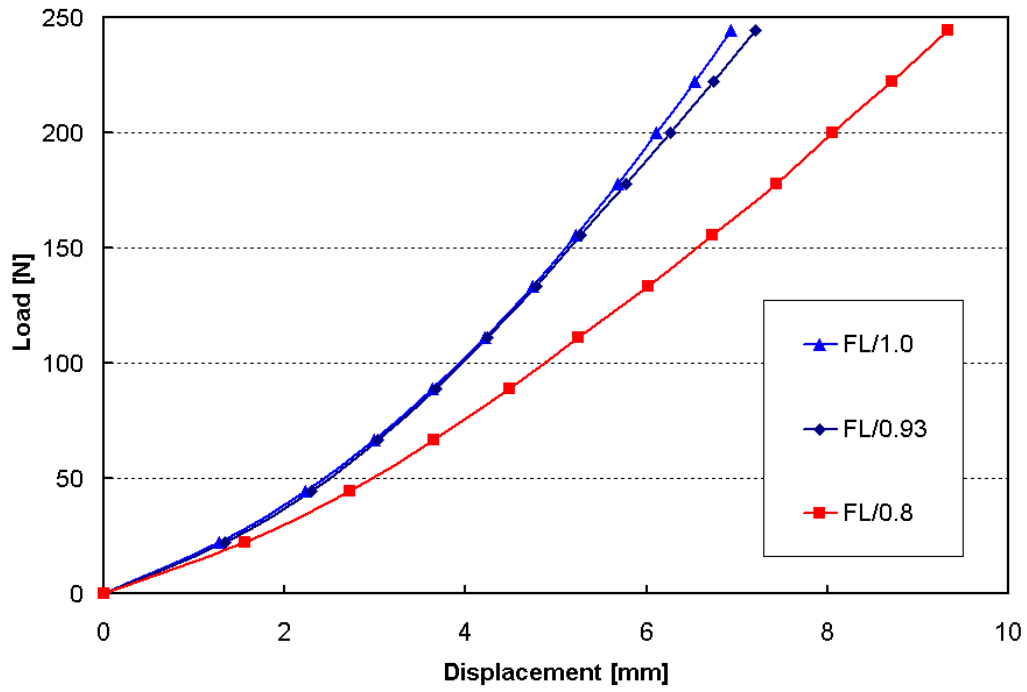
Figure 95: Static stiffness responses at site B for flat assemblies of three outer panel thickness values.
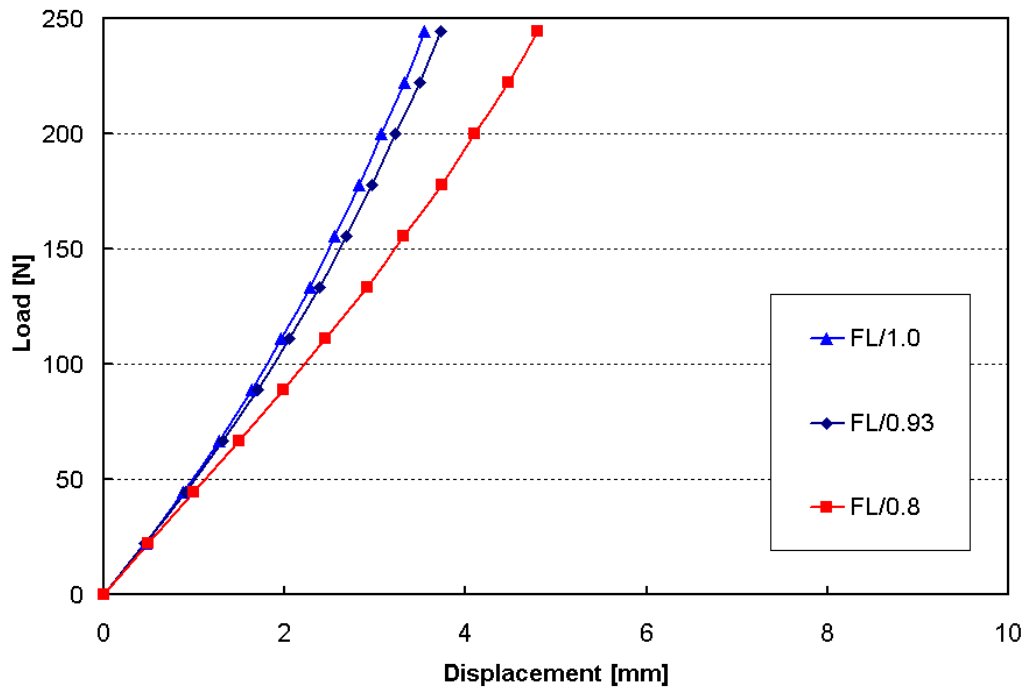
Figure 96: Static stiffness responses at site C for flat assemblies of three outer panel thickness values.

The results for the flat panel stiffness responses, for varying thickness, exhibit more predictable trends. For both sites B and C the expected increase in stiffness with increase in thickness is observed. Only site A, shown in Figure 94, exhibits opposing results. The initial stiffness of site A is higher than the other sites, before softening occurs and the stiffness reduces below that of the other sites. It appears that the thinner sheet at site A maintains it's initial stiffness for a longer period of time before dramatically softening. Teacup related effects might be contributing to the results, as site A generally displays the most complex deflection response.

5.2.4 Effect of Panel Thickness on Static Dent Depth

Comparisons of static dent depths for the medium curvature assemblies for a range of thickness are shown in Figure 97, Figure 98 and Figure 99, for sites A, B and C respectively. The static dent depths for the flat assemblies are compared in Figure 100, Figure 101 and Figure 102 for sites A, B and C respectively. The dent depths are equivalent to the residual displacement after unloading. In some cases, gaps in the dent vs. load curves are present. This is due to measurement errors or omissions during testing.
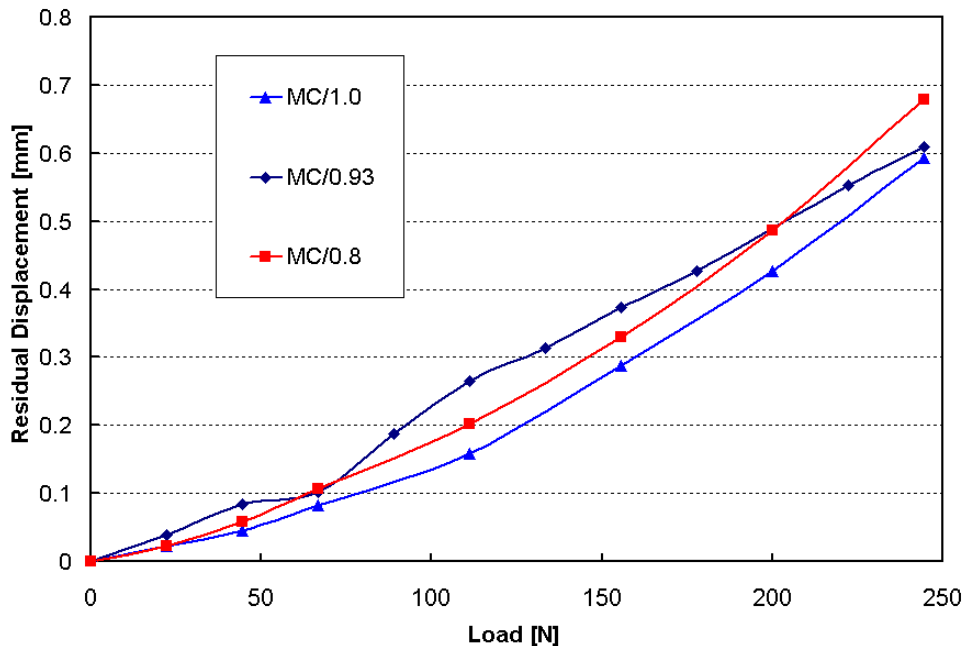
Figure 97: Static dent depths at site A for medium curvature assemblies of three outer panel thickness values.
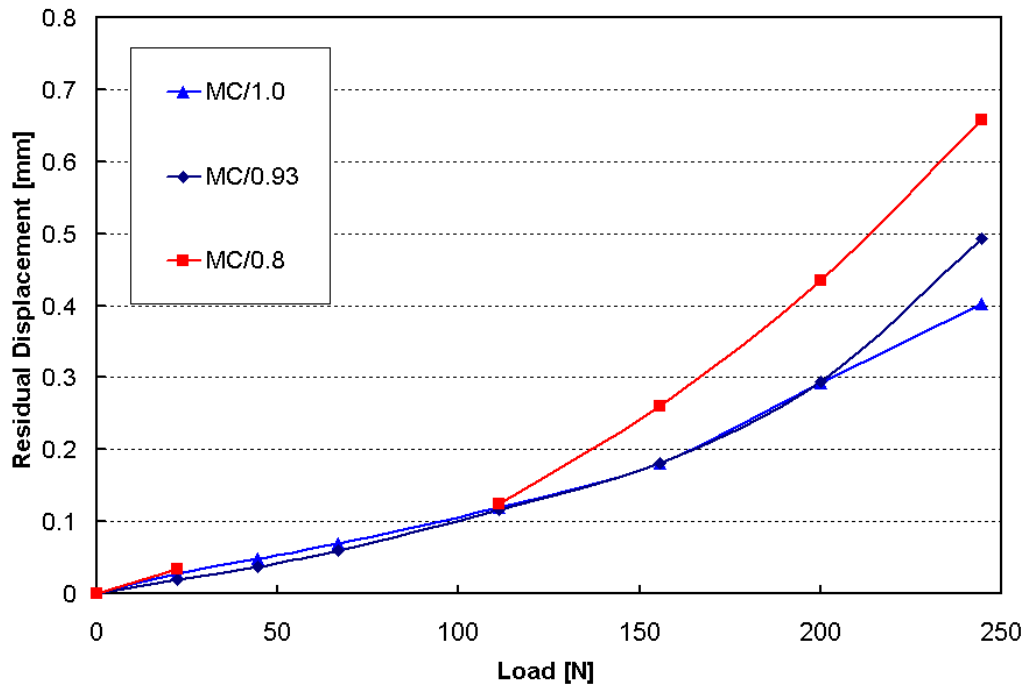
Figure 98: Static dent depths at site B for medium curvature assemblies of three outer panel thickness values.
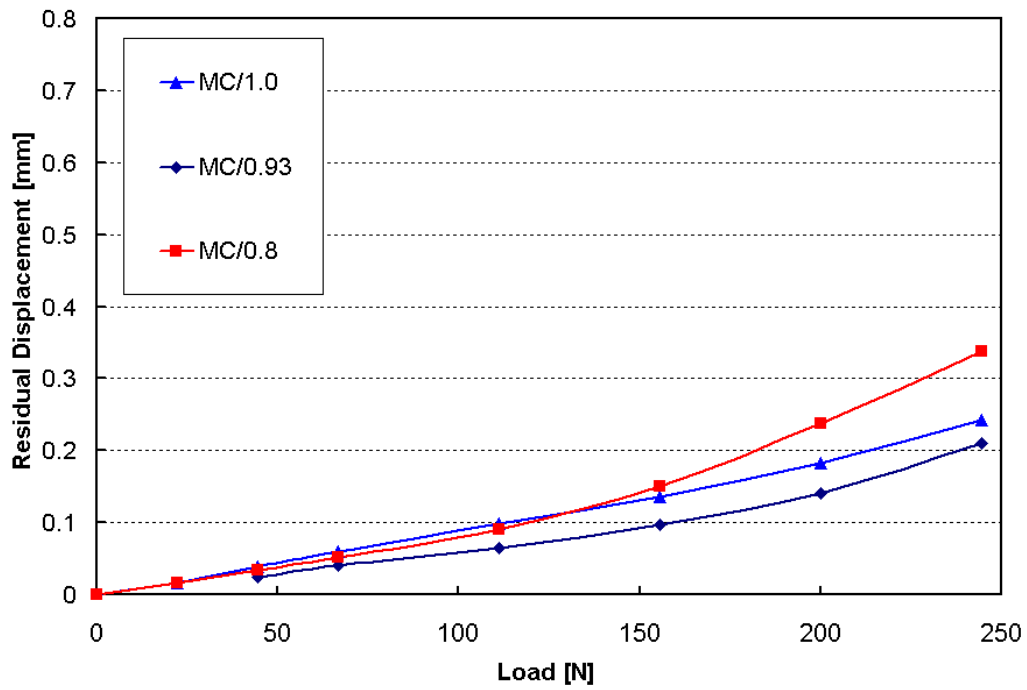
Figure 99: Static dent depths at site C for medium curvature assemblies of three outer panel thickness values.

The results for the medium curvature assemblies are inconsistent with respect to thickness related trends for the various sites. The residual displacement will be highly sensitive to teacup and mastic related issues, as previously discussed. The expected loss of dent resistance for decreasing thickness is only consistently observed for site B, Figure 98, the unsupported site, which is least likely to be influence by teacup and mastic issues. For the other sites the 0.93mm thickness sheet presents unexpected results. The two gauges of the less aged material, 1.0mm and 0.8mm, display consistent and expected behaviours. The 0.8mm sheet offers inferior dent resistance than the thick sheet, with the effect becoming more pronounced as the load level increases. The irregular behaviour of the 0.93mm gauge sheet is difficult to explain. The lower strength of the 0.93mm sheet, as shown in Figure 24, may contribute to the observed behaviour. For site A, where the dent depths are large, the lower strength of the 0.93mm sheet should contribute to the poorer dent resistance. However, the superior performance of the 0.93mm sheet at site C appears to contradict such a conclusion. Site C is the stiffest site, with the smallest dent depths, which should reduce the degree of yielding and thus limit the range of the strength response that applies. The 0.93mm sheet has smaller differences in strength properties at low strain levels, which may at least partially explain the improved dent resistance.
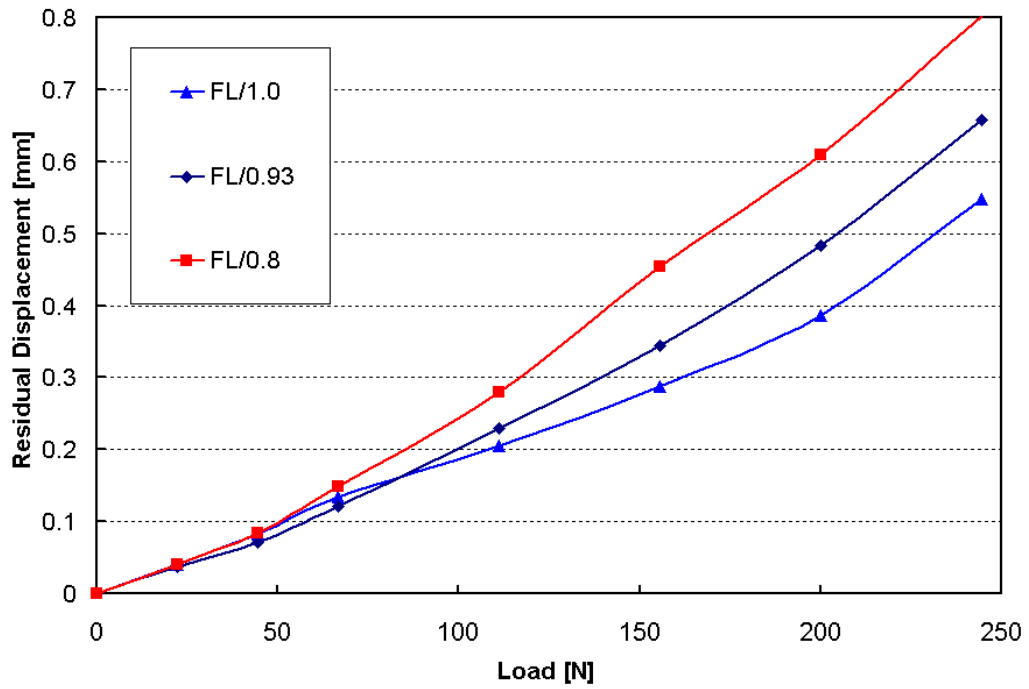
Figure 100: Static dent depths at site A for flat assemblies of three outer panel thickness values.
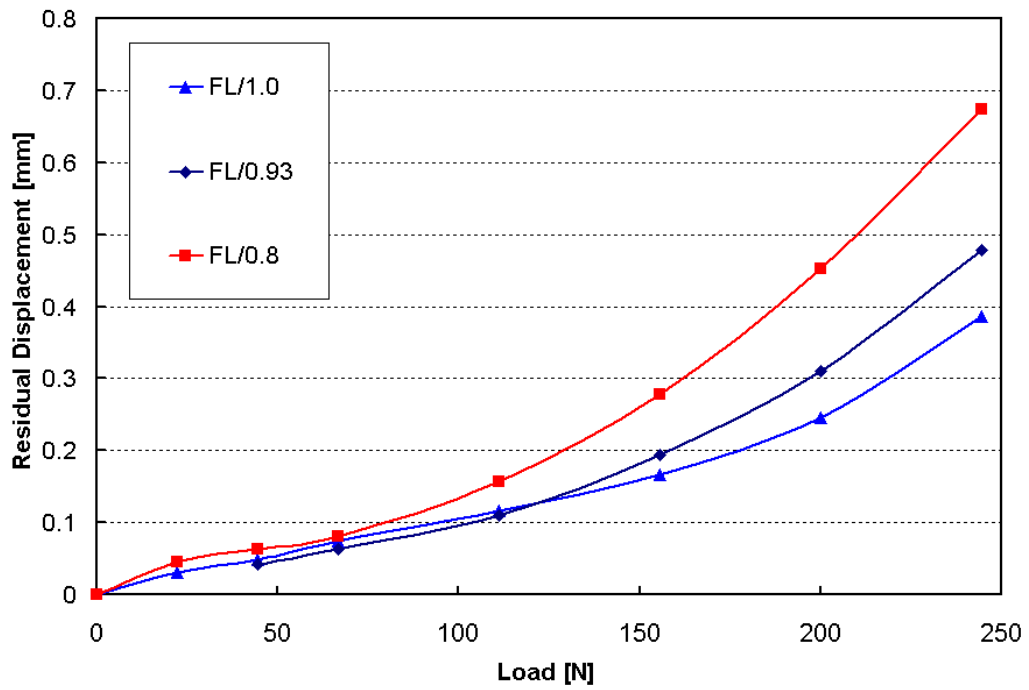
Figure 101: Static dent depths at site B for flat assemblies of three outer panel thickness values.

145
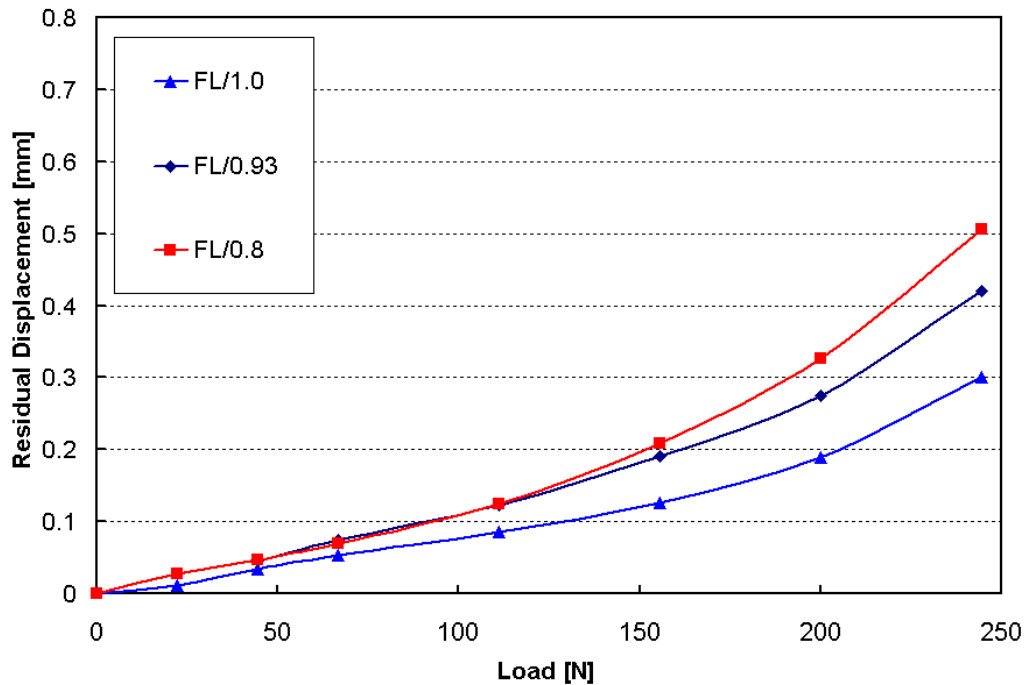
Figure 102: Static dent depths at site C for flat assemblies of three outer panel thickness values.

The thickness effect is consistent for all dent sites for the flat panels. The expected increase in dent resistance, or lower dent depths, with increasing thickness is observed for all locations. Also, as the load level increases, the degree of the thickness effect increases as well. The thickness effect is least pronounced for the stiffest site, site C, shown in Figure 102, where the level of panel deflection is limited to a nearly linear response. The lack of a stiffness transition for site C translates into less divergence of the dent depths at higher loads. The consistent nature of the thickness effect for the flat panels, when compared to the varied results for the medium curvature panel should be noted. The flat panels were generally easier to assemble, as less welding distortion and misalignment occurred. In comparison, the medium curvature panels are more susceptible to variations in the inner panel geometry, which in turn contributes to increased experimental differences from site to site, and from assembly to assembly. The resulting panel geometry is more consistent for the flat panels, which it is believed contributed to more consistent results and trends.

146

5.2.5 Effect of Panel Curvature on Static Stiffness

The effect of panel curvature on static stiffness is examined, for the 0.93mm assemblies, in Figure 103, Figure 104 and Figure 105, for sites A, B and C respectively. The curves are presented without their unloading portions for improved clarity.
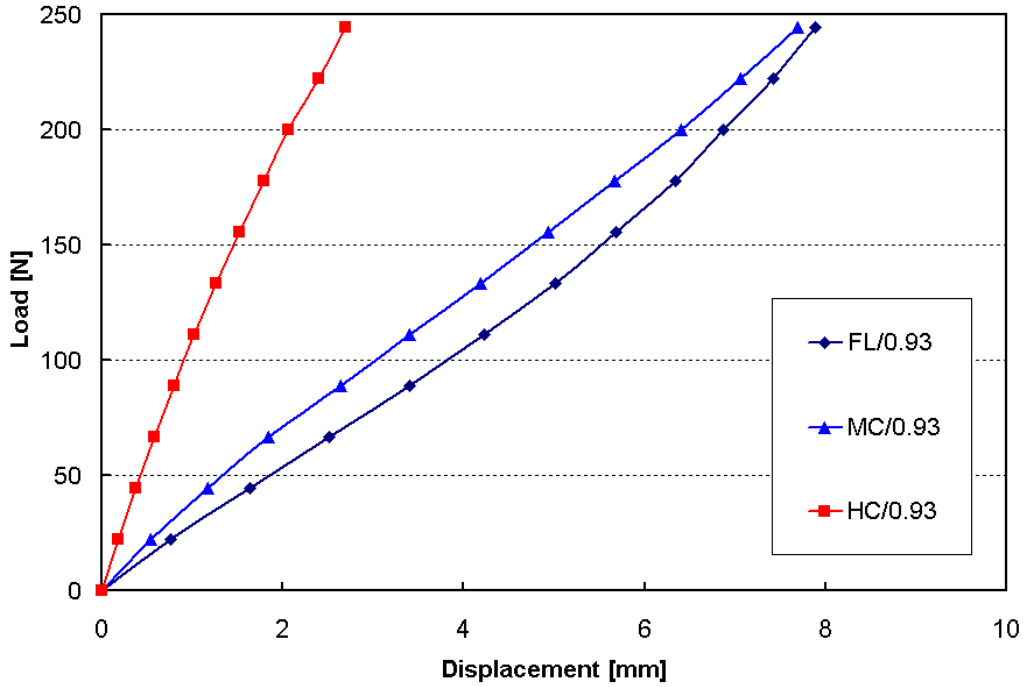
Figure 103: Static stiffness responses at site A for the 0.93mm outer panel assemblies with three panel curvatures.
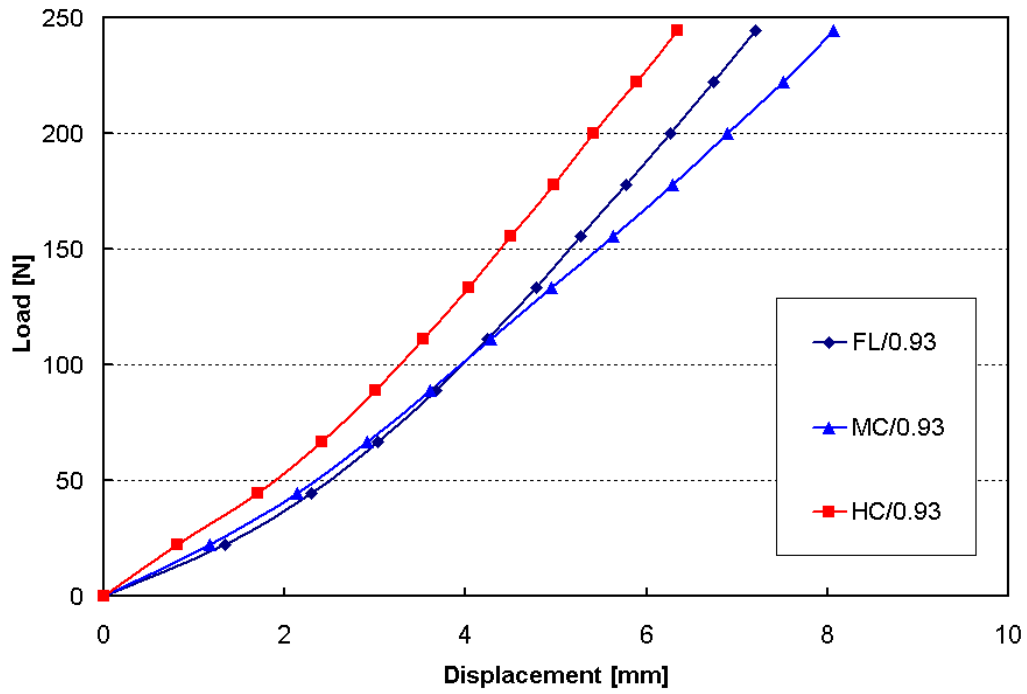
Figure 104: Static stiffness responses at site B for the 0.93mm outer panel assemblies with three panel curvatures.
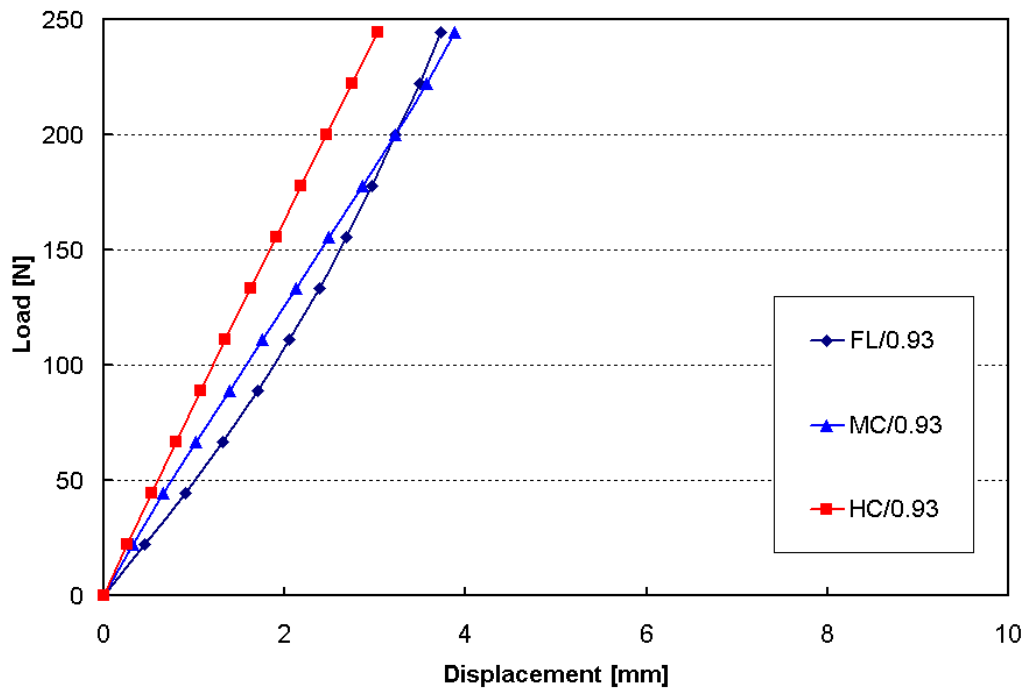
Figure 105: Static stiffness responses at site C for the 0.93mm outer panel assemblies with three panel curvatures.

The effect of curvature on the stiffness response is generally as expected. For all cases the high curvature panel provides superior stiffness response. Of particular interest are the results at Site A, Figure 103, where the high curvature panel retains a relatively linear stiffness response while the other panels display a multi-stage response. The response of the high curvature panel at site A resembles the response of all panels at site C. This suggests that the high curvature panel provides equivalent reinforcement at site A, to that of the surrounding flange and sidewalls at site C. The increased reinforcement of the high curvature panel prevents the snap-through response typical of site A, leading to the linear response common to site C. This highlights interaction of global curvature and local supports on the stiffness response.

5.2.6 Effect of Panel Curvature on Static Dent Depth

The effect of panel curvature on the static dent depths of the 0.93mm assemblies is shown in Figure 106, Figure 107 and Figure 108 for sites A, B and C respectively. The dent depths are taken after unloading from the increasing applied loads.
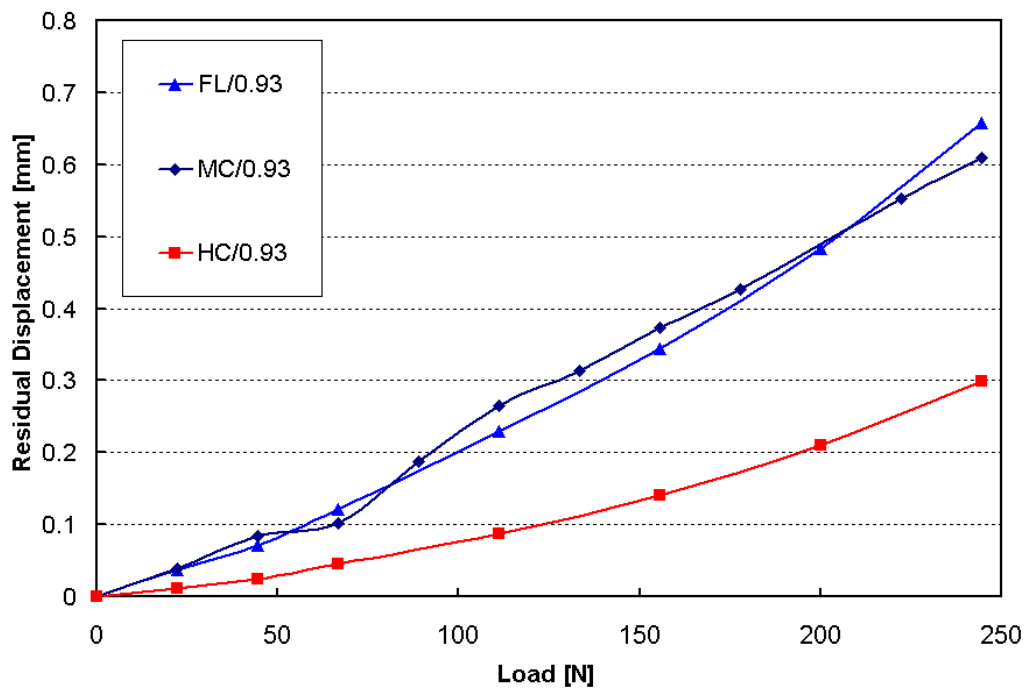
Figure 106: Static dent depths at site A for the 0.93mm outer panel assemblies with three panel curvatures.
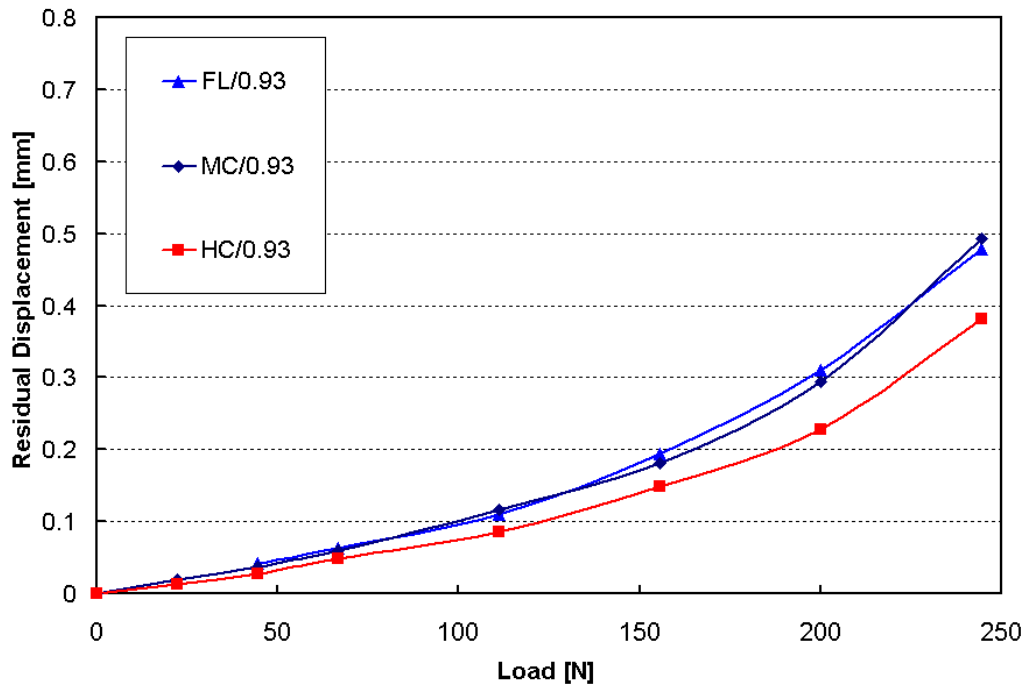
Figure 107: Static dent depths at site B for the 0.93mm outer panel assemblies with three panel curvatures.
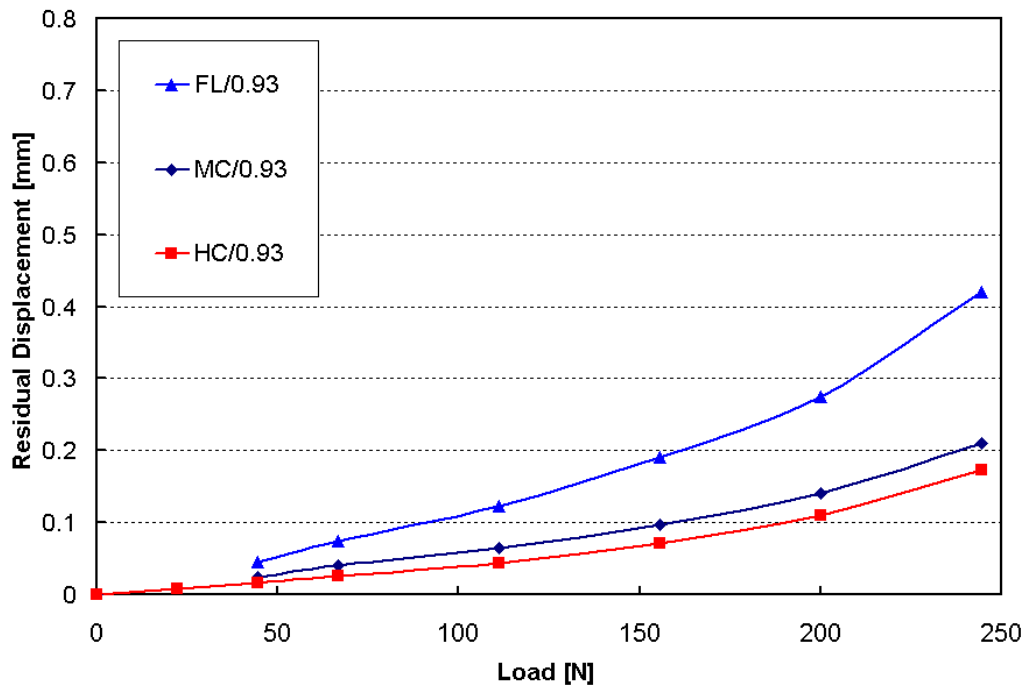
Figure 108: Static dent depths at site C for the 0.93mm outer panel assemblies with three panel curvatures.

150

The results for the static dent depths for the various curvatures reflect the trends observed in the analysis of the stiffness response. The high curvature panels, that exhibited the highest stiffness, consistently yield the lowest dent depths. This correlates well with the expected behaviour that suggests high stiffness causes superior dent resistance. The most dramatic illustration of the stiffness effect on static dent depth is seen in Figure 106, for site A. The high curvature panel had a substantially stiffer response, as shown in Figure 103, which translates into the far lower dent depths observed. The difference in dent depths between the flat and medium curvature panels also relates back to their respective stiffness responses. For site C, where the medium curvature panel was stiffer than the flat panel, the medium curvature panel provides lower dent depths. For sites A and B, where the stiffness responses were less consistent, the dent depths are very similar for the flat and medium curvature assemblies.

5.3 Comparison of Dynamic and Static Dent Behaviour

The results for the dynamic and static denting offer some interesting perspective into the competitive nature of the two denting processes. The number of static sites tested limits the number of sites that can be used to compare the static and dynamic denting behaviour. For both teacup configurations, there are two dent sites that were tested both statically and dynamically, one site centered between four teacups and the other located above an outer teacup. The measured dent depths are presented in Table 5 for all panel assembly configurations. The static results are shown for an intermediate load, 111N and for the peak load of 245N. Sites are designated using the test locations outlined in Figure 52 and Figure 53 for the dynamic sites and Figure 59 and Figure 60 for the static sties. The difference in response, depending on the type of dent, is illustrated in Figure 109. The chart compares the supported and unsupported sites for all the panel combinations tested using the 245N static load data. In comparing the static and dynamic results it is important to recall that the relative magnitudes of the static and dynamic dent depths are not overly important. The more important result is the change in dent depth, for a given type of denting, from the supported to the unsupported sites.

Panel	Sites	Static Dent Depth [mm]		Dynamic Dent Depth [mm]
		111N Load	245N Load	
Teacup Configuration #1				
MC/1.0	B/E - Between 4 Teacups	0.119	0.402	0.019
MC/1.0	C/K - Above Outer Teacup	0.099	0.243	0.263
MC/0.93	B/E - Between 4 Teacups	0.116	0.493	0.029
MC/0.93	C/K - Above Outer Teacup	0.065	0.210	0.305
MC/0.8	B/E - Between 4 Teacups	0.124	0.657	0.076
MC/0.8	C/K - Above Outer Teacup	0.090	0.337	0.472
FL/1.0	B/E - Between 4 Teacups	0.116	0.386	0.021
FL/1.0	C/K - Above Outer Teacup	0.085	0.301	0.287
FL/0.93	B/E - Between 4 Teacups	0.110	0.479	0.053
FL/0.93	C/K - Above Outer Teacup	0.123	0.420	0.318
FL/0.8	B/E - Between 4 Teacups	0.157	0.674	0.079
FL/0.8	C/K - Above Outer Teacup	0.125	0.506	0.463
HC/0.93	B/E - Between 4 Teacups	0.086	0.381	0.026
HC/0.93	C/K - Above Outer Teacup	0.044	0.173	0.300
Teacup Configuration #2				
MC/0.93	B/E - Between 4 Teacups	0.067	0.389	0.037
MC/0.93	C/G - Above Outer Teacup	0.062	0.234	0.339

Table 5: Comparison of static and dynamic dent depths for both teacup configurations. The relative magnitudes of the dent depths illustrate the competing nature of the two denting processes.
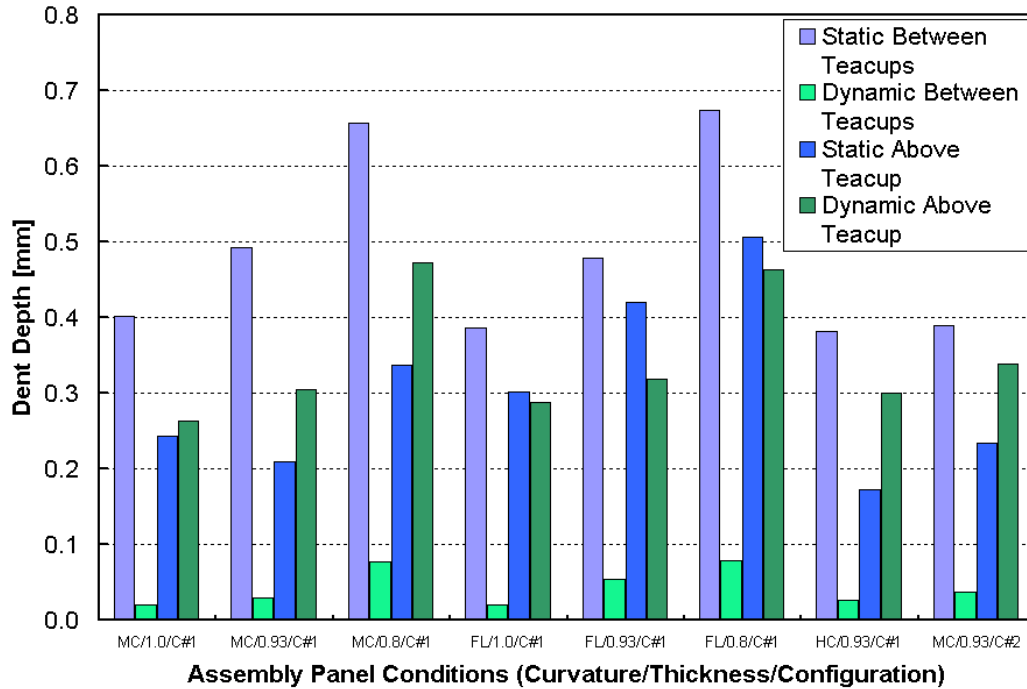
Figure 109: Comparison of static and dynamic dent depth for various panel combinations. The sites above and between teacups are compared using the 245N static load.

The comparisons of the static and dynamic results illustrate the competitive nature of the two denting processes, as shown in previous studies [4,63]. The static dent resistance is superior at the supported sites, directly above the teacups, while the dynamic dent resistance is worse at the teacup locations. A clear drop in dent depth is seen when comparing the static results from the unsupported sites to the supported sites. Conversely, an increase in dynamic dent depth is seen between the unsupported and supported sites. These results are consistent for all panel combinations. The local reinforcement provided by the teacup prevents the panel from absorbing the dynamic impact energy leading to large localized deformation. The same location is highly stiff due to the teacup and the edge supports, which results in low static dent depths. At the unsupported region, the panels are able to store the energy elastically, allowing the indentor to rebound with less plasticity, leading to small dynamic dent depths. The static dent depths at these sites are relatively high, due to the low stiffness at these sites.

Attempting to correlate the static stiffness with the dynamic dent resistance may not always be possible. As noted in the examination of the static dent site locations, the stiffness and dent resistance of two teacup supported sites, A and C, can be vastly different. While the

153

static results appear to be strongly influenced by proximity to the sidewalls and flanges, which provided additional stiffness, the dynamic results are indifferent to these global factors. The dynamic results for all teacup locations are very similar, suggesting that although the stiffness may vary at each teacup, the local reinforcement is similar and controls the dynamic dent process. The thin mastic layer may artificially over estimate the importance of the local reinforcement. However, a more representative mastic layer might offer a similarly localized dampening effect that would override more global stiffness effects. Further examination to clarify the role of mastic thickness on static stiffness and dynamic dent resistance should be pursued.

The effect of panel curvature on the different types of denting suggests that the global curvature is more significant in static denting. As outlined in Sections 5.2.5 and 5.2.6, the high curvature panels exhibited much stiffer responses that translated into lower dent depths. The dependence was quite significant, with dramatically superior dent resistance in some cases. In contrast, the variation in dynamic dent resistance for the range of panel curvatures tested was minimal, as examined in section 5.1.4. This again reinforces the highly localized nature of dynamic denting, where small changes in global curvature have little effect on dynamic dent depth. Static dent resistance is quite dependent on global effects such as curvature and edge conditions.

The effect of thickness is similar for both static and dynamic denting. The dynamic denting process appears to be more sensitive to thickness effects than curvature effects, as the reduction in thickness will affect even a small, localized dent region. The loss of strength as thickness is reduced will affect both static and dynamic dent resistance. The loss of thickness will be coupled with the stiffness response of the panel and thus is harder to isolate in the static cases. Still, the thickness effect is clearly evident in the static dent results.

6 Numerical Results

6.1 Dynamic Denting Results

All of the dynamic denting results presented are for simulations using solid elements to represent mastic. The Young's modulus is 3.93MPa unless stated otherwise. The plots compare the measured and predicted dent depths at all the dynamic test sites as outlined in Figure 52 for teacup configuration #1 and Figure 53 for teacup configuration #2. The numerical predictions of dent depth were calculated using the averaging method outlined in section 4.4.3.

6.1.1 Comparison of Panel Deflection During Dynamic Denting

The various dynamic denting simulations exhibit different deformation histories, prior to reaching their final dent depth, depending primarily on the location of the dent site. The denting simulations at the unsupported sites show a more distributed deflection and require a longer simulation time as a result. The corresponding displacement contours can be examined to illustrate the different deflection behaviours. Figure 110 compares the contours of displacement in the vertical direction after 1ms for supported and unsupported sites, A and E, respectively, for the 1.0mm thick, medium curvature assembly with teacup configuration #1. At 1ms, the teacup dent site has reached its peak displacement and the indentor has begun to rebound. The unsupported site has not yet reached its peak displacement at 1ms. The more compliant, unsupported site is developing both wider and deeper deflection contours than the teacup site.
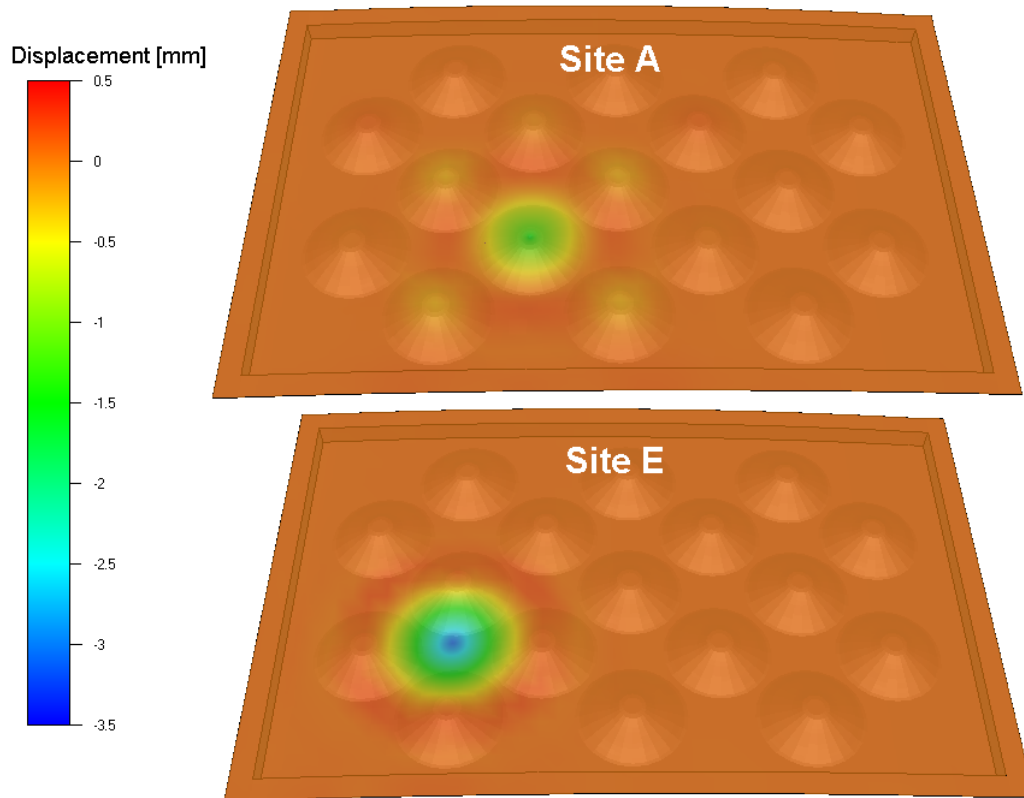
Figure 110: Comparison of vertical displacement contours [mm], after 1ms, between a site directly above a teacup, site A, and an unsupported site, site E. The contours are shown for the 1.0mm, medium curvature assembly with teacup configuration #1.

Figure 111 shows the vertical displacement contours after 2ms, when the unsupported site is near its peak deflection, and the teacup site is free of any indentor contact and is oscillating prior to switching to the springback solution. The contours for site A show a spreading of the panel deflection from the teacup with relatively small magnitudes of deflection. The unsupported site has deflected to a deeper depth around the denting region, and is exhibiting an outer ring where the panel is actually deflecting upward (seen as the dark red areas). The displacement profile at the unsupported site highlights the elastic "catching" of the indentor typical of low stiffness regions. The contours for both sites illustrate the influence of the teacups as the displacement patterns focus around the support points.
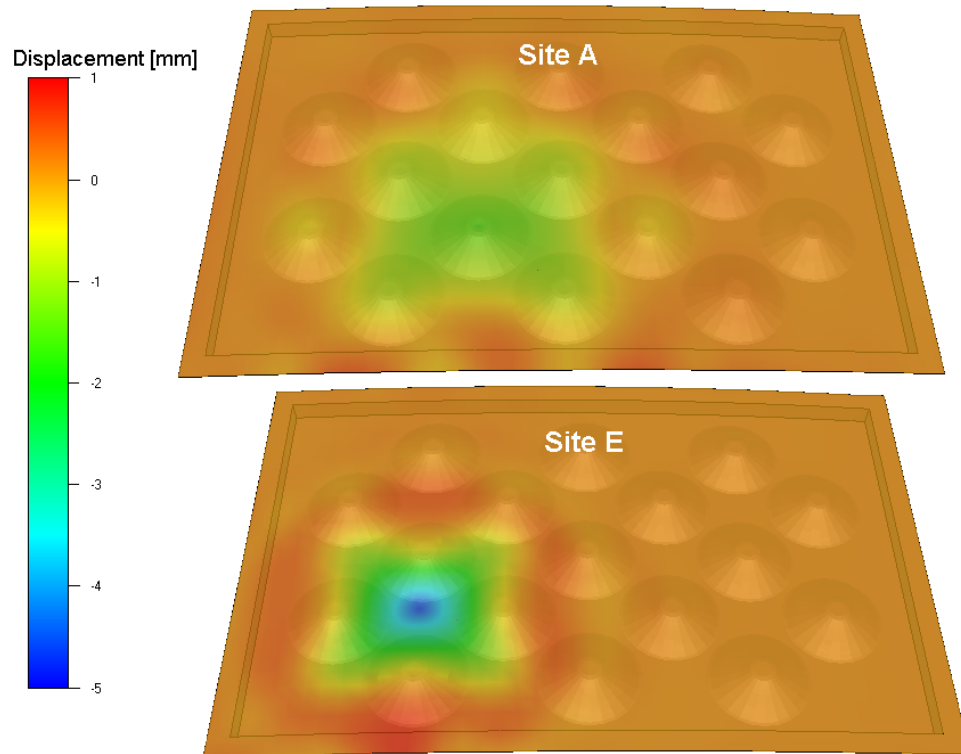
Figure 111: Comparison of vertical displacement contours [mm], after 2ms, between a site directly above a teacup, site A, and an unsupported site, site E. The contours are shown for the 1.0mm, medium curvature assembly with teacup configuration #1.

6.1.2 Comparison of Predicted and Measured Results for All Test Conditions

The predictions for the medium curvature assemblies are presented in Figure 112, Figure 113 and Figure 114 for the 1.0mm, 0.93mm and 0.8mm cases respectively. The predictions are generally quite good at the teacup locations, sites A D, F and K, with slightly lower predictions compared to the measurements. However, as the dent site moves away from the teacup supports the prediction become increasingly less accurate, although the magnitude of the dent depth decreases. The least supported site, site E, shows a large over prediction of the dynamic dent depth. There is over prediction at the intermediate sites B, C, I and J, but not to the same degree. These trends are the same for all thickness values, however the thin sheet predictions seem to be more accurate. The supported sites are correctly predicted as the most susceptible to dynamic denting, and the unsupported sites are predicted to provided the best dent resistance.

The results for the flat panel assemblies are presented in Figure 115, Figure 116 and Figure 117 for the 1.0mm, 0.93mm and 0.8mm thickness outer panels respectively. The

predicted dent depths are again reasonably accurate at the teacup locations, with a tendency to under predict actual dent depth. Similarly, over prediction of dent depth is observed at the unsupported sites, with the worst agreement occurring at site E. The numerical simulations predict the basic trends with respect to dent performance relative to thickness and support conditions for most cases. The results for the 0.8mm sheet thickness show nearly identical dent depths at both the teacup sites and the sites between two teacups. This loss of predictive capability may be tied to the larger panel deflections typical of the thinnest sheet.

The high curvature assembly predictions, shown in Figure 118, and the predictions for the alternative teacup configuration, shown in Figure 119, are similar to the other results. The high curvature results again reflect the effect of support conditions, but offer poor numerical accuracy at the least supported sites. The results for the second teacup configurations also follow the expected trends, with the same relative degree of accuracy. This suggests that the simulations are not overly sensitive to the small change in teacup spacing or variations in global stiffness. The dynamic simulations are consistent for the teacup-supported locations, and are mainly a function of the local geometry, mesh and material properties. The ability of the simulations to successfully predict the best and worst sites from a dynamic dent resistance perspective is encouraging, but the degree of accuracy limits the predictive ability of the simulations. Recognition of poor dent sites is valuable, but the uncertainty of the expected dent depths makes quantitative analysis difficult. Relative comparison of different panels is possible, as the predictions do reflect the changes in dent depth associated with thickness and curvature changes.
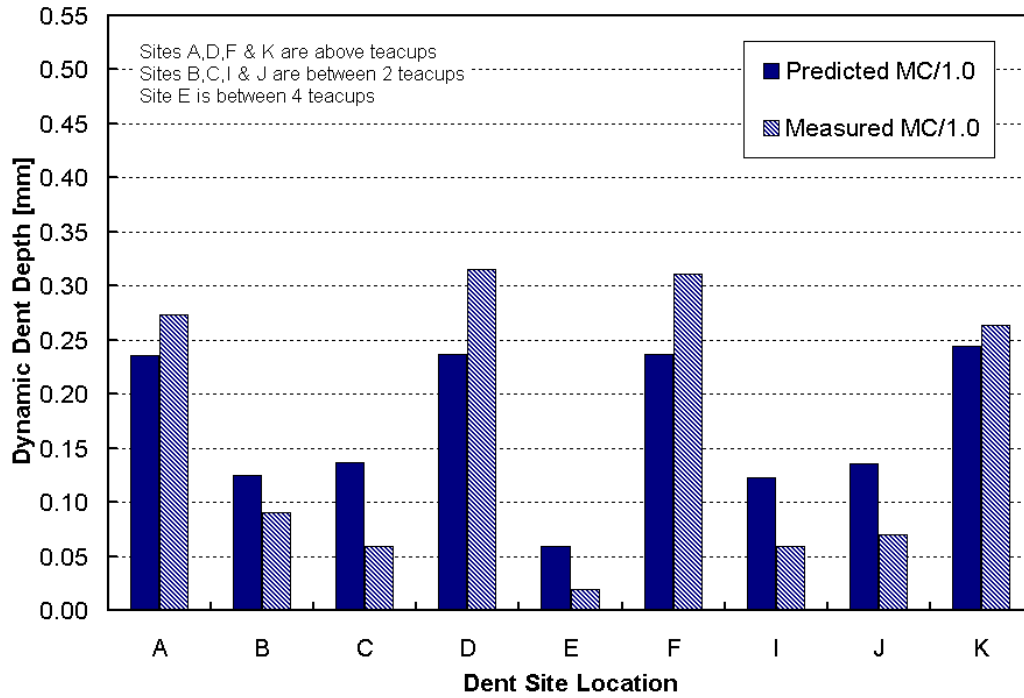
Figure 112: Comparison of predicted and measured dynamic dent depths for the medium curvature, 1mm assembly with teacup configuration #1.
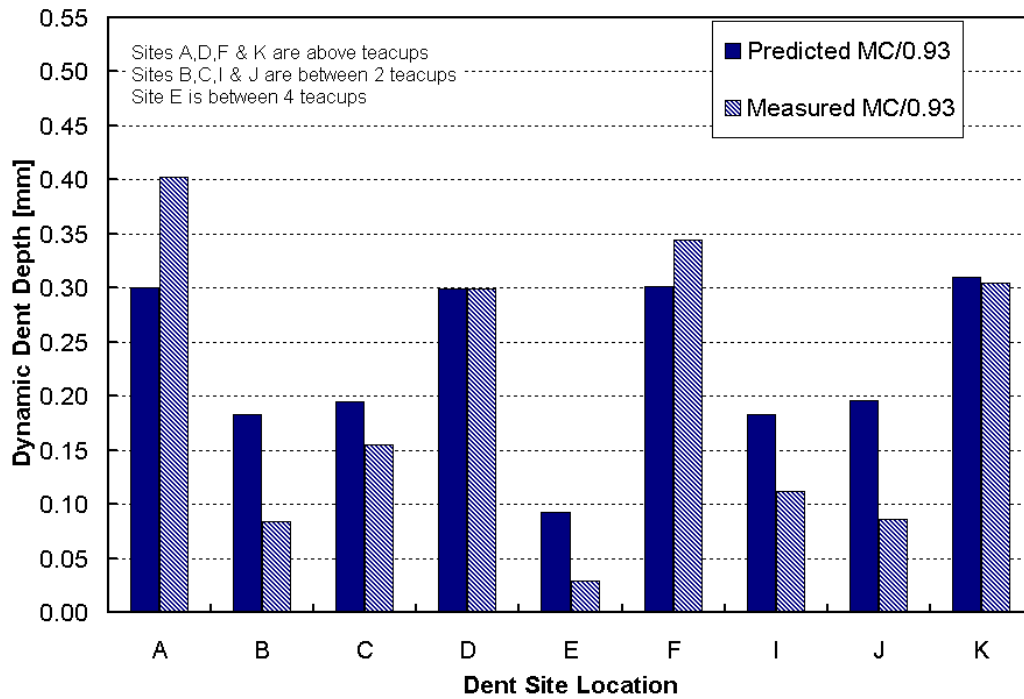
Figure 113: Comparison of predicted and measured dynamic dent depths for the medium curvature, 0.93mm assembly with teacup configuration #1.

159
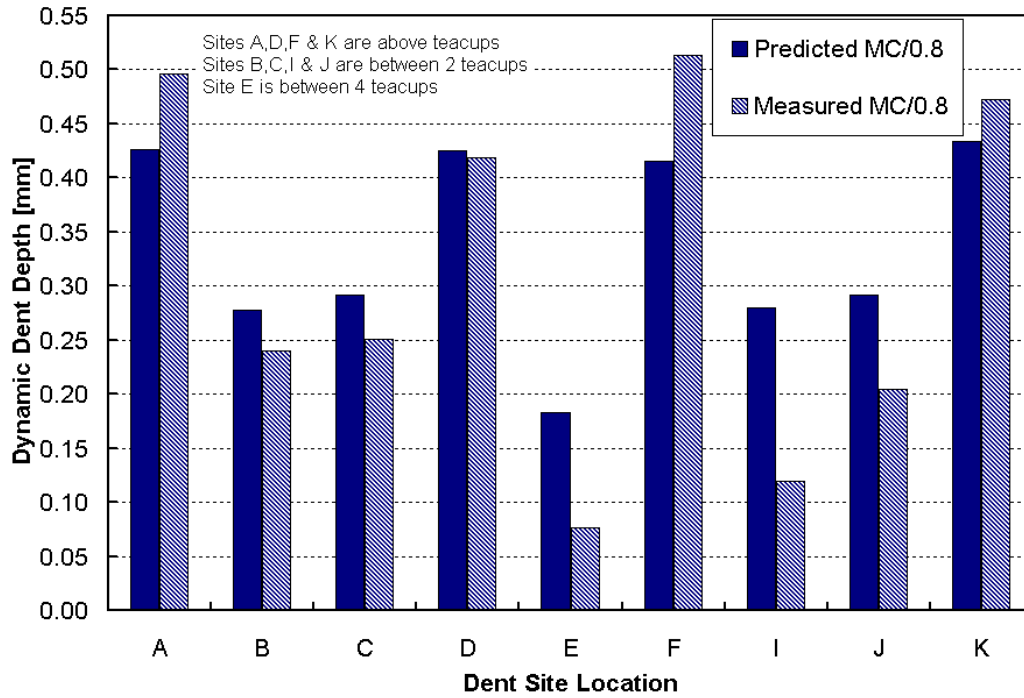
Figure 114: Comparison of predicted and measured dynamic dent depths for the medium curvature, 0.8mm assembly with teacup configuration #1.
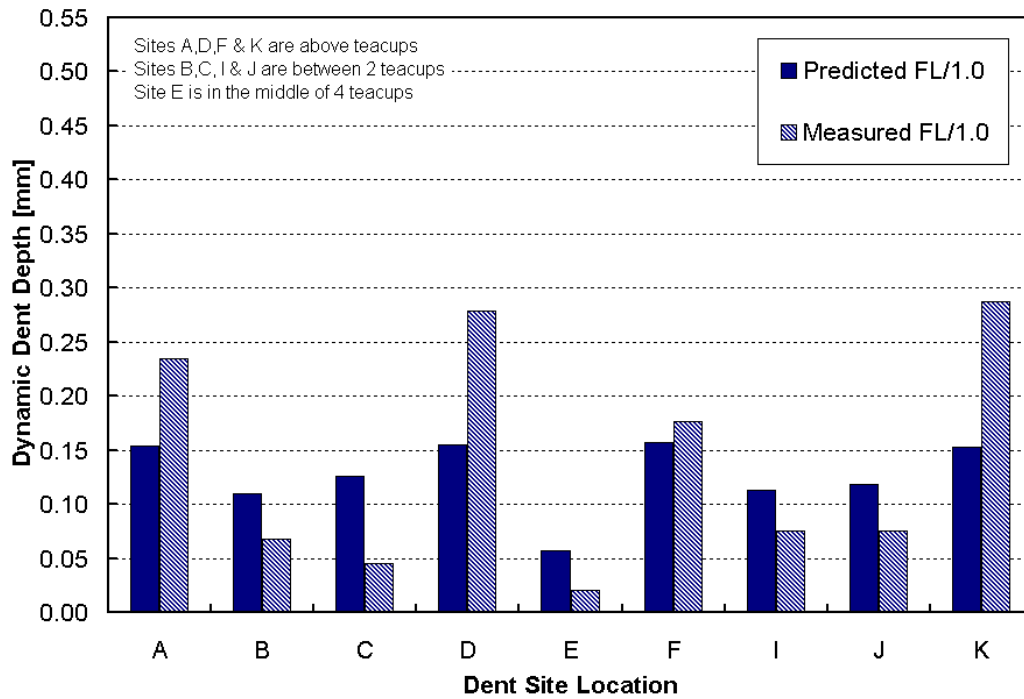
Figure 115: Comparison of predicted and measured dynamic dent depths for the flat, 1mm assembly with teacup configuration #1.

160
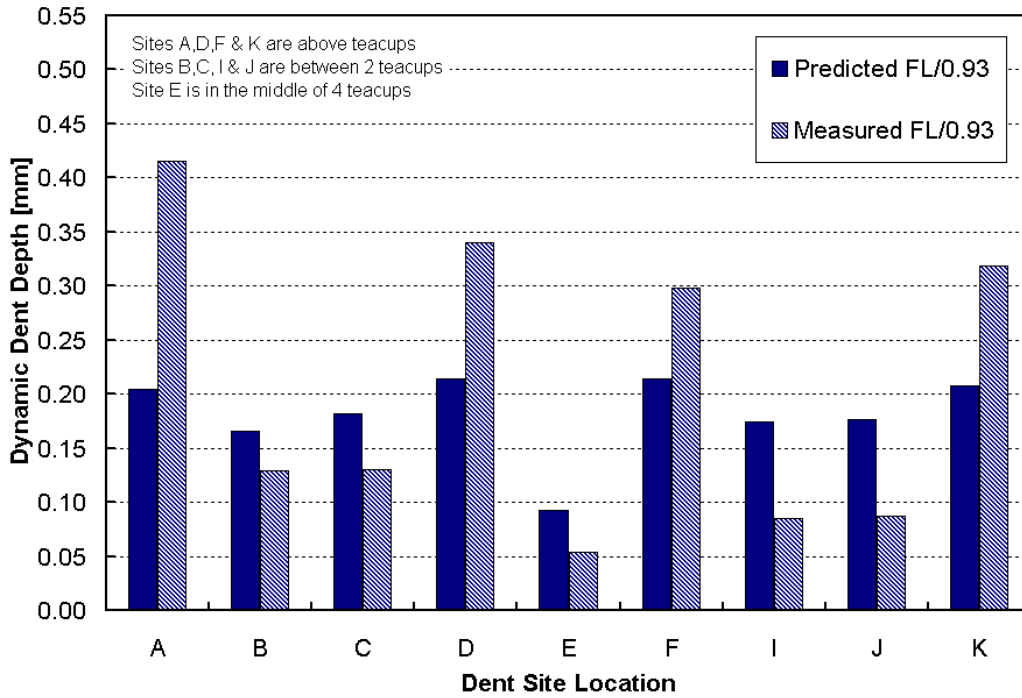
Figure 116: Comparison of predicted and measured dynamic dent depths for flat, 0.93mm assembly with teacup configuration #1.
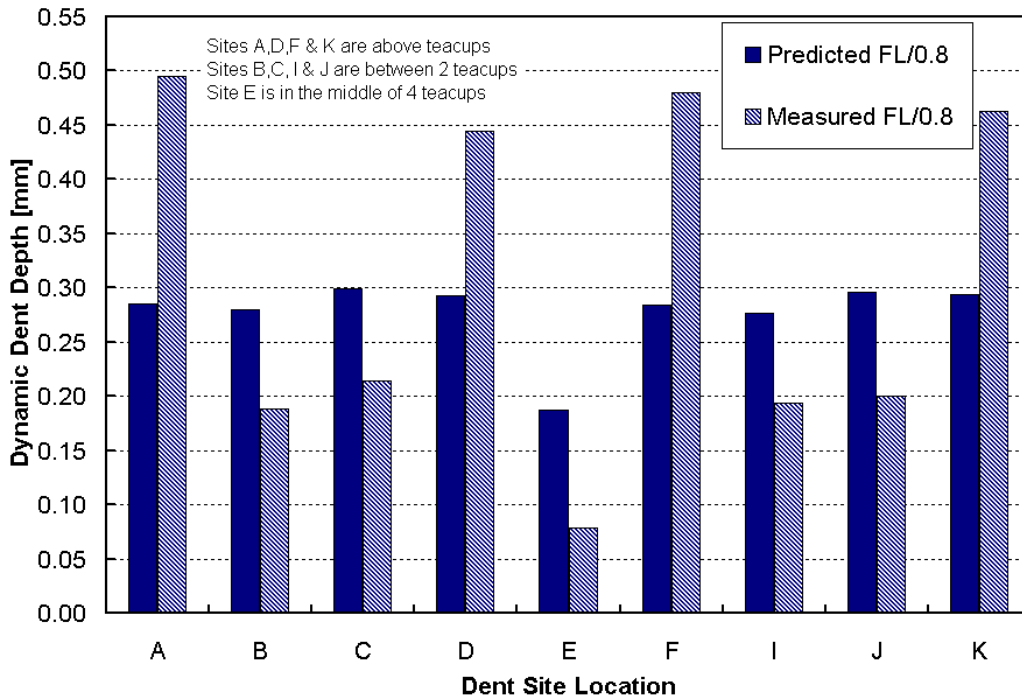
Figure 117: Comparison of predicted and measured dynamic dent depths for the flat, 0.8mm assembly with teacup configuration #1.

161
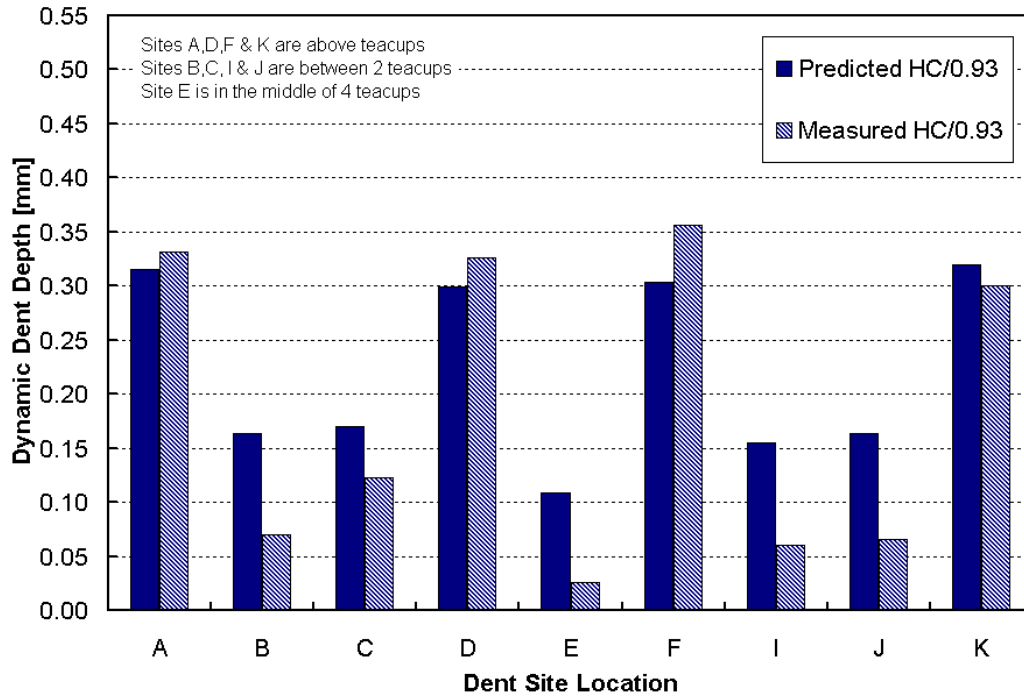
Figure 118: Comparison of predicted and measured dynamic dent depths for the high curvature, 0.93mm assembly with teacup configuration #1.
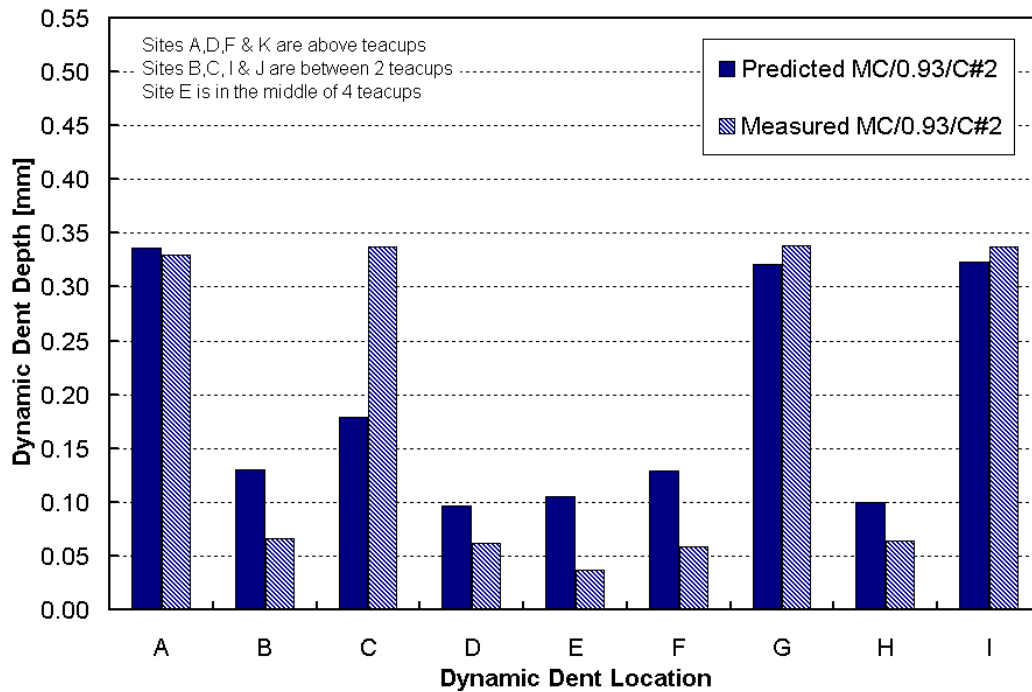
Figure 119: Comparison of predicted and measured dynamic dent depths for the medium curvature, 0.93mm assembly with teacup configuration #2.

6.1.3 Thickness Effect on Dynamic Dent Depth Predictions

An examination of the influence of outer panel thickness on the dynamic dent depth predictions is presented in Figure 120 and Figure 121 for the medium curvature and flat assemblies, respectively. Both figures show that the numerical simulations successfully predict the loss of dent resistance with reduced thickness. The numerical predictions show a linear increase in dent depth as the sheet thickness is reduced for both the flat and curved assemblies. The linear increase is similar to that shown in the experimental results, with the predictions providing a more uniform trend. The numerical results are not affected by teacup and mastic layer variations, leading to the more consistent trends observed. The trends are consistent for all dent locations, regardless of panel support conditions. This indicates that the local yielding at the dent site is closely tied to the sheet thickness in the numerical simulations and is captured for all support cases. The successful prediction of the thickness trends suggests that relative comparisons of numerical results are possible, when absolute dent depths are not considered. The numerical predictions offer potential insight into down-gauging effects on the general denting performance.
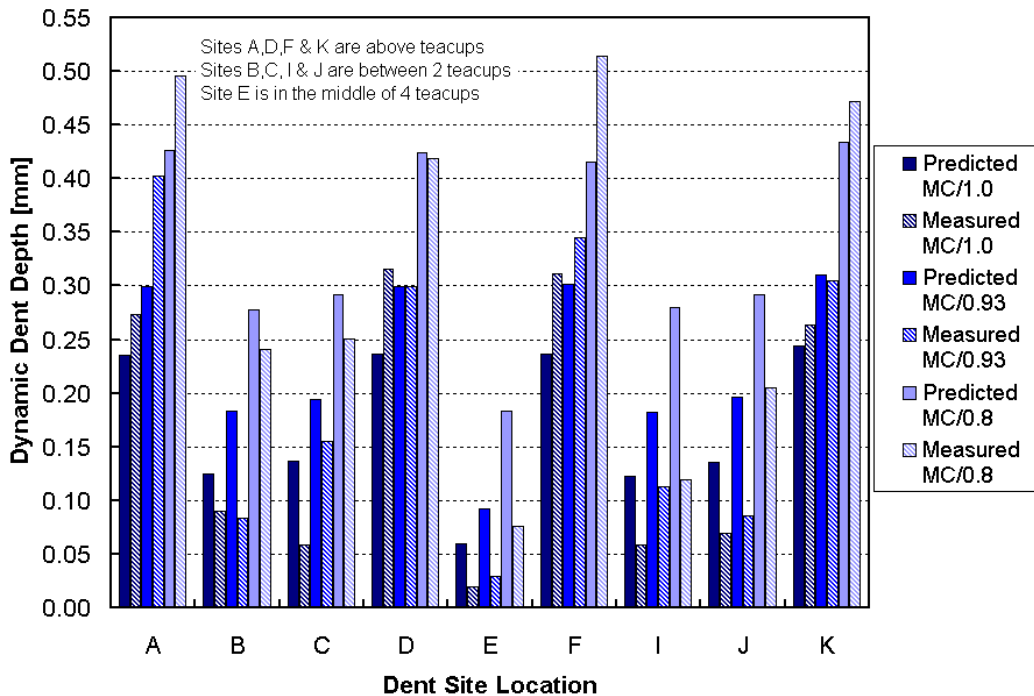
Figure 120: Comparison of predicted and measured dynamic dent depths for the medium curvature assemblies for all three thickness outer panels.
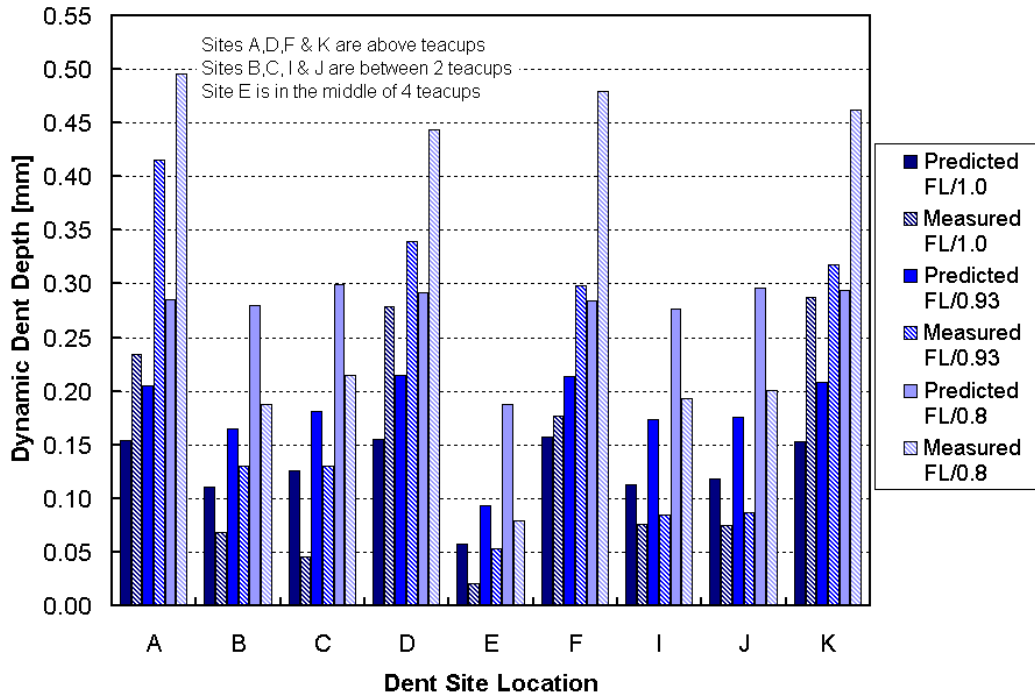
Figure 121: Comparison of predicted and measured dynamic dent depths for the flat assemblies for all three thickness outer panels.

6.1.4 Curvature Effect on Dynamic Dent Depth Predictions

The effect of panel curvature on the dynamic dent depth predictions is presented in Figure 122, for the 0.93mm thick, outer panel assemblies. The numerical predictions show a significant increase in dent depth, at the teacup sites, when comparing the flat and curved panels. There is little change in the predicted results at the teacup locations when comparing the medium and high curvature assemblies. The predictions at the unsupported sites between two teacups are consistently highest for the medium curvature assemblies. The observed numerical trends are not reflected in the measured results that exhibit limited trends with curvature. It should be noted that the experimental results are generally very similar for all curvatures, as discussed in section 5.1.4, and the numerical predictions are also very similar for all curvatures. This suggests that while the accuracy of the results remains sensitive to the local support conditions, the relative effect of curvature can be captured. This again suggests that relative assessment of panel curvature is possible using the numerical approach.
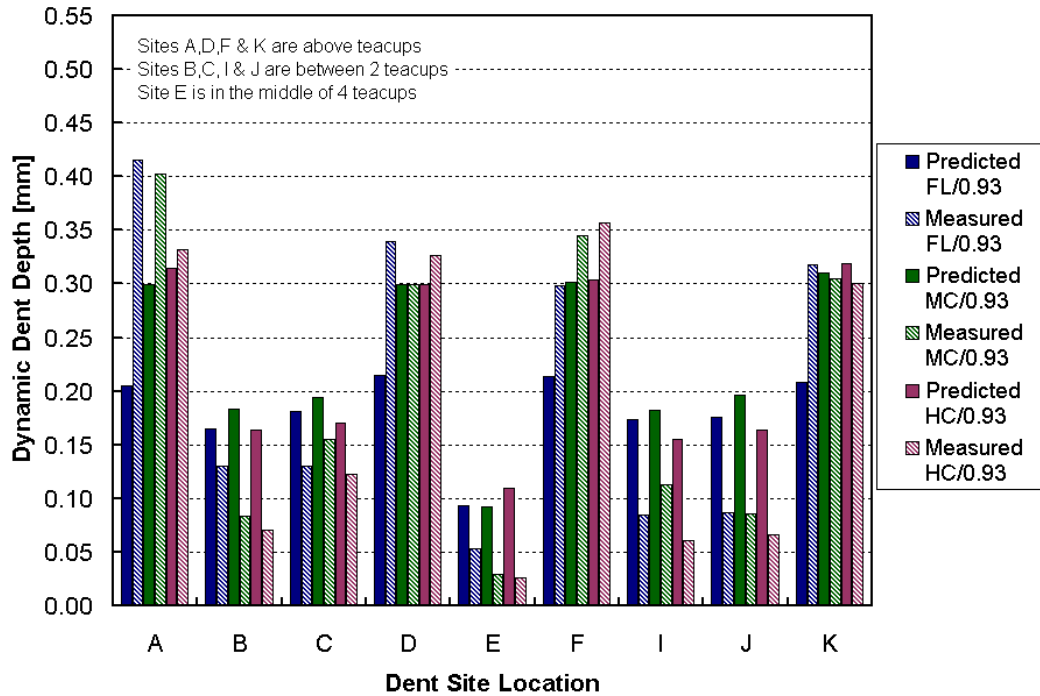
Figure 122: Comparison of predicted and measured dynamic dent depths for the 0.93mm outer panel assemblies for all assembly curvatures.

6.1.5 Predicted Contact Forces During Dynamic Denting

As discussed in section 4.2.2, the modelling approach used for the mastic assumed a linear elastic material response. This response is incapable of capturing the non-linear force-displacement behaviour displayed by the mastic, which limits the predictive capabilities of the simulations. A typical set of contact force vs. time history profiles is shown in Figure 123 for all the modelled dent sites. The dynamic dents at the teacup locations experience large contact forces, between the outer panel and the indentor, that exceed 500N. In contrast, the contact forces developed in the denting of the unsupported sites are around 200N to 250N. For the dents directly above a teacup, the majority of the force is transferred to the mastic pad below the dent site. For the unsupported sites, the contact force curve represents the combined forces experienced at the surrounding pads. As such, for the sites between two cups, the actual force at each pad is expected to be on the order of one-half the value recorded and for the central site E, the force would be roughly one quarter the reported value.

165
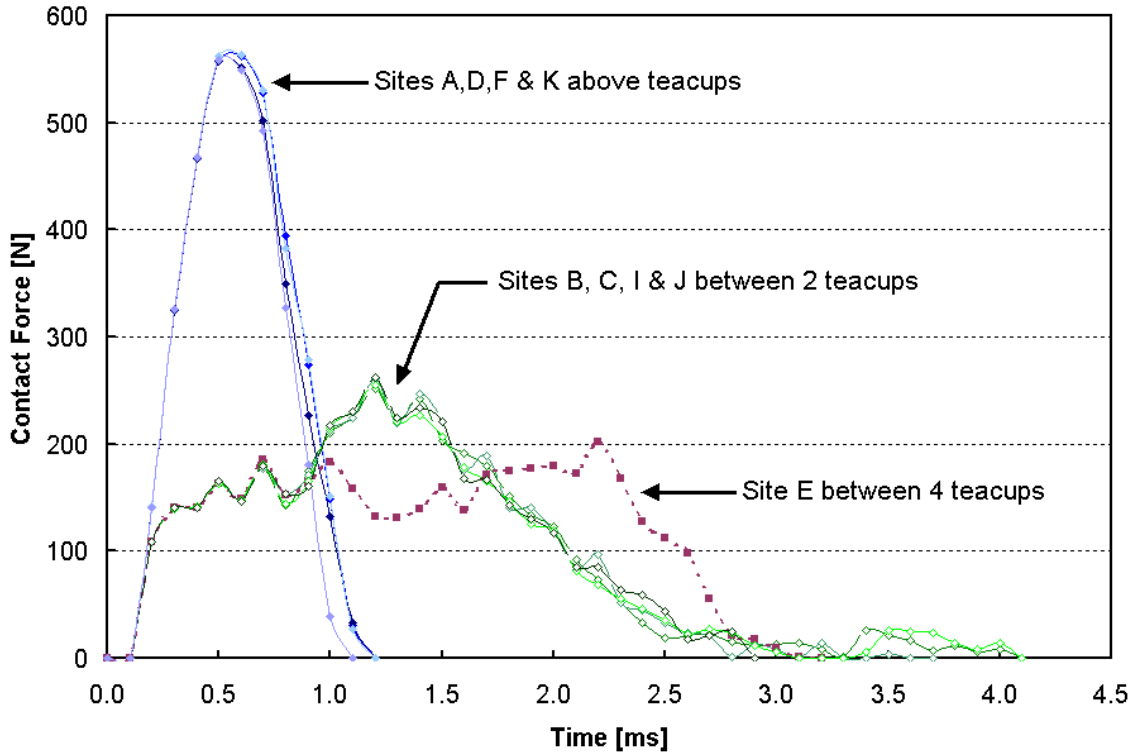
Figure 123: Contact forces between the outer panel and the indentor for dynamic denting simulations of the 1.0mm, medium curvature assembly with teacup configuration #1.

Based on the examination of the mastic response in Figure 44, a linear elastic model is incapable of capturing this response. The mastic stiffness used for the numerical results was based on a 500N applied load, which helps explain the good agreement of the results when denting at the teacup locations.

The mastic thickness coupled with the tied contact surfaces used to connect the mastic to the inner and outer panels are also a concern from a more general perspective. The very thin, constrained mastic layer may introduce an artificially stiff response as it does not deform sufficiently when the impact occurs away from the teacups. If the models are incapable of deflecting and absorbing the indentor energy this may contribute to the high dent predictions. The very thin mastic layer is introducing error in the numerical results due to the complicated mastic response and interactions. Subsequent modelling of full hood assemblies by Viertel *et al.* [65], using a thicker mastic layer, showed superior results for dents between teacup supports. In these models the thicker mastic layer was better represented, in both tension and compression, when using a linear approximation for mastic

166

stiffness. For the thicker mastic layer, the contact forces developed were significantly lower, even at teacup locations, rendering the non-linearity of the mastic response much less significant.

6.1.6 Effect of Mastic Stiffness on Numerical Predictions

Based on the problems resulting from the mastic stiffness, simulations using alternative stiffness values were performed. Only a limited number of dent sites were used on a single panel assembly. Sites A, B and E were modelled with the 1.0mm, medium curvature assembly with teacup configuration #1. This provided one site with each of the typical support conditions, site A above a teacup, site B between 2 teacups and site E between 4 teacups. A high stiffness mastic, based on the stiffness response of the mastic beyond 400N, as shown in Figure 44, was modelled using a Young's Modulus of 16.44MPa. This stiffness should better represent the high contact force cases occurring at the teacup sites. A low stiffness simulation, using a Young's Modulus of 1.01MPa corresponding to the tensile stiffness, was also run. The results for the dynamic dent depth predictions for varying mastic stiffness are compared in Figure 124. The measured dent depths and the predicted dent depths for the base model with 3.93MPa mastic stiffness are included for comparison.
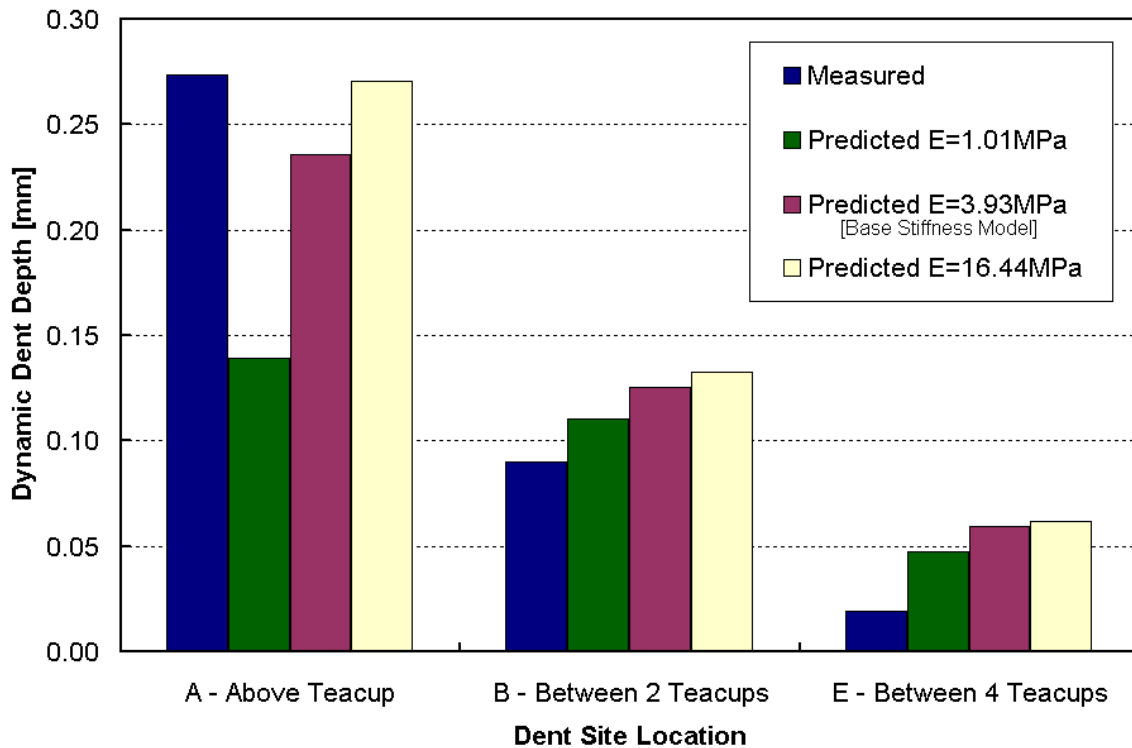
Figure 124: Effect of variation in mastic stiffness on dynamic dent predictions at typical dent sites for the 1.0mm, medium curvature assembly with teacup configuration #1. The base model used a mastic stiffness of 3.93MPa.

The higher stiffness models better predict the dynamic dent depth at the teacup location. This illustrates that the mastic stiffness can be used to adjust the model to match measured results at teacup sites. However, the increase in stiffness translates into more severe over prediction of dent depth at the unsupported sites. A more detailed material model, that incorporates an increased stiffness response at higher forces, would offer the same improvement at the teacup sites without hindering the results at the unsupported sites. The results for the lower stiffness model show a reversed effect on dent depth. The Low stiffness model produced the lowest, and worst, dent depth prediction at the teacup site, while offering improved accuracy at the unsupported sites. This suggests that the unsupported dent site results should improve if a more representative stiffness response is implemented for the mastic. However, other numerical factors may be contributing to the overly stiff response at the unsupported sites compounding the prediction error. The simulation sensitivity to mastic properties highlights the need for further improvements in the mastic modelling.

6.1.7 Effect of Refinement on Dynamic Dent Depth

The effect of mesh refinement was examined for the unsupported test site, site E, of the medium curvature, 1.0mm thick assembly with teacup configuration #1. Mesh refinement was expected to have the most significant effectt on the unsupported site, with broader panel deflections. As a result, the effect of refinement was not examined for the teacup sites, where global deflections were less critical. Predicted dynamic dent depths for four refinement combinations, for different refinement radii and re-meshing algorithms, are compared in Figure 150. The refinement algorithms were detailed in Section 4.3, with typical resulting meshes shown in Figure 70. Recall that the second re-meshing algorithm produces a larger region of highly refined, small, elements with small transition regions to the original mesh. The base dynamic denting models used a 100mm radius of refinement with re-meshing algorithm #1. A simulation using re-meshing algorithm #2 with a 100mm radius of refinement, the same mesh used for the static dents was also performed. Two simulations, for each refinement algorithm, were performed at a larger radius of refinement. Both large refinement radii saw the edges of the refined mesh reach the surrounding teacups, providing a large region of refinement to capture the panel deflection. The large radius, algorithm #2 mesh required a substantially longer run time and large implicit memory requirements, rendering this degree of re-meshing prohibitive for a more extensive set of predictions.
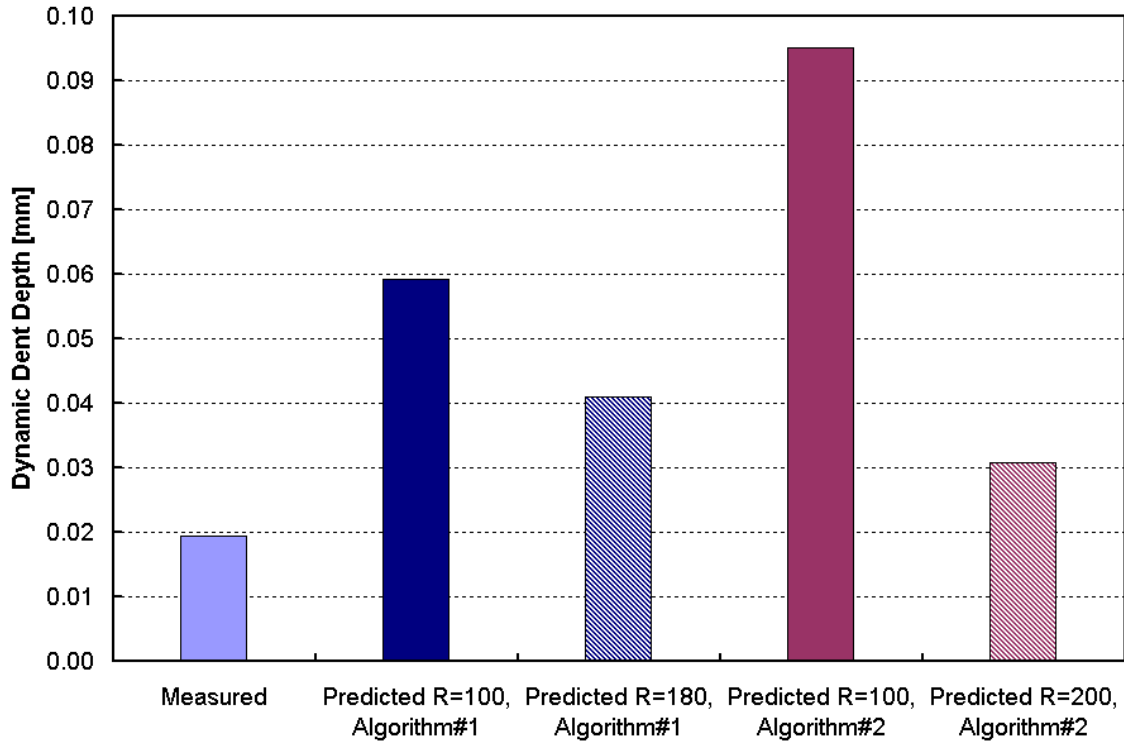
Figure 125: Comparison of dynamic dent depth at site E, of the medium curvature, 1.0mm assembly with teacup configuration #1, for various mesh refinement radii and the two re-meshing algorithms.

The results shown in Figure 150 illustrate the improvement in dent predictions with increased refinement radius regardless of re-meshing algorithm. All meshes over predict the measured dent depth. The best results are achieved for the 200mm radius of refinement, using the second re-meshing algorithm. This mesh offers a large region of highly refined elements that better capture the complex panel deflection. In extracting the dent depths the benefits of the highly refined mesh were pronounced. The dent depth is a function of both the displacement of the node below the dent site and the displacement of the surrounding ring of nodes, as discussed in Section 4.4.3. The degree of dent site, nodal displacement was a function of mesh refinement, with smaller displacements observed at the highly refined sites. In contrast, the displacement of the surrounding ring of nodes was quite similar for all meshes, except the R=200mm, algorithm #2 case. This is attributed to the mesh for this single case being better able to capture the more global panel displacements. The results for the R=100mm, algorithm #2 mesh are troubling due to the large increase in the predicted

170

dent depth. It was expected that this mesh would offer comparable results to the base model. Perhaps the rapid transition from highly refined to coarse elements, at a radius near the transition in bending of the panel, is the source of the increased error. Despite the improvements in prediction associated with increased refinement, the results are still poor for the unsupported site. For limited dynamic dent evaluation, where precision is a key concern, a large radius of very small elements is desirable. However, the numerical cost of using large degrees of refinement becomes prohibitive for large arrays of test sites and conditions.

6.2 Static Denting Results

All the static denting results presented are for simulations using solid mastic elements with Young's modulus of 3.93MPa. The plots compare the measured and predicted static stiffness and static dent depths at all the static test sites as outlined in Figure 52 for teacup configuration #1 and Figure 53 for teacup configuration #2.

6.2.1 Comparison of Predicted and Measured Static Stiffness for All Test Conditions

The static stiffness predictions are presented with only the loading portion of the curves for improved clarity. The predicted and measured results are presented for each of the test configurations in Figure 126 to Figure 133, with all test sites included on each plot. The various plots will vary somewhat from case to case as the numerical load step sizes used were adjusted as required to achieve convergence of the simulations. This was done mainly in the low load regions where the initial 22.2N load step was often omitted to ensure sufficient contact over the first implicit iteration. The numerical results still reflect the overall loading conditions used in the experimental testing.
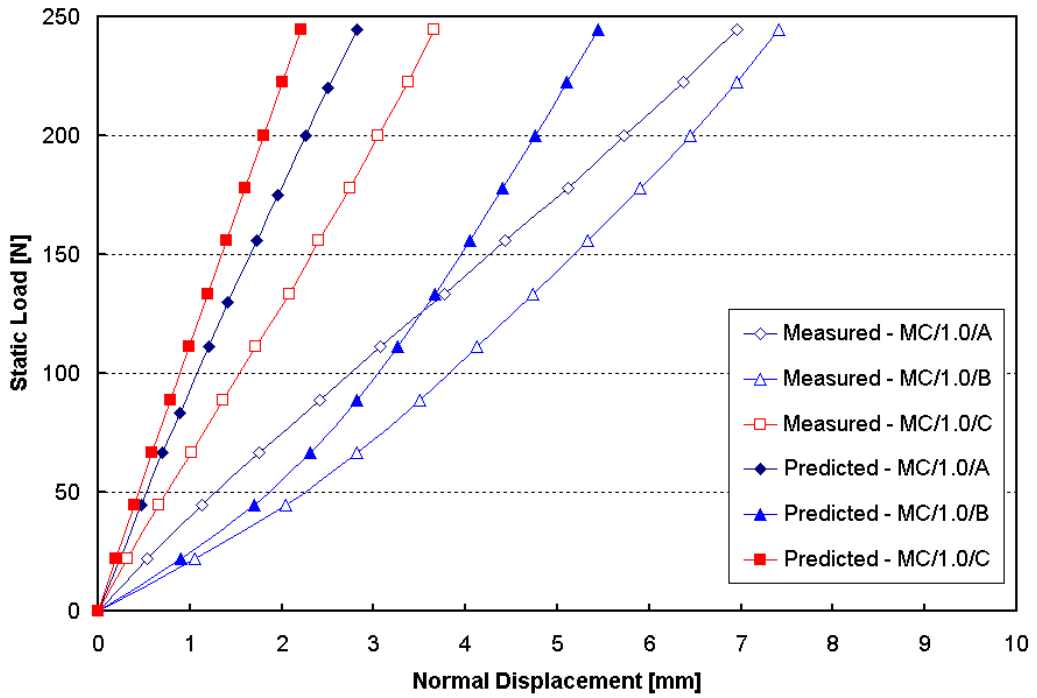
Figure 126: Predicted static stiffness response at all sites for medium curvature, 1.0mm thick, panel assemblies with teacup configuration #1.
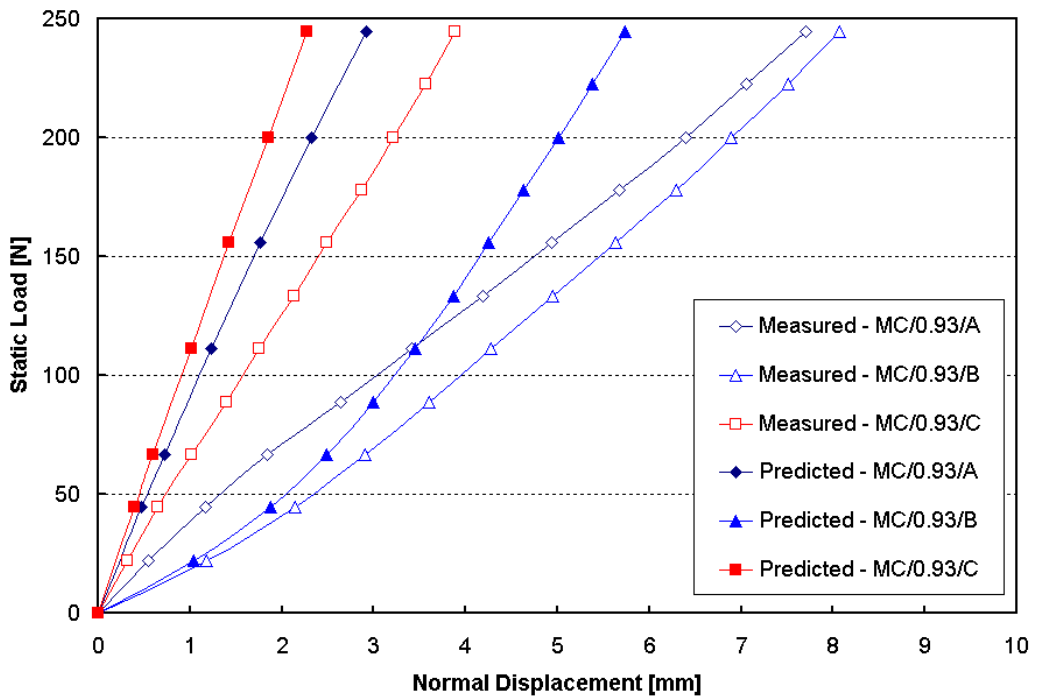
Figure 127: Predicted static stiffness response at all sites for medium curvature, 0.93mm thick, panel assemblies with teacup configuration #1.
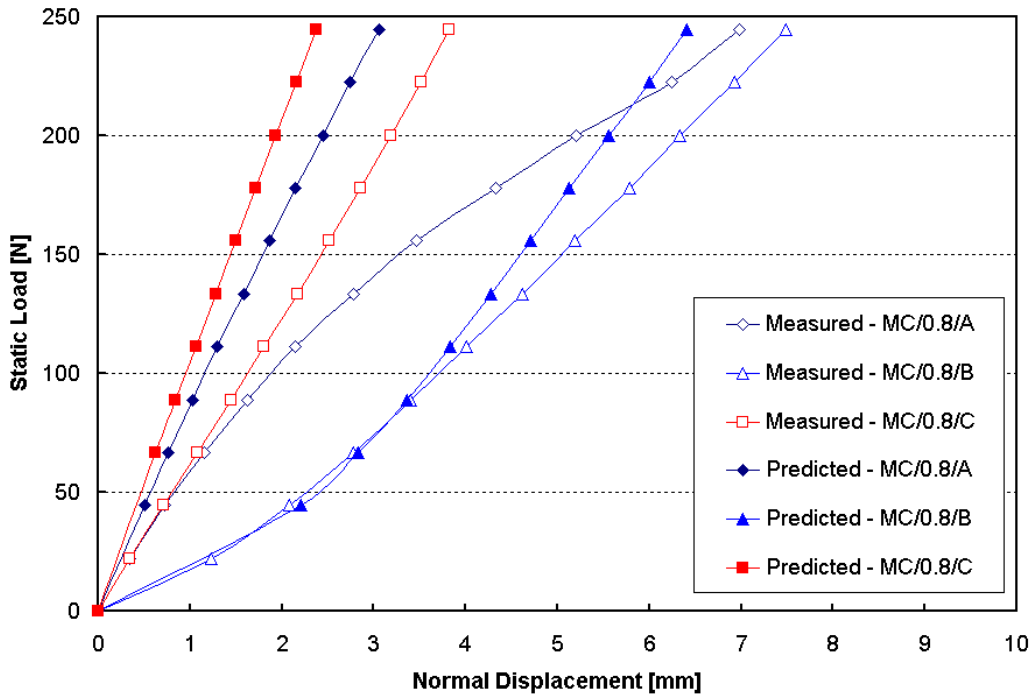
Figure 128: Predicted static stiffness response at all sites for medium curvature, 0.8mm thick, panel assemblies with teacup configuration #1.

The predictions for the medium curvature assemblies are presented in Figure 126 to Figure 128 for decreasing values of outer panel thickness. The predictions offer several consistent trends, regardless of thickness, with respect to stiffness response of the various test locations. Site C, above a teacup near the outer edge of the assembly, consistently offers the stiffest response. This agrees with the observed experimental results, where site C was always the stiffest site. The predictions for site A are the next stiffest, which again agrees with the measured responses. Finally, the predicted and measured results for site B are consistently the least stiff responses. This general capture of the relative stiffness from site to site should be noted.

The degree of agreement of the particular stiffness responses varies for each site and with thickness. The profile of the stiffness response is predicted well at site C for all thickness values. The numerical models predicted similar, principally linear responses for site A, while the measured results exhibit much softer, multi-stage stiffness responses that are poorly predicted by the models. The predictions for site B, the unsupported site, more accurately capture the displacement profiles of the measured results. The degree of agreement improves as the thickness of the outer panel is reduced. At low load levels, all site

173

B predictions are quite close but as higher load levels are reached the models exhibit an overly stiff response.
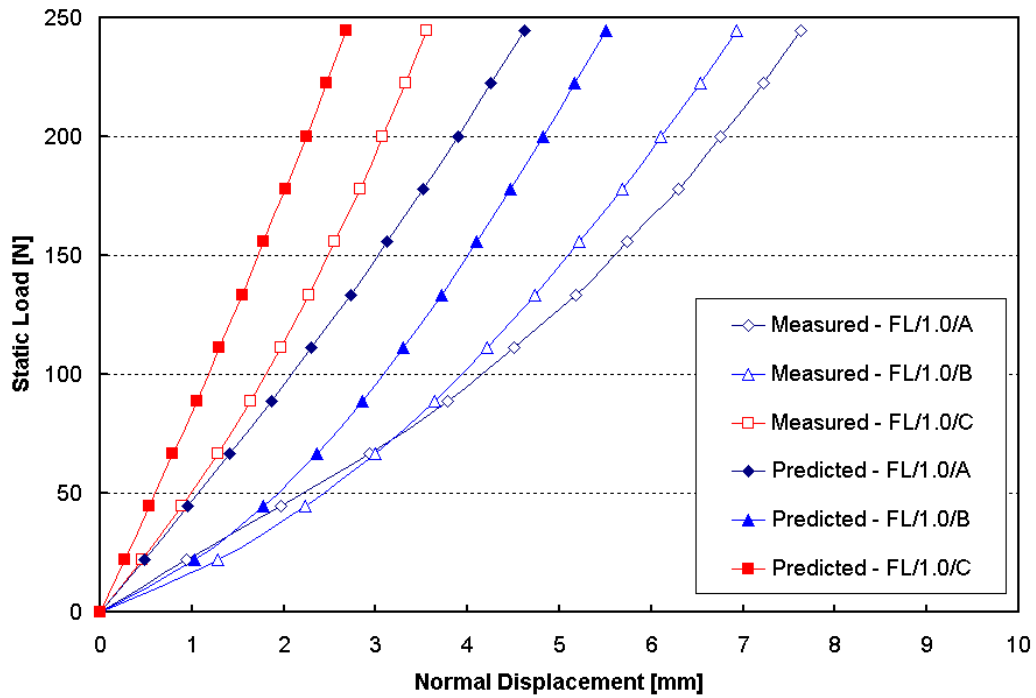
Figure 129: Predicted static stiffness response at all sites for flat curvature, 1.0mm thick, panel assemblies with teacup configuration #1.
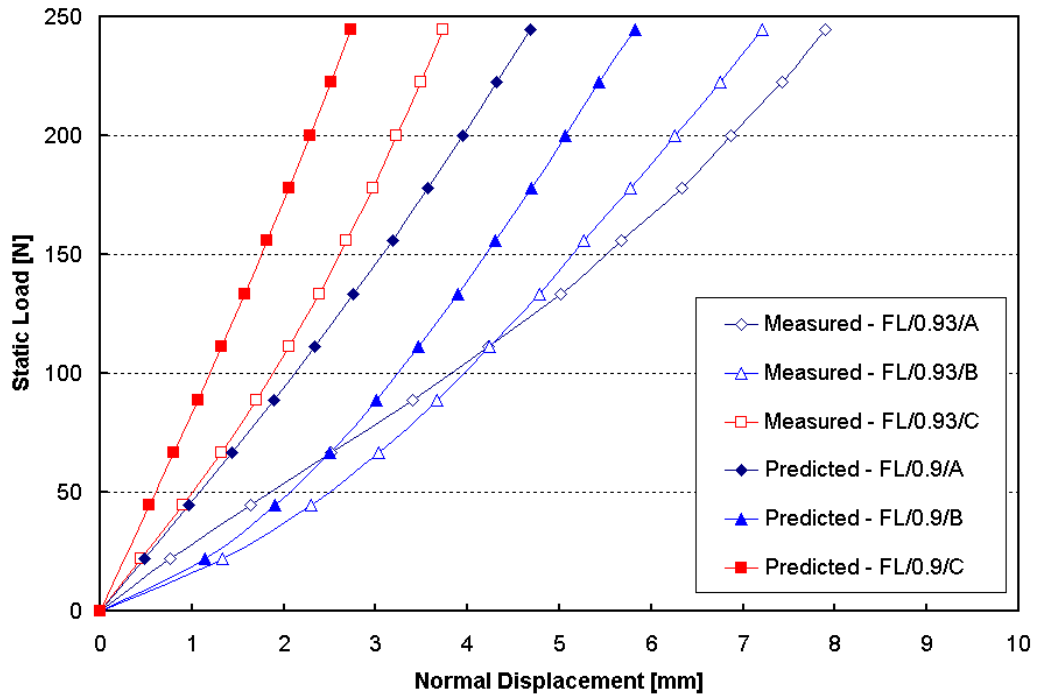
Figure 130: Predicted static stiffness response at all sites for flat curvature, 0.93mm thick, panel assemblies with teacup configuration #1.
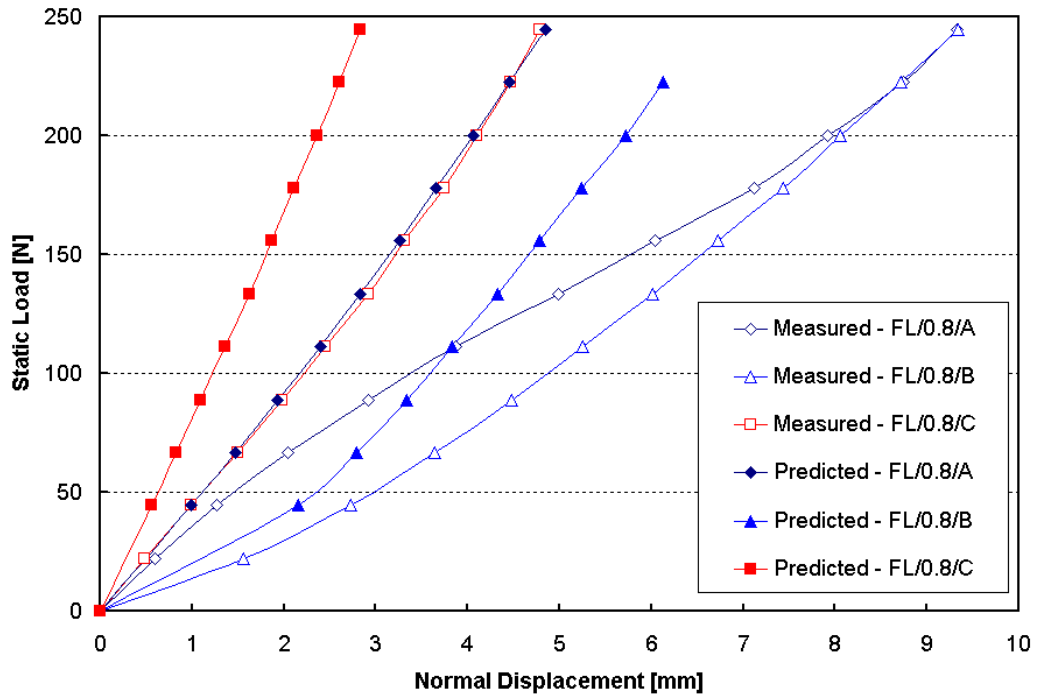
Figure 131: Predicted static stiffness response at all sites for flat curvature, 0.8mm thick, panel assemblies with teacup configuration #1.

The stiffness predictions for the flat panel assembly are presented in Figure 129 to Figure 131. The predictions are similar to those for the medium curvature assemblies. The relative stiffness from site to site is again captured, with site C being the stiffest and site B the softest. This reinforces that the numerical models can successfully capture the relative stiffness behaviour at various sites of a given assembly. This offers good potential for qualitative assessment of relative stiffness performance of a given panel. It appears that the model of the teacup support may be limiting the displacement behaviour and producing the consistently linear responses predicted at the teacup locations.
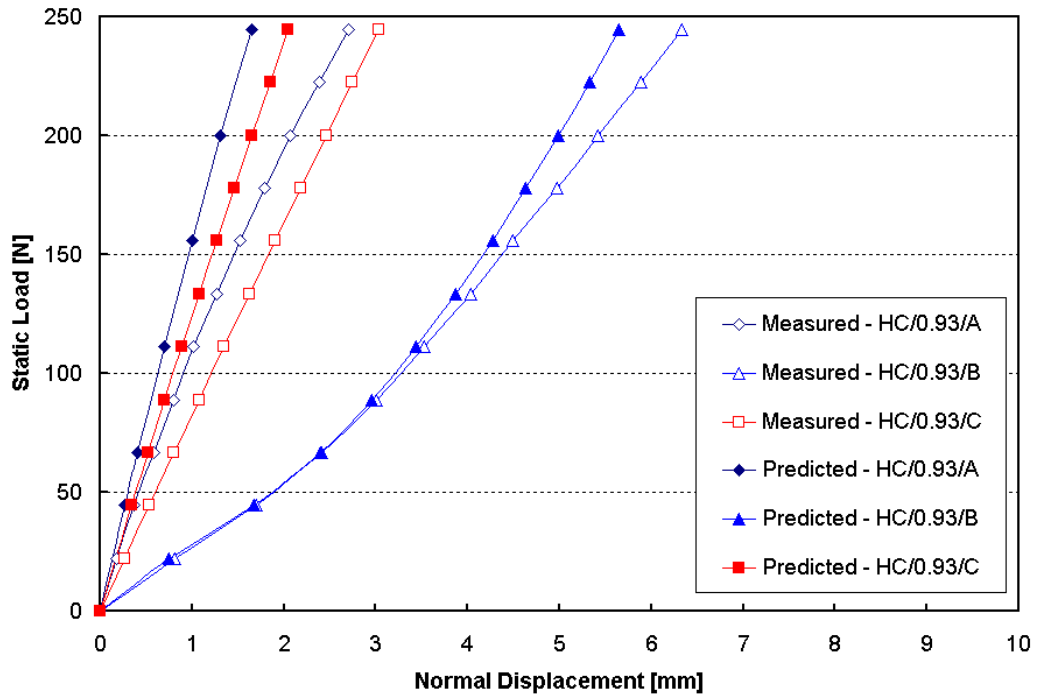
Figure 132: Predicted static stiffness response at all sites for high curvature, 0.93mm thick, panel assemblies with teacup configuration #1.

The high curvature stiffness predictions are shown in Figure 132. The best agreement between the predicted and measured results is observed for this panel curvature. The relative stiffness between the sites is again predicted correctly. It should be noted that for this curvature, site A is actually both predicted and measured as the stiffest site.
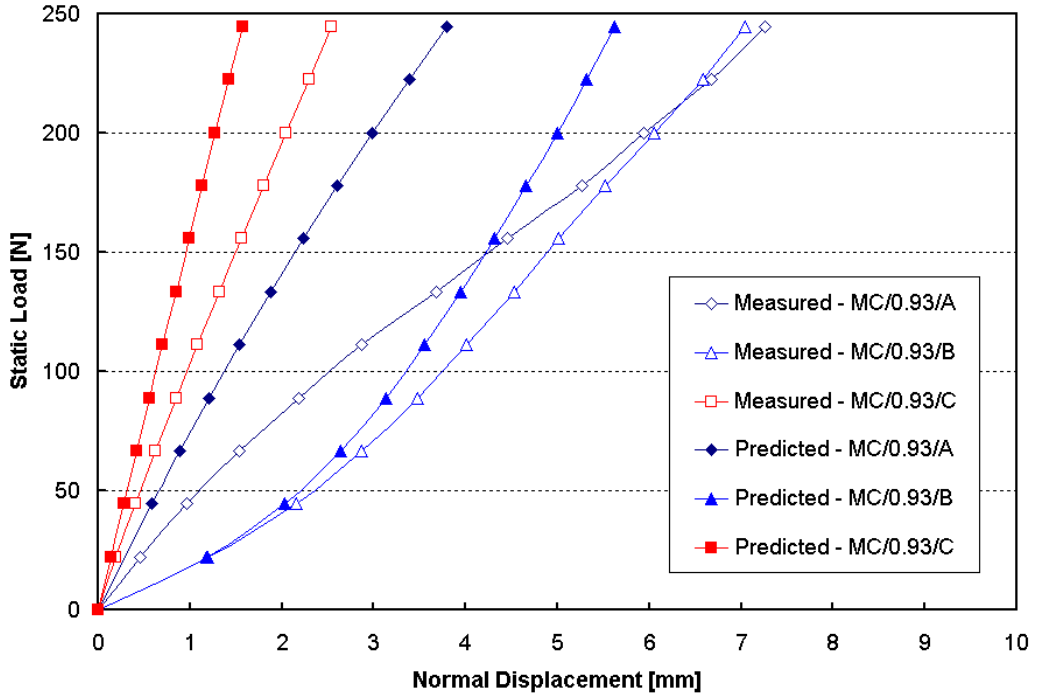
Figure 133: Predicted static stiffness response at all sites for medium curvature, 0.93mm thick, panel assemblies with teacup configuration #2.

The stiffness results for the second teacup configuration are presented in Figure 133. The results for this teacup configuration are similar to those observed with teacup configuration #1. The relative stiffness trends between sites are again captured correctly.

6.2.2 Thickness Effect on Static Stiffness Predictions

The effect of panel thickness is examined for both the medium curvature and flat assemblies in Figure 134 and Figure 135, respectively. The black arrows included on the plots indicate the direction of increasing outer panel thickness. The plots include the measured stiffness responses for comparison.
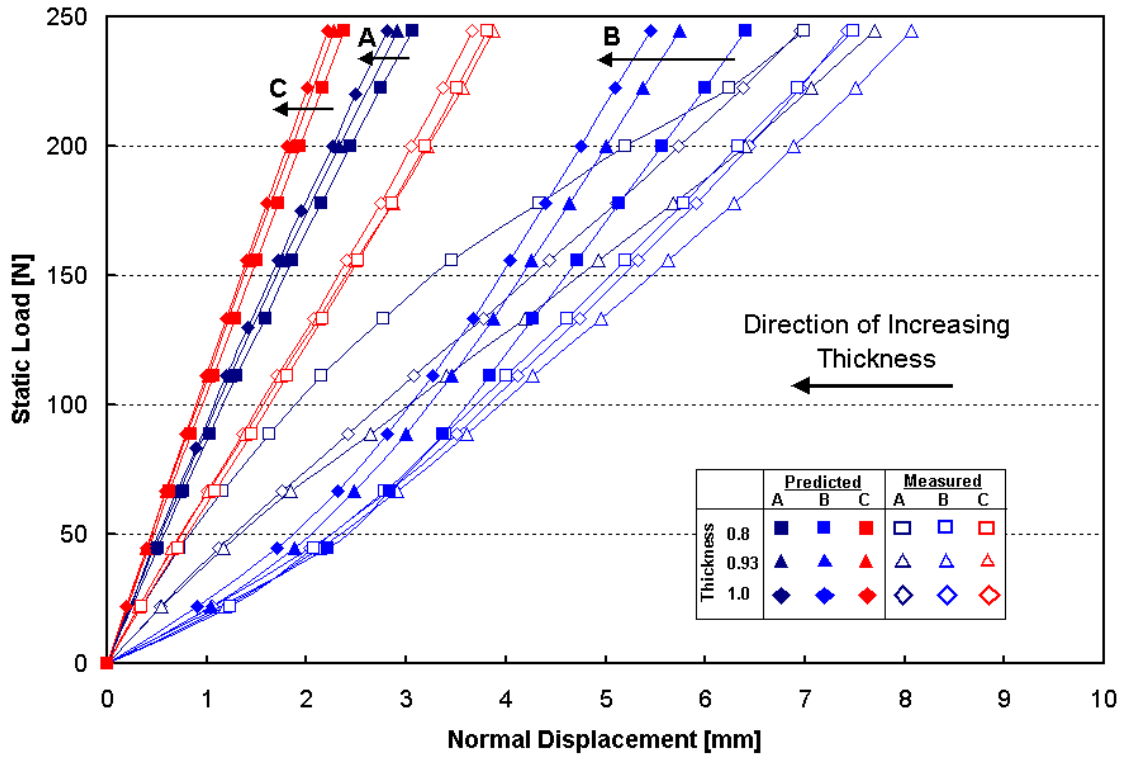
Figure 134: Effect of thickness on static stiffness predictions for medium curvature assemblies with teacup configuration #1.

The medium curvature results (Figure 135) exhibit a consistent predicted increase in stiffness with thickness at all test locations. The effect of thickness is quite small at the two teacup supported locations, A and C, suggesting that the supports are playing a more critical role than changes in thickness. The variation with thickness at site B, the unsupported site, is more pronounced as the influence of the teacups is lessened. The measured trends with thickness, discussed previously in section 5.2.3, are less consistent than the trends of the numerical models. Changes in mastic thickness and other geometric variations are absent in the numerical models, which accounts for the observed thickness trends.
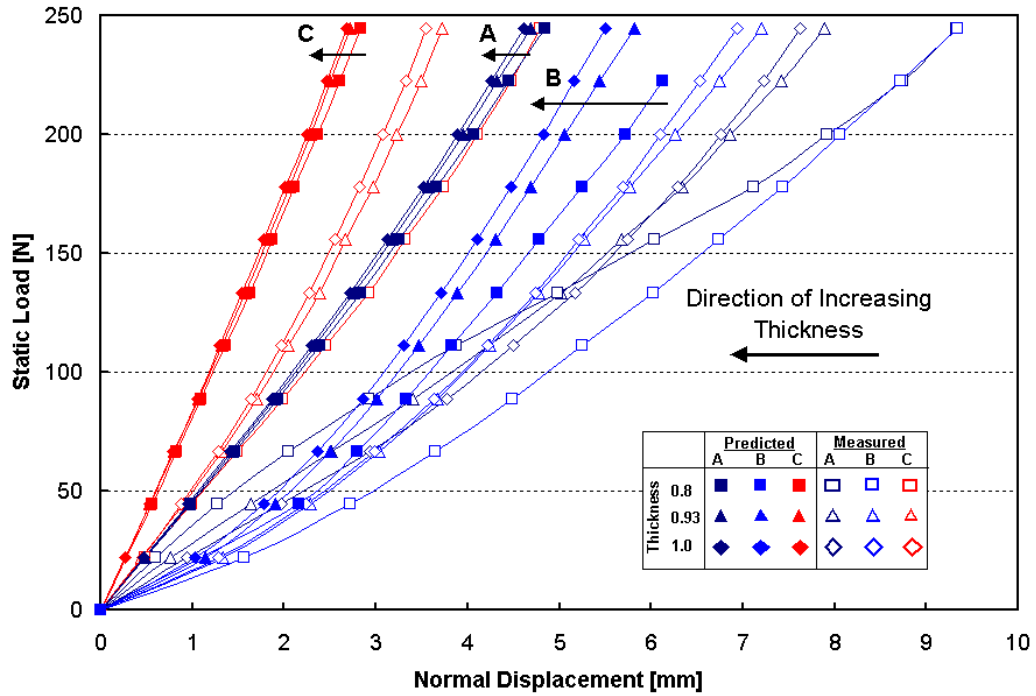
Figure 135: Effect of thickness on static stiffness predictions for flat assemblies with teacup configuration #1.

The thickness trends observed in Figure 135, for the flat assemblies, again predict an increase in stiffness as thickness is increased. Similarly small variation with thickness is observed at the teacup test sites, A and C, where the support condition controls the displacement response. Again, a wider spread in the predicted stiffness responses is observed at the unsupported site B.

6.2.3 Curvature Effect on Static Stiffness Predictions

The effect of panel curvature on static stiffness predictions is presented in Figure 136 for the 0.93mm assemblies with teacup configuration #1. The results are presented for all test sites, along with the measured results for comparison. A consistent increase in panel stiffness is observed with increasing panel curvature, indicated with the solid black arrows, for each test site. While the thickness effect was most pronounced at the unsupported site the opposite is true with curvature. The predictions for the unsupported site B are quite similar with the high curvature assembly offering a stiffer prediction at low loads that is reduced with increasing load.
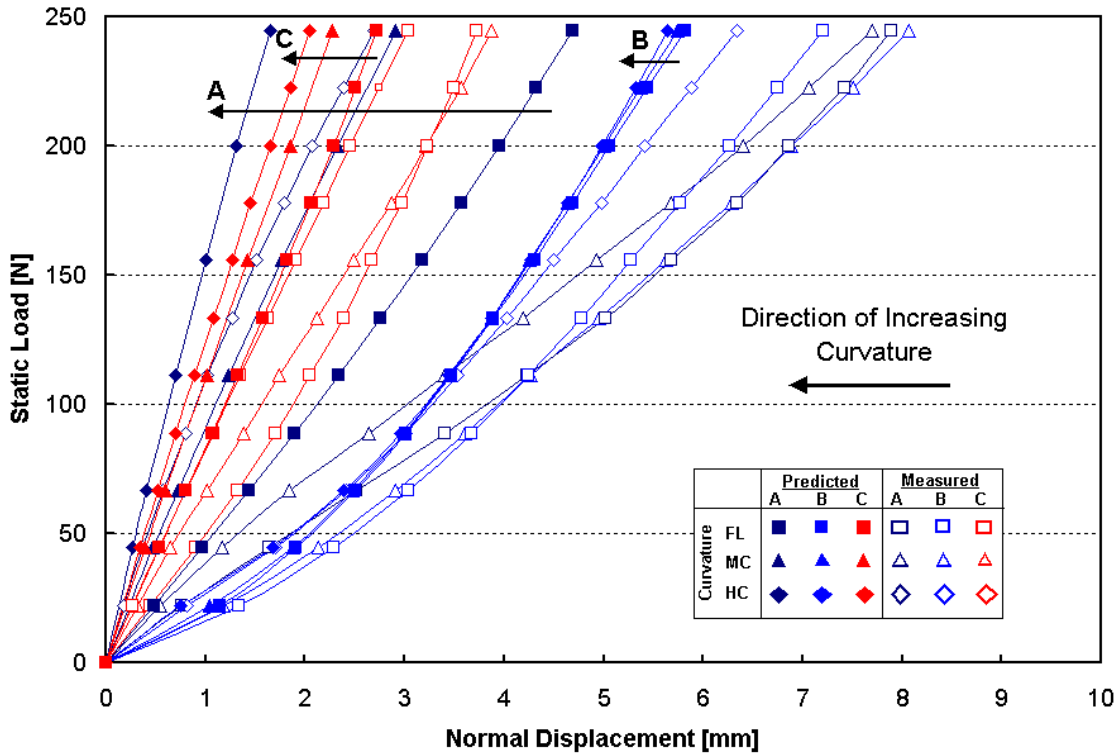
Figure 136: Effect of curvature on static stiffness predictions for 0.93mm assemblies with teacup configuration #1.

6.2.4 Effect of Mesh Refinement on Static Stiffness Response

Based on the overly stiff predictions observed at most of the test sites, concerns that the degree of mesh refinement was insufficient arose. An inadequate level of mesh refinement would lead to models that poorly captured the wider, global deflections observed in static denting, resulting in an overly stiff response. A highly refined mesh was created, using the same re-meshing algorithm outlined in the discussion of the static models in Section 4.3, with a refinement radius of 200mm. This radius assured highly refined elements in the entire region around the dent site, extending to the surrounding teacups. Both meshes are identical in the region directly surrounding the dent site. The large radius mesh is shown, along with an outline of the base mesh, in Figure 137.
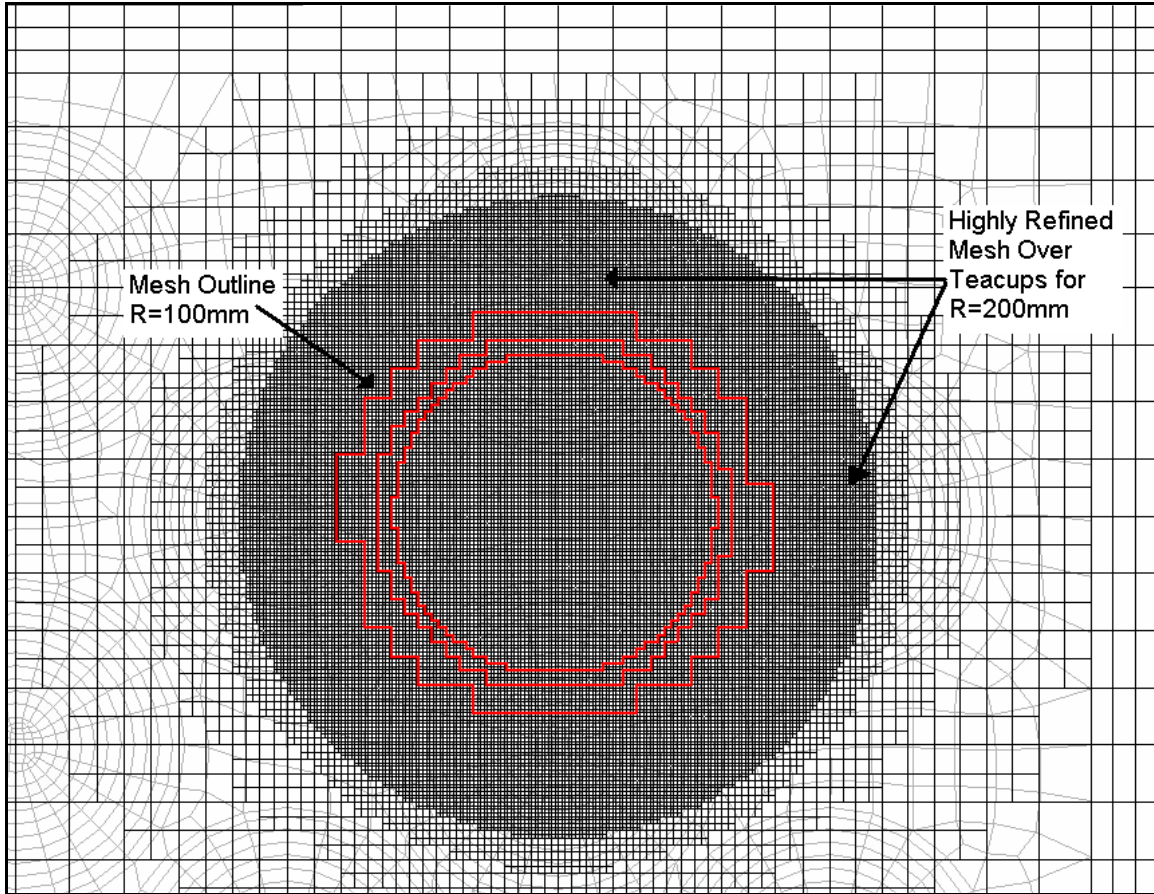
Figure 137: Comparison of highly refined mesh, R=200mm, and the base mesh, R=100mm, used in static stiffness analysis of the unsupported test site, site B.

The highly refined mesh was only used for the unsupported site B, of the 0.8mm thick, medium curvature assembly. The numerical cost associated with this degree of mesh refinement is prohibitive for a wide array of test conditions, particularly if a complete load/unload history is modelled. For the case evaluated here only a single loading cycle was modeled and the simulation time was roughly six times longer than the base model simulation time. The results are present in Figure 138, and include the measured results and the predictions for both the base refinement radius, R=100mm, and the large refinement radius, R=200mm. The results show an improvement in the predictions at the higher load levels, but the predictions remain overly stiff.
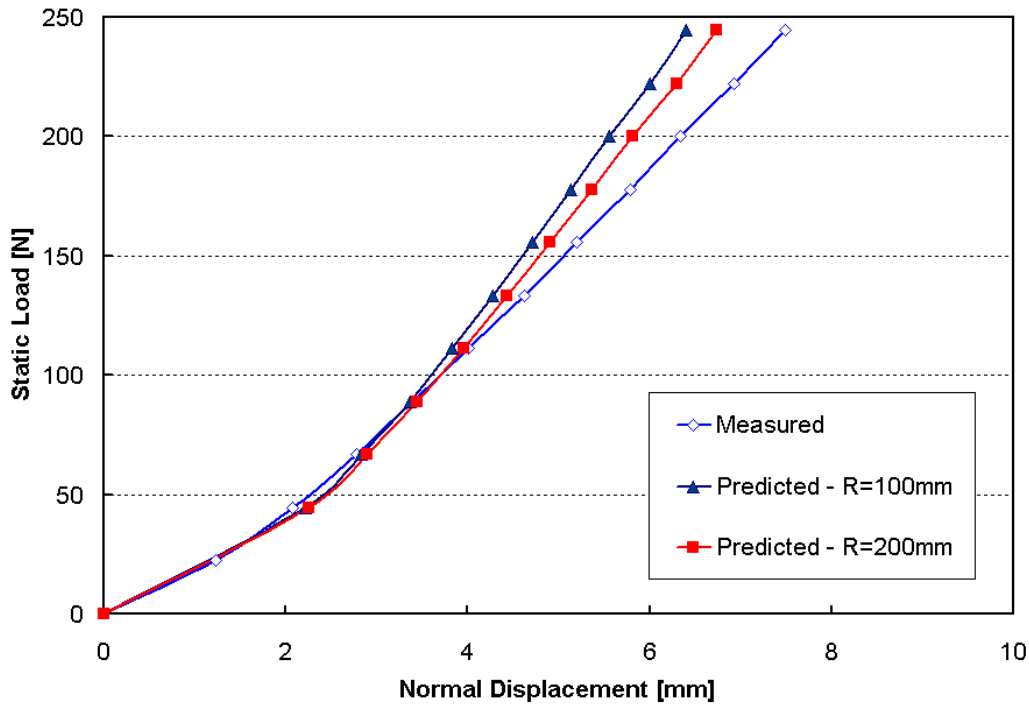
Figure 138: Effect of mesh refinement on static stiffness response at site B of the 0.8mm thick, medium curvature assembly with teacup configuration #1. Both meshes used refinement algorithm #2 with refinement radii of 100mm and 200mm respectively.

The improvement with increased refinement is attributed to the improved capture of the panel deflection and interaction with the supports. At higher load levels, a wider region of the panel surrounding the dent site is deflecting and the transition in panel bending is moving outward. The displacement profiles for the two meshes under the peak static load of 244.7N are compared in Figure 139. The more widely refined mesh predicts an increased peak displacement and covers the deflecting region of the assembly better.
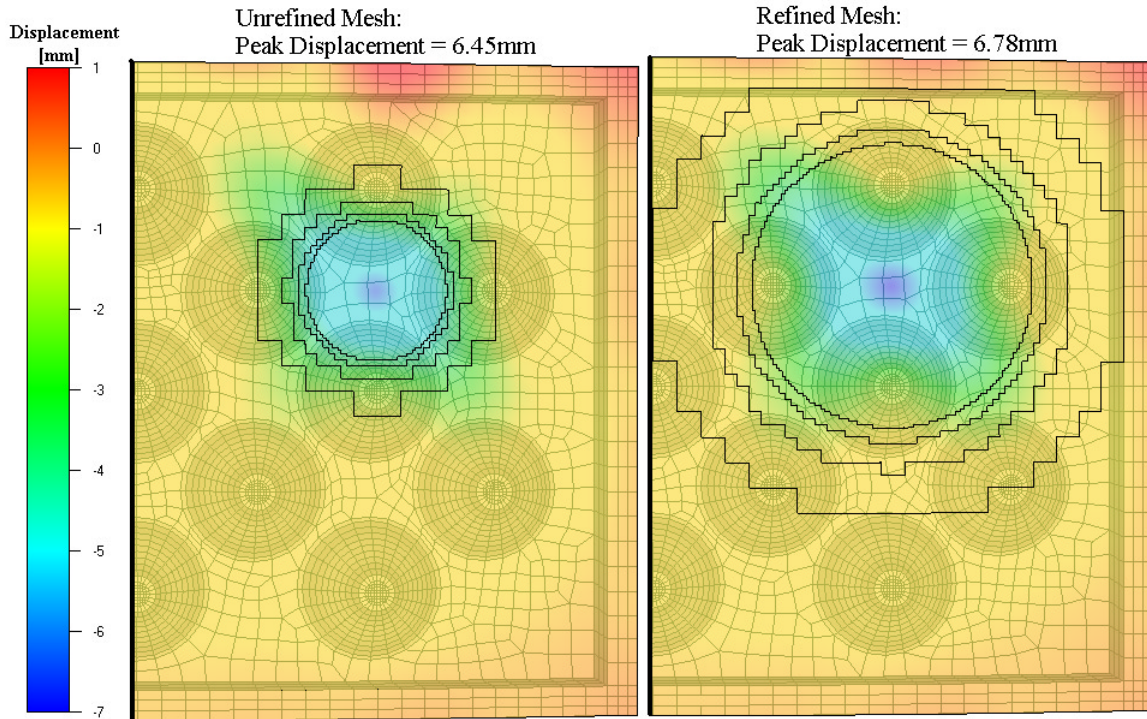
Figure 139: Displacement contours for the refined and unrefined meshes at a peak static load of 244.7N. The inner panel mesh is shown along with the outlines of the refined regions of the outer panel mesh.

6.2.5 Comparison of Predicted and Measured Static Dent Depths for all Test Conditions

Comparisons of predicted and measured static dent depths are presented in Figure 140 to Figure 144 for the various panel combinations. All figures present comparisons for all the test locations where possible. The static dent depth predictions were extracted from simulated load/unload cycles. In some cases, numerical convergence issues prevented complete predictions for all test sites for a particular panel. It proved particularly difficult to achieve convergence with the flat panel assembly models, and no results are presented. Also, the number of unloading steps were not always consistent from site to site, but variations in implicit time steps used in unloading were found to have no significant effect on predicted dent depths.

184
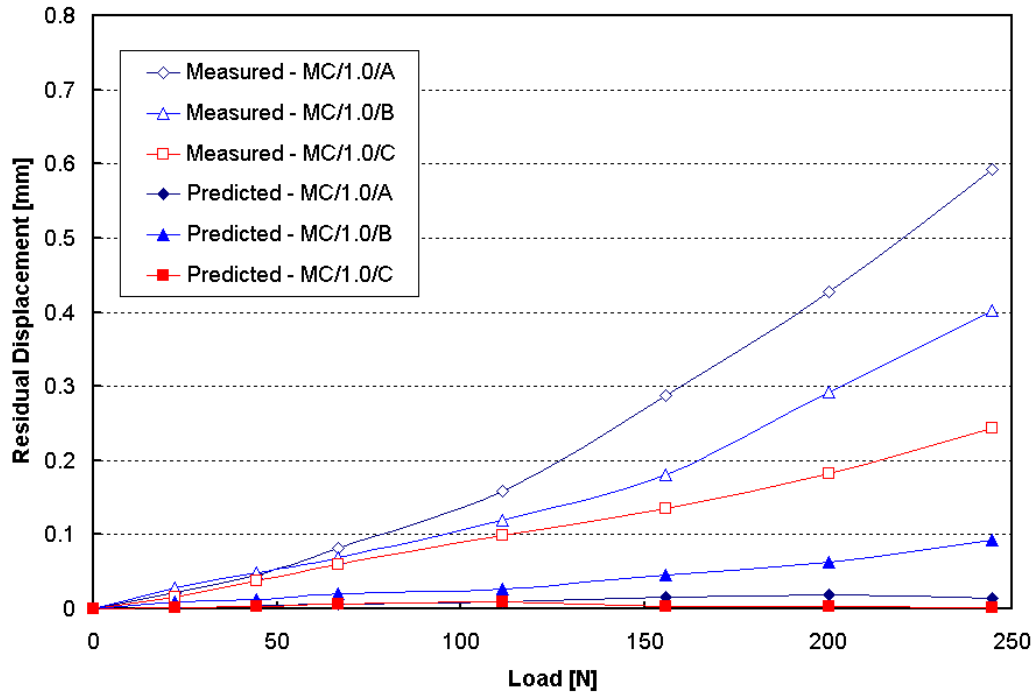
Figure 140: Comparison of predicted and measured static dent depths for the 1.0mm thick, medium curvature assemblies with teacup configuration #1.
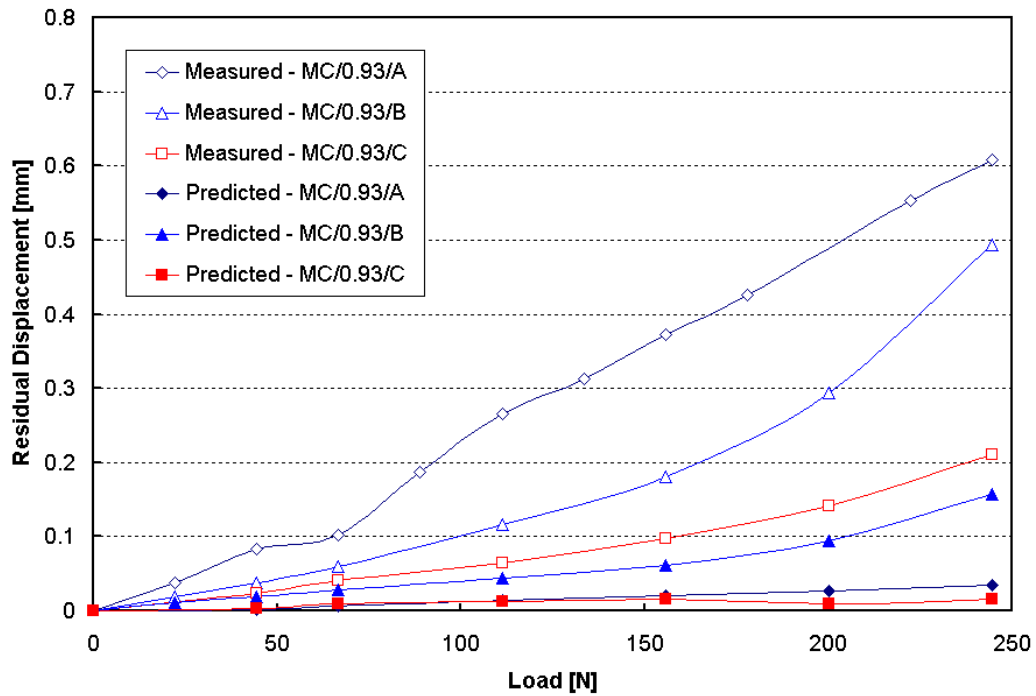
Figure 141: Comparison of predicted and measured static dent depths for the 0.93mm thick, medium curvature assemblies with teacup configuration #1.

185
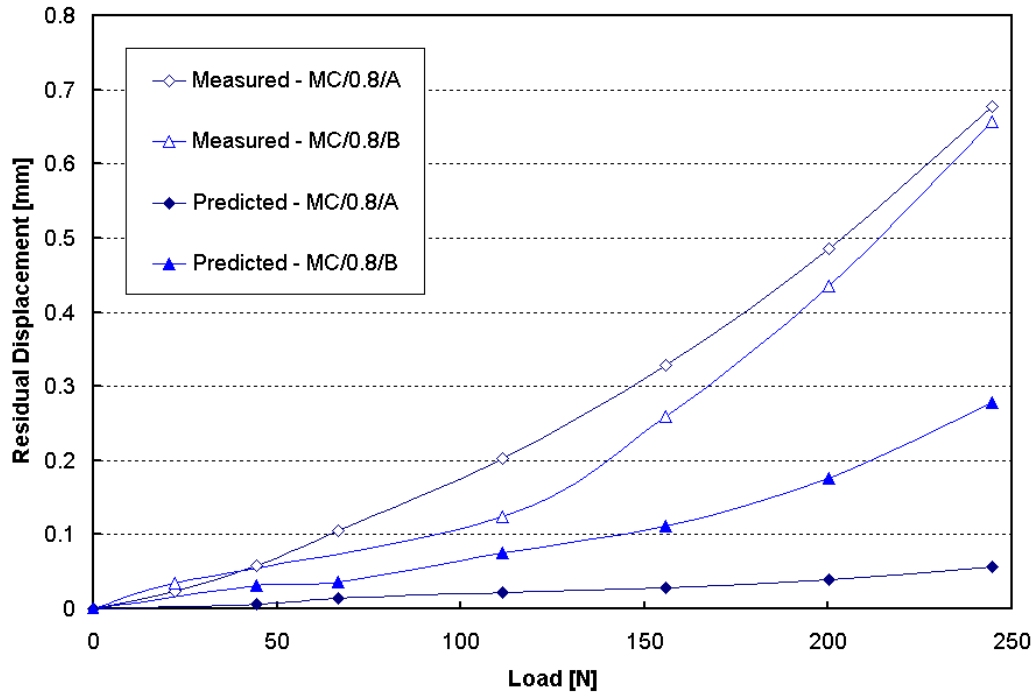
Figure 142: Comparison of predicted and measured static dent depths for the 0.8mm thick, medium curvature assemblies with teacup configuration #1.

The static dent predictions for the medium curvature assemblies are presented in Figure 140 to Figure 142 for decreasing values of outer panel thickness. The predictions all lie well below the measured results for all test sites. The static dent depths are consistently under predicted. The predicted results for the two teacup locations, A and C, are very low, with only minimal residual deformations at all load levels. The teacup-supported sites resist any permanent deformation as the panels barely yield, even at the highest load levels. In some cases the predicted dent depths actually decrease as the load is increased, a clearly incorrect response. In these cases the degree of predicted denting is very small and the variation in results is more likely attributed to numerical noise than any real effect. The predictions for site B are also low, but some level of permanent deformation is occurring. As the load level is increased the predicted deflections at site B increase in a similar manner to the measured results. This suggests that the models can capture the denting behaviour at the unsupported sites.

The superior results at the unsupported sites are likely linked to the stiffness predictions discussed earlier. The predicted stiffness responses for the teacup sites were always overly stiff, particularly at site A. This overly stiff response will inhibit static

186

denting, contributing to the poor predictions at the teacup locations. Conversely, the stiffness response at site B was much softer, which will allow static denting in the simulations.

The limited predicted results obtained for the flat assemblies are not shown. These results are limited by convergence difficulties, particular for the thinnest outer panel case. The most difficult site to achieve convergence at was site C, the site closest to the surrounding wall. As the loading is increased, the number of iterations to achieve implicit convergence increases. This is likely due to the spreading of the panel deflection towards the perimeter where interaction with the stiff sidewalls and riveted constraints becomes a factor. In cases where convergence was obtained, the results are similar to those for the medium curvature assemblies, showing only slight yielding and residual displacement at the unsupported sites.
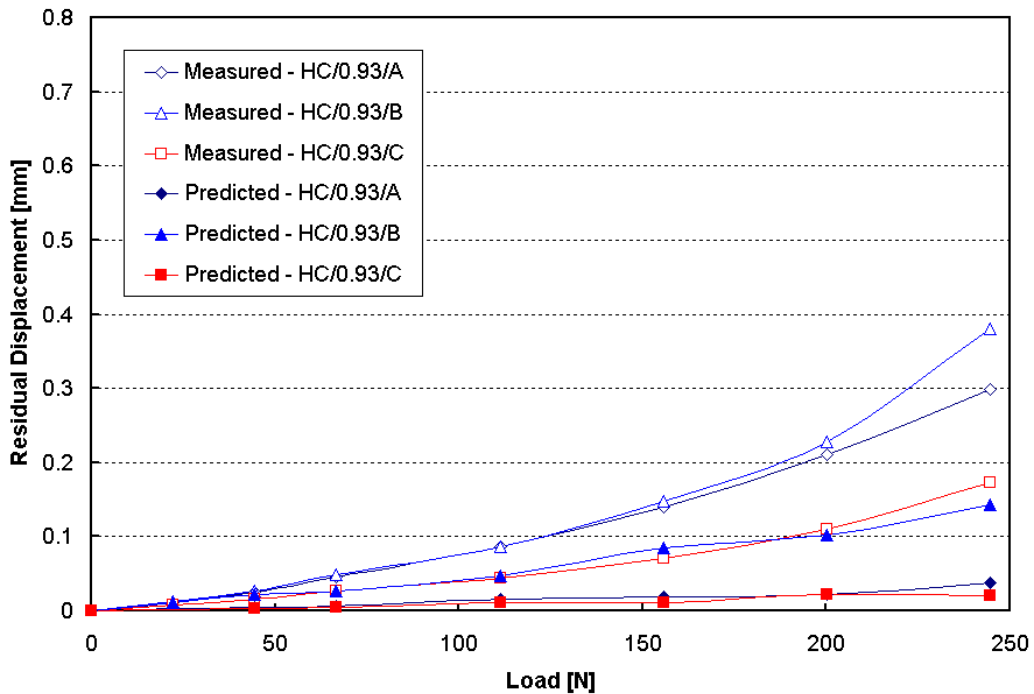
Figure 143: Comparison of predicted and measured static dent depths for the 0.93mm thick, high curvature assemblies with teacup configuration #1.

The results for the high curvature assembly presented in Figure 143 have the same level of agreement between the predicted and measured results as observed with the medium curvature assemblies. The teacup-supported sites again resist permanent panel deformation and exhibit negligible predicted static dent depths.
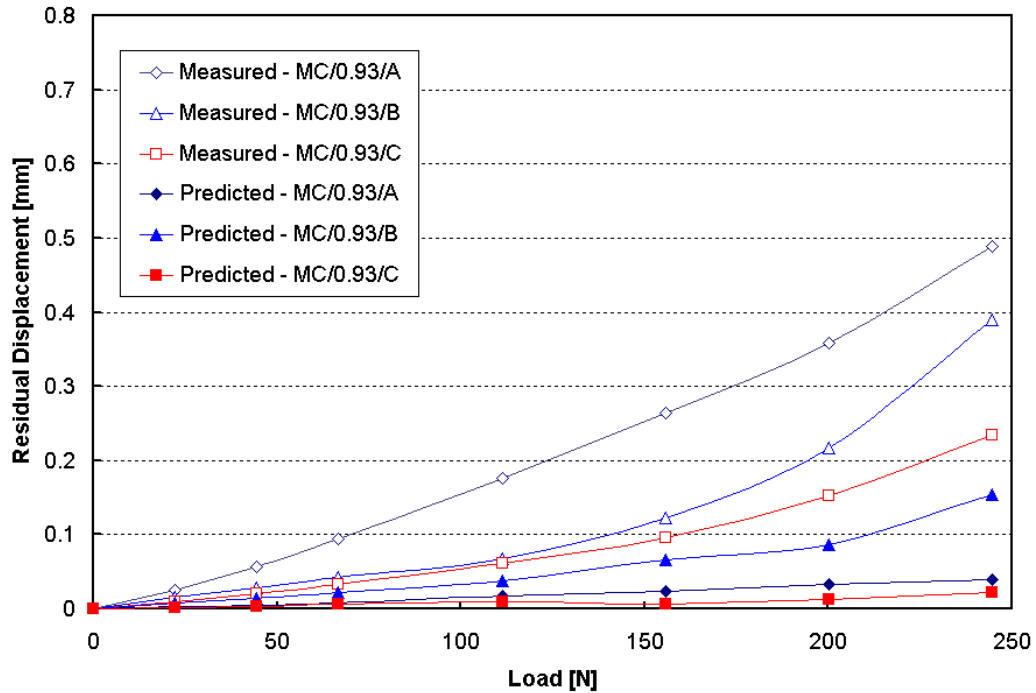
Figure 144: Comparison of predicted and measured static dent depths for the 0.93mm thick, medium curvature assemblies with teacup configuration #2.

The predicted and measured static dent depths for the medium curvature assembly with the second teacup configuration are presented in Figure 144. The results again follow the same trends as seen for the primary teacup configuration. The variation in teacup spacing has a no noticeable effect on the dent depth predictions. The teacup sites continue to show little permanent deformation leading to the under prediction of dent depth. The predicted results for the unsupported site are also low, but the dent depth response does follow the measured trend.

6.2.6 Thickness Effect on Static Dent Depth Predictions

Comparison of the predicted results for the range of outer panel thicknesses is presented in Figure 145 for the medium curvature assemblies. Only the results for the unsupported site are compared. The results at the teacup sites are very similar and offer little insight into the effect of thickness on the predicted results. The exclusion of the results at the supported sites limits any observations with respect of thickness on the unsupported panel locations.

The predicted results exhibit an increase in dent resistance with an increase in outer panel thickness. The predicted trend agrees with the measured trend, showing lower dent

depths for the thickest outer panel. Also, as the static load level increases the divergence in dent depths for panels of different thickness, seen in the measured results, appears in the predicted results. This indicates that the numerical models correctly capture the thickness effect on static denting and offer potential for relative assessment of static dent resistance for a range of thickness.
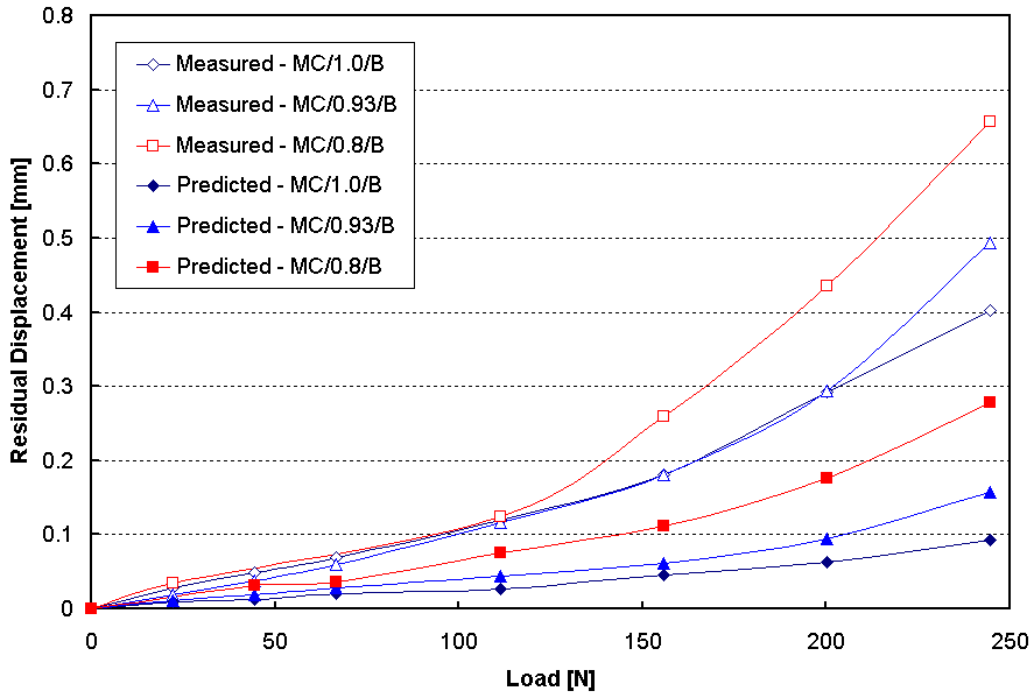
Figure 145: Thickness effect on predicted static dent depths for the unsupported site, site B, of the medium curvature assemblies with teacup configuration #1.

6.2.7 Curvature Effect on Static Dent Depth Predictions

The effect of panel curvature on static dent depth predictions is shown in Figure 146 for the 0.93mm assemblies. Again, only the predictions for the unsupported site are presented as the teacup sites offer little for relative comparison. The measured and predicted trends, with respect to curvature are reversed. While both sets of results present closely grouped dent depths, the predictions suggest superior dent resistance with decreased curvature, for most loads, the opposite of the measured results. The predicted stiffness responses for the various curvatures, Figure 146, should be recalled in examining the denting results. The stiffness predictions found almost no change in stiffness for the various curvatures, which translates into the similarly small variation in the denting predictions. The curvature effect is generally

small for the range of curvatures examined, which is reflected in both the experiments and models.
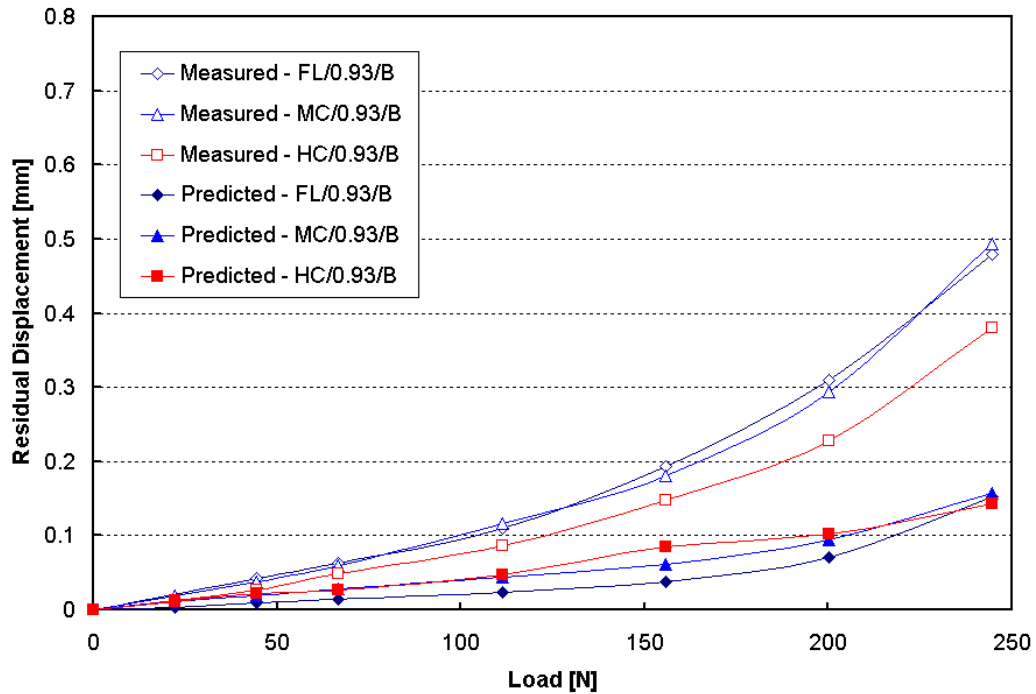
Figure 146: Curvature effect on predicted static dent depths for the unsupported site, site B, of the 0.93mm thick assemblies with teacup configuration #1.

6.2.8 Effect of Outer Panel Yield Strength on Static Dent Depth Predictions

The under prediction of static dent depth raised concerns with regard to the ability of the models to accurately capture the static denting process. The observed level of permanent deformation, measured as the effective plastic strain, was very low for the majority of the simulations. As a result a limited number of simulations were performed using a reduced outer panel yield strength. The stress-strain curve of the outer panel was reduced by a factor of 25% to promote the onset of panel yielding. By promoting the onset of plastic deformation a better understanding of the performance of the model is obtained. The effect of reduced yield strength is presented in Figure 147 for the medium curvature assembly with the lowest panel thickness. Comparison with the measured and the base model results are shown for the unsupported site B and the teacup supported site A. The panel stiffness responses are unaffected by the changes in yield strength and are not shown.

190

The reduction in yield strength provides little change in the results at low load levels. In the low load regions the deformation of the outer panel remains elastic and the predicted results remain identical to the base model predictions. Depending on the dent site, the two models diverge at the onset of yielding in the reduced strength models for a given load. The unsupported site is affected by the reduction in yield strength at the 111N load and the results after this point follow the measured dent depth profile much more closely. The results for the supported site require a much greater load level before divergence of the predicted results occurs.

The improved results for the unsupported site suggests that the original model is too resistant to the onset of yielding. The artificial reduction of yield strength overcomes this numerical problem and reveals the models ability to more accurately capture the denting response at the unsupported site. The results at the teacup site remain poor, as the 25% reduction in yield strength is insufficient in overcoming the over prediction of static stiffness.
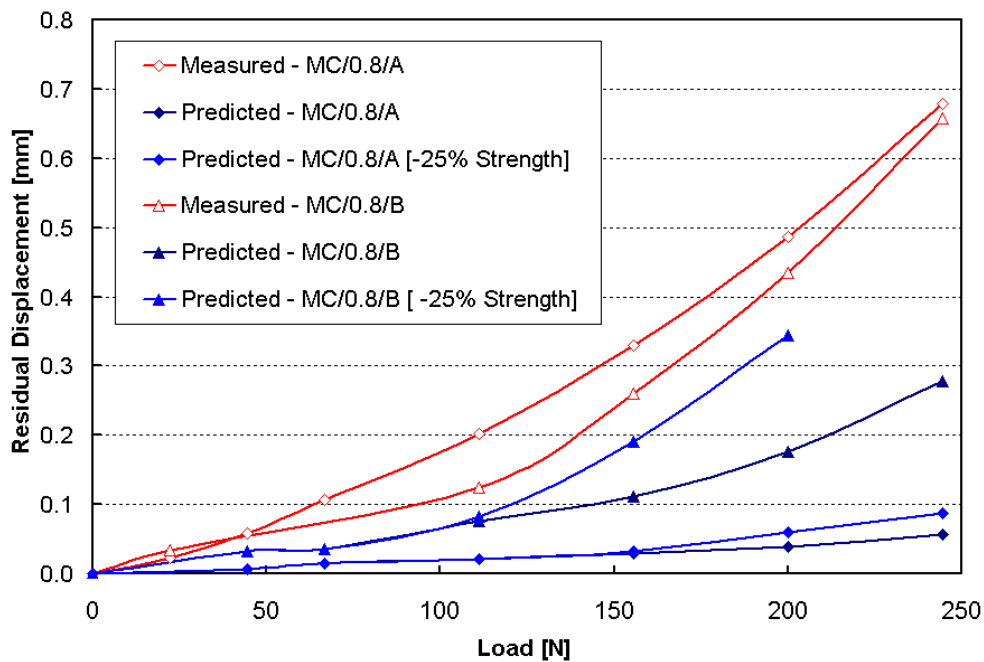
Figure 147: The effect of outer panel yield strength on static dent depth prediction for the medium curvature, 0.8mm thick, assembly with teacup configuration #1. The outer panel yield strength has been reduced by 25% in the numerical models.

191

6.2.9   Effect of Mesh Refinement on Static Dent Depth Predictions

The effect of mesh refinement on static dent depth predictions was explored for a single test case. The need to model a complete load-unload cycle to obtain a predicted static dent depth profile introduces high numerical costs. The same model used in Section 6.2.4 for the comparison of stiffness responses took over five days, roughly 20 times the simulation period of the unrefined model, to solve. The comparison of predicted static dent depths for site B of the medium curvature, 0.8mm thick assembly with teacup configuration #1 is presented in Figure 148.   The predicted results show no appreciable improvement in static dent predictions with increased radius of refinement.   The limited improvement in stiffness, shown in Figure 138, does not translate into any increase in dent depth prediction accuracy.
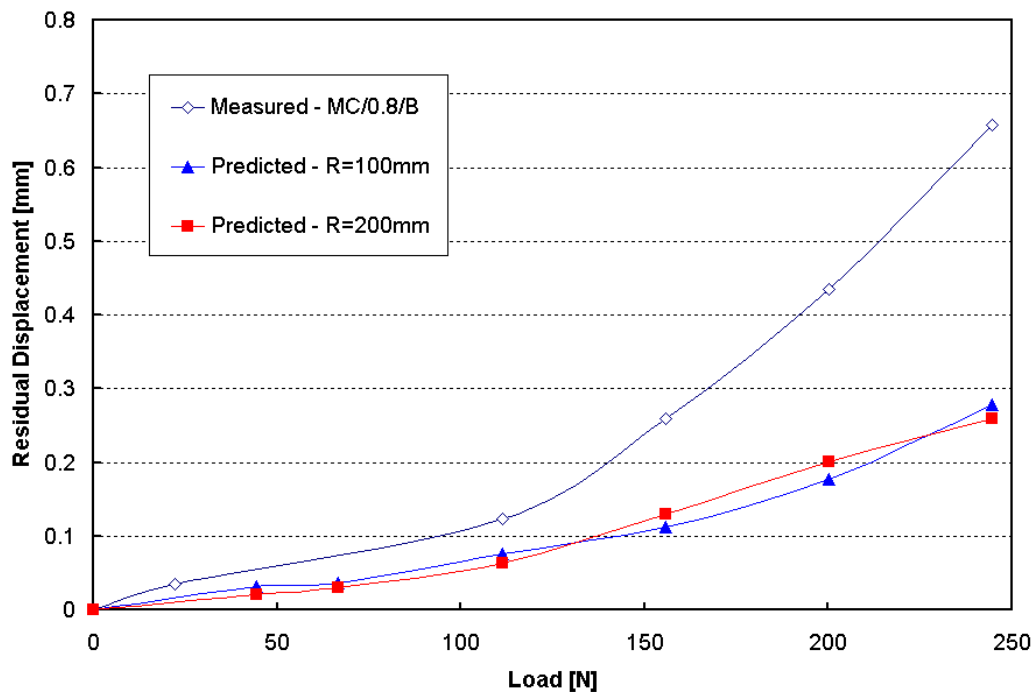
Figure 148: Effect of mesh refinement on static dent depth predictions at site B of the medium curvature, 0.8mm assembly with teacup configuration #1.

7 Discussion

The results of this work provide a broad insight into the denting behaviour of automotive structural panels. The experimental results provide a parametric assessment of various factors affecting dent resistance in multi-part panel assemblies with structures typical of automotive hoods. The numerical simulations offer varying degrees of predictive ability for both static and dynamic denting analysis, while providing a foundation for future examination of full-scale hood models. The results of this work have revealed several issues that require further discussion. These concerns are divided into experimental and numerical issues. Also presented is an examination of on-going work on the transfer of the modelling techniques to full-scale automotive hoods.

7.1 Experimental Results

The experimental program has involved the parametric assessment of the effect of panel curvature, sheet thickness, inner support configuration and local dent site support conditions on static and dynamic dent resistance. The results have provided an understanding of the effect of the various parameters on dent resistance. The competing nature of static and dynamic dent resistance is clearly illustrated by the measured results. While the static dent resistance is superior directly above the teacup supports, the dynamic dent resistance is poor at these locations due to the restriction of panel deflection. Conversely, the unsupported dent sites provide superior dynamic dent resistance as the panel elastically "catches" and releases the indentor with little permanent deformation. The low stiffness at the unsupported sites leads to a loss of static dent resistance since the sheet must support the load in local bending, its weakest mode. The trends observed offer potential for dent resistance improvements in design of automotive panels. However, the experimental results raised various concerns with regard to experimental test procedures.

The most notable concern with the experimental program was the overly thin mastic layer chosen and the resulting effect on the observed static and dynamic dent resistance. The thin mastic layer led to concerns that the medium-scale panels were not as representative of actual hoods as desired. It has become apparent that a mastic thickness on the order of at least 5mm can be expected in actual hoods, a substantial increase over the approximately 1mm thickness tested. This low mastic thickness introduces a highly non-linear stiffness response in the mastic for the range of contact forces developed. The thin mastic layer becomes highly compressed, losing its dampening characteristics and foam-like consistency. This increase in mastic stiffness leads to overly stiff support conditions at the teacup locations. This increased stiffness in turn leads to dent resistance performance that may not be typical of actual automotive hoods. Clearly, future work should consider thicker mastic layers and more detailed examination of the non-linear mastic response.

Another experimental concern is the geometric variation across the array of panel configurations and within a given assembly. The fabricated nature of the assemblies introduces variability in the test geometry that may contribute to variations in the experimental results. Weld distortions due to sidewall and teacup attachment introduce variations in panel geometry that limit the repeatability of the testing. As seen in the examination of test results at mirrored dent sites, the degree of variability for nominally similar sites was of particular concern at teacup locations. While small variations due to welding and slight differences in teacup shape are a factor, the principal cause of the variations is again manifested within the mastic response. The geometric variations led to an inconsistent mastic thickness at each teacup, as the nominal 1mm thickness was often times not achieved. The sensitivity to these variations was exacerbated by the initially thin choice of mastic layer. At some sites, the mastic thickness was much smaller, leading to near metal-to-metal contact between the top of the teacup and the outer panel. This loss of mastic thickness greatly increases the stiffness at the support points, which translates into measurement variability. The variation in mastic thickness is lessened at the unsupported sites where the impact of teacups is effectively averaged.

The measurement of dent depths is also an area of concern. For both the static and dynamic dent tests the measurement techniques are required to measure small local changes in panel curvature. Accurate capture of this deformation is non-trivial, as the precision of the

measurement techniques was a limiting factor. For the dynamic dent measurements the tripod platform and dial gauge method is limited by the manual determination of the dent site and positioning of the tripod before and after the test. The measurement technique can lead to small scratching of the panel surface as the deepest displacement is located. This may contribute small errors in the measured dynamic results. A more advanced measurement method could avoid these problems and improve the accuracy of the dynamic results. Manual locating of the dent site does not hamper the static results, as the indentor motion is directly recorded throughout the test. However, the large degree of panel recovery observed during testing hinders the static results, particularly the static dent depth measures. The tendency of the unloaded panel displacement to recover over time led to an arbitrary one minute delay prior to recording of the static dent depth. This drifting of the unloaded displacement limits the static dent measures to relative comparisons, as the absolute measures are artificially high. Due to the nature of the static load and unload cycles it is not possible to remove the loading arm to take more detailed intermediate dent depth measures. Replacing the loading arm at the same location would be impossible and would lead to more pronounced experimental variations. Clearly an automated loading and measurement system would help to alleviate these problems.

7.2 Numerical Results

The experimental static and dynamic dents have been simulated using finite element techniques. The complicated interactions of typical automotive panels have been successfully captured in the simulations, providing a foundation for future models of complete automotive panel assemblies. The numerical predictions offer varying degrees of accuracy, and are highly dependent on the type of denting and the dent location. The results reproduce the measured denting trends quite well, suggesting the models offer good potential for qualitative assessment of denting behaviour. The role of curvature and thickness is well captured for both types of denting. The static results show good correlation between stiffness and static dent depths for the unsupported dent sites. The accuracy of the results is a function of several numerical factors that have varying degrees of influence on the different simulations.

The representation of the mastic was an area of critical importance in the numerical simulations. The limitations associated with the mastic representation are among the key factors causing the inaccuracies of the predictions. The mastic was modelled using solid elements with a linear elastic material response. The linear stiffness approximation for the mastic led to concerns, particularly with the dynamic denting simulations, when the range of contact forces encountered is considered. For the dynamic denting simulations, the variation in contact forces evolving during a dent differed substantially between the teacup-supported and unsupported sites. The linear representation of the mastic stiffness was incapable of reflecting the non-linear mastic response observed in material testing. This leads to an arbitrary load condition of 500N being chosen as the basis of the linear stiffness approximation. Consequently, the dynamic predictions will generally be good at the teacup sites, where the very stiff linear mastic is appropriate, but poor at the unsupported sites. Furthermore, the material representation assumes an identical response in tension and compression. For the thin mastic layer this is inappropriate, as the mastic is stiffer in compression than tension. Attempts to use a non-linear elastic foam material model for the mastic proved unsuccessful due to limitations with its current implementation in LS-DYNA implicit.

The tied contact surfaces joining the mastic to the inner and outer panel, coupled with the linear stiffness of the mastic, limit the static stiffness and dent depth predictions. The contact between the mastic and surrounding panels maintains a constant offset of one-half of a sheet thickness. The very thin mastic layer combined with the constraints at the top and bottom of the mastic appear to severely limit the local deformation of the assemblies under static load conditions. The tied interface will constrain the bending of the sheet due mismatch of the mastic and outer panel mesh. In the future, a matched mesh between the mastic and outer panel should be explored to assess whether more representative local panel deflection can be obtained. The static stiffness is uniformly over predicted for all test sites. The mastic stiffness and teacup supports substantially contribute to this over prediction. The more problematic numerical results are the static dent depth predictions at the teacup locations. The models dramatically under predict the static dent depth at these sites, which cannot be solely attributed to the high stiffness predictions. The models are highly resistant to permanent deformation at the teacup sites, even for large reduction in panel yield strength,

suggesting that other numerical factors are controlling the response. The constraints of the contact surface, coupled with the elastic mastic stiffness, are viewed as a likely cause of the poor predictions. The narrow mastic layer restricts panel deformation and prevents panel yielding. For thicker mastic a less constrained numerical condition is expected that should improve the predicted results. A non-tied interface, coupled with a thicker mastic layer, will greatly relieve the numerical issues, while at the same time matching current panel design practice better.

Implicit convergence also proved to be a concern in the static simulations, which was not unexpected since automotive panels often lead to ill-conditioned stiffness matrices. The latest version of LS-DYNA offers improvements in its implicit solvers that allowed for the successful simulation of the majority of the static test cases. For some simulations, the multi-stage load/unload cycles proved to be difficult numerically, limiting the predictions to single load cycle simulations. The majority of the convergence issues occurred in the thinnest outer panel assemblies at the dent site closest to the assembly perimeter. Also, the flat assemblies proved more difficult to model than the curved panels. These difficulties are attributed to the spreading of the panel deflection towards the outer wall where a sharp increase in stiffness is expected. This rise in stiffness may be difficult for the implicit solver to handle as the stiffness matrix changes substantially. Previous work by Thomas [4], on single panels, was done on an alternative implicit code, ABAQUS, after difficulties were encountered with an earlier version of LS-DYNA implicit. It is uncertain whether the alternate code would offer improved convergence for the more complex, multi-part assembly models. Also, it is possible that the convergence issues encountered with LS-DYNA may have been resolved in the latest version of the code used in this thesis. The development of the current models required substantial debugging and adjustment to ensure all the panel interactions were correctly modelled. As this work progressed, limited attempts to explore modelling the static dents in ABAQUS proved unsuccessful, and it remains uncertain whether ABAQUS is capable of capturing all the necessary interactions within the panel assemblies. The time required to incorporate the necessary panel interactions and material responses was deemed too great for the timeframe of this work. Finally, the use of a common base-model for both static and dynamic dent analysis is beneficial, as only a single code and approach must be

learned when transferring the methods to other users. Thus LS-DYNA was used for all the panel assembly simulations.

The predicted results display varying degrees of mesh sensitivity. The element size in the region surrounding the dent sites was roughly 1.3mm by 1.3mm. Further reduction of element size was not explored, as the computational time was deemed prohibitive. The more important consideration related to mesh refinement was the size of the radius of refinement. A wider region of highly refined elements was examined for a limited set of test conditions. The level of mesh refinement is more important at unsupported sites where larger regions of panel deflection occur and accurate capture of panel buckling or snap-through is essential. For both the static and dynamic simulations an increased radius of refinement improved the predicted results at the unsupported test location. For the dynamic simulations, the increased radius of mesh refinement lessens the numerical stiffness, leading to more accurate capture of the catching and releasing of the indentor by the outer panel. The static stiffness response is also improved with a wider region of highly refined elements. The effect of increased mesh refinement in the static simulations appears at higher loads when the nodal point of deflection moves further from the dent site. The improvement in static stiffness prediction offers little corresponding improvement in static dent depth predictions. Unfortunately, the run times associated with this larger radius of refinement were deemed prohibitive to study a wide array of test conditions.

7.3 Application to Full Scale Automotive Hood Applications

The end goal of the overall research effort at Waterloo, outlined in Chapter 2, was the application of the numerical methods to actual automotive hoods. The work of this thesis provided the basis for the modelling of typical structural interactions between inner and outer panels and their sandwiched mastic layer found in current hoods. The modelling techniques have now been successfully implemented as part of a numerical down-gauging analysis of static and dynamic dent resistance completed for three prototype hoods by the author of this thesis and others [65].

The numerical modelling was based on existing finite element meshes used in structural analysis of the hoods. The creation of denting models was accomplished using modelling techniques similar to those presented in this thesis. The mastic layer between the

inner and outer panel was modelled with solid elements. The mastic thickness was on the order of 7mm, a significantly larger thickness than that of the mastic layer used in this thesis.

A validation study was performed prior to the numerical down-gauging assessment in which numerical dent depth predictions were compared to measurements from actual hoods. A typical hood model was shown earlier in Figure 25. The results of the validation study were good for most dent locations, as shown in Figure 149, with the notable exception of one site where insufficient local refinement, caused by a highly distorted initial mesh, prevented accurate prediction. The improved results for the full hood, relative to the results for the medium-scale assemblies in this thesis, are mainly attributed to the higher mastic thickness. The thicker mastic experiences less variation in its stiffness response thereby rendering a linear approximation of mastic stiffness more appropriate. Also, the larger mastic thickness translated into superior dent resistance at teacup locations, both numerically and experimentally, suggesting that the poor performance observed in the medium-scale panel assemblies is not reflective of actual hood behaviour. The thicker mastic appears to act as damper, absorbing the indentor impact energy and reducing residual deformation of the outer panel.
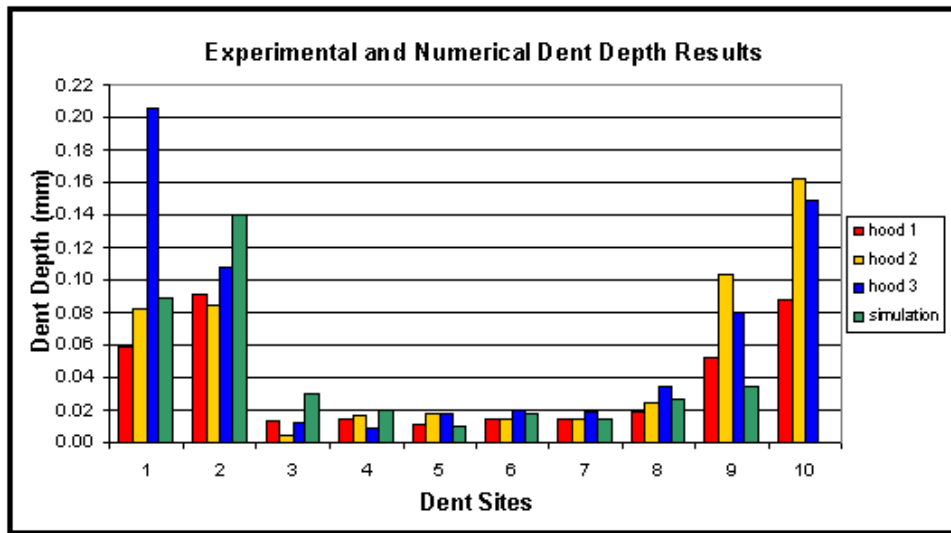
Figure 149: Comparison of experimental and predicted dynamic dent depths for a full hood assembly at various dent sites.

The validated modelling approach was then used to assess the impact of down gauging, from 1.0mm to 0.9mm to 0.8mm, on three prototype hoods. The effect of down-gauging from 1.0 to 0.8mm is minimal for most dent sites, as seen in Figure 150. For most

sites the change in dent depth between the thickest and thinnest sheet is less than 0.05mm, and the dent depths for the 0.8mm sheet remain below the threshold of 0.1mm.   The one exception is the dent depth at a hood featureline (site 10), an area of high local stiffness. Dynamic dent depths at this extremely stiff region are noticeably larger than all other sites, as expected.   Regardless of sheet thickness, the dent depths all exceed the 0.1mm threshold, reflecting that any denting on the feature line will be visible.
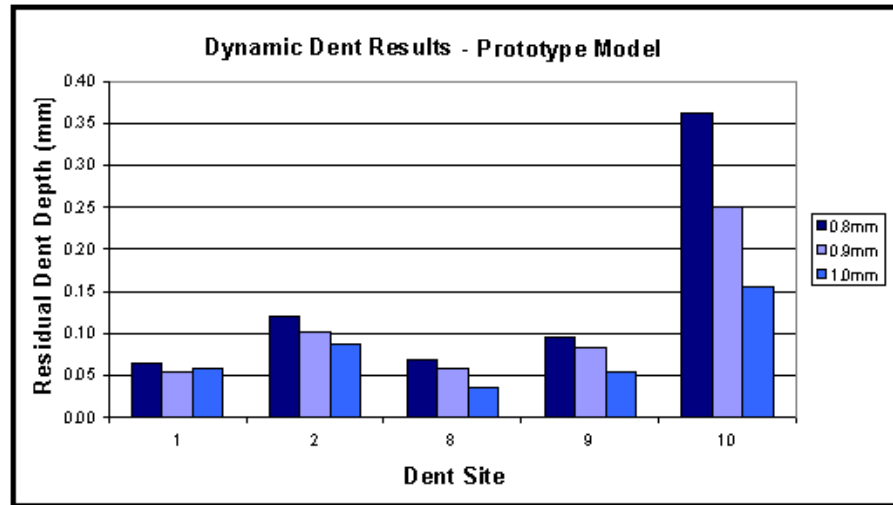
Figure 150: Comparison of predicted dynamic dent depths at various sites for 3 outer panel thickness values.

Comparisons of the predicted results for the different prototypes showed little influence of inner enhancements on dent resistance, as presented in Figure 151.   The three hoods compared had the same basic construction but included additional inner panel supports. The small effect of the inner stiffener variation on dynamic dent depth is due to the highly localized nature of dynamic denting, where global stiffening plays a limited role. The results of this follow-on work have proven the predictive capabilities of the modeling approaches developed in this thesis for actual automotive panel applications.
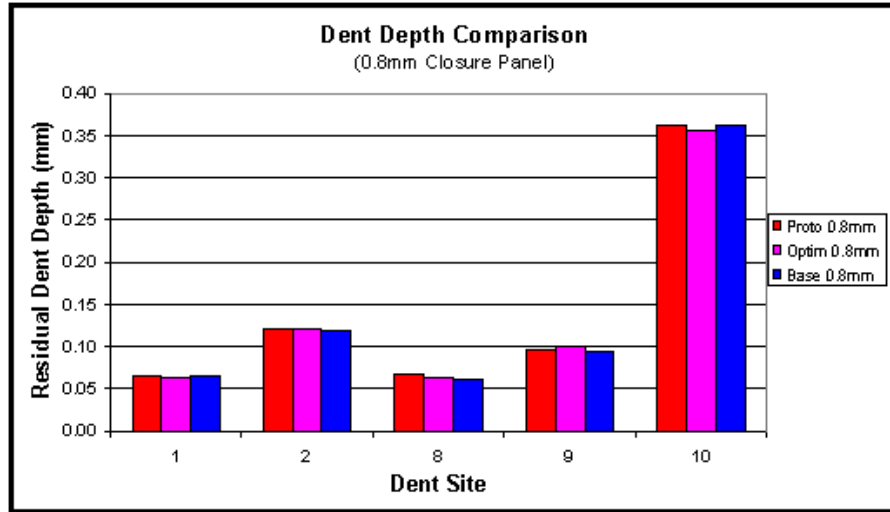
Figure 151: Comparison of predicted dynamic dent depths at various sites for 3 inner panel designs.

8 Conclusions and Future Work

8.1 Conclusions

The following are the principal conclusions drawn from this research:

- A parametric examination of factors affecting dent resistance, including panel curvature, panel thickness, spacing of inner panel supports and dent site location, has been performed. The experimental results offer a qualitative assessment of the various factors effecting static and dynamic denting in multi-part panel assemblies.

- The experimental results are hindered by the selection of an overly thin mastic layer between the inner and outer panels. The thin mastic layer leads to a non-linear material response with high stiffness in the range of loads tested. As such, the experimental results may not reflect the typical behaviour of actual automotive panels with thicker mastic pads.

- Increased sheet thickness improves both static and dynamic dent resistance for the load conditions tested.

- Global panel curvature has a small effect on the highly localized dynamic denting process for the large radii of curvature panels considered. Increased panel curvature does improve static stiffness response, which translates into improved static dent resistance.

- The surrounding boundary conditions imparted by the panel sidewalls and flanges, dramatically increase panel stiffness at a teacup location near the perimeter and improve the static dent resistance. However, dynamic denting above various teacup locations exhibits no significant variation. Dynamic denting is largely controlled by local support conditions, while static denting influenced more by global support conditions.

- The competitive nature of static and dynamic denting is revealed in comparing the results at the supported and unsupported sites. The local reinforcement of the teacup supports is

beneficial for static stiffness and dent resistance, but promotes dynamic denting. Conversely, the low stiffness unsupported sites offer superior dynamic dent resistance due to their ability to effectively transfer the momentum of the indentor during impact.

- A numerical modelling approach for evaluation of static and dynamic dent resistance incorporating features typical of real world automotive assemblies has been developed. Interactions between an inner support panel, an outer closure panel, the adjoining mastic layer and the peripheral rivets are all successfully implemented.

- The numerical predictions offer varying degrees of accuracy. The numerical results reproduce the measured trends for the various parametric combinations tested, offering potential for qualitative prediction of dent resistance.

- The numerical representation of the thin mastic layer is limited in the current version of LS-DYNA used. The linear approximation of the mastic stiffness used is incapable of fully capturing the actual mastic response limiting the accuracy of numerical predictions.

- The models poorly predict static dent depths at teacup-supported sites. This is attributed to an overly stiff model that is highly resistant to local yielding under static loading at the dent sites directly above the teacups.

- The use of a tied contact interface between the mastic and surrounding panels leads to numerical constraint of sheet bending at the teacup sites.

- Implicit convergence difficulties were encountered with the thinnest outer panel assemblies at load levels where the panel deflection was restricted by the surrounding sidewalls.

8.2 Future Work

Further dent resistance research should address several outstanding issues arising from the current work.

- Improvements to the dent testing setups will improve the accuracy of the measured results. These improvements could include an electric or hydraulic loading system for the static dent testing, a more precise laser-based alignment method for the dynamic tests and a more accurate residual displacement measurement system.

- Assessment of more traditional inner support configurations should be explored to assess the relative effectiveness of the teacup based inner panels.

- Detailed examination of the effect of mastic thickness is required. The variation in results between the medium scale assemblies with a 1mm thick mastic layer and the actual hood results with a 7mm mastic layer indicate that mastic thickness is a crucial component in multi-part panel assemblies. Experiments with the medium-scale panel assemblies using a thicker mastic layer should be undertaken.

- A thorough characterization program for the automotive mastic to develop a complete understanding of the material response under a variety of load conditions is recommended. This should include consideration of dynamic effects encountered at strain rates typical of current dynamic dent testing.

- Improved numerical representation of the mastic response is required. A fully non-linear material model that works with both the explicit and implicit solvers may be required to achieve accurate predictions.

- Alternative implicit codes could be explored to assess their potential to achieve more accurate static denting predictions. The necessary boundary conditions and inter-panel interactions must be considered.

- Transfer of the modelling approach to a wider range of automotive panels to better assess the predictive ability of the current method is required.

- Integration of the various modelling techniques, specific to multi-part assemblies, into a more advanced version of the re-meshing software D-Mesh, leading to a comprehensive dent resistance analysis tool is desirable.

9 References

1   R. Bamberger. "Automobile and Light Truck Fuel Economy: Is CAFE Up To Standard?", The National Council for Science and the Environment (NCSE), Paper: IB901222, Sept. 2000.

2   ULSAB webpage, "http://www.ulsab.org/index.html", 1997.

3   ULSAC webpage, http://www.ulsac.org/, 1998.

4   D. Thomas. "The Numerical Prediction Of Panel Dent Resistance Incorporating Panel Forming Strains", *Master's Thesis*, Department of Mechanical Engineering, University of Waterloo, Waterloo, Ontario, Canada, 2001.

5   "New Dent Resistance data", Dow Metal Products News, December 1960.

6   J. A. DiCello and R.A. George. "Design Criteria For The Dent Resistance Of Auto Body Panels", *Paper 740081*, SAE, 1974.

7   R.H. Frazier. "Improving Dent Resistance", Metal Progress, (93):30, 1968.

8   S.H. Greenfield. "Hail resistance of roofing products", *Paper, United States Department of Commerce, National Bureau of Standards*, August 1969. CODEN: BSSNB.

9   T.E. Johnson Jr. and W.O. Schaffnit. "Dent resistance of cold-rolled low-carbon steel sheet", *Paper 730528*, SAE, 1973.

10   C.E. Burley, B.A. Niemeier and G.P. Koch. "Dynamic denting of autobody panels", *Paper 760165*, SAE, 1976.

11   C.E. Burley and B.A. Niemeier. "Denting properties of aluminum autobody components", *Paper 770199*, SAE 1977.

12   B. A. Niemeier and C.E. Burley. "Hailstone response of body panels – real and simulated", *Paper 780398*, SAE, 1978.

13   R.L. Rolf, M.L. Sharp and H.H. Stroebel. "Structural characteristics of aluminum body sheet", *Paper 770200*, SAE, 1977.

14   D.C. Chang and R.P. Khetan. "Surface damage of steel, aluminum, and chopped-fiber composite panels due to projectile impact*", Journal of Reinforced Plastics and Composites*, 3:193-203, July 1984.

15   S. Nomura, Y. Yutori, J. Iwaya, M. Miyahara and I. Kokubo. "A study of the dynamic dent resistance", *In IDDRG Conference Proceedings*, p. 394-402. IDDRG, 1984.

16   M.B. Motwani. "Application of aluminum in body weight reduction", *Paper 770306*, SAE, 1977.

17   A. Daglish and D.J. Cunnane. "The static dent resistance of autobody alloys as a function of strain", *Technical Report BR-81/77*, ALCAN, 1981.

18   Y. Yutori, S. Nomura, I. Kokubo and H. Ishigaki. "Studies On The Static Dent Resistance", *Memoires Scientifiques Revue Metallurgie*, 77(4):561-569, April 1980.

19   D.J. Schaeffer. "Procedures for dent resistance evaluations of automotive outer body panels and assemblies under quasi-static and dynamic indenting conditions", *Technical Report 1.0, Auto/Steel Partnership Standardized Dent Resistance Task Force*, January 1997.

20   C.L. Alaniz and J.E. Borchelt. "Study of parameters that affect body panel performance perdictions", *Paper 910289*, SAE, 1991.

21   G. Ekstrand and N. Asnafi. "On testing of the stiffness and the dent resistance of autobody panels", *Materials and Design*, (19):145-156,1998.

22   P.T. Vreede, P.J. Tamis and M.E. Roelofsen. "The influence of material properties and geometry on dynamic dent resistance: Experiments and simulations", *In IBEC'95 Materials and Body Testing*, p. 79-86, IBEC, 1995.

23   M.A. Sabbagh, RN. Chavali and J.S. Montgomery. "Quasi-static dent depth simulation using non-linear fea", *In IBEC'95 Materials and Body Testing*, p. 87-90. IBEC, 1995.

24   J. Montgomery and A. Brooks. "Influence of geometry on outer panel dent resistance as demonstrated through fea", *In IBEC'94 Automotive Body Materials*, p.85-89. IBEC 1994.

25   M.F. Werner. "Finite element simulation of steel body panel performance for quasi-static dent resistance", *In IBEC'93 Automotive Body Materials*, p. 87-90. IBEC 1993.

26   M.A. McCormick, D.J. Meuleman, J.R. Fekete and M.F. Shi. "Effect Of Steel Strengthening Mechanisms On Dent Resistance Of Automotive Body Panels", *Paper 980960*, SAE, 1998.

27   B. Dauby, P. Magain, R. Kergen, F. Beco, S. Vandierendonck, M. Van Overmeire and J. Vereecken. "Improvement of dent resistance of autobody panels taking advantage of the strain hardening properties of steel sheets", *In the 19th Biennial Congress International Deep Drawing Research Group*, IDDRG, June 1996.

28   M.F. Shi and J.S. Wilczynski. "Potential weight savings versus dent resistance performance of high strength steel body panels", *In IBEC'93 Automotive Body Materials*, IBEC, 1993.

29   R.P. Krupitzer and R.P. Harris. "Improvements in the dent resistance of steel body panels", *Paper 920243*, SAE, 1992.

30   H.J. Thorburn. "Comparative tests of stiffness and dent resistance on aluminum and steel fenders", *In IBEC'94 Automotive Body Materials*, p.105-112. IBEC 1994.

31   C. Lahaye, J. Soderlund, D. ten Have and H. Schwenk. "Development of an aluminum prototype bonnet for Saab 9-3", *Paper 98IBECB-16*, 1998.

32   J. Zijp, I. Van Stijn, and M. Roelofsen. "Processing and applications of rephosphorized IF steels", *In 39th MWSP Conference Proceedings*, (35):31-35, 1998.

33   K.S. Raghavan and N. Arwashan. "Analysis of quasi-static denting behavior of automotive sheet steels", *Paper 970984*, SAE, 1997.

34   C.H. Chen, P.K. Rastogi and C.D. Horvath. "Effects of steel thickness and mechanical properties on vehicle outer panel performance: Stiffness, oil canning load and dent resistance", *In IBEC'93 Automotive Body Materials*, IBEC, 1993.

35   B. van Veldhuizen, W. Kranendonk, and R. Ruifork. "The Relation Between The Curvature Of Horizontal Automotive Panels", The Panel Stiffness And The Static Dent Resistance", *In Materials and Body Testing IBEC'95*, p. 62-70. IBEC, 1995.

36   M.F. Shi, D.J. Meulemanm C.L. Alaniz and S.J. Zurdosky. "An evaluation of the dynamic dent resistance of automotive steels", *Paper 910287*, SAE, 1991.

37   M.F. Shi, J.A. Brindza, P.F. Michel, P. Bucklin, P.J. Belanger and J.M. Prencipe. "Static and dynamic dent resistance performance of automotive steel body panels", *Paper 970158*, SAE, 1997.

38   T.N. Seel. "Bake hardening steel application study – key factors of dent resistance improvement", *Paper 910291*, SAE, 1991.

39   A.V. Vadhavkar, M.G. Fecek, V.C. Shah and W.E. Swenson. "Panel optimization program (P.O.P) ", *Paper 810230*, SAE, 1981.

40   K. Gong. "Structural And Dent Resistance Test On Prototype Aluminum Hoods", *KR-99/026 Internal Report*, Alcan International Limited, KRDC, October 1999.

41   K.K. Chen and P.A. Salamie. "A mathematical model for calculating dent initiation loads at the door centers", *Paper 841201*, SAE, 1984.

42   N. Asnafi. "On strength, stiffness and dent resistance of car body panels", *Journal of Materials Processing Technology*, (49):13-31, 1995.

43   H.F. Mahmood. Dent resistance of surface panel and slam area", *Paper 810099*, SAE, 1981.

44   A.A. Konieczny, Y. Qiu and b. Singh. "A practical program set for stiffness/dent resistance calculation of autobody outer panels", *In IBEC'97 Automotive Body Materials*, p. 54-58. IBEC, 1997.

45   W.E. Swenson Jr. and R.J. Traficante. "The influence of aluminum properties on the design, manufacturability and economics of an automotive body panel", *Paper 820385*, SAE, 1982.

46   M.F. Shi, D.J. Meuleman, C.L. Alaniz and S.J. Zurdosky. "Prestrain effects on static dent resistance of automotive steels", *Paper 910288*, SAE 1991.

47   H. Sakai, K. Saito and H. Tsukada. "Stiffness and dent characteristics of body outer surface panel – finite element analysis and experiment", *International Journal of Vehicle Design*, 4(1):13-22, 1983.

48   M.F. Shi and J.S. Wilczynski. "Estimation of yield strength for a formed panel", *In IBEC'95 Materials and Body Testing*, p.55-61, IBEC, 1995.

49   J. Bottema, C. Lahaye, R. Baartman, L. Zhuang and P. DeSmet. "Recent developments in AA 6016-T4 aluminum type body sheet product", *Paper 981007*, SAE, 1998.

50   R. Chavali and W. Song. "Coupling forming and denting simulations for automotive closure panels", *Paper Number 96NM098*, Unknown Origin, 1996.

51   J.D. Bryant. "The effects of pre-aging treatments on formability and paint bake response in aluminum autobody sheet alloys", *In the TMS Annual Meeting Automotive Alloys*, p.19-36, The Minerals, Metals and Materials Society, 1997.

52   C.M. Ni. "Analysis of panel dent resistance", *Internal Report N77 10290*, General Motors, 1976.

53   F. Gatto and D. Morri. "Forming properties of some aluminum alloy sheets for car-body use", *In the 12th Biennial Congress International Deep Drawing Research Group*, IDDRG, May 1982.

54   R. Hill. "Theoretical Plasticity of Textured Aggregates", *Math. Proc. Comb. Phil. Soc.*, 85:179-191, 1979.

55   H. Sakai, K. Saito and H. Tsukada. "Stiffness and dent characteristics of body outer surface panel – finite element analysis and experiment", *International Journal of Vehicle Design*, 4(1):13-22, 1983.

56   N. Oda, K. Hamano, T. Umemura and M. Kusuhara. "A method of predicting dent resistance of automobile body panels", *Paper 950574*, SAE, 1995.

57   D.G. Adams. "Automobile panel sweep-stiffness analysis", *Paper 740080*, SAE, 1974.

58   K.V. Williams. "The Numerical Prediction of Strain Distribution in Sheet Metal Forming Operations", *Master's Thesis*, Ottawa-Carleton Institute for Mechanical and Aerospace Engineering, Carleton University, Ottawa, Ontario, Canada, December 1993.

59   E.T. Harpell. "Numerical Prediction Limiting Draw Ratio in Aluminum Cylindrical Cup Drawing", *Master's Thesis*, Ottawa-Carleton Institute for Mechanical and Aerospace Engineering, Carleton University, Ottawa, Ontario, Canada, May 1996.

60   C.G. Lamontagne. "Numerical Simulation of Aluminum Sheet Forming Incorporating Plastic Anisotropy", *Master's Thesis*, Ottawa-Carleton Institute for Mechanical and Aerospace Engineering, Carleton University, Ottawa, Ontario, Canada, May 1996.

61   X. Zhou. "Numerical Prediction of Springback in U-Channel Forming of Aluminum Tailor Welded Blanks", *Master's Thesis*, Ottawa-Carleton Institute for Mechanical and Aerospace Engineering, Carleton University, Ottawa, Ontario, Canada, October 1999.

62   C.L. Alaniz, L.E. Brookes and T.N. Seel. Investigation of body panel stiffness as predicted by finite element analysis", *Paper 900716*, SAE, 1990.

63   M.J. Worswick, M.J. Finn and H.J. Thorburn. "A numerical study of the geometric and material parameters affecting static and dynamic denting", *Internal Report KR-97/025*, Alcan International Limited, Kingston Research and Development Centre, November 1997.

64   Thomas, D.N., Hodgins, B., Worswick. M.J., Oddy, A.S., Gong, K., Finn, M.J., FEM *Technique for Static and Dynamic Dent Modelling of Aluminum*, Proceedings, Numisheet'99, France, September, 1999.

65   A. Viertel, M.J. Worswick, B. Hodgins and D. Thomas. "Numerical Modelling Of Dynamic Denting On An Aluminum Automotive Hood*", Progress Report*, Department of Mechanical Engineering, University of Waterloo, May 2001.

66   L. Sutak, ALCAN, Private Communications.

67   L. Sutak, "Automotive Hood "Gum-Drop" Mechanical Properties", *Internal Report,* Alcan International Limited, KRDC, September, 2000.

68   SDRC, "IDEAS User Manual", Structural Dynamics Research Corporation, Milford , Ohio, 1993.

69   LSTC. "LS-DYNA Keyword User's Manual: Nonlinear Dynamic Analysis of Structures", Livermore Software Technology Corporation, December, 2000.

70   M.J. Worswick. "IDZDYNA – A Translator System for the I-DEAS and DYNA3D Codes", M.J. Worswick Analysis Ltd., February, 1993.

71   B.N. Maker and X. Zhu. "Input Parameters for Metal Forming Simulation using LS-DYNA", Livermore Software Technology Corporation, February, 2000.

72   J.C. Simo and F. Armero. "Geometrically non-linear enhanced strain mixed methods and the method of incompatible nodes", *International Journal for Numerical Methods in Engineering*, 33:1413-1449, 1992.

73   B.N. Maker, LSTC, Private Communications.

74   F. Barlat and J. Lian, "Plastic behaviour and stretchability of sheet metals. Part 1: A yield function for orthotropic sheets under plane stress conditions. *International Journal of Plasticity,* 5:51-66, 1989.

75   J. O. Hallquist. "LS-DYNA Theoretical Manual", Livermore Software Technology Corporation, May, 1998.